

THESIS ON MECHANICAL AND INSTRUMENTAL ENGINEERING E27

**Deposition of Solid Particles
from Aerosol Flow
in Laminar Flat-Plate Boundary Layer**

SERGEI TISLER

Faculty of Mechanical Engineering
Department of Thermal Engineering
TALLINN UNIVERSITY OF TECHNOLOGY

Dissertation was accepted for the defence of the degree of Doctor of Philosophy
in Engineering on May 5, 2006

Supervisors:

Prof. Ph D Aadu Paist, Faculty of Mechanical Engineering
D Sc Alexander Kartushinsky, Faculty of Science

Opponents:

Prof. Ph D Sergei Sazhin, University of Brighton, Brighton, UK
Prof. D Sc Leonid Zaichik, Scientific Association for High Temperatures,
Moscow, Russia

Commencement: June 9, 2006

Declaration

Hereby I declare that this doctoral thesis, my original investigation and
achievement, submitted for the doctoral degree at Tallinn University of
Technology has not been submitted for any degree or examination.

Copyright Sergei Tisler 2006
ISSN 1406-4758
ISBN 9985-59-625-0

MASINA- JA APARAADIEHITUS E27

**Tahkete osakeste väljasadenemine
aerosoolvoolustest tasapinnalise plaadi
laminaarses piirkihis**

SERGEI TISLER

TAHKETE OSAKESTE VÄLJASADENEMINE AEROSOOLVOOLUSTEST TASAPINNALISE PLAADI LAMINAARSES PIIRKIHS

Sergei Tisler

Mitmefaasiliste keskkondade füüsika teaduslaboratoorium

Tallinna Tehnikaülikool

Akadeemia tee 23A, 12618, Tallinn

Eesti

Kokkuvõte

“Gaas-tahked osakesed” tüüpi kahefaasilised aerosoolvoolused on looduses laialt levinud. Näiteks liiva tormid, liikuvad liivadüünid, kosmiline tolm, lumelaviinid aga samuti tolmu liikumine atmosfääris.

Mitmefaasilised, eriti aga kahefaasilised aerosoolvoolused, leiavad laialdast kasutamist tehnikas. Need protsessid moodustuvad või organiseeritakse spetsiaalselt paljude tööstusharude tehnoloogiliste protsesside läbiviimiseks, näiteks energeetikas, farmaatsiatööstuses, toiduainetööstuses jne.

Aerosoolvoogude kasutamine kahjulike gaasiliste ühendite eraldamiseks tahketel kütustel töötavate elektrijsüsteemide suitsugaasidest, tööstusjäätmete filtreerimisel ja tolmupüüdmisel võimaldavad oluliselt vähendada ümbritseva keskkonna saastumist. Hingamise toksikoloogia ja atmosfääri reostumise kontroll on samuti otseselt seotud aerosoolvoolustega.

Aerosoolvoolusi kasutatakse laialdaselt tsemendi, teravilja, väetiste ja teiste puistematerjalide pneumotranspordi süsteemides.

Kõige kujukam näide aerosoolvooluste kasutamise kohta on keevkihtseadmed, mida kasutatakse kütuste põletamiseks energeetikas, aga samuti kütuste gaasistamiseks ja kahjulike orgaaniliste- ning bioloogiliste ühendite eraldamiseks keemiatööstuses.

“Gaas-tahked osakesed” tüüpi aerosoolvooluseid kasutatakse laialdaselt nii uute materjalide tootmisel kui ka materjalide töötlemise tehnoloogilistes protsessides. Näidena sellest valdkonnast võib tuua materjalidele katete pealekandmise pihustamise teel. Seda meetodit kasutatakse ülipeene struktuuriga ja paljudest komponentidest koosnevate materjalide tootmisel.

Suurem enamus ülalnimetatud looduslikest nähtustest ja tööstuslikest protsessidest on seotud tahkete aerosoolsete osakeste väljasadenemisega mitmesugustele pindadele, nagu maapind, hooned, mitmesuguste seadmete tööpinnad jne. Üks kasutatav kasulik väljasadenemise meetod on erineva kuju või tihedusega tahkete osakeste tööstuslik separeerimine. Tahkete kütuste põletamisel tekivad katelde soojusvahetuspindadele lendtuha sadestised, tahkete osakeste sadestised võivad tekkida ka turbiini labadele. Need sadestised põhjustavad energeetiliste seadmete tööparameetrite halvenemist.

Järelikult on tahkete osakeste väljasadenemise füüsikaliste mehhanismide tundmaõppimine üks vajalikust tingimustest erinevate tööstusprotsesside

optimaalsel väljatöötamisel ja looduslike protsesside modelleerimisel. Väljasadenenud tahkete osakeste koguse ja erinevatel pindadel jaotumine hindamine on abiks paljude tööstuslike agregaatide ja seadmete projekteerimisel ning konstrueerimisel.

Seega on tahkete osakeste väljasadenemise prognoosimine aerosoolvoolustest üks aktuaalse(i)m probleem käesoleval ajal.

Vaatamata sellele, et viimastel kümnenditel on tehtud ja tehakse jõupingutusi, selleks et süvendada arusaamist tahkete osakeste väljasadenemisest erinevatele pindadele, mida uhub aerosoolvoog, on paljud probleemid siin veel ebaselged. Puudub selge ja loogiline teooria katseliselt määratud tahkete osakeste seaduspärasuste kirjeldamiseks piirkihis, mis moodustub aerosoolvooga uhutava pinna lähedal. See puudutab ka väljasadenevate osakeste hüdrodünaamiliste protsesside matemaatilist modelleerimist, aga ka adhesiooni protsesse, milledest paljuski oleneb osakeste väljasadenemine pinnale. Vaatamata sellele, et on tehtud palju eksperimentaalseid ja teoreetilisi uuringuid tahkete osakeste väljasadenemise kohta erinevatele pindadele, ei ole seni veel täpseid ja usaldusväärseid meetodeid mitte ainult osakeste väljasadenemise koguse jaotumise kohta piki pinda, vaid ka nende osakeste üldise massi kohta. Sellised meetodid on aga väga vajalikud efektiivsete abinõude väljatöötamiseks, et kaitsta pindu nende tekkivate tahkete sadestiste vastu.

Järelikult tahkete osakeste väljasadenemise põhjalik eksperimentaalne ja teoreetiline uurimine aerosoolvooluse poolt uhutavale pinnale ja meetodi väljatöötamine, mis võimaldab prognoosida väljasadenenud osakeste kogust, omavad väga suurt praktilist tähtsust.

Paljude eksperimentaalsete ja teoreetiliste uuringute analüüsi tulemusena on leitud, et erinevate kehade uhumisel aerosoolvoolustega, võib tahkete osakeste väljasadenemisel nende pindadele eristada järgmisi etappe:

- 1) osakeste kandumine pinna lähedale kuni pinnaga kontakti momendini;
- 2) osakeste ja pinna vaheline adhesioon.

Esimene etapp on määratud ainult osakeste käitumise iseärasustega laminaarse hüdrodünaamilise piirkihi sees, mis moodustub aerosoolvooga uhutava pinna lähedal, arvestamata muutusi, mis on tingitud pinnale moodustunud osakeste sadestistest. Teine etapp on tingitud osakeste ja pinna vastastikusest mõjust ja paari "osake-pind" adhesiooni omadustest antud väliskeskkonna tingimuste juures. Seepärast võib pindadele väljasadenevate osakeste koguse hindamise ülesande jagada kaheks allülesandeks.

Esimene nn. hüdrauliline allülesanne on seotud piirkihi mõju väljaselgitamisega väljasadenemise protsessile. Selle ülesanne käigus määratakse aerosoolvooluse kiirusi ja osakeste kontsentratsioone pinna lähedal.

Teine allülesanne on seotud osakeste ja pinna vastastikuse mõjuga. See ülesande lahendamine võimaldab määrata pinnale moodustuvate sadestiste massi ja selle jagunemist piki pinda. Seda ülesannet on võimalik lahendada juhul kui on teada paari "osake-pind" adhesiooni omadused.

Seega oli vaja pinnale väljasadenevate osakeste koguse hindamise usaldusväärse meetodika väljatöötamiseks läbi viia järgmised eksperimentaalsed ja teoreetilised uuringud:

- 1) määrata aerosooli osakeste käitumise hüdrodünaamilised iseärasused pinna lähedases laminaarses piirkihis;
- 2) uurida paari "osake-pind" adhesiooni omadusi.

Käesolevas tööks valiti uuringute objektiks tasapinnaline plaat. Antud valik oli tingitud ühest küljest sellest, et tasapinnalise plaadi hüdrodünaamilised omadused on puhta, tolmuva voolusega uhumisel hästi uuritud ja teisest küljest seepärast, et paljud eksperimentaalsed ja teoreetilised uurimustulemused, mis on saadud tasapinnalise plaadi uhumisel aerosoolvoogude, on vasturääkivad.

Käesoleva uurimistöö ülesandeks oli järgmiste parameetrite kvalitatiivse ja kvantitatiivse mõju hindamine väljasadenemise protsessile:

- vooluse kiirus,
- tahkete osakeste mõõt,
- osakeste masskontsentratsioon vooluses,
- osakeste ja pinna adhesiooni omadused
- saadud katsetulemuste alusel tasapinnalisele plaadile väljasadenenud osakeste koguse määramise meetodi väljatöötamine.

Tahkete osakeste käitumise iseärasuste uuringud piirkihi sees plaadi pinna lähedal viidi läbi kahefaasilises avatud aerodünaamilises torus kahel vooluse kiirusel 1,5 ja 3 m/s. Disperse keskkonna loomiseks kasutati elektrokorundi osakesi keskmise läbimõõduga 12, 23 ja 32 μm . Aerosoolvooluse dispersse faasi tihedus oli 0,01 kg/m^3 . Aerosoolvooluse kiirust ja osakeste kontsentratsiooni piirkihi sees mõõdeti vastavalt laser-doppleranemomeetriga ja kontsentratsiooni laser mõõdikuga. Plaadi pinnale väljasadenenud osakeste jaotumist määrati kaalumise teel.

Osakeste hüdrodünaamiliste karakteristikate (kiiruse ja massi kontsentratsiooni) arvutamiseks piirkihi sees töötati välja kahefaasilise laminaarse piirkihi matemaatiline mudel, mis rahuldavalt kirjeldab osakeste käitumist tasapinnalise plaadi lähedal.

Paari "osake-pind" adhesiooni omaduste uurimiseks töötati välja spetsiaalne stend, millel tsetrifugaalse lahtirebimisjõu meetodil määrati uuritavate osakeste adhesiooni arv olenevalt lahtirebimise jõust.

Saadud eksperimentaalsete ja teoreetiliste uuringute tulemuste alusel töötati välja meetodika tahkete osakeste väljasadenenud koguse kvantitatiivseks hindamiseks tasapinnalisele plaadile selle pikkuse ulatuses. See meetod põhineb nii plaati uhuva aerosoolvooluse hüdrodünaamiliste iseärasuste, kui ka osakeste ja pinna adhesiooni omaduste tundmisel koos tõenäose lähenemisega väljasadenemise protsessile.

Läbiviidud uurimuste alusel saadud tulemused võimaldavad teha järgmised järeldused:

1. Väljatöötatud tahkete osakeste tasapinnalisele plaadile väljasadenemise koguse hindamise meetodika põhineb selle protsessi kompleksel hindamisel ja arvestab nii tasapinnalist plaati uhuva aerosoolvooluse hüdrodünaamilisi iseärasusi kui ka osakeste ja pinna adhesiooni omadusi.

2. Osakeste pinnale väljasadenemise protsess sõltub olulisel määral nende osakeste hüdrodünaamilise käitumise iseärasustest pinna lähedal moodustuva laminaarse piirkihi sees ja nimelt osakeste massi kontsentratsiooni jagunemise maksimumi suurusest, selle maksimumi asendist pinna suhtes, aga samuti massi kontsentratsiooni gradiendist kihi sees.

3. Adhesioon, mis ilmneb peale osakeste kontakti ja haaramist pinna poolt ning millel on tõenäoline iseloom, määrab olulisel määral pinnale tekkiva tahkete aerosooli osakeste sadestiste koguse.

Väljatöötatud sadestiste massi hindamise meetodikat saab kasutada isotermilistest aerosoolvoogudest mitmesugustele pindadele väljasadenevate sadestiste koguste arvutamiseks, näiteks torudes puistematerjalide pneumotransportimisel, ventilatsioonikanalites, gaasipuhastusseadmetes jne.

DEPOSITION OF SOLID PARTICLES FROM AEROSOL FLOW IN LAMINAR FLAT-PLATE BOUNDARY LAYER

Sergei Tisler

Laboratory of Multiphase Media Physics
Tallinn University of Technology
Akadeemia tee 23A, 12618, Tallinn
Estonia

Abstract

The given thesis is dedicated to the experimental and theoretical investigations of the deposition of fine solid particles from the aerosol flow in the laminar flat-plate boundary layer.

The objective of the investigations was to estimate qualitatively and quantitatively the influence of parameters of the aerosol flow and the adhesive properties of particles and surface on the deposition properties of particles under the conditions of the laminar flat-plate boundary layer and elaborate the estimation technique for the amount of the deposited particles.

The streamflow velocity was 1.5 and 3 m/s. Electrocorundum powders with the particle size of 12, 23 and 32 μm were used as the dispersed phase of the aerosol flow. The bulk density of the dispersed phase was 0.01 kg/m^3 .

The local air velocity and the particles mass concentration inside the laminar boundary layer were measured by the laser Doppler anemometer and the laser concentration measurer. The amount of the particles deposited at the surface from the flow was measured by the weighing method.

The mathematical model elaborated to describe adequately the behaviour of aerosol particles inside the laminar boundary layer was applied for the calculations of the hydrodynamic parameters of particles near the plate.

The investigations have revealed that the amount of particles deposited at the surface was substantially conditioned by a character of distribution of the particle mass concentration occurred inside the boundary layer, the disposition of maximum of the particle mass concentration relative to the surface as well as the gradient of the particle mass concentration within the boundary layer.

The results of the investigations of the adhesive properties of pair “particle-surface” have shown that the adhesion factor was also of primary importance for the particles deposition.

The elaborated estimation technique for the particles deposition takes into account both the hydrodynamics of the flow past the flat plate and the adhesive properties of particles and surface. The given technique can be applied for the assessment of amount of solid deposits at various surfaces streamlined by the air-solid particles aerosol flows, namely, the acting faces of the constructional elements of the solid fuel power plants, the pneumo-conveying devices as well as various gas-purifying equipment.

FORMATTING OF THE THESIS

The given thesis may be divided into three main parts – the experimental and the theoretical investigations concerning the behaviour of solid aerosol particles inside the laminar flat-plate boundary layer, the experimental study of the adhesive properties of the aerosol particles and the considered surface, and the elaboration of the estimation technique for the particles deposition.

The theoretical and the experimental parts of the thesis, dedicated to the hydrodynamics of the streamlining of the plate by the aerosol flow, as well as the adhesive properties of the pair “particle-surface” are based mainly on the publications that completely cover the investigations of the behaviour of the particles within the laminar boundary layer. At the same time, the contents of these publications is presented here in the revised form due to the better understanding of the studied phenomena by the author of the given thesis.

The remaining part of the thesis presents the probabilistic approach for the particles deposition and describes the estimation technique for the deposition amount, which have not been published until now, and so they are presented in more detailed form.

The dissertation is based on the following publications:

- I. Hussainov, M., Kartushinsky, A., Mulgi, A., Shcheglov, I., Tisler, S., 1994, Properties of solid particle distribution in two-phase laminar boundary layers of various shapes and particle sedimentation. *Proc. Estonian Acad. Sci. Physics Mathematics*, Vol. 43(4), pp. 237-249.
- II. Hussainov, M., Kartushinsky, A., Mulgi, A., Rudi, Ü., Tisler, S., 1995, Experimental and theoretical study of the distribution of mass concentration of solid particles in the two-phase laminar boundary layer on a flat plate. *Int. J. Multiphase Flow*, Vol. 21(6), pp. 1141-1161.
- III. Hussainov, M., Kartushinsky, A., Shcheglov, I., Tisler, S., 1998, Some results of investigation of solid particles distribution in the vicinity of various shapes in two-phase flow and sedimentation on their surfaces. *In: Proceedings of 27th Israel Conference on Mechanical Engineering*, Haifa, Israel, 19-20 May, (Ed.) Ben-Haim, Ya., Technion - Israel Institute of Technology, Haifa, Israel, pp. 356-358.
- IV. Hussainov, M., Kartushinsky, A., Tisler, S., 2002, Experimental study of adhesive behaviour of pair “solid particle-streamlined surface”. *In: Proceedings of 10th Workshop on Two-Phase Flow Predictions*, Merseburg, Germany, April 9-12, (Ed.) Sommerfeld, M., Martin-Luther-Universität, Halle, Germany, pp. 401-405.
- V. Hussainov, M., Kartushinsky, A., Rudi, U., Shcheglov, I., Tisler, S., 2004, An experimental investigation of effect of the velocity slip on modification of the grid-generated turbulence in a gas-solid particles flow. *In: Proceedings of 3rd International Symposium in Two-Phase Flow Modelling and Experimentation*, Pisa, Italy, September 22-25, CD-ROM, as04.
- VI. Kartushinsky, A., Mulgi, A., Tisler, S., Michaelides, E. E., 2005, An experimental study of the effect of particles on the shear stress in

- particulate turbulent pipe flow. *Proc. Estonian Acad. Sci. Engineering*, Vol. 11(2), pp. 161-168.
- VII. Hussainov, M., Kartushinsky, A., Rudi, U., Shcheglov, I., Tisler, S., 2005, Experimental study of the effect of velocity slip and mass loading on the modification of grid-generated turbulence in gas-solid particles flows. *Proc. Estonian Acad. Sci. Engineering*, Vol. 11(2), pp. 169-180.

The personal contribution of the competitor

Articles I, II, III, V, VI, VII: The author took an active part in the elaboration of the research program of the experimental and theoretical investigations concerning the deposition of solid aerosol particles at various surfaces, as well as in the designing and building of the experimental set-up intended for these investigations. The author has developed the techniques for the measurements of amount of the deposited particles along the plate and other surfaces which were under investigation in the given articles and elaborated and built the appropriate test rig. The author took part directly in the running of the experiments and discussions of the obtained data. The author took part in the writing of the presented joint papers.

Article IV: The author has suggested the methodology of the experimental procedure concerning the investigation of the adhesive behaviour of pair “particle-surface”. The author has designed and built the test rig for these investigations. The author has performed the experiments and the appropriate experimental data processing.

Unpublished material: The author has suggested the estimation technique for the particles deposition and performed the calculations concerning this technique with the applying of the probabilistic approach for the particles deposition.

The subject of the defence:

The subject of the defence is the estimation technique for the aerosol solid particles deposition at the surface under the conditions of the flat-plate laminar boundary layer, the results of the experimental and numerical investigations of influence of parameters of the aerosol flow on the deposition of particles at the surface of the flat plate, the measurement technique for the particles deposition and the appropriate experimental test rig, the results of the experimental investigation of the adhesive behaviour of pair “particle-surface” and the appropriate test rig.

Scientific novelty of the obtained results:

The estimation technique for the solid particles deposition from the aerosol flow has been elaborated for the laminar flow past a flat plate at the isothermal conditions, which simultaneously accounts the hydrodynamics of the flow past and the adhesive properties of the deposited particles and a surface.

SCOPE OF THE THESIS

The thesis consists of introduction, five chapters and conclusion.

Chapter 1 considers the parameters of the two-phase aerosol flow, surveys the published results of the experimental and theoretical investigations concerning various aspects of the deposition of solid particles from the aerosol flow on various surfaces. The analysis of influence of different critical parameters of a two-phase aerosol flow on the phenomenon, which is under consideration, is also included. The first part is concluded by the problem statement for the investigation and the general concept of the investigations of the particles deposition from the aerosol flow.

Chapter 2 contains the description of the experimental set-up and the procedures of measurements of the particles concentration inside the laminar boundary layer near the plate surface, as well as the intensity of the particles deposition. This chapter also presents the discussion of the obtained experimental results concerning the particles behaviour in the boundary layer near the plate and their deposition at the plate surface.

Chapter 3 gives the concise description of technique of the numerical modelling applied in the given thesis. It includes the problem statement, the mathematical formulation with the description of the applied model and the initial and boundary conditions, as well as the procedure of the modelling. The comparison of the obtained numerical results with the experimental data is also presented in this chapter.

Chapter 4 presents the description of the experimental set-up and the procedure of the measurements for the adhesive behaviour of solid particles and a surface, as well as the discussion of the obtained results concerning the obtained experimental dependencies for the adhesion number from the detaching force.

Chapter 5 contains the description of the estimation technique for the calculation of the particles deposition based on the simultaneous account of the hydrodynamics of the laminar boundary layer, which is formed close to the plate surface, and the adhesive properties of the particles and the surface with the applying of the probabilistic approach for the deposition phenomenon. The discussion and comparison of the numerical results, obtained by the given technique, with the experimental data on the particles deposition, is also presented in this chapter.

PREFACE

The author gratefully acknowledges the Estonian Science Foundation and Tallinn University of Technology for the financial support of this research. The present investigations were fulfilled in the framework of the current studies carried out in the Laboratory of Energy Processes Diagnostics of Estonian Energy Research Institute under the project “*Theoretical and experimental investigations of mass transfer inside two-phase boundary layers and determination of thermo-optical characteristics of dust surfaces*” (the government financing project No. F92/12) and “*Development of theory of the two-phase gas-solid particles flows*” (the Estonian Science Foundation financing project SF0070055s98) and in the Laboratory of Multiphase Media Physics, Faculty of Science of Tallinn University of Technology under the project “*Development of the theory of dispersed (gas-solid particles) flows and its implementation in energy processes*” (the Estonian Science Foundation financing project SF0812526s03). This work was carried out partly under the financial support of the International Science Foundation (grant No. LG 6000) and within the international project “*Mars 94/96*” in the frame of the cooperation between the Russian and French Space Agencies.

I would like to express my gratitude to everyone who has in one way or another contributed to this work.

The author would like to express his deepest gratitude to his supervisors, Prof. Ph D A. Paist and D Sc A. Kartushinsky, for their excellent guidance and support during the research.

I am also deeply thankful to my colleagues and collaborators from the Laboratory of Multiphase Media Physics for their collaboration in conducting laborious experiments and useful discussion of the obtained results.

I owe my sincere gratitude to those persons whose disciple I consider myself, firstly, A. Mulgi and Ph D M. Hussainov for taking care during my initial study in the field of multiphase flow, and secondly, Dr. Ü. Rudi for his incessant care and support while writing this thesis.

I wish to express my thankful appreciation to my dear wife V. Tisler and to my friends for their continuous support, understanding and encouragement during this work.

Table of Contents

NOMENCLATURE	17
INTRODUCTION	22
1. DEPOSITION FROM AEROSOL FLOWS.....	23
1.1. The Definition of Aerosol and the Main Parameters of the Aerosol Flow	23
1.2. Deposition of Aerosol Solid Particles at Streamlined Surfaces	25
1.2.1. <i>Hydrodynamical mechanisms of the particles deposition</i>	26
1.2.2. <i>The particles adhesion</i>	32
1.2.3. <i>The particles detachment</i>	37
1.3. The Statement of Problem for the Investigation	40
1.3.1. <i>Goal and objectives</i>	40
1.3.2. <i>The concept for the investigations of deposition of the aerosol particles</i>	41
2. THE INFLUENCE OF PARAMETERS OF THE AEROSOL FLOW ON DEPOSITION OF SOLID PARTICLES AT FLAT SURFACE.....	42
2.1. Experimental Set-Up.....	42
2.2. Experimental Conditions.....	43
2.3. Experimental Technique	46
2.4. Results.....	48
2.4.1. <i>The particle mass concentration in the laminar boundary layer on the flat plate</i>	48
2.4.2. <i>The particles deposition on the flat plate</i>	50
2.5. Discussion of Results	53
3. THEORETICAL MODEL OF THE TWO-PHASE LAMINAR BOUNDARY LAYER ON A FLAT SURFACE.....	54
3.1. Prerequisites for Numerical Modelling.....	54
3.2. System of Equations.....	56
3.3. Initial and Boundary Conditions	59

3.4. Results of the Computations and Validation of the Model	62
4. ADHESION BEHAVIOUR OF PAIR “SOLID PARTICLE- STREAMLINED SURFACE”	69
4.1. Experimental Conditions.....	69
4.2. Measurement Technique	69
4.3. Results and Discussion.....	72
5. THE ESTIMATION TECHNIQUE FOR THE PARTICLES DEPOSITION AT THE FLAT PLATE.....	76
5.1. Probabilistic Nature Of Particles Deposition	76
5.2. Estimation of Deposition Intensity.....	77
5.3. Results And Discussion.....	80
CONCLUSIONS	83
REFERENCES	84
ORIGINAL PUBLICATIONS.....	90
CURRICULUM VITAE.....	164
ELULOOKIRJELDUS (CV).....	165
LIST OF THE MOST IMPORTANT PUBLICATIONS	166

NOMENCLATURE

Roman Symbols

A	-	the constant of van der Waals, [N m]
B_1	-	the constant
B_2	-	the constant
a	-	the constant
b	-	the constant
C	-	mass concentration of the dispersed phase, $\left[\frac{\text{kg}}{\text{m}^3}\right]$
C_N	-	the numerical concentration of particles in the flow, $\left[\frac{1}{\text{m}^3}\right]$
C_x	-	the aerodynamic drag coefficient of a particle
C'_D	-	the drag coefficient
D	-	a pipe diameter, [m]
D_p	-	the particle Brownian diffusion coefficient, $\left[\frac{\text{m}^2}{\text{s}}\right]$
D_s	-	the pseudoviscosity coefficient for the particles mass transport equation
dx_L	-	the width of the test cross-section of the conic model, [m]
E	-	Young's modulus, $\left[\frac{\text{N}}{\text{m}^2}\right]$
E_e	-	the electric field, $\left[\frac{\text{N}}{\text{C}}\right]$
e	-	the electron charge, $1.6 \cdot 10^{-19}$, [C]
F_A	-	the adhesive force, [N]
F_{ad}	-	the aerodynamic drag force, [N]
F_C	-	the Coulomb force, [N]
F_{im}	-	the image force, [N]
F_M	-	the molecular force, [N]
F_{cap}	-	the capillary force, [N]
F_{el}	-	the elastic force, [N]
F_{fr}	-	the frictional force, [N]
F_{gr}	-	gravity, [N]
F_{press}	-	the pressing force, [N]

f_u	-	the coefficient characterizing the loss of the particles tangential velocity due to their collisions with the plate surface
$f(x)$	-	the numerical function
g	-	acceleration of gravity, $\left[\frac{\text{m}}{\text{s}^2} \right]$
H	-	the distance between molecules, [m]
I_A	-	the deposition intensity occurred under the absence of the blowing-off of particles, $\left[\frac{\text{kg}}{\text{m}^2 \text{ s}} \right]$
I_{bl}	-	the intensity of the blowing-off of some portion of the deposited particles, $\left[\frac{\text{kg}}{\text{m}^2 \text{ s}} \right]$
I_d	-	the intensity of the particle deposition, $\left[\frac{\text{kg}}{\text{m}^2 \text{ s}} \right]$
J_w	-	the mass flux of particles to the wall per unit area, $\left[\frac{\text{kg}}{\text{m}^2 \text{ s}} \right]$
K_{el}	-	the constant defined by the physical properties of materials of surface and particles
K_s	-	the numerical constant
Kn	-	the particle Knudsen number
k	-	Boltzmann's constant, $1.38 \cdot 10^{-23}$, $\left[\frac{\text{J}}{\text{K}} \right]$
k_t	-	the roughness coefficient
L	-	the length of the plate, [m]
l	-	the mean free path of a gas molecule, [m]
l_{el}	-	the approach of the centre of a spherical particle and the surface, [m]
m_p	-	the mass of a particle, [kg]
N	-	the number of particles
N_0	-	the initial number of particles
N_{det}	-	the number of particles detached from a surface
n	-	the rotational speed of the model, [rps]
P_A	-	the probability of adhesion of a particle
P_{bl}	-	the probability of the blowing-off of a particle from a surface
P_{en}	-	the probability of entrainment of a particle by a surface
P_{st}	-	the sticking probability

p_{max}	-	the maximum tension in the zone of contact of a particle and a surface, $\left[\frac{\text{N}}{\text{m}^2} \right]$
p_s	-	the normal stress for the dispersed phase, $\left[\frac{\text{N}}{\text{m}^2} \right]$
q_p	-	a particle charge, [C]
q_{sur}	-	a surface charge, [C]
R	-	a distance between a particle and a surface, [m]
R_i	-	the radius of the cross-section of the model, [m]
Re_p	-	the particle Reynolds number
Re_x	-	the Reynolds number defined for the current cross-section of the flat plate
Re_{xcrit}	-	the critical Reynolds number
Re_{Δ}	-	the Reynolds number defined by a thickness of a boundary layer
r_p	-	a particle radius, [m]
S	-	the area of the stripe, [m ²]
S_c	-	the contact area of a particle and surface, [m ²]
S_p	-	the area of the midsection of a particle, [m ²]
S_z	-	the area of the zone of contact, [m ²]
Sc	-	the particle Schmidt number
St	-	the Stokes number
St_{cr}	-	the critical value of the Stokes number
T	-	the temperature of a flow, [°C]
t	-	the time period, [s]
v_t	-	the terminal velocity of a particle, $\left[\frac{\text{m}}{\text{s}} \right]$
U, u	-	the axial component of air velocity, $\left[\frac{\text{m}}{\text{s}} \right]$
U_0	-	the flow velocity at the outer boundary of the laminar boundary layer, $\left[\frac{\text{m}}{\text{s}} \right]$
U_d	-	the axial component of the flow velocity near the centre of a particle, $\left[\frac{\text{m}}{\text{s}} \right]$

U_p	-	the axial component of a particle velocity, $\left[\frac{\text{m}}{\text{s}}\right]$
U_s, u_s	-	the axial component of velocity of the dispersed phase, $\left[\frac{\text{m}}{\text{s}}\right]$
u_*	-	the friction velocity, $\left[\frac{\text{m}}{\text{s}}\right]$
V, v	-	the transversal component of air velocity, $\left[\frac{\text{m}}{\text{s}}\right]$
V_{dep+}	-	the dimensionless deposition velocity
V_s, v_s	-	the transversal component of velocity of the dispersed phase, $\left[\frac{\text{m}}{\text{s}}\right]$
x	-	the distance from the leading edge of the plate, [m]
x_L	-	the coordinate of the cross-section of the conic model, [m]
y	-	the transverse coordinate calculated from the plate surface, [m]

Greek Symbols

α	-	the particles adhesion number defined by the number of particles detached from the surface
β	-	the vertex angle of the conic model, [deg]
β_s	-	the volumetric concentration of the dispersed phase
χ	-	the dynamic friction coefficient
Δ_l	-	the theoretical thickness of the laminar boundary layer defined for the given cross-section of the plate, [m]
ΔM	-	the mass difference, [kg]
δ_p	-	a particle diameter, [μm]
δ_{pmin}	-	the minimum value of the particle size, [μm]
ε	-	the permittivity of medium within a clearance space
ε_0	-	the electric constant, $\left[\frac{\text{C}^2}{\text{N} \cdot \text{m}^2}\right]$
ϕ	-	a characteristic contact angle, [radian]
γ	-	the particles adhesion number defined by the number of particles remained at the surface
γ_u	-	the restitution coefficient
η	-	the self-similar coordinate
λ	-	the interparticle distance, [m]
μ	-	Poisson's ratio

ν	-	the kinematic viscosity of air, $\left[\frac{\text{m}^2}{\text{s}} \right]$
ν_s^1	-	the pseudoviscosity coefficient for the momentum balance in the streamwise direction
ν_s^2	-	the pseudoviscosity coefficient for the momentum balance in the transversal direction
ρ	-	physical density of air, $\left[\frac{\text{kg}}{\text{m}^3} \right]$
ρ_p	-	material density of particles, $\left[\frac{\text{kg}}{\text{m}^3} \right]$
ρ_{pm}	-	the mean particle density, $\left[\frac{\text{kg}}{\text{m}^3} \right]$
ρ_s	-	bulk density of the dispersed phase, $\left[\frac{\text{kg}}{\text{m}^3} \right]$
σ	-	the root-mean-square deviation
σ_s	-	the density of charges of the electric double layer, $\left[\frac{\text{C}}{\text{m}^2} \right]$
τ	-	a representative time of a flow, [s]
τ_a	-	the shear stress of air, $\left[\frac{\text{N}}{\text{m}^2} \right]$
τ_p	-	a particle relaxation time, [s]
τ_{p+}	-	dimensionless particle relaxation time
τ_s	-	the shear stress of the dispersed phase, $\left[\frac{\text{N}}{\text{m}^2} \right]$
τ_w	-	a wall shear stress, $\left[\frac{\text{N}}{\text{m}^2} \right]$
ξ	-	a liquid surface tension, $\left[\frac{\text{N}}{\text{m}} \right]$

Subscripts

m	-	refers to a material properties
p	-	refers to a single particle properties
s	-	refers to the dispersed phase properties
i	-	i^{th} component
j	-	j^{th} component
k	-	k^{th} component
W	-	refers to the properties occurred at a wall
x	-	refers to the streamwise direction
∞	-	refers to the free stream properties

INTRODUCTION

Aerosol gas-solid particles two-phase flows are of high relevance in various natural phenomena, such as sand storms, moving sand dunes, cosmic dusts, snow avalanches, dust explosions and settlements, as well as the sedimentation of dust in atmosphere.

The multiphase and, especially, two-phase aerosol flows are very important in many engineering applications. These flows are specially generated for industrial processes taken place in power engineering, chemical, pharmaceutical, food and other branches of industry.

It should be noted the commercial applications of the aerosol flows, like the removal of harmful solid combustion products from the exhausted gases of power plants, filtration of the production residue and dust separation, that allow to reduce an environmental pollution. Inhalation toxicology and micro-contamination control are also among the areas where the aerosol flows play a critical role.

Another important industrial application of the aerosol flows is the pneumo-conveying. The pneumatic transport is widely used for the transportation of cement, grains and other granular material.

One of the most striking examples of the applying of the aerosol flows is the fluidized bed plants, which are used for the combustion of the fossil fuels in power engineering and for many chemical techniques, e.g. coal gasification, removal of organic, biological and other injurious additives.

The aerosol gas-solid particles flows are applied for the manufacturing of the advanced materials as well as for the material processing. One of the technological areas is the producing of the spray coatings that is applied for the manufacturing of the ultra-fine structured multi-component materials.

The overwhelming majority of the above mentioned natural phenomena and the industrial processes are accompanied by the deposition of solid particles onto various surfaces, among them are earth surface, buildings, the working surfaces of various devices etc.

One of the helpful applications of deposition of solid particles from the aerosol flows and their deposition at the surfaces is the industrial separation of particles of different densities or sizes.

The formation of deposits of the unburned solid fuel components often results in fouling of a boiler furnaces, turbine blades, chimney flues and so on, that leads to a depreciation of performance of power equipment.

Therefore, the understanding of the physical mechanisms that govern the deposition of solid particles at various surfaces is essential for the optimal design of the industrial processes and for the modelling of natural phenomena. In particular, the assessment of the deposition amount of solid particles and their distribution along various surfaces is of great importance in the optimal designing of various apparatuses and devices for the industrial application.

Thus, the problem of the prediction of deposition of solid particles from the aerosol flows remains one of the most actual nowadays.

1. DEPOSITION FROM AEROSOL FLOWS.

1.1. The Definition of Aerosol and the Main Parameters of the Aerosol Flow.

The first definition of the aerosol has been stated by Fuchs (1955). He considered the *aerosol* as a dispersion, consisting of a *fluid medium* (air) and solid/liquid *dispersed phase*. In other words, the aerosol is the assemblage of solid or/and liquid particles suspended in air. There is not so far any common classification generally accepted for the aerosols. One of the most appropriate classifications has been proposed by Fuchs (1955). It is based on the difference that exists between the dispersions containing solid and liquid dispersed phases, as well as the difference of manner of formation of the aerosols.

According to Fuchs (1955), the aerosols are subdivided into the *dispersing* and *condensing*.

The dispersing aerosols are formed as a result of disintegration or atomization of an initial substance with a subsequent transfer into the suspension state. The given aerosols can contain both liquid and solid particles. One of the examples of the dispersing aerosols, containing a liquid dispersed phase, is the one that is generated by the static, air stream or other ways of a liquid atomization. The case of the dispersing aerosol, which contains a solid dispersed phase, is the powder suspension formed by the grinding of an initial substance in the ball crushers.

The condensing aerosols are generated either by the volume condensation of the supersaturated vapours or as a result of the gas chemical changes, which cause the formation of the non-volatile products. The examples of the condensing aerosols are a natural fog and soot.

Generally, the dispersing aerosols contain the particles with the sizes varying from units up to hundreds microns, whereas the condensing aerosols consist of the fine particles with the size less than 1 μm , but sometimes more larger particles can be generated due to coagulation, that, for example, occurs in the clouds. In many case the dispersing aerosols are more polydispersed than the condensing ones, due to the peculiarities of the formation process. The solid particles of the dispersing aerosols are weakly aggregated, and their shape is rather irregular, except for the cases, when the particles are fused due to the engineering process. The solid particles of the condensing aerosols are often aggregated into large formations that consist of a large number of the initial particles of spherical or regular crystal shape.

The distinction of the aerosols containing the solid and liquid particles consists in the fact that the liquid particles have a shape, which is spherical or close to an ellipsoid of revolution (for example, polarization of droplets by an electric field), while the shape of solid particles is either irregular or crystal. The coagulation of the liquid droplets results in formation of droplet of globular or spheroidal shape. In case of solid particles the coagulation can form the aggregates of various shape (from loose spherical to an open-chain).

The subject of inquiry of the given thesis is the dispersing aerosol containing solid particles.

The single aerosol solid particles are characterized by a set of parameters, that defines the behaviour of a particle under the conditions of the aerosol flow. The most significant are the particle size, its shape, the particle material density, as well as the electrical parameters, such as conductivity and electric permittivity. The optical properties of particles, in particular, their optical diffraction, are relevant in case of diagnostics of the aerosol flow by the laser Doppler anemometry.

The *material density* of a particle is the parameter, which conditions its inertia, deposition velocity etc. Here it should distinguish the *real density* of particle, that coincides with the particle material density, and the *apparent density*, which is determined by the loose packing of particles in aggregates. The apparent density can be in order of magnitude less than the real one. One of the kinds of the apparent density is the *bulk density* of powders, which is determined by mass and volume of a powder portion. The ratio between the bulk and the real densities is in the range (0.1...0.7).

Most of aerosols are substantially polydispersed, i.e. they contain particles of a wide range of size. There are no completely monodispersed aerosols. The aerosols are called monodispersed, if the size spread of particles is negligible as compared with the average size.

It is quite enough to know the average particle size for the description of the monodispersed aerosol, while the polydispersed one is described by the *particles size distribution*.

There are several methods of setting of the particles size distribution. The most prevalent is the particle radius distribution. Another way is the particle mass or volume distribution.

The consideration of the aerosol flow needs in the introduction of the certain quantitative parameters that characterize both the gas (air) and the dispersed phases. These are the *physical density of air* ρ ; the *material density of particles* ρ_p ; the *bulk density (or apparent density) of the dispersed phase* ρ_s , i.e. the mass of the dispersed phase per unit volume of a mixture; the *mass concentration of the dispersed phase* C :

$$C = \frac{\rho_s}{\rho} \quad (1.1.1)$$

which is the ratio of the mass of the dispersed phase to that of air in a mixture.

Another important criteria, characterizing the relations between the parameters of air and dispersed phase of an aerosol flow, are the *particle Reynolds number* Re_p , the *Stokes number* St and the *terminal velocity* v_t of a particle.

Re_p is determined according to Schlichting (1974) as follows:

$$Re_p = \frac{|U_p - U| \delta_p}{\nu} \quad (1.1.2)$$

where U_p is the axial component of a particle velocity, U is the axial component of air velocity, δ_p is a particle diameter, ν is the kinematic viscosity of air.

The Stokes number St is determined according to Crowe et al. (1996) as follows:

$$St = \frac{\tau_p}{\tau} \quad (1.1.3)$$

where τ_p is a particle relaxation time, τ is a representative time of a flow. The particle relaxation time τ_p is the time taken by a particle to accelerate from rest to the velocity $(1 - e^{-1})U$. Stokes (1851) have shown for the streamlining of a spherical particle that:

$$\tau_p = \frac{(2\rho_p + \rho)\delta_p^2}{36\rho\nu} \quad (1.1.4)$$

In case of $\rho_p \gg \rho$ this formula transforms as follows:

$$\tau_p = \frac{\rho_p\delta_p^2}{18\rho\nu} \quad (1.1.5)$$

This Stokes streamlining takes place only for the very small values of Re_p , i.e. $Re_p \ll 1$.

The terminal velocity of a particle is the ultimate velocity which a particle achieves in free fall, that is, when the acceleration is zero. For the Stokes streamlining the terminal velocity is as follows:

$$v_t = g\tau_p = \frac{g\rho_p\delta_p^2}{18\rho\nu} \quad (1.1.6)$$

where g is the acceleration due to gravity.

1.2. Deposition of Aerosol Solid Particles at Streamlined Surfaces.

The deposition of solid particles in the aerosol flows has received considerable attention for more than last four decades. Particularly, the problem of the predicting of the deposition amount of the particles suspended in a gas flow was and remains still to be of great interest for the researchers in many countries. The investigations of the particles deposition have undoubtedly been stimulated by its practical relevance to many areas of technology and science, but the interest has also been aroused by the intellectual challenge of the problem and the inability of any theory to provide a truly satisfying physical explanation of the observed facts.

The numerous theoretical and experimental researches are dedicated to the study of sedimentation and deposition of solid particles at various surfaces and the influence of hydrodynamics of the aerosol flows on the peculiarities of these phenomena. But, unfortunately, most of them mainly deal with the theoretical

aspects. The existing experimental ones do not consider the particles deposition as the complex phenomenon, involving various physical processes that occur during the deposition.

The particles sedimentation and deposition at the surfaces can be divided conventionally into two processes: 1) the transport of the particles to a surface till the coming in contact with it and 2) the adherence of the particles with a surface. The first one is determined exclusively by the hydrodynamics of the streamlining of the surface by the aerosol flow without taking into account the effect of change of the surface behaviour due to the particles deposition. The second process is conditioned by the interaction of the particles with the surface and the adhesive contact “surface-particle” at the given environmental conditions.

Let us consider separately the both processes that determine the deposition of the aerosol particles.

1.2.1. Hydrodynamical mechanisms of the particles deposition.

Despite the longstanding use of sedimentation and deposition in practical applications, much remains unknown about the fundamental properties of the sedimenting suspensions, such the mechanisms that stipulate the formation of the particles deposits at various surfaces, and the correlations between the hydrodynamics of the aerosol flows and the deposition amount of the particles.

Extensive experimental and computational studies related to the particle transport in the aerosol flows, which were reported by Hinze (1975), Wood (1981), Papavergos & Hedley (1984), have revealed the presence of the *boundary layer*, which formed close to the surface, streamlined by the flow, and in many respects determined the sedimentation of particles from the flow towards the surface and their deposition immediately at the surface.

The influence of the boundary layer on the particle motion near the streamlined surfaces was mostly studied theoretically by Soo (1967), Stulov (1979), Osyptsov (1980, 1985), Asmolov (1992). The first rough estimations by Fuchs (1989) showed that the influence of the boundary layer should be included in the calculations of the inertial sedimentation of the fine particles. One of the latest reviews of the experimental and theoretical studies of influence of the boundary layer on the particles deposition onto the streamlined surfaces was made by Varaksin (2003).

Osyptsov (1985), neglecting an inertial sedimentation, suggested the transport equations for the motion of fine particles near a body. He showed that the particles accumulated close to a body surface, and even for the insignificant values of the particles mass concentration the velocity and temperature fields of a gas flow were distorted substantially due to the accumulation of the particles near the surface. The generalization of the given results for the compressible gas flow has been made by Osyptsov & Shapiro (1986). The increase of the particles mass concentration in vicinity of the surface of a flat plate in the laminar boundary layer have been also observed by Soo (1967), Asmolov (1992), Osyptsov (1980). As the monodispersed (i.e. of the same size) particles were engaged in these theoretical studies, the models elaborated for the two-phase

laminar boundary layer did not take into account the interparticle collision mechanism and, hence, the mass transfer induced by the diffusion was excluded from the consideration.

Spokoinij & Gorbis (1981) have studied experimentally the aerosol air-solid particles flow in a pipe. They have shown that there was the critical value of the Stokes number St_{cr} , which determined the condition of the particles sedimentation towards the surface of an obstacle installed within the aerosol flow. The sedimentation is absent at the conditions of the isothermal flow if $St \leq St_{cr}$. Here St was determined as follows:

$$St = \frac{\rho_p \delta_p^2 U}{18 \rho \nu D} \quad (1.2.1)$$

where D is a pipe diameter. St_{cr} allows to determine the minimum value of the particle size $\delta_{p\ min}$, that can still deposit at the surface. As St_{cr} is larger for the other equal status, the worse conditions for the deposition take place.

When studying the sedimentation in a suspension flow system (the large monodispersed particles in liquid), Davis & Acrivos (1985) have shown a significant influence of the volume particle concentration on the magnitude of the settling velocity near the surface. They have also examined the structure of the suspension layer, which width was comparable with the length scale of the inter-particle spacing.

In the review of the current state of knowledge of the flow past a flat plate at small Reynolds numbers $Re_\Delta \leq 5000$, where Re_Δ is the Reynolds number determined by a thickness of the boundary layer, Robinson (1991) pointed out on influence of the coherent motions, which occur in the turbulent boundary layers, on a hydrodynamics of a boundary layer and, finally, on the deposition processes on the streamlined surfaces. Such coherent motion was detected by various experimental techniques, such as laser Doppler anemometer (LDA) and the hot-wire anemometer, and with the help of the numerical simulation, namely the large-eddy simulations (LES) and direct numerical simulations (DNS), as well as the conceptual models based on the idealized layer approximation (sublayer, buffer and wake zones). According to Robinson (1991), the open issues still remained for the understanding of the relationship between a vortical structure and an internal shear layer. Among them he listed a correlation between the turbulence production and its dissipation, the passage frequencies, study of effect of the pressure gradient, compressibility, density stratification, wall roughness as well as the dimensionality, unsteadiness, free-stream turbulence for the non-canonical boundary layers etc.

The theoretical description of sedimentation of fine particles on the vertical surface was carried out by Johansen (1991), who disclosed the influence of the gravitational and lift forces along with the electrostatic effects on the particle sedimentation. It was shown that there were different regimes of sedimentation depending on the particle relaxation time. For a short relaxation time, the Brownian sedimentation regime dominates, while the turbulent sedimentation

occurs for the long and medium relaxation times. It was found that for the Brownian diffusion of particles in vicinity of the surface the distribution of concentration had a maximum at the wall and the concentration value decreased with the increasing of the particle relaxation time.

The systematic investigations of influence of the boundary layer on the dynamics, the flow structure and the properties of the inertial sedimentation were carried out by Tsirkunov (1993), who has analysed the influence of the boundary layer on a motion of particles near the streamlined surface and drawn the following conclusions:

- 1) it is necessary to take into account the impact of the boundary layer on the particle trajectories in vicinity of the streamlined surface together with the influence of the viscous drag force and the lift Magnus and Saffman forces;
- 2) it should take into account that inside the boundary layer the particles of different sizes behave in different ways, namely, large particles move through the boundary layer keeping their velocities and direction, whereas fine particles decelerate in the boundary layer and drift along the surface. The density of the particle mass flux in each point at the forehead of the streamlined surface is definitely determined by the trajectories of particles;
- 3) the boundary layer obstructs the particles sedimentation, rejecting the particles out.

The DNS of the particles deposition in the wall-bounded turbulent aerosol flows were performed by McLaughlin (1989) and Ounis et al. (1991). These studies concerned the clarifying of the particle deposition mechanisms. Brooke et al. (1992) performed the detailed DNS studies of the vortical structures in the viscous sublayer. Pedinotti et al. (1992) used the DNS technique to investigate the particle behaviour in the wall region of the turbulent flows. They reported that an initially uniform distribution of particles tended to segregate into the low-speed streaks and resuspension occurred by particles being ejected from the wall. The DNS simulation was used by Soltani & Ahmadi (1995) to study the particle entrainment process in a turbulent channel flow. They found that the wall coherent structure played a dominant role on the particle entrainment process.

Squires & Eaton (1991a) simulated a homogeneous isotropic non-decaying turbulent flow field by imposing an excitation at low wavenumbers, and studied the effects of inertia on the particles dispersion. They also used the DNS procedure to study the preferential micro-concentration structure of particles as a function of the Stokes number in the turbulent near-wall flows (see Squires & Eaton, 1991b). Rashidi et al. (1990) performed the experimental study of the particles turbulence interactions near a wall. They reported that the particles transport was mainly controlled by the turbulent burst phenomena.

Young & Leeming (1997) summarized the results of numerous experimental studies concerning the prediction of the deposition rate of small particles suspended in a turbulent aerosol flow in a pipe (see Figure 1.2.1).

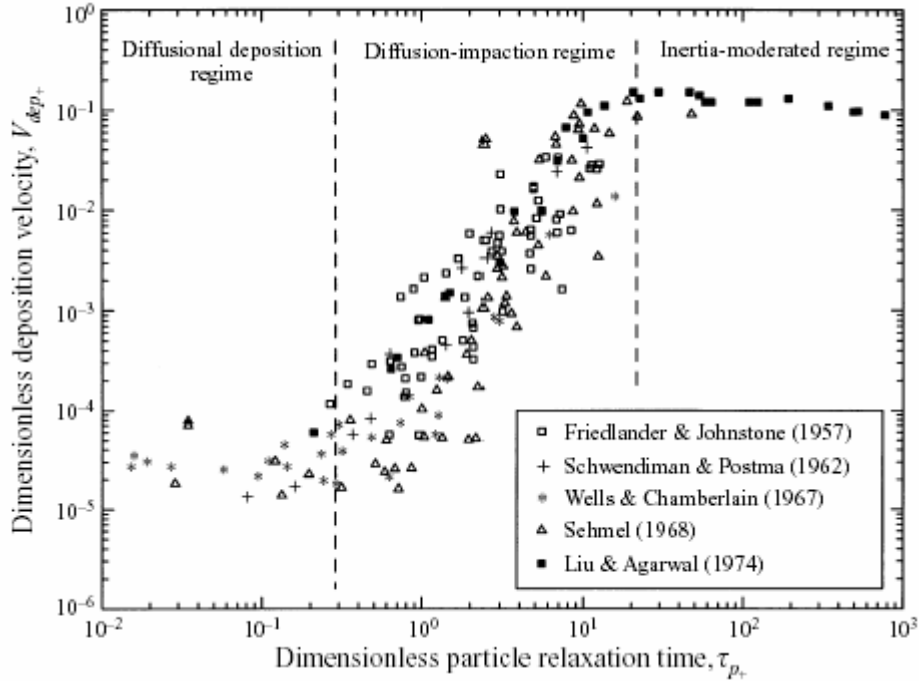


Figure 1.2.1 The particle deposition from fully developed turbulent pipe flow: a summary of the experimental data

Figure 1.2.1 shows the rate of the particle deposition on the wall of a circular pipe as a function of the particle size. Here, the dimensionless deposition velocity V_{dep+} is calculated according to Liu & Agarwal (1974) as follows:

$$V_{dep+} = \frac{J_w}{\rho_{pm} u_*} \quad (1.2.2)$$

where J_w is the mass flux of particles to the wall per unit area, ρ_{pm} is the mean particle density in a pipe, i.e. the mass of particles per unit volume, u_* is the friction velocity ($u_* = \sqrt{\tau_w / \rho}$, where τ_w is the wall shear stress). The dimensionless particle relaxation time τ_{p+} is defined as:

$$\tau_{p+} = \tau_p u_*^2 / \nu \quad (1.2.3)$$

$$\tau_p = \frac{\rho_p \delta_p^2}{18 \rho \nu} \cdot (1 + 2.7 Kn) \quad (1.2.4)$$

where $Kn = l / \delta_p$ is the particle Knudsen number, l is the mean free path of a gas molecule. Here the expression for τ_p derived by Stokes (1851) was modified by the correction factor $(1 + 2.7 Kn)$ entered by Cunningham (1910), which models the deviations from a continuum behaviour when the particle diameter is comparable with the molecular mean free path.

As one can see from Figure 1.2.1, there are nominally three regimes of the particles deposition. In the "diffusional deposition" regime, V_{dep+} is a monotonically decreasing function of τ_{p+} and also depends on the particle Schmidt number, $Sc = \nu / D_p$, D_p is the particle Brownian diffusion coefficient. D_p is assumed to be given by the Einstein equation:

$$D_p = R_p T \tau_p \quad (1.2.5)$$

where T is the temperature (the flow is assumed to be isothermal), $R_p = k / m_p$, (k is Boltzmann's constant and $m_p = \pi \delta_p^3 \rho_p / 6$ is the mass of a particle). In this regime, the particle transport to the wall is well represented by a gradient diffusion model, that is by the turbulent diffusion in the core of the pipe and the Brownian diffusion in a very thin layer directly adjacent to the wall.

In the "diffusion-impaction" regime, a dramatic increase in the deposition rate of several orders of magnitude is observed corresponding to about a fourfold increase in a particle diameter. From the early days, this was recognized as the result of the interaction between the particles having a significant inertia and the fluid turbulent eddies. Starting from the work of Friedlander & Johnstone (1957), a theory, variously referred to as the "free-flight" or "stop-distance" model, was developed over a period of more than twenty years. The essence of the model is that the particles are transported by the gradient diffusion to within one "stop-distance" of the wall where they acquire sufficient inertia to "coast" across the viscous sublayer.

The free-flight model lacks rigour, but it does provide an attractive physical explanation with the exception of one, very serious, shortcoming. In order to obtain agreement with experiment, it is necessary to assume that the particles acquire a velocity towards the wall at the stop distance approximately equalled to the friction velocity u_* . However, at these locations of between about 1 and 10 wall units from the surface (one wall unit corresponds to a distance equalled ν / u_*), the root mean square (r.m.s.) fluctuating velocity of gas is very much less than u_* , and it has never been satisfactorily explained how the particles acquire the necessary wallwards momentum from the prevailing low level of turbulence. Indeed, a more formally correct interpretation of the free-flight model made by Davies (1966) has predicted the deposition rates some two orders of magnitude less than those observed experimentally.

The third region is known as the "inertia-moderated" regime. Here, the gradient diffusion is assumed to play little or no part, the very massive particles acquiring sufficient momentum from the large eddies in the turbulent core to reach the wall directly. The reduction in the deposition rate with increasing of the particle size is explained by the fact that the increasing of the particle inertia results in a decreasing response to the turbulence.

A sublayer models for the particles resuspension and deposition in the turbulent aerosol flows were proposed by Cleaver & Yates (1973, 1975, 1976), Fichman et al. (1988) and Fan & Ahmadi (1993). In the last work, the effect of a

wall roughness was included, and an empirical equation for the particle deposition rate was proposed.

Zaichik & Alipchenkov (2001) developed the statistical model for the prediction of transport and deposition of high-inertia colliding particles (massive droplets) in the vertical pipe turbulent air flow. On the basis of analysis of the obtained results the authors drew the next conclusions: 1) the elastic collisions increase the deposition rate, while the inelastic collisions may result in a deposition decrease; 2) the decrease in the particle turbulence through the inelastic particle-particle collisions is not of great importance.

Shams et al. (2000) used a Lagrangian simulation of transport and deposition of aerosol nano- and micro-particles (from 10 nm to 50 μm) including a Brownian motion effects in the sublayer of the turbulent boundary layer flow in the vertical and horizontal ducts. They extended the sublayer model for the turbulent deposition process to cover the effects of gravity, Brownian and lift forces. The given model was based on the detailed analysis of the particle trajectories in the turbulence coherent structures near a wall. The Stokes drag, the Saffman lift and the Brownian excitation were included in the particle equation of motion. On the basis of the results by Shams et al. (2000) one can draw some important conclusions: 1) the coherent near-wall eddies of the turbulent boundary layer flows play an important role in the particle deposition process; 2) the applying of the sublayer model for the evaluating of the particle deposition is a reasonable approach.

Zhang & Ahmadi (2000) studied the aerosol deposition from the turbulent air streams in the vertical and horizontal ducts. It was revealed that the particle-to-fluid density ratio, the shear-induced lift force, the flow direction and the shear velocity affect the particle deposition rate. For both vertical and horizontal ducts, the DNS results showed that the effect of gravity and its direction on the particle deposition rate became more significant at low shear velocities.

In the work by Zhang et al. (2000) the motion and deposition of the ellipsoidal particles of a wide range of size in turbulent air flows were theoretically investigated. It was shown that the deposition velocity followed a V-shape variation with the particle relaxation time, i.e. the particle size. The authors also obtained that the character of distributions of the particle concentration near the wall (normal and parallel to the wall) was different for different particle sizes. The particles of the intermediate size accumulated in the vicinity of the wall in contrast to the small and large ones. As to the longitudinal distribution, the intermediate particles tended to accumulate in the low-speed streaks of the turbulent boundary layer flow.

Wang & Levy (2003) experimentally obtained the velocity and concentration profiles for the 60 μm coal particles within the turbulent boundary layer on a vertical flat plate. These profiles were appreciably non-uniform and had the peak values in the outer region of the boundary layer, that was attributed to the transverse lift force and the particle-wall interactions in the boundary layer, as well as the occurrence of the vortical structures and the associated coherent

motions throughout the boundary layer, not only in the wall region, but also in the outer region of the boundary layer.

Marchioli & Soldati (2002), Botto et al. (2003), Marchioli et al. (2003) using DNS for the study of the particles deposition in a fully developed turbulent open channel flow have also revealed the strong accumulation of the particles very close to the wall in the form of the streamwise oriented streaks. They attributed this phenomenon to the effect of turbophoresis, which is caused by a gradient in the particles velocity fluctuations, associated with a gradient turbulence intensity of the gas flow.

Thus, based on the reviewed studies, one can distinguish the next mechanisms of the particles transport to the surface, that take place in the isothermal aerosol flows:

- the diffusion;
- the convective;
- the inertial.

The transport of the particles in the non-gradient laminar flows is realized only by the Brownian diffusion.

In case of the gradient flows, when the particle material density approximately equals to the gas physical density, the convective transport of the particles solely determines sedimentation and deposition of the particles.

When the particle material density is much more than the gas physical density, i.e. $(\rho_p / \rho) \rightarrow \infty$, that implies the particles to be highly massive, the particles are not entrained by the gradient flow, but continue coasting at the constant velocity and direction, and the sedimentation is carried out exclusively by the inertial mechanism.

Actually, the motion of the aerosol particles close to the surface is conditioned by the interaction of all the above mentioned mechanisms, but in every specific case, depending on the relation between the local parameters of a flow, one mechanism predominates.

1.2.2. *The particles adhesion.*

Along with purely hydrodynamics of the aerosol flows, there are another mechanisms, which stipulate the particles deposition at the streamlined surface.

When delivered to the streamlined surface and touched it, a particle can be 1) entrained by a surface and further adheres to it, 2) rebounds, and then it is reentrained by the gas flow or 3) damages a surface.

The adherence of the particles takes place under the condition of a prevailing of the surface attractive forces over the elastic repulsion forces. The adhesion phenomenon is complex in itself, and it depends on the overall effect of such factors, as the conditions of a particle-surface interaction, the properties of a particle and a surface (particle size and shape, surface roughness), electric charge of particle and a surface, as well as the ambient conditions (humidity, temperature, chemistry). All these factors in whole determine the phenomenon called *adhesion* of the particles with each other or with a surface. The measure of adhesion is *the adhesive force*.

Zimon (1976) has expounded the fundamentals of adhesion and reviewed the results of numerous theoretical and experimental investigations concerning the mechanisms of adherence of the particles to a surface.

According to Zimon (1976), when the single particles are brought into contact with a homogeneous surface, the occurred adhesive forces effected on each particle are the different. This is due to the specific conditions of contact of the single particle. Therefore, when the same *detaching force* impacts on all the adhered particles, some portion of particles remain on a surface. The ratio between the number of particles N remained at the surface after the effect of the detaching force F_{det} and the number of particles N_0 initially adhered to a surface is assigned as the particles *adhesion number* $\gamma(F_{det})$, which is as follows:

$$\gamma(F_{det}) = \frac{N}{N_0} 100\% \quad (1.2.6)$$

The adhesion of particles with a surface can be also characterized by the ratio $\alpha(F_{det})$ between the number of particles N_{det} detached from a surface by the force F_{det} and the initial number of particles N_0 :

$$\alpha(F_{det}) = \frac{N_{det}}{N_0} 100\% = 1 - \gamma(F_{det}) \quad (1.2.7)$$

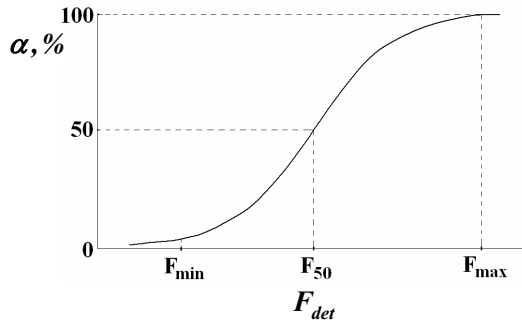


Figure 1.2.2 The adhesion number vs. the detaching force

Generally, the dependence of the adhesion number on the detaching force for the given pair “particle-surface” looks like Figure 1.2.2 shows, i.e. the detaching of particles from a surface is the probabilistic process. Here $F_{det} = F_{50}$ is the detaching force that provides the detaching of 50% of all adhered particles.

Since at the time of the detaching the adhesive force is numerically equal and oppositely directed to the detaching force, the dependences $\gamma(F_{det})$ and $\alpha(F_{det})$ can be considered as the dependences of the adhesion number on the adhesive force for the given detaching force, i.e. $\gamma(F_A)$ and $\alpha(F_A)$. If the data concerning the adhesive force distribution of the particles is presented in the probability-logarithmic coordinate system, where $\lg F_A$ is along the abscissa axis and the probability of the given adhesive force α is along the ordinate axis, the distribution looks like a straight line. This means that the adhesive force distribution of the particles obeys the normal-logarithmic law. Thus, the adhesive properties of the pair “particle-surface” are characterized by two constants a and b of the equation of line $\alpha(F_A) = a + b \lg F_A$. The inclination

of line determined by the coefficient b determines the root-mean-square deviation of the adhesive force distribution.

Generally, according to Zimon (1976), the adhesive force is the totality of the forces (components of the adhesive force) that differ in nature, namely the molecular force, the image force, the Coulomb force and the capillary force.

The molecular force. The molecular force F_M acts before the direct contact of a particle with a surface. It is determined by the geometry of the contacting bodies and the properties of air. For the spherical particles this force is calculated as follows:

$$F_M = \frac{A r_p}{6H^2} \quad (1.2.8)$$

Here A is the constant of the molecular interaction (the constant of van der Waals), H is the distance between molecules, r_p is a particle radius.

The image force. The image force F_{im} acts during the contact of a particle with a surface, and it emerges from the contact potential difference as follows:

$$F_{im} = 2\pi\sigma_s^2 S_c \quad (1.2.9)$$

Here $\sigma_s = \frac{q_p}{S_c}$ is the density of charges of the electric double layer, which is formed in the contact zone, and q_p is the particle charge. The contact area of a particle and a surface S_c is determined by Hertz' formula:

$$S_c = \pi(0.75rF_{press}(k_1 + k_2))^{2/3} \quad (1.2.10)$$

where F_{press} is the pressing force, $k_i = \frac{1-\mu_i}{E_i}$, $i=1, 2$, μ_1, μ_2 are Poisson's ratios and E_1, E_2 are Young's modules for materials of a particle and a surface, respectively.

The effect of the electrostatic charge is often important in the powder handling processes, particularly in pneumatic conveying. During the powder handling operations, particles make frequent contacts with a surface of a wall and invariably become electrically charged due to the process of the contact electrification. The materials of pipe, ranging from conductor to insulator, play a crucial role in the charge transfer process. The electrostatic charge may, in some cases, alter the dynamics of the transport process of solid particles. Many studies have shown that the electrostatic charges might cause a significant increase of a pressure drop in the transport line (see, for example, Richardson & McLeman, 1960). Normally, the larger electrostatic charge per particle is expected with the smaller particles (Marcus et al., 1990). However, Bowling (1986) considered the electrostatic factor as the predominant one only for the particles with a diameter larger than 50 μm . He suggested that with the suspensions of very fine particles, the entire inside surface of the pipe might have been coated with a layer of the solids, so that the column wall had identical surface properties to the flowing particles, and therefore the charge transfer was attenuated. The presence of

moisture in the clearance between the contacting surfaces suppresses an electric force.

The Coulomb force. The Coulomb force F_C becomes to be significant for the preliminary charged particles. The necessary condition for this force is a clearance space taken place between a particle and a surface during the initial time of contact. The Coulomb force is calculated as follows:

$$F_C = \frac{q_p q_{sur}}{4\pi\epsilon_0\epsilon R^2} \quad (1.2.11)$$

where q_p and q_{sur} are the electric charges of a particle and a surface, respectively; ϵ is the permittivity of medium within a clearance space; ϵ_0 is the electric constant, $\epsilon_0 = 8.85 \cdot 10^{-12}$, $C^2/N \cdot m^2$; R is a distance between a particle and a surface.

The capillary force. The capillary force F_{cap} originates from a liquid meniscus taken place within a clearance space between a particle and a surface and appears after an attaching of a particle at the surface. The expression of the capillary force for a spherical particle of radius r_p looks as follows:

$$F_{cap} = 4\pi r_p \xi \cos(\phi) \quad (1.2.12)$$

where ξ is a liquid surface tension, ϕ is a characteristic contact angle, i.e. the angle at which the meniscus contacts the surface.

During the process of adhesion, the ratio between the above mentioned forces changes. For example, before the contact, the Coulomb and the molecular forces are considerable, but during the contact, the molecular, electric and capillary forces are most prevailing.

It is known that when even absolutely identical particles contact with a uniform surface, the adhesive forces differ in quantity, i.e. the scatter of the forces takes place. There are several reasons of this scatter: an energy inhomogeneity of a surface, an inequality of the initial charges of the particles, as well as an indeterminacy of a contact area.

The dependence of the adhesive force on a particle size is one of the main questions in the theory of adhesion. At the same time, the available results on this issue are the most discrepant. This is caused by the scatter of the adhesive forces occurred for the particles of the same size. There is no unique dependence of the total adhesive force on the particles size, since the components of the adhesive force depend on a particle size in different ways.

According to Zimon (1976), the adhesive force strongly depends on the surface roughness, since the roughness changes the contact area of particle with a surface. Depending on the ratio between the sizes of particle and the roughness protuberances, the adhesive force may increase or decrease.

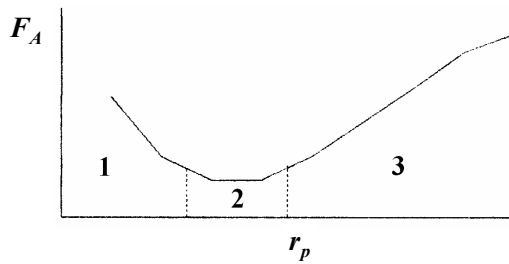


Figure 1.2.3 The adhesive force vs. the particle radius in case of a rough surface

The second case (region 2) realizes when the particle radius and size of the protuberances of the mechanical roughness are comparable. In the third case (region 3) the particle is much larger than the protuberances of the mechanical roughness, and the adhesive force grows with the increasing of the particle size. The second case is the most practicable.

Figure 1.2.4 shows the dependencies of the adhesive force on the particle size. Curve 1 corresponds to the spherical particles, while curve 2 corresponds to the particles of an irregular shape. In general, the adhesive force acted on the particles of an irregular shape is larger than for the spherical particles (Zimon, 1976).

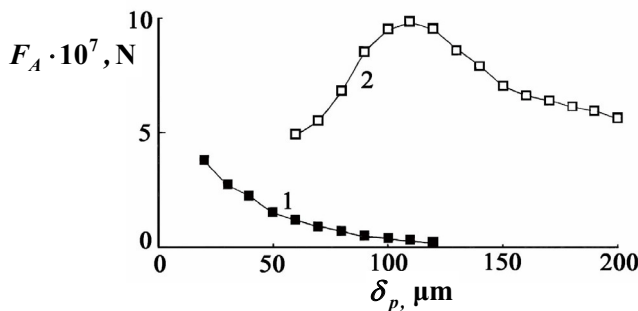


Figure 1.2.4 The adhesive force vs. the particle size for various shapes of particles

The adhesive force for a particle occurred on a clean surface or on a surface along with a layer of the precipitated particles influences on the deposition or on the further deposition of the particles. In the survey by Corn (1961) it has been shown that the adhesive forces are either electrical or

liquid in the origin. The electrical forces include those due to the contact potential difference and due to the dipole effect (Penny & Klingler, 1962; Niedra & Penny, 1965) and the space charges (Kottler et al. 1968).

In the adhesion of an individual particle to a particle from the multilayers adhering to a substrate, a space charge effect exists between the individual particles giving a force equalled $(q_p E_e)$, where E_e is the electric field. In the particles multilayers, the inter-particle distance is large compared to the particle diameter and there is a force due to repulsion of such charges. Krupp (1967) has measured the adhesive force acted between the 5 and 30 μm polymer particles and a layer of amorphous selenium by the centrifuging after a contact time of 1 hour. The charges obtained triboelectrically were $(3 \cdot 10^4 \dots 4 \cdot 10^5) e$ per particle,

where e was the electron charge. The forces for both multilayers and selenium surfaces were measured.

The phenomenon of adhesion of the particles to a surface is the stochastic process influenced by many factors. Löffler & Muhr (1972) were the first who reported that the sticking probability of 2.8 μm quartz particles on the polyamide and glass fibers of 19 μm diameter decreased with a particle velocity. The experimental data of the sticking probability P_{st} , presented by Löffler (1977) and shown in Figure 1.2.5, were obtained for the quartz and glass particles with the sizes of 5 and 10 μm on 20 μm polyamide and glass fibers.

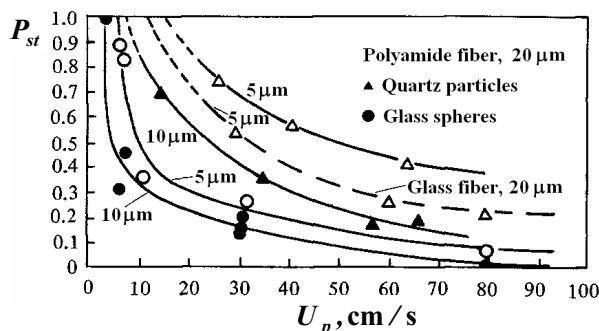


Figure 1.2.5 The sticking probability of the quartz particles and glass spheres on 20 μm fibers of polyamide and glass as a function of the particles velocity

One can see that the rebounding starts at about (5...15) cm/s. As the particles velocity increases, P_{st} is also less for 10 μm than for 5 μm particles.

1.2.3. The particles detachment.

When the aerosol flow velocity is sufficiently high, the deposited particles can be *detached* from a surface and *reentrained* by a flow, i.e. the *resuspension* of the particles takes place. This phenomenon is the essential part of the total deposition process and it should be taken into account for the estimating of the quantity of the deposited particles.

The reentrainment of fine particles from the surfaces in the aerosol flows has been the focus of numerous theoretical (Cleave & Yates, 1973; Reeks & Hall, 2001; Wen & Kasper, 1989; Soltani & Ahmadi, 1994; Vainstein et al., 1997; Lazaridis et al., 1998) and experimental (Wen & Kasper, 1989; Taheri & Bragg, 1992; Braaten et al., 1993; Phares et al., 2000; Ibrahim et al., 2003) investigations, but the mechanism of a particle detachment remains still unclear. Both the normal lift forces (Cleave & Yates, 1973; Reeks & Hall, 2001; Wen & Kasper, 1989; Lazaridis et al., 1998) and the tangential shear forces (Soltani & Ahmadi, 1994; Vainstein et al., 1997; Braaten et al., 1993; Ingham & Yan, 1994) have been proposed as the impetus for the resuspension. Efforts to resolve the controversy have been hindered by the variability of the properties of the particles on the surfaces that leads to ambiguous experimental observations. Only by studying the reentrainment of particles of the uniform properties, e.g. shape, size, the mechanical properties, from a well-characterized surface and with known interaction potentials these questions can be resolved. The experimental investigations to date have involved a relatively broad distribution of particle-surface interactions and that the flows have been highly turbulent,

theorists have developed statistical models aimed at predicting the probability of particle resuspension upon exposure to a series of random turbulent impulses. Although such models can be empirically related to the observed resuspension rates in turbulent flows, neither the previous experiments nor the models are well suited to resolving the mechanics of flow-induced particle detachment.

Few experimental studies have observed and reported the actual mode of detachment. Masironi & Fish (1964) observed the combinations of lift-off and motion along the surface (i.e., rolling and/or sliding). Similarly, few experimental studies mention the repeatability of their detachment/resuspension data. Wu et al. (1992) and Braaten et al. (1990) have found large changes in resuspension for the experimental runs repeated under the same conditions. Smedley et al. (1999) have achieved small variability in their particles removal experiments by careful surface preparation.

Extensive reviews devoted to the particles resuspension have been made by Bowling (1986), Ranade (1987) and Ziskind et al. (1995). However, few experiments have investigated systematically the effects of a microparticle size, shape, material and humidity, and few investigators have reported directly observed modes of resuspension or the repeatability of their results. Phares et al. (2000) have studied experimentally the aerodynamic reentrainment of the monodisperse spheres from the glass substrates. It was found that the threshold (critical) flow velocity, at which the detachment took place, was more sensitive to the particle size than predicted by the existing resuspension theories, which were based on the equilibrium adhesion models. Furthermore, the resuspension was also found to be sensitive to the duration of the applied shear stress. This sensitivity depends upon the particle size and material properties.

The resuspension rate is reduced at high relative ambient humidity. This is because of the adsorption of water vapor at the particle-surface interface and its effects on adhesion. Corn (1961) has found almost no change in the adhesive forces with relative humidity up to 30% and a rapid increase thereafter. Despite the large dependence of the resuspension on relative humidity, many experiments do not report the value of the relative humidity. Many studies were made on different days at different relative humidity, which further added to uncertainty in the results.

The effects of a surface roughness on the resuspension also must be considered since the actual surfaces are rough. Roughness of the order of the atomic scale always is present, even for nominally "smooth" surfaces. Soltani (1993) has shown for the hard elastic materials that a surface roughness of the order of the atomic scale could reduce adhesion significantly. According to the results of Cheng et al. (2002) a standard deviation of heights of 17 \AA can cause the detaching force to be reduced to 1% of its smooth-surface value.

The particle-particle collisions have a significant effect on resuspension. Once a few particles are detached, they move along the surface and impact other particles. This process supplies enough momentum to the stationary particles to overcome their adhesion with the substrate, and they detach and may resuspend into the flow. Fairchild & Tillery (1982) have found that the saltation of the

200 μm diameter particles increased the maximum vertical particle flux by two orders of magnitude. Theerachaisupakij et al. (2003) have shown that the wall collision of an aerosol particle larger than several micrometers played an important role in the reentrainment, whereas, the effect of the aerodynamic drag dominated for the sub-micron particles.

The experimental study by Ibrahim et al. (2003) of detachment of fine solid particles of different sizes, materials and shapes has revealed that the given process was governed by a balance of the moments of aerodynamic drag and rough-surface detaching forces.

Reeks & Hall (2001) experimentally investigated the adhesion mechanism of the 10 and 20 μm alumina spheres and (6...20) μm graphite particles on a polished stainless-steel substrate by the centrifugal technique. They obtained the log-normal distribution of the adhesive forces. The detaching force tangential to the surface (tangential adhesive force) was about 1/100th of the normal detaching force. This latter result has the important implications for the way the particles are resuspended from the surfaces and highlights the dominance of the drag force over the lift force even though both forces are of similar magnitude for the considered particles.

Many theoretical investigations of the particles reentrainment applied the concept of the turbulent bursts to explain the detachment and reentrainment of the particles. A number of investigators (e.g., Kline et al., 1967 and Robinson, 1991) have studied the turbulent-burst phenomenon. Yung et al. (1989) applied a flow visualization in the turbulent flow of water to examine the interaction between the turbulent burst-sweep events and fine particles completely embedded within the viscous sublayer, which was generated close to the streamlined surface. These results suggested that, in general, the turbulent burst-sweep events were insignificant in the reentrainment process, although some of the particles were reentrained by such events.

Numerous investigations dealt with the reentrainment of a single particle preliminarily adhering to a wall. However, the research of the reentrainment should not be restricted to a single particle. In fact, fine particles in the aerosol flow easily form aggregates or a particle deposition layer. Kousaka et al. (1980) observed the breaking of the interparticle bonds when the soft aggregates adhering to a surface were reentrained. They analyzed the critical condition for the reentrainment using the tensile strength derived by Rumpf (1970). Adhiwidjaja et al. (2000) have presented the model for the reentrainment of a small aggregate with the breaking particle-wall interactions.

In the aerosol flow, a particle deposition layer is formed below a certain critical value of a flow velocity. Above this critical value, the particles layers are formed as a result of the simultaneous deposition and reentrainment processes (see, e.g., Adhiwidjaja et al., 2000 and Theerachaisupakij et al., 2001). When the particles deposition and reentrainment are in equilibrium, the state of the deposition layer is controlled by the balance of the moments of forces (Adhiwidjaja et al., 2000). As the flow velocity is increased gradually, the amount of the deposited particles decreases, and the particles deposition layer

changes into small aggregates. According to Matsusaka et al. (2001), if all the aggregates are reentrained, the deposition layer will be completely removed.

1.3. The Statement of Problem for the Investigation.

As the results of numerous experimental and theoretical investigations of solid particles deposition on various surfaces show, this physical process is rather complicated, and its consideration requires to take into account the effect of various factors.

In spite of the great efforts made for a better understanding of the particles deposition on various surfaces streamlined by the aerosol flows, many things are still incomprehensible. In particular, there is a lack of clear and logical theoretical description for the experimentally measured features of the distribution of the particle concentration within the boundary layer near the bodies. This also concerns the theoretical simulation of the deposition processes on the streamlined surfaces as well as the adhesion mechanism of the deposits formation. All this does not allow to develop the robust analysis methods for various processes and devices that concern the flow past various bodies by the aerosol flows. Despite numerous investigations concerning solid particles deposition on the surfaces have been carried out, up to now there are no reliable methods of assessment even of the total amount of the deposited particles, not to mention the distribution of the deposits along a surface, which is necessary for the design of sufficiently effective methods of the deposits protection for various surfaces.

Thus, the full-scale experimental and theoretical studies of the deposition of solid particles on a surface streamlined by an aerosol flow and the elaboration of the method of assessment for the particles deposition are of great practical interest and importance.

1.3.1. Goal and objectives.

The main goal of the study is the comprehensive investigation of the deposition of solid particles from the aerosol flow at a surface. It is necessary to consider the particles deposition as the complex phenomenon with taking into account both the hydrodynamics of streamlining of the surfaces and the processes that determine the adhesion of the particles to the surfaces for the wide-ranging properties of the air-solid particles aerosol flow, such as:

- the flow velocity,
- the size of solid particles,
- the particles mass concentration of the aerosol flow,
- the adhesive properties of the particles and the surface.

There are the following main objectives to accomplish this goal:

- The strategy generation for the experimental and theoretical investigations for the particles deposition.
- The development and building-up of the experimental set-ups, which would enable to investigate various mechanisms of the deposition.

- The elaboration of the measurement procedures which would allow to obtain the reliable relevant data.
- The elaboration of the mathematical model which adequately describes the behaviour of the particles close to the streamlined surface.

1.3.2. The concept for the investigations of deposition of the aerosol particles.

Summarizing the results of the above reviewed investigations one can distinguish the next stages in the particles deposition for the aerosol flow at various surfaces:

- 1) the transfer of particles towards a surface till the time of a contact occurrence;
- 2) the adhesion of the particles to the surface.

The first stage is determined only by the hydrodynamics of the streamlining of a surface under the condition of absence of effect, caused by the changing of the surface properties due to the deposited particles.

The second stage is conditioned by the mechanism of the particle-surface interaction and the adhesive properties of the pair “particle-surface” for the given ambient conditions.

Thus, the general problem of assessment of deposition of the particles at a surface can be subdivided into two corresponding subproblems.

The first subproblem, called the hydrodynamical, concerns the influence of the boundary layer on the process of deposition on a surface. The solution of this subproblem enables to determine the dynamical properties of the particles and air close to a surface, namely the velocity and concentration of the particles.

The second subproblem involves the interactions between the particles and a surface. Solving this subproblem one can determine the quantity of the deposited particles. This subproblem can be solved based on the known adhesive properties of the pair “particle-surface”.

Therefore, for the elaboration of the reliable method of assessment of the amount of the deposited particles, it is necessary to conduct the experimental and theoretical investigations in the following directions:

- 1) the behaviour of the aerosol particles in the laminar boundary layer formed near the streamlined surface;
- 2) the adhesive properties of the pair “particle-surface”.

2. THE INFLUENCE OF PARAMETERS OF THE AEROSOL FLOW ON DEPOSITION OF SOLID PARTICLES AT FLAT SURFACE.

2.1. Experimental Set-Up.

The experiments were carried out in a disconnected vertical two-phase wind-channel with an open working space (Figure 2.1.1), which was described in detail in Articles I, II and III.

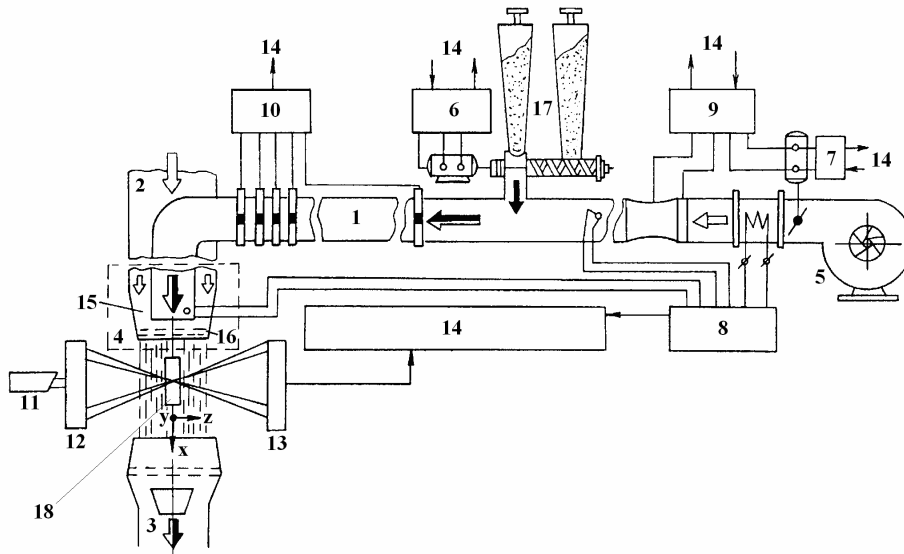


Figure 2.1.1 Experimental set-up: 1 – main channel; 2 – channel of cocurrent pure air flux; 3 – dust suck-out channel; 4 – outlet; 5 – blower; 6, 17 – particle screw feeder; 7 – air flow governor; 8 – thermocontroller; 9 – flowmeter; 10 – pressure converter; 11 – He-Ne laser; 12 – transmitting optics; 13 – receiving optics; 14 – registering, processing and controlling system; 15 – confuser; 16 – system of grates; 18 – model

The experimental set-up consisted of the following parts: main channel (Pos. 1) intended for the formation of the two-phase flow; a channel of cocurrent pure air flow (Pos. 2); the inlet (Pos. 4) for the formation of a flow field having the given parameters in the working space of the wind-channel; the dust suck-out channel (Pos. 3). Besides, the experimental set-up contained various power (Pos. 5, 17), processing (Pos. 6, 7, 8), controlling (Pos. 9, 10) and measuring (Pos. 11, 12, 13, 14) equipment, which provided the formation and transport of the aerosol two-phase flow with the given parameters.

The wind-channel started functioning by the injecting of the dispersed phase into the open working space of the wind-channel with its following ejection through the confuser (Pos. 15). The two-phase flow was formed by the outlet (Pos. 4) consisted of a cylindrical tube with a diameter of 100 mm and a length of 3 m, which was installed along the axis of the forming device for the input of the two-phase admixture. After the exit from the cylindrical tube and passing

through the system of grates (Pos. 16), the formed two-phase flow expanded and entered the open working space supported by the cocurrent flow of pure air on either side. Three grates with the mesh sizes of 0.63, 0.315 and 0.315 mm and with the distance of 12 mm between them were used for the smoothing of the parameters of the inflow. The uniformity of the aerosol flow having the given parameters in the test section of the wind-channel was obtained by the varying of the pure air flow in the main channel, in the channel of cocurrent air flux and also in the dust suck-out channel. The temperature of the aerosol flow in the test section was kept constant by the thermocontroller and equalled $(20\dots21)^{\circ}\text{C}$ that corresponded to the air density $\rho_{\infty}=1.2\text{ kg/m}^3$ and the kinematic viscosity of air $\nu=1.5\cdot 10^{-5}\text{ m}^2/\text{s}$.

The distributions of the local averaged parameters (axial velocity and particle mass concentration) of the aerosol flow in the vicinity of a flat plate were measured with the help of the forward-scatter laser Doppler anemometer (LDA) and laser concentration measurer (LCM) (Pos. 11, 12, 13, Figure 2.1.1), which optical arrangements were specially designed for the given investigations in the Laboratory of Energy Processes Diagnostics of Estonian Energy Research Institute and described in detail in Articles I and II. The optical parts of LDA and LCM have been installed on a special coordinate device controlled by PC. This allowed scanning of the flow continuously or discretely in any given direction with an accuracy of 0.1 mm. The optical system included a 50 mW helium-neon laser of 0.6328 μm wavelength. The LDA receiving optics contained two channels: one has been tuned for the registering of signals from small electrocorundum particles that traced air, and the second one was intended for the measuring of the dispersed phase. Each channel consisted of the receiving optics, the fiber cable, the photomultiplier (PM) and a special counter processor. The tuning of the channels was based on the amplitude discrimination of the Doppler signals. The channel of the dispersed phase has been tuned for registering signals only from the particles of this phase by selecting the geometry of reception and sensitivity of PM. The particle mass concentration was obtained by the measurements of the light intensity of the beam scattered at some angle and an attenuated direct beam in the optical heterogeneous medium.

2.2. Experimental Conditions.

Flow. The model of the flat surface was streamlined by the fully uniform vertical downward aerosol flow which had the given parameters. The parameters of the aerosol flow in the test section of the wind-channel (the mean axial velocity of air in the free stream U_{∞} , the mean particle size δ_p and the bulk density of the dispersed phase in the free stream ρ_{sco}) were chosen based on the condition of the generating of the steady-state two-phase laminar boundary layer near the flat surface, the uniform feeding of the dispersed phase into the test section as well as the eliminating of influence of the dispersed phase on the air flow (the condition of $\rho_{sco} \ll 1$).

The mean axial flow velocity in the free stream U_∞ was 1.5 and 3 m/s.

The mean bulk density of the dispersed phase $\rho_{s\infty}$ in the aerosol flow was 0.01 kg/m^3 .

Figure 2.2.1 shows the distributions of the mean axial air velocity and the relative mass concentration of the dispersed phase for the particles $\delta_p=23 \mu\text{m}$ in the test section of the wind-channel measured by LDA and LCM at the location 200 mm from the exit section of the outlet (Pos. 4, Figure 2.1.1). Here C is the current value of the particle mass concentration, $C_\infty = \rho_{s\infty} / \rho_\infty$ is the particle mass concentration at the flow axis, y is the transversal coordinate. It is clear from Figure 2.2.1 that the flow field in the test section was sufficiently uniform. The diameter of the uniform aerosol flow in the test section was (150...180) mm depending on the mean flow velocity.

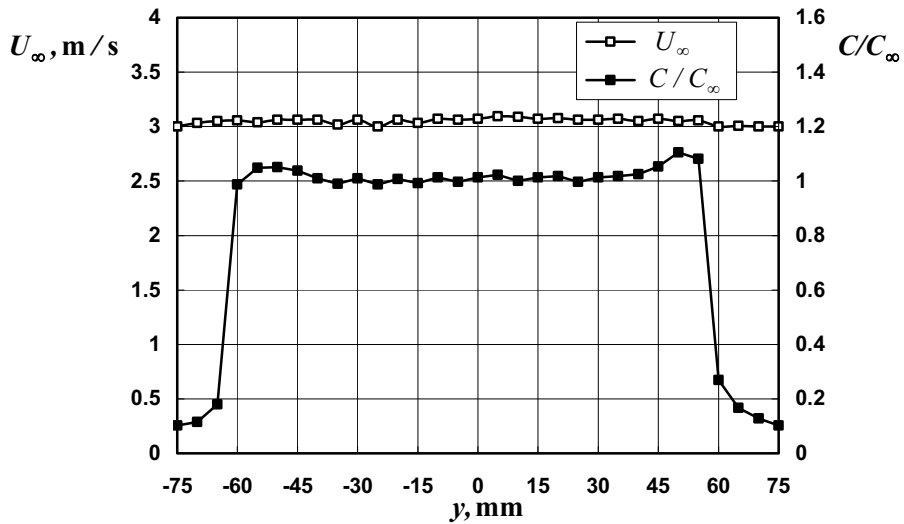


Figure 2.2.1 The cross distributions of the mean axial velocity of air and mass concentration of the dispersed phase in the test section of the wind-channel; $\delta_p=23 \mu\text{m}$

Particles. The manufactured abrasive electrocorundum Al_2O_3 powders ($\rho_p=3950 \text{ kg/m}^3$, Young's modulus of elasticity $E_p=7 \cdot 10^{11} \text{ N/m}^2$, Poisson's ratio $\mu_p=0.3$) with the particle mass mean sizes $\delta_p=12 \mu\text{m}$, $23 \mu\text{m}$ and $32 \mu\text{m}$ were used in the experiments as the dispersed phase of the aerosol flow. The material of particles and their size were chosen based on the Stokes criterion, i.e. the particles should meet the condition $Re_p \ll 1$ (Schlichting, 1974). According to the given criterion the particles had to be sufficiently low-inertia.

A large number of natural and manufactured dispersed abrasive materials have a granulous form and a high polydispersity, i.e. they contain particles with different sizes (the so-called fractions). Since the physical properties of the

dispersed systems depend significantly on the fractional composition of the powders, it is necessary to know the particle size distributions, and thus the analysis of a granulometric composition of the applied powders was made beforehand. Figure 2.2.2 shows the results of the given analysis.

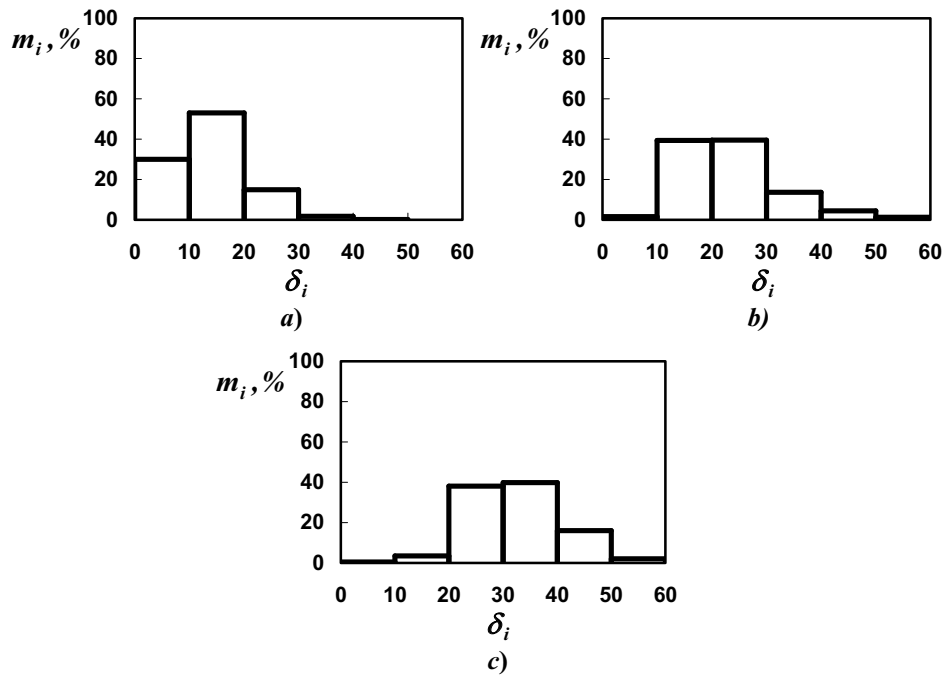


Figure 2.2.2 The mass distributions of the particles sizes for the applied powders:
 a) $\delta_p = 12 \mu\text{m}$, b) $\delta_p = 23 \mu\text{m}$, c) $\delta_p = 32 \mu\text{m}$

Here the upper and lower limits δ_i of the fractions size are on the abscissa axis, the mass percentage content of the given fraction m_i is on the ordinate axis. The root-mean-square deviation of the particles size σ was less than $(0.3\delta_p)$.

Model. A stainless steel flat plate was used as the model for investigations (Figure 2.2.3). The choice of a flat plate was based on a simplicity of its surface shape, and that the hydrodynamic characteristics of the boundary layer, which was generated near the flat surface in case of the pure air flow (i.e. without solid particles in it), had been already well studied.

The flat plate had the following dimensions: 0.5 m length, 0.1 m width, 0.002 m thickness. The quality of the surface treatment was characterised by the average roughness height which was about $6.3 \mu\text{m}$.

The model was installed into the test section of the wind-channel (Figure 2.1.1) with the help of the specially designed holder under the zero incidence.

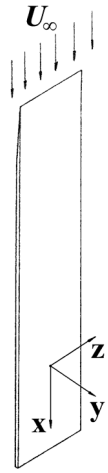


Figure 2.2.3 The flat plate

According to Schlichting (1974), for a flat plate at the zero incidence, the critical Reynolds number $Re_{x_{crit}}$ for the transition from the laminar boundary layer to the turbulent one is as follows:

$$Re_{x_{crit}} = \left(\frac{U_{\infty} x}{\nu} \right)_{crit} = (3.5 \dots 5) \cdot 10^5 \quad (2.2.1)$$

where x is the distance from the leading edge. At $U_{\infty} = 3$ m/s and $x=L=0.5$ m, Re_x was about 10^5 . Here L is the length of the plate. This indicates that the boundary layer was the laminar over all the plate length. The measurements were made at the locations $x=0.05, 0.1$ and 0.17 m, where x was counted

from the leading edge of the plate. The Reynolds number in these cross-sections did not exceed $4 \cdot 10^4$ for the considered values of the flow velocity.

The main parameters of experiments are presented in Table 2.2.2.

Table 2.2.2 Parameters of experiments

Mean flow velocity U_{∞} , m/s	Particle material	Mean particle size δ_p , μm	Density of particles material ρ_p , kg/m^3	Bulk density of the dispersed phase $\rho_{s\infty}$, kg/m^3
1.5; 3	Electrocorundum	12; 23; 32	3950	0.01

2.3. Experimental Technique.

The investigated surface of the flat plate was degreased by a spirit and dried out before the experiments. Then the plate was installed into the test section of the wind-channel and blown by the aerosol flow at the given values of the experimental conditions during the time period t . Simultaneously, the axial air velocity U and the mass concentration of particles C were measured inside the boundary layer with the help of LDA and LCM, respectively, by the traversing of the measuring volume along the y axis (see Figure 2.1.1).

The profiles of the relative particle mass concentration C/C_{∞} , have been obtained by the averaging of data got from more than 10 measurement series for every cross-section of the plate.

The concentration profiles C/C_{∞} were determined as the dependencies on the self-similar coordinate $\eta = y/\Delta_{l_x}$, which is usually applied for the analysis

of the parameters of the boundary layer (Schlichting, 1974). Here y is the transverse coordinate calculated from the plate surface. The theoretical thickness of the laminar boundary layer $\Delta_{l,x}$, calculated for the given cross-section of the plate x , according to Schlichting (1974), is as follows:

$$\Delta_{l,x} = 5 \sqrt{\frac{\nu x}{U_\infty}} \quad (2.3.1)$$

which has been confirmed by the measurements of the clean air boundary layer flow in the given set-up.

Thus, η can be calculated as follows:

$$\eta = \frac{y}{\Delta_{l,x}} = \frac{y}{5} \sqrt{\frac{U_\infty}{\nu x}} \quad (2.3.2)$$

The boundary layer thickness was between 3 and 7 mm for the considered cross-sections and the values of the flow velocity.

The uncertainty in the measurements of the velocity and the particle mass concentration inside the boundary layer was caused by the temporal instability, the non-uniformity of the particle concentration over the cross-section of the flow and the procedural error of LDA and LCM. The non-uniformity of the particle mass concentration for various particle sizes was almost the same and did not exceed 5%. The temporal instability of the concentration arose from the functioning of the particle screw feeder and the particles deposition both on the walls of the main channel of transportation of the two-phase flow and on the

surfaces of the outlet (Pos. 4, Figure 2.1.1). This instability became appreciable only for 12 μm particles due to their high adhesive features. The procedural errors of LDA and LCM were 3% and 6%, respectively.

Thus, the experimental uncertainties for the measurements of the flow velocity and the particle mass concentration, which were calculated according to Moffat (1988), were less than 5% and

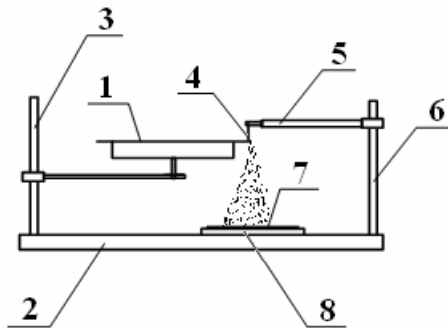


Figure 2.3.1 Test rig for removing particles from the plate

10%, respectively.

The distribution of mass of the deposited particles along the plate was measured by the weighing method. The test rig for the removing of the deposited particles from the surface of the flat plate is shown in Figure 2.3.1.

After the blowing by the aerosol flow during the given period of time t , the plate (Pos. 1) covered with the particles was installed on the fixed bottom (Pos. 2) by means of the holder (Pos. 3). The particles were removed from the surface in various cross-sections with the help of the cardboard head (Pos. 4), which

could move across the plate with the help of the telescopic bar (Pos. 5) installed on the holder (Pos. 6). The removed particles fell down on the surface of the 6 μm mylar film specimen (Pos. 7) installed on the slab (Pos. 8). The net weight of the specimen was measured beforehand. The width of the head determined the width of the stripe on the plate surface from which the particles were removed by the head (Pos. 4). The width of the head was 3 mm. The mass of the film specimen covered with the deposited particles was determined by the laboratory balance. The uncertainty of the measurements was less than 1%. The difference of the masses of the film specimen with and without particles was assigned as the mass ΔM of the particles deposited on the plate surface in the given cross-section during the given period of time t . The intensity of the particle deposition I_{dx} was calculated in various cross-sections along the plate as follows:

$$I_{dx} = \frac{\Delta M}{S t} \quad (2.3.3)$$

where S is the area of the stripe on the plate surface from which the particles were removed by the head (Pos. 4).

2.4. Results.

The results of the experimental investigations concerning the particle mass concentration in the laminar boundary layer on the flat plate and the particles deposition were reported in Articles I, II and III.

2.4.1. *The particle mass concentration in the laminar boundary layer on the flat plate.*

Let us consider separately the influence of the experimental parameters of the aerosol flow on the distribution of the particle concentration close to the plate surface.

The longitudinal coordinate x . Figure 2.4.1 shows the distributions of the relative mass concentration of 32 μm particles in the boundary layer obtained in the cross-sections $x=0.05$, 0.1 and 0.17 m for the flow velocity 1.5 m/s and the distribution of the axial air velocity in the boundary layer for $x=0.1$ m.

It is evident that the distribution of the particles concentration has its maximum within the boundary layer. The value of this maximum grows downstream while it immerses into the boundary layer. The similar tendency was observed for 12 and 23 μm particles.

The profile of the air velocity almost coincides with the solution of Blasius (Schlichting, 1974) that proves once more that the formed boundary layer was the laminar.

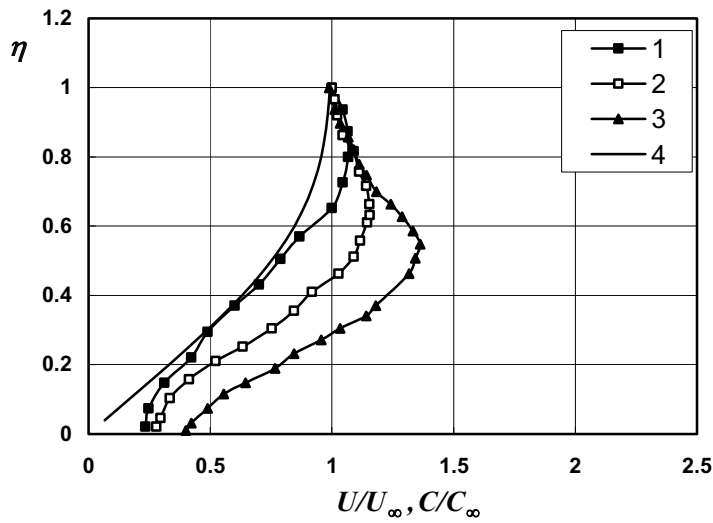


Figure 2.4.1 Axial air velocity U/U_∞ and particles concentration C/C_∞ profiles for $\delta_p=32 \mu\text{m}$ and $U_\infty=1.5 \text{ m/s}$; 1 - $x=0.05 \text{ m}$, 2 - $x=0.1 \text{ m}$, 3 - $x=0.17 \text{ m}$, 4 - U/U_∞

The flow velocity. The distributions of the relative mass concentration of $12 \mu\text{m}$ particles measured for the flow velocity 1.5 and 3 m/s at those cross-sections of the plate, where the thickness of the laminar boundary layer was the same, i.e. for the same Reynolds number Re_x (Re_x was $1.03 \cdot 10^4$), are shown in Figure 2.4.2.

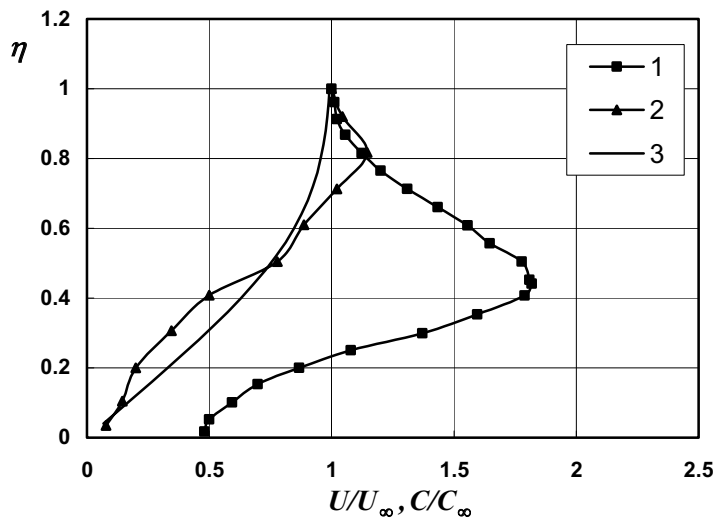


Figure 2.4.2 Axial air velocity U/U_∞ and particles concentration C/C_∞ profiles for $\delta_p=12 \mu\text{m}$ for $Re_x=1.03 \cdot 10^4$; 1 - $U_\infty=1.5 \text{ m/s}$, 2 - $U_\infty=3 \text{ m/s}$, 3 - U/U_∞

One can see from Figure 2.4.2 that the increase in the flow velocity results in the decrease of the concentration maximum and its shift towards the outer border of the boundary layer. The particles concentration that occurred close to the plate surface decreases.

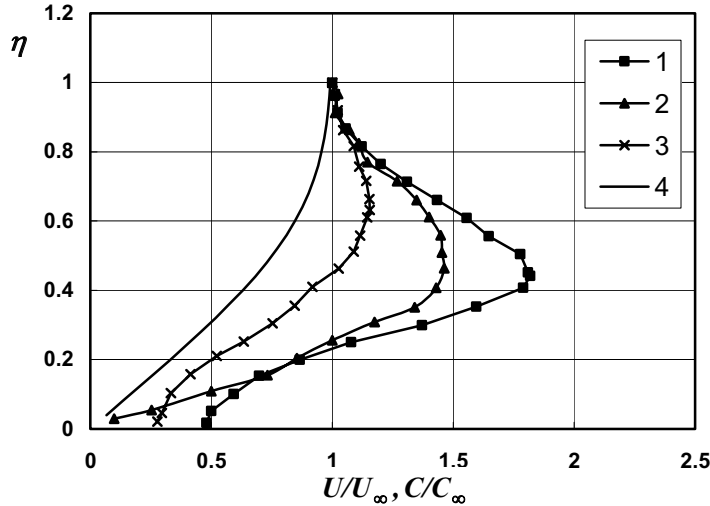


Figure 2.4.3 Axial air velocity U/U_∞ and particles concentration C/C_∞ profiles for various particle sizes in the cross-section $x=0.1$ m, $U_\infty=1.5$ m/s, $Re_x=1.03 \cdot 10^4$; 1 – $\delta_p=12$ μm , 2 – $\delta_p=23$ μm , 3 – $\delta_p=32$ μm , 4 – U/U_∞

The size of the aerosol particles. The influence of the particles size on the distributions of their concentration in the boundary layer is shown in Figure 2.4.3, where the concentration profiles measured for three particle sizes in the cross-section $x=0.1$ m are presented. Here the flow velocity $U_\infty=1.5$ m/s and $Re_x=1.03 \cdot 10^4$.

One can see from Figure 2.4.3 that the increase in the particles size affects on the distribution of their concentration that takes place in the boundary layer similarly to the increase in the flow velocity, i.e. the concentration maximum decreases and shifts towards the outer limit of the boundary layer.

2.4.2. The particles deposition on the flat plate.

Now let us consider separately the influence of the experimental parameters of the aerosol flow on the intensity of deposition of the particles on the surface of the plate surface. The distributions of the deposition intensity were measured for the particle sizes $\delta_p=12$ and 23 μm .

The flow velocity. Figures 2.4.4 and 2.4.5 show the experimental data and the trendlines for the distributions of the deposition intensity of 12 and 23 μm particles along the plate surface, respectively, which were measured for the flow

velocities 1.5 and 3 m/s. Here the deposition is presented versus the Reynolds number $Re_x = U_\infty x / \nu$ for the more convenience.

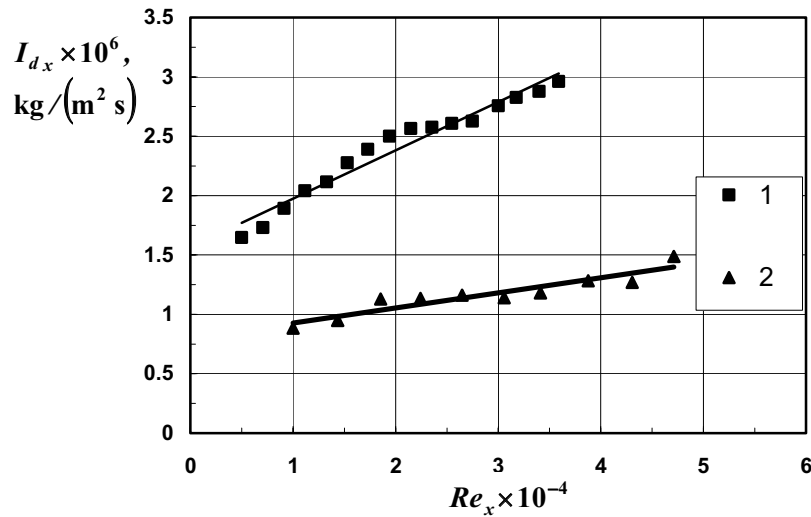


Figure 2.4.4 The distributions of the deposition intensity of the particles $\delta_p=12 \mu\text{m}$ along the plate for various flow velocities; 1 – $U_\infty=1.5 \text{ m/s}$, 2 – $U_\infty=3 \text{ m/s}$

One can see that the growth of the flow velocity causes the decrease in the deposition. This decrease is the more, the particles are larger.

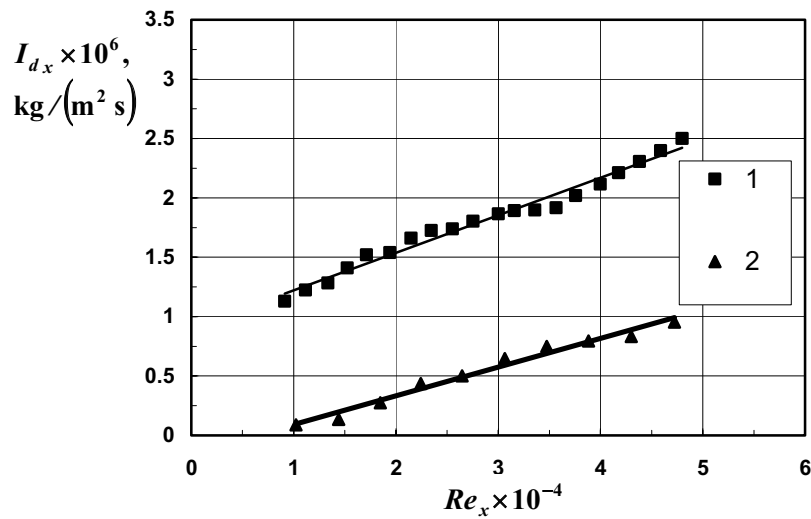


Figure 2.4.5 The distributions of the deposition intensity of the particles $\delta_p=23 \mu\text{m}$ along the plate for various flow velocities; 1 – $U_\infty=1.5 \text{ m/s}$, 2 – $U_\infty=3 \text{ m/s}$

The size of the aerosol particles. The influence of the particles size on the deposition intensity along the plate is shown in Figures 2.4.6 and 2.4.7 (the experimental data and the trendlines). It is evident that the transition to the larger particles results in the decrease of the deposition for the considered flow velocities.

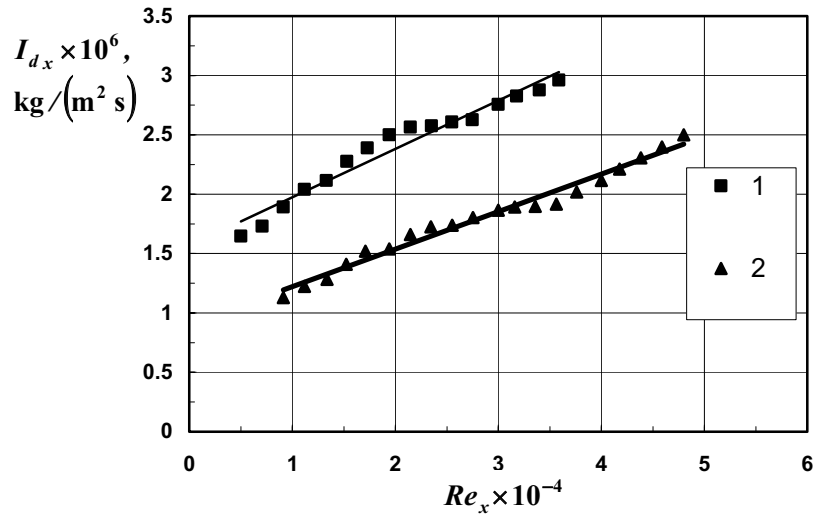


Figure 2.4.6 The distributions of the deposition intensity of various particles along the plate for the flow velocity $U_{\infty}=1.5$ m/s; 1 – $\delta_p=12$ μm , 2 – $\delta_p=23$ μm

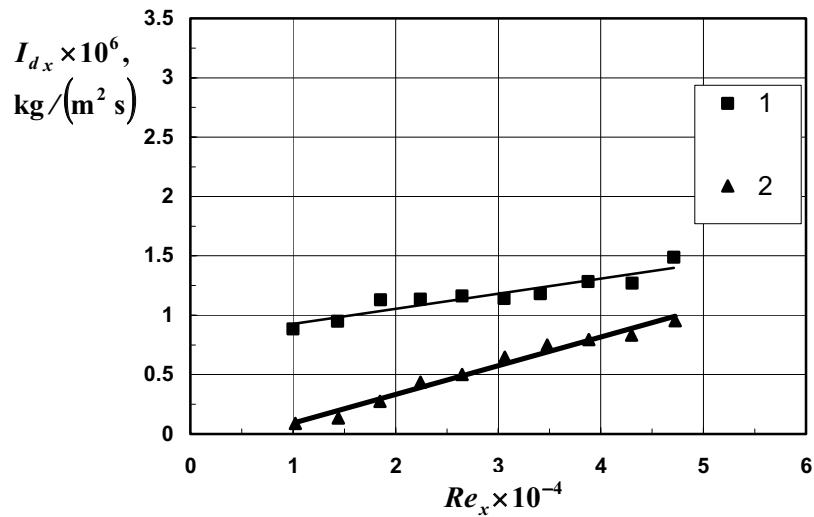


Figure 2.4.7 The distributions of the deposition intensity of various particles along the plate for the flow velocity $U_{\infty}=3$ m/s; 1 – $\delta_p=12$ μm , 2 – $\delta_p=23$ μm

One can see that the deposition intensity increases downstream, but it reduces with the increase in the flow velocity. This reduction is more pronounced for the larger particles ($\delta_p = 23 \mu\text{m}$).

2.5. Discussion of Results.

The considered aerosol particles are sufficiently low-inertia in the free stream, since their material and sizes satisfy the Stokes criterion, i.e. the particles meet the condition $Re_p \ll 1$. When such particles are brought into the laminar boundary layer, formed close to the flat plate, their transport in different regions of the layer is conditioned by the different mechanisms.

The outer region of the boundary layer is characterized by the inertial transport of the particles. This is caused by the fact that the particles cannot move along the streamlines due to the substantial difference between the air and particles physical density and get to the region of the boundary layer where the air velocity is smaller. The particles decelerate and accumulate in this region resulting in the increase of the concentration.

The convective transport which takes place in the more interior parts of the boundary layer, located closer to the surface of the plate, balances the inertial transport, and this conditions no further increase of the concentration.

Immediately near the surface the transport of the particles is already carried out by the diffusion which is caused mainly by the interactions between the particles, realized directly or implicitly by air, and also by the interactions between the particles and the surface. The gradient of the concentration in this region of the boundary layer is determined by the ratio between the kinematic viscosity of air and the coefficient of the particles diffusion D_p , i.e. by the Schmidt number Sc .

Thus, the number of the particles that occur close to the surface and, hence, the number of the deposited particles are determined by the value of the concentration maximum, its location relative to the surface and the concentration gradient near the surface. This fact is confirmed by the concentration distributions measured in various cross-sections of the plate (see Figure 2.4.1) and the distributions of the particles deposited along the surface (see Figures 2.4.4 and 2.4.5).

The influence of the parameters of the aerosol flow on the deposition appears as the changing of character of the concentration distribution which occurs near the surface.

The increase of the flow velocity results in the decrease of the concentration maximum and its shift towards the outer border of the boundary layer (see Figure 2.4.2), and the concentration which take place immediately near the surface reduces and, correspondingly, the deposition intensity also reduces (see Figures 2.4.2, 2.4.4 and 2.4.5). The increase of the particle size causes the similar changing of the concentration distribution (see Figure 2.4.3) and, as a consequence, the reduction of the deposition intensity (see Figures 2.4.6 and 2.4.7).

3. THEORETICAL MODEL OF THE TWO-PHASE LAMINAR BOUNDARY LAYER ON A FLAT SURFACE.

3.1. Prerequisites for Numerical Modelling.

One of the main objectives of the given investigation was to elaborate the mathematical model which would describe adequately the behaviour of the aerosol particles close to the streamlined surface of a flat surface, in particular, the distributions of the particle mass concentration occurred within the laminar boundary layer near the flat surface that was obtained in the experimental part of this work.

The given model should meet the next requirements:

- the considering of the real composition of the aerosol particles, i.e. the polydispersity of their size and shape;
- the model must take into account all the physical phenomena, which occur within the boundary layer near the streamlined surface of the flat plate and determine the particles deposition at this surface;
- the computed profiles of the particle mass concentration should reproduce the ones obtained by the experiments with a satisfactory accuracy that is the main criterion of validity of the given model.

The mathematical model being proposed in the given thesis and applied for the calculations of the particles velocity and mass concentration within the boundary layer near the flat plate has been described in detail in Article II.

The laminar boundary layer which develops while the zero incidence flowing past the flat plate by the air-solid particles aerosol flow takes place, is considered within the Eulerian approach, where the dispersed phase is modelled as the continuous medium. The dispersed phase is described within the mutually-penetrating continua by Nigmatulin's theory (1978), since the interparticle distance λ is much smaller than the characteristic flow scale which here is the thickness of the boundary layer Δ_l . This also issues from the necessity of the theory validation. As the calculations have shown, e.g., for the 10 μm particles at the particle mass concentration $C_\infty=0.01$ kg/kg, the ratio between the interparticle distance λ and the thickness of the boundary layer Δ_l was an order of $\lambda/\Delta_l \approx O(10^{-1})$.

Unlike the approach of an ideal gas description of the dispersed phase in a two-phase laminar boundary layer, suggested by Soo (1967), Osipov (1980), and Asmolov (1992), where the interparticle collisions and friction were not taken into account, the transport equations of the particles mass and momentum of the dispersed phase are written within the given model using the approximation of the Newtonian viscous fluid. Soo (1967), Osipov (1980) and Asmolov (1992) calculated the two-phase laminar boundary layer, developed near a flat plate, considering the dispersed phase to be monodisperse, and Asmolov (1992) took into account the influence of the Saffman lift force on the motion and distribution of the dispersed phase. Therefore, they considered only

the convective transfer of the dispersed phase in the boundary layer. In addition to the convective transfer and the particle-gas interaction, occurred via the drag force and the Saffman lift force, the proposed model takes into account the diffusion transfer of the particles, that is described by the consideration of the interparticle collision mechanism. As a result of such theoretical description, the so-called pseudoviscosity coefficients of the dispersed phase are brought into consideration. The interparticle collisions result from the velocity differences of the particles of various fractions. These differences in turn arise from the polydispersity of the real solid particles. As the results of the experimental part of the given work show (see Chapter 2), the composition of the electrocorundum powder applied as the dispersed phase of the aerosol flow in the given study is non-uniform, and the particles themselves have an irregular form, while the r.m.s. deviation of the particle size is up to 30%.

The real continuous particle size distribution is modelled by the finite number of the particle fractions of the discrete size for the mathematical description of the dispersed phase. Each fraction is characterized by its own properties, such as the particle size, concentration and velocity. This allows to take into consideration the collision process, occurred between the particles that have different velocities. Hence, one can write the transport equations and set the boundary conditions for each particle fraction. The correlations between the different particle fractions are calculated by introducing the pseudoviscosity coefficients derived from the collision mechanism.

The theoretical consideration within the given model is restricted to the description of the two-dimensional motion of two-phase aerosol flow in the laminar boundary layer. So, there are not the turbulent momentum and transfer. The proposed model is based on the so-called one-way coupling, i.e. the influence of air on a behaviour of the particles is considered only, due to very diluted aerosol flow conditions at the very low mass concentration of the dispersed phase C_∞ , which is about 0.01 kg/kg. The composition of the polydisperse dispersed phase is modelled by three fractions of particles: the fraction, which contains the particles of the largest percentage by mass (the so-called “main fraction”, which is denoted below by index 2, and two additional particle fractions of the smaller percentage by mass. One of these additional fractions (index 1) consists of the particles of the smaller size as compared with the size of particles of the main fraction. The other additional fraction (index 3) includes the particles of the larger size than the particles of fraction 2. The dispersed phase is considered as the polydisperse one and characterized by the following parameters: the particle sizes of the fractions δ_{pi} ; the velocity projections u_{si} and v_{si} in the streamwise and transversal directions, respectively, and the particle mass concentration of the fractions C_i .

It should be noted that the number of the particles fractions, which can be considered within the given model, is not the principal item. It can consider two, four and more particles fractions. The increase of the fractions results in the

complication of the problem and the expansion of the computing power. The crucial issue of the given model approximation is the relation between the mass portions of the particles fractions and their sizes. According to the investigation by Frishman et al. (1997), the mass portions of the fractions 1, 2 and 3 are 25, 50 and 25% of the total dispersed phase, respectively. The particles size of the fraction 1 is 85% of the particles size of the fraction 2, while this value for the fraction 3 is 108% of the particles size of the fraction 2. The substitute of the real polydisperse dispersed phase for only three particles fraction within the given model is caused by the limitations of the computing power only, that has affect finally on the calculation accuracy of the particles deposition.

The impact of the air flow on a motion of the dispersed phase in the laminar boundary layer is realized by taking into account the drag force, the Saffman lift force, which is caused by the gradient distribution of the air velocity within the boundary layer. With the applying of the spatial averaging method by Nigmatulin (1978) for the equations of the translational motion of a single particle, the equations for the description of the dispersed phase as the continuum one are obtained. There is a prerequisite for the consideration of the Saffman lift force in the laminar boundary layer, since the parameter $u/\sqrt{\nu(\partial u/\partial y)}$ used by Saffman (1961) is of a unit value unlike for the turbulent boundary layer, where it is much higher than a unit. Here u is the axial velocity component of air and ν is the kinematic viscosity of air. Gravity is neglected due to the insignificance of the particle terminal velocity relative to the particle velocity originating from the drag force. Other force factors, such as the Basset force, the force of the added masses and so on, are also neglected, as the ratio between the material density of the particles and the air density is very high.

3.2. System of Equations.

Let us consider the two-dimensional motion of air and dispersed phase inside the laminar boundary layer. The equations of the two-phase laminar boundary layer in the Cartesian coordinate system are as follows:

$$\frac{\partial(\rho u)}{\partial x} + \frac{\partial(\rho v)}{\partial y} = 0 \quad (3.2.1)$$

$$\rho u \frac{\partial u}{\partial x} + \rho v \frac{\partial u}{\partial y} = \frac{\partial \tau_a}{\partial y} \quad (3.2.2)$$

$$\frac{\partial(\rho_s u_s)}{\partial x} + \frac{\partial(\rho_s v_s)}{\partial y} = \frac{\partial}{\partial y} \left(D_s \frac{\partial \rho_s}{\partial y} \right) \quad (3.2.3)$$

$$\rho_s u_s \frac{\partial u_s}{\partial x} + \rho_s v_s \frac{\partial u_s}{\partial y} = \frac{\partial \tau_s}{\partial y} + \frac{\rho_s}{\rho_p} \frac{18C'_D \nu (u - u_s)}{\delta_p^2} \quad (3.2.4)$$

$$\rho_s u_s \frac{\partial v_s}{\partial x} + \rho_s v_s \frac{\partial v_s}{\partial y} = \frac{\partial p_s}{\partial y} + \frac{\rho_s}{\rho_p} \left[\frac{18C'_D \nu (v - v_s)}{\delta_p^2} + \right.$$

$$+ \frac{6K_s \sqrt{\nu}}{\pi \delta_p} (u - u_s) \sqrt{\frac{\partial u}{\partial y}} \quad (3.2.5)$$

where ν is the transversal air velocity component. The drag coefficient C'_D is determined for the different Reynolds numbers of a particle Re_p according to Kravtsov (1968) by the formula:

$$C'_D = \frac{24}{Re_p} = 1 + 0.275 \sqrt{Re_p} + 0.0138 Re_p \quad (3.2.6)$$

where $Re_p = \delta_p \sqrt{(u - u_s)^2 + (v - v_s)^2} / \nu$. The density of the dispersed phase ρ_s is related to the physical density of incompressible gas ρ by $\rho_s = C\rho$ according to the Eq. (1.1.1), which is valid if the volumetric concentration of particles β_s is very low, i.e. $\beta_s \ll 1$. τ_a , τ_s are the shear stresses of air and the dispersed phase, respectively, and p_s is the normal stress for the dispersed phase. $K_s = 1.61$ is the numerical constant which value is chosen according to Shraiber et al. (1980).

The combined transport equations Eqs. (3.2.1) – (3.2.5) contain the continuity equation Eq. (3.2.1), the equation of the momentum balance of gas Eq. (3.2.2), the transport equation of the particle mass Eq. (3.2.3) and the momentum balance of the dispersed phase in streamwise and transversal directions Eqs. (3.2.4) and (3.2.5), respectively. These equations are obtained by the applying of the theory by Nigmatulin (1978) of the mutually-penetrating continua. The drag force and the Saffman lift forces are taken into account on the right-hand side of Eqs. (3.2.4) and (3.2.5).

It is suggested that the behaviour of the dispersed phase obeys the approximation of the Newtonian fluid. Therefore, analogously to the air flow, the stress tensor components of the dispersed phase are correlated with the rate of strain via the introduced pseudoviscosity coefficients, which can be written in the simplest form using the approximation of the laminar boundary layer according to Schlichting (1974) (see Eqs. (8) – (10), Article II).

The pseudoviscosity coefficients for the particles mass transport equation and for the momentum balance in the streamwise and transversal directions are D_s , ν_s^1 , ν_s^2 , respectively. These coefficients describe the transfer of mass and momentum of the dispersed phase by the diffusion process originated from the interparticle collisions. This transfer is considered in addition to the convectational transfer and the interphase momentum exchange, which is caused by various forces (the viscous drag force and the Saffman lift force). The pseudoviscosity coefficients are varied both over the width and the length of the boundary layer. As the calculations have shown, the values of these coefficients at the leading edge of the plate, where the distributions of velocity of the dispersed phase changes from the uniform taken place in the free stream flow to the typical occurred in the boundary layer, were comparable with the values of the coefficient of the laminar viscosity of the air flow.

The transport equations are written for each particle fraction denoted by the index “ i ”. The pseudoviscosity coefficients ν_{si}^i , D_{si} can be determined for each particle fraction by knowing the velocity and mass concentration fields of the interacting fractions, i.e. u_{si} , ν_{si} , C_i . The detailed description of the definition of the pseudoviscosity coefficients is presented in Article II.

Since while solving the equations of the two-phase laminar boundary layer it is more convenient to consider the parameters of air of the aerosol flow expressed in the self-similar variables, as it was done, for example, by Schlichting (1974), the combined transport equations Eqs. (3.2.1) – (3.2.5) are transformed to the new coordinate system with $x=x$, $\eta = y\sqrt{U_\infty/\nu x}$ using the transformation by Anderson et al. (1990) as follows:

$$x \frac{\partial \bar{U}}{\partial x} - \frac{\eta}{2} \frac{\partial \bar{U}}{\partial \eta} + \frac{\partial \bar{V}}{\partial \eta} = 0 \quad (3.2.7)$$

$$x \bar{U} \frac{\partial \bar{U}}{\partial x} + \left[\bar{V} - \frac{\eta \bar{U}}{2} \right] \frac{\partial \bar{U}}{\partial \eta} = \frac{\partial^2 \bar{U}}{\partial \eta^2} \quad (3.2.8)$$

$$\sqrt{x} \frac{\partial}{\partial x} \left[\sqrt{x} \bar{C}_i \bar{U}_{si} \right] + \frac{\partial}{\partial \eta} \left[\bar{C}_i \left(\bar{V}_{si} - \frac{\eta \bar{U}_{si}}{2} \right) \right] = \frac{\partial}{\partial \eta} \left[\frac{D_{si}}{\nu} \frac{\partial \bar{C}_i}{\partial \eta} \right] \quad (3.2.9)$$

$$x \bar{U}_{si} \frac{\partial \bar{U}_{si}}{\partial x} + \left[\bar{V}_{si} - \frac{\eta \bar{U}_{si}}{2} \right] \frac{\partial \bar{U}_{si}}{\partial \eta} = \frac{\partial}{\partial \eta} \left[\frac{\nu_{si}^1}{\nu} \frac{\partial \bar{U}_{si}}{\partial \eta} \right] + \frac{\rho}{\rho_p} \frac{x}{\delta_{pi}} \left[\frac{18 C'_{Di} (\bar{U} - \bar{U}_{si})}{Re_{pi}} \right] \quad (3.2.10)$$

$$x \bar{U}_{si} \frac{\partial \bar{V}_{si}}{\partial x} + \left[\bar{V}_{si} - \frac{\eta \bar{U}_{si}}{2} \right] \frac{\partial \bar{V}_{si}}{\partial \eta} = \frac{\partial}{\partial \eta} \left[\frac{2 \nu_{si}^2}{\nu} \frac{\partial \bar{V}_{si}}{\partial \eta} \right] + \frac{\rho}{\rho_p} \frac{x}{\delta_i} \left[\frac{18 C'_{Di} (\bar{V} - \bar{V}_{si})}{Re_{pi}} + \frac{6 K_s (\bar{U} - \bar{U}_{si})}{\pi 4 \sqrt{Re_x}} \sqrt{\frac{\partial \bar{U}}{\partial \eta}} \right] + \frac{\bar{U}_{si} \bar{V}_{si}}{2} \quad (3.2.11)$$

where $\bar{U} = u/U_\infty$, $\bar{U}_{si} = u_{si}/U_\infty$, $\bar{V} = v\sqrt{x}/(\nu U_\infty)$, $\bar{V}_{si} = v_{si}\sqrt{x}/(\nu U_\infty)$, $\bar{C}_i = C_i/C_\infty$ are the non-dimensional stretched variables, Re_{pi} is the Reynolds number of the particles for the different fractions:

$$Re_{pi} = \frac{U_\infty \delta_{pi} \sqrt{(\bar{U} - \bar{U}_{si})^2 + (\bar{V} - \bar{V}_{si})^2}}{\nu} \quad (3.2.12)$$

and U_∞ , C_∞ are the axial velocity of air and the mass concentration of the dispersed phase occurred in a free stream, respectively.

One can see that the equations of the two-phase laminar boundary layer include the non-self-similar terms which depend on the axial (streamwise) coordinate x . They characterize the influence of the force factors in the equations of the momentum balance of the disperse phase. One can also see that as far as

the streamwise coordinate extends, the ratio δ_{pi}/x decreases resulting in the reduction of the influence of the force terms. The first terms on the right-hand side of the equations of the particle mass transfer Eq. (3.2.9) and momentum transfer in axial Eq. (3.2.10) and transversal directions Eq. (3.2.11) describe the diffusion of mass and momentum of the different fractions, and they are determined via the introduced pseudoviscosity coefficients of the dispersed phase ν_s^1, ν_s^2, D_s . The terms in square brackets on the right-hand side of the equations of the momentum balance, Eqs. (3.2.10) and (3.2.11), characterize the impact of the drag force and the Saffman lift force, respectively. The fourth term takes into account the influence of the Saffman force, and the last term on the right-hand side of Eq. (3.2.11) is a sequence of the transform of equations into a new self-similar coordinate system.

3.3. Initial and Boundary Conditions.

Since the one-way coupling (i.e. the influence of air on a behaviour of the solid particles takes place only, without the effect of the particles on the parameters of air) is considered in the given model, and, hence, the non-self-similar terms (the force factors) on the right-hand side of Eqs. (3.2.7) and (3.2.8) are absent, the velocity distribution of air is the self-similar for the new coordinates x, η . This solution results from the joint decision of Eqs. (3.2.7) and (3.2.8) for the cross-section of the boundary layer $x=0$. The initial fields of the axial velocity components of the dispersed phase of the aerosol flow are set as the uniform distributions in the cross-section of the boundary layer for the different fractions and the particle mass concentrations:

$$\bar{U}_{si} = 1 \quad (3.3.1)$$

$$\bar{C}_1 = \bar{C}_3 = 0.2, \bar{C}_2 = 0.6 \quad (3.3.2)$$

where \bar{C}_2 is the initial value of the relative particle mass concentration for the main particle fraction, \bar{C}_1 and \bar{C}_3 are the initial values of the relative particle mass concentration for other particle fractions.

The distribution of the transversal velocity components of the dispersed phase at the cross-section $x=0$ is set as:

$$\bar{V}_{si} = 0 \quad (3.3.3)$$

The boundary conditions for the equations of air are set as the sticking and impenetrability conditions at the surface of the plate:

$$\bar{U}|_w = 0 \quad (3.3.4)$$

$$\bar{V}_w = 0 \quad (3.3.5)$$

Here and below index “ W ” denotes the conditions occurred immediately on the surface.

At the outer part of the boundary layer the axial velocity component of air is set to be equal to the velocity in free stream, and the gradient of the transversal velocity equals zero:

$$\bar{U}\Big|_{\infty} = 1 \quad (3.3.6)$$

$$\frac{\partial \bar{V}}{\partial \eta}\Big|_{\infty} = 0 \quad (3.3.7)$$

The boundary conditions for the equations of the dispersed phase, i.e. for the equations of the axial particle velocity component, are set assuming the relative particle velocity along the surface as it was done in the theory of the rarefied gases (Chapman & Cowling, 1990). The given expression includes the restitution coefficient of the linear momentum of the particles at the interaction with the surface:

$$\bar{U}_{si}\Big|_W = -\gamma_u \frac{\partial \bar{U}_{si}}{\partial \eta}\Big|_W \quad (3.3.8)$$

where the restitution coefficient γ_u , which characterizes the loss of the particles axial velocity due to their collisions with the plate surface, is determined according to Chapman & Cowling (1990) as follows:

$$\gamma_u = \frac{\lambda - f_u}{f_u} \lambda \quad (3.3.9)$$

The expression for the coefficient f_u , which characterizes the loss of the particles tangential velocity due to their collisions with the plate surface, is obtained using the results of Babukha & Shraiber (1972):

$$f_u = \frac{5 + 2k_t}{7} \quad (3.3.10)$$

The roughness coefficient k_t , taking into account the surface roughness of the plate and particles, was introduced by Babukha & Shraiber (1972). It neglects the relative velocity of the particles along the surface, and thus differs from those introduced by Matsumoto & Saito (1970), who considered two types of the particle-wall interaction – with and without the consideration of the relative velocity along the surface. According to Babukha & Shraiber (1972), k_t can vary in the range $(-1...1)$, and its value is set to be 0.75 in the calculations for the given pair “surface-particle”.

The impenetrability conditions at the surface for each particle fraction are set for the transversal velocity component of the dispersed phase as follows:

$$\bar{V}_{si}\Big|_W = 0 \quad (3.3.11)$$

In order to explain the boundary conditions set for the particle mass concentration at the surface, the balance of the mass flow rates near the surface in the volume element with thickness Δ_1 and length Δ_2 along the plate surface is considered. For the given volume element the difference between the input and output mass flow rates in the axial direction is not equal to zero due to the sliding friction of the particles against the plate surface. The total mass flow rate in the axial direction can be balanced by the convective and diffusion particle transfers occurred in the transversal direction. But, as the convective transfer in the transversal direction is negligible due to the insignificance of the

transversal particle velocity component near the surface, one can only take into account the diffusion transfer. Thus, one can write the boundary condition for the particle mass concentration as follows:

$$\left. \frac{D_{si}}{\nu} \frac{\partial \bar{C}_i}{\partial \eta} \right|_w = \bar{C}_i f(x) \quad (3.3.12)$$

The expression for the function $f(x)$ in the new coordinates is written as follows:

$$f(x) = B_1 x \left(\sqrt{1 + \frac{\Delta_2}{x}} \bar{U}'_{si} - \bar{U}_{si} \right) \quad (3.3.13)$$

During the interaction of a particle with the surface it loses its velocity. This velocity loss is determined as $\bar{U}'_{si} = \bar{U}_{si} [(5 + 2k_t)/7]$ according to Babukha & Shraiber (1972). The velocity loss is calculated along the length Δ_2 . The coefficient B_1 in Eq. (3.3.13) equals the ratio between Δ_1 and Δ_2 . One can assume in the calculations that $\Delta_1 = \Delta\eta$ and $\Delta_2 = \Delta x$, where $\Delta\eta$ and Δx are the calculation steps in the transversal and streamwise directions, respectively. So, one can write that $B_1 = \Delta\eta / \Delta x$.

In the outer part of the boundary layer the axial velocity component of the particles and the particle mass concentration for the different fractions are set equalled to those in the free stream:

$$\bar{U}_{si}|_{\infty} = 1 \quad (3.3.14)$$

$$\left(\bar{C}_1 = \bar{C}_3 \right)|_{\infty} = 0.2, \quad \bar{C}_1|_{\infty} = 0.6 \quad (3.3.15)$$

The gradient type of the boundary conditions are set similar to those of air for the transversal velocity component in the outer part of the layer. But, unlike air, the velocity gradient is set to be equal to constant, which in turn may be determined as the streamline inclination in the outer part of the layer towards the particle velocity direction of the free stream. Thus, there is some definite particle flow rate coming from the free stream into the boundary layer. This constant does not depend on a particle size. The boundary condition for the transversal particle velocity in that case can be written:

$$\left. \frac{\partial \bar{V}_{si}}{\partial \eta} \right|_{\infty} = -B_2 \quad (3.3.16)$$

The constant B_2 is computed based on a good agreement with the experimental data, and according to the given investigations $B_2 = 0.1$ for all experiments.

Eqs. (3.2.7) – (3.2.11) in the aggregate with the initial conditions Eqs. (3.3.1) – (3.3.3) and the boundary conditions Eqs. (3.3.4) – (3.3.8), (3.3.11), (3.3.12), (3.3.14) – (3.3.16) were solved numerically by the tridiagonal algorithm using the six-point formula for the numerical scheme by the standard software C++. The linearization of the non-linear terms on the left-hand side of the transport equations was carried out by Newton's method (Anderson et al.

1990), and the upwind difference were used according to Roache (1980) for the approximation of the derivatives in the transversal direction.

The obtained values of the particles velocity V_{sw} and particle mass concentration C_w occurred inside the boundary layer immediately near the surface will be applied afterwards for the calculation of the particles deposition at the plate surface.

3.4. Results of the Computations and Validation of the Model.

The results of the numerical modelling concerning the particle mass concentration were reported in Article II.

The results of the numerical modelling of the distributions of the axial velocity components of air and the aerosol particles and the relative particle mass concentration within the laminar flat-plate boundary layer, and the comparison of the numerical and experimental data obtained by the given investigation are shown in Figures 3.4.1 – 3.4.6. Here the data are presented depending on the self-similar coordinate $\eta = y\sqrt{U_\infty / (\nu x)}$.

The axial component of the air velocity within the boundary layer coincides with the well-known self-similar solution of Blasius (see Schlichting, 1974), since due to the low mass concentration of the solid particles (i.e. $C \approx O(10^{-2})$) the given model neglects their influence on the parameters of the air flow, i.e. the air flow is calculated as in case of the single-phase laminar boundary layer on a flat plate. The transversal component of the air velocity is also assumed to be described by the profile by Blasius (see Schlichting, 1974).

As one can see from Figures 3.4.1 – 3.4.6, the numerical distribution of the relative particle mass concentration in the laminar boundary layer is appreciably non-uniform. The concentration increases monotonously from the outer part of the boundary layer, reaches its maximum (the so-called concentration peak) at some distance from the surface and decreases towards the wall up to 20% of its value occurred in the free stream. The increase of the particle mass concentration in the outer part of the boundary layer can be explained by the penetration of the inertia particles inside the boundary layer, where they decelerate. The further reduction of the concentration towards the surface can be explained by the diffusion mechanism caused by the interparticle collisions and by their collisions with the surface. The prevalence of the diffusion transfer over the convective transfer near the surface firstly relates to the decrease of the convective transfer near the surface, secondly, the intensification of the diffusion process. This intensification arises from the enhancement of the particles velocity disturbances due to both their interactions with the surface and the different influence of the drag force and the Saffman lift force, that impose on the particles of the different size.

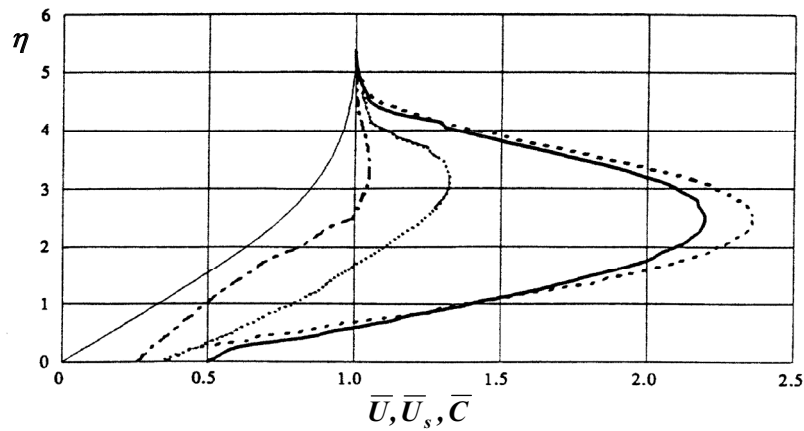


Figure 3.4.1 Numerical profiles of the axial velocity component of air and the dispersed phases (— \bar{U} , \bar{U}_s , $x=0.1$ m, $\delta_p=12$ μm) and the particle mass concentration \bar{C} (— $x=0.1$ m, $\delta_p=12$ μm ; - - - $x=0.17$ m, $\delta_p=12$ μm ; ····· $x=0.1$ m, $\delta_p=23$ μm ; - - - - $x=0.1$ m, $\delta_p=32$ μm). The free stream velocity $U_\infty=1.5$ m/s

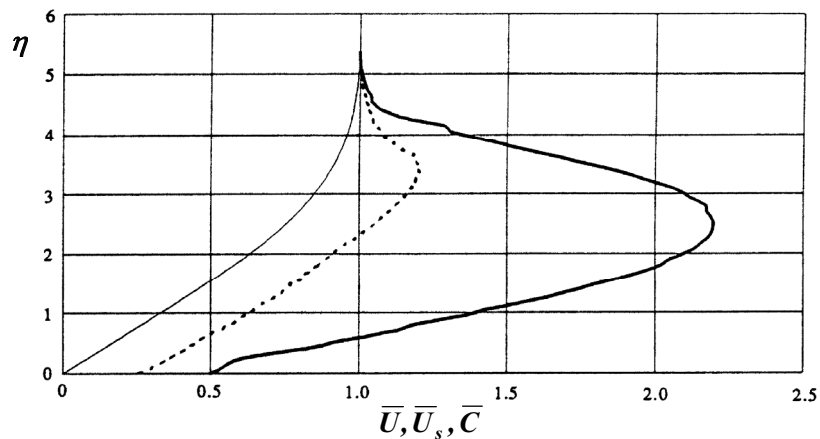


Figure 3.4.2 Numerical profiles of the axial velocity component of air and the dispersed phases (— \bar{U} , \bar{U}_s , $U_\infty=1.5$ m/s) and the particle mass concentration \bar{C} for $\delta_p=12$ μm in the cross-section $x=0.1$ m for the different free stream velocities (— $U_\infty=1.5$ m/s; - - - $U_\infty=3$ m/s)

According to the numerical investigations, the distribution of the particle mass concentration has its maximum value in case of fine 12 μm particles (see Figures 3.4.1 and 3.4.3). The maximum of the mass concentration decreases with the growth of the particle size, and the profile becomes more uniform for the larger 23 and 32 μm particles (Figures 3.4.1 and 3.4.4). It also follows from Figure 3.4.1 that the concentration maximum shifts towards the outer part of the boundary layer in case of the larger particles. The influence of the increase of the

free stream velocity on the concentration distribution is similar to the influence of the increase of the particle size (Figure 3.4.2).

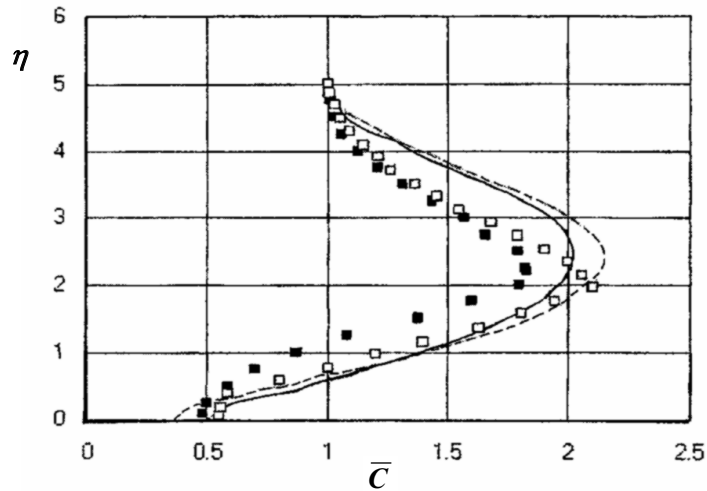


Figure 3.4.3 The profiles of the particle mass concentration for $U_\infty=1.5$ m/s and $\delta_p=12$ μm in the cross-sections $x=0.1$ m (— numerical calculation, ■ experiment) and $x=0.17$ m (----- numerical calculation, □ experiment)

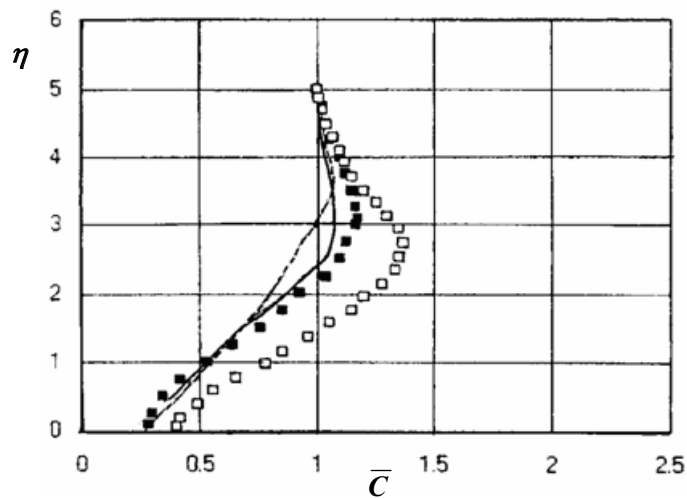


Figure 3.4.4 The profiles of the particle mass concentration for $U_\infty=1.5$ m/s and $\delta_p=32$ μm in the cross-sections $x=0.1$ m (— numerical calculation, ■ experiment) and $x=0.17$ m (----- numerical calculation, □ experiment)

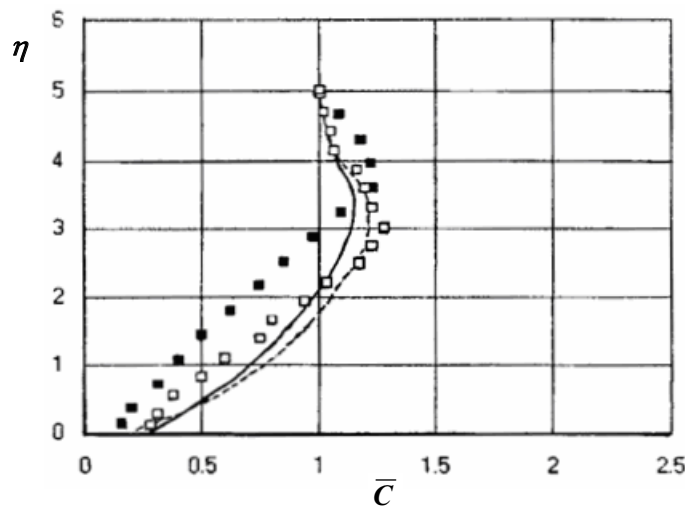


Figure 3.4.5 The profiles of the particle mass concentration for $U_\infty=3$ m/s and $\delta_p=12$ μm in the cross-sections $x=0.1$ m (— numerical calculation, ■ experiment) and $x=0.17$ m (----- numerical calculation, □ experiment)

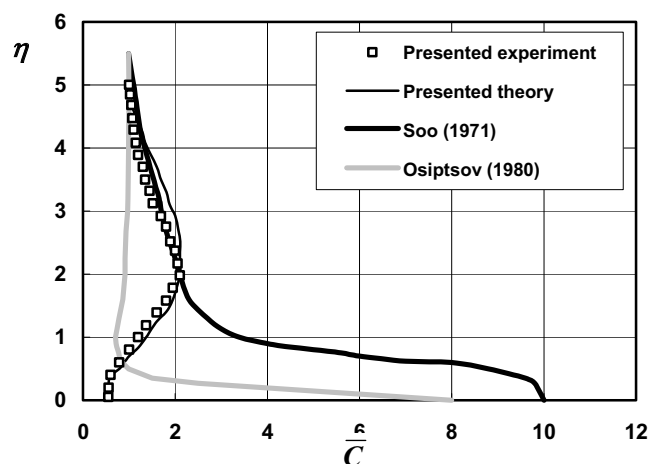


Figure 3.4.6 Comparison of the experimental and numerical profiles of the particle mass concentration with the results of other investigations for the condition $U_\infty=1.5$ m/s, $\delta_p=12$ μm , $x=0.17$ m

The comparison of the experimental and theoretical results obtained by the given investigation with the calculations by Soo (1971) and Osipitsov (1980) is presented in Figure 3.4.6. The existing models of the two-phase laminar boundary layer generated close to the flat plate (Soo, 1971; Osipitsov, 1980) based on the description of the dispersed phase of the aerosol flow within the conception of the ideal gas cannot provide the experimentally observed distributions of the relative particle mass concentration, since the mass transfer due to the diffusion is not taken into account by those models. Soo (1971) and

Osipov (1980) calculated the two-phase laminar boundary layer in case of the monodisperse particles only. Thus, they excluded the interparticle collision mechanism from the consideration and, thereby, the diffusion transfer.

Presenting the dispersed phase within the concept of the Newtonian fluid, by introducing the pseudoviscosity coefficients and specifying the boundary conditions for the dispersed phase, one can obtain the distributions of the particle mass concentration by the numerical calculations, which is in a good agreement with the experimental results obtained by this investigation. The given model also describes the tendency of the modification of the particle mass concentration with the parameters of the free stream. For example, according to the obtained numerical results, the increase of the particles size or the free stream velocity leads to the more uniform distribution of the particle mass concentration (see Figures 3.4.1 and 3.4.2).

Some discrepancy in the experimental and numerical results obtained by the given investigation is due to the approximate description of the composition of the dispersed phase, when it is substituted only by three fractions of particles, and the boundary conditions on the surface, specifically, when the impenetrability condition on the surface implies the particle collision with the surface to be elastic.

Figures 3.4.7 – 3.4.10 show the numerical distributions of the axial and transversal components of the particles velocity along the plate, which were obtained within the boundary layer at the distance $\eta = 0.2$ from the surface.

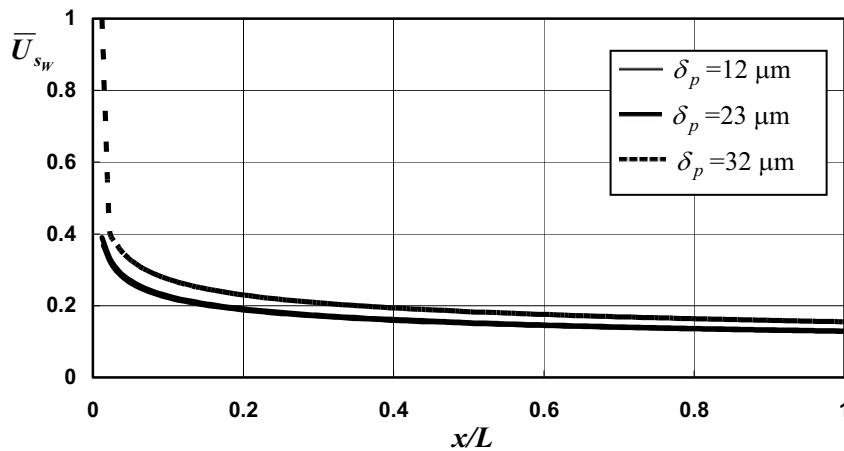


Figure 3.4.7 The distribution of the axial velocity component of the dispersed phase along the plate calculated inside the boundary layer for $\delta_p = 12, 23$ and $32 \mu\text{m}$ at the free stream velocity $U_\infty = 1.5 \text{ m/s}$

One can see that the axial component of the particles velocity has its maximum located at the leading edge of the plate, decreasing downstream and submerging into the boundary layer (Figures 3.4.7 and 3.4.8). This situation is slightly determined by the flow conditions, namely the flow velocity and the particles size.

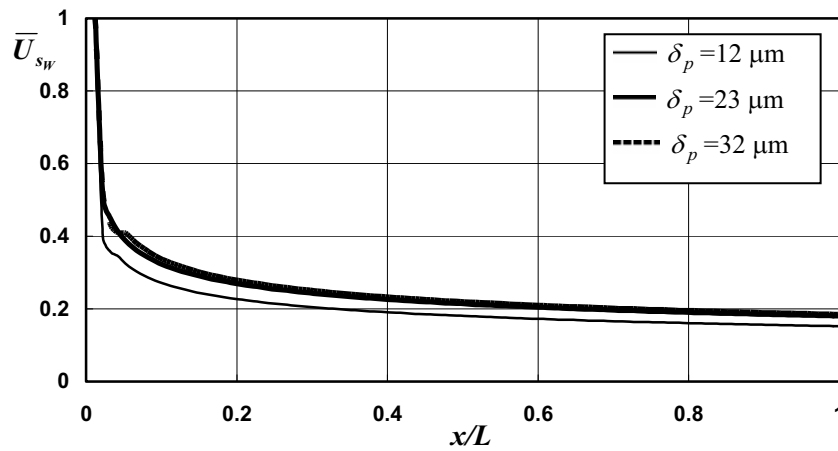


Figure 3.4.8 The distribution of the axial velocity component of the dispersed phase along the plate calculated inside the boundary layer for $\delta_p = 12, 23$ and $32 \mu\text{m}$ at the free stream velocity $U_\infty = 3 \text{ m/s}$

Conversely, the transversal particles velocity has its minimum located at the leading edge of the plate. It increases downstream (Figures 3.4.9 and 3.4.10) due to the side motion that is generated by the flow itself along with the main stream.

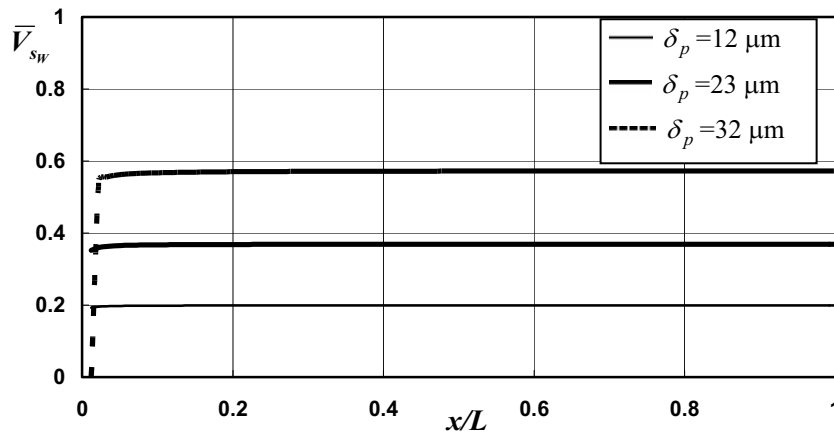


Figure 3.4.11 The distribution of the transversal velocity component of the dispersed phase along the plate calculated inside the boundary layer for $\delta_p = 12, 23$ and $32 \mu\text{m}$ at the free stream velocity $U_\infty = 1.5 \text{ m/s}$

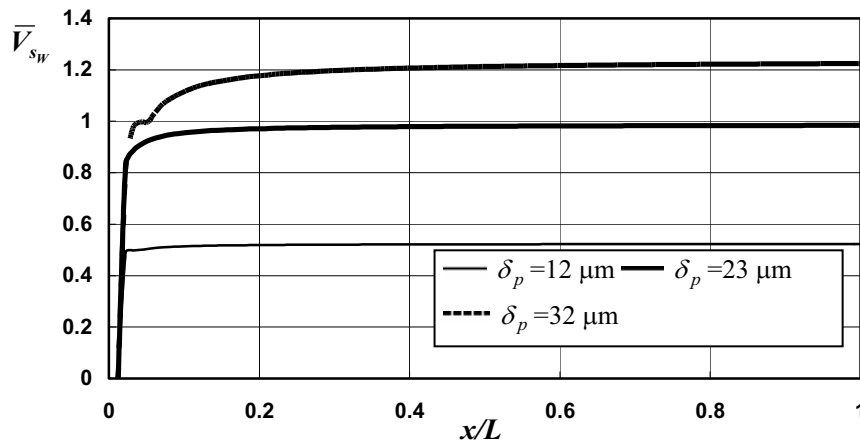


Figure 3.4.10 The distribution of the transversal velocity component of the dispersed phase along the plate calculated inside the boundary layer for $\delta_p = 12, 23$ and $32 \mu\text{m}$ at the free stream velocity $U_\infty = 3 \text{ m/s}$

Thus, the obtained numerical results and its comparison with the experimental ones allow to draw the next conclusions:

- the presented numerical model shows the principle possibility for the applying of the pseudoviscosity approach for the description of behaviour of the solid aerosol particles in the two-phase laminar flat-plate boundary layer at the zero incidence condition;
- the numerical distributions of the particle mass concentration inside the boundary layer show a good agreement with the ones got from the experiments;
- the elaborated model satisfactory describes all the tendencies of the behaviour of the aerosol particles within the laminar boundary layer, specifically the non-uniform distribution of the particle mass concentration and the presence of the concentration peak inside the boundary layer.
- the calculated values of the particles transversal velocity V_{sw} and mass concentration C_w were applied afterwards for the calculation of amount of the deposited particles.

4. ADHESION BEHAVIOUR OF PAIR “SOLID PARTICLE-STREAMLINED SURFACE”.

The given part of the investigations was carried out for the purpose of the ascertainment of the relations that would allow to describe quantitatively the process of adhesion, which takes place when delivering the streamlined surface and touching, the aerosol particles adhere to it.

4.1. Experimental Conditions.

The electrocorundum powders described in Chapter 2 of the given thesis were used in the experiments. The surface of the stainless steel hollow conic model with the vertex angle $\beta = 60^\circ$ and the base diameter of 100 mm was used as the surface for the particles deposition. The model was made of the same stainless steel as the flat plate was. The surface material had the next properties: the physical density $\rho_m = 7800 \text{ kg/m}^3$, Young's modulus of elasticity $E_m = 2.1 \cdot 10^{11} \text{ N/m}^2$, Poisson's ratio $\mu_m = 0.27$. The quality of the surface treatment was characterised by the average roughness height, which was about $6.3 \text{ }\mu\text{m}$, i.e. the surface was sufficiently smooth.

4.2. Measurement Technique.

The experiments were carried out at the special test rig (Figure 4.2.1) designed for the investigations of the adhesive properties of the particles and the surface and described in detail in Article IV.

During the tests the dependence of the particles adhesion number α from the detaching force F_{det} was determined by the centrifugal technique consisted in the separating of the particles from the rotating surface initially covered by the particles.

The square $20 \times 20 \text{ mm}$ specimens (Pos. 10, Figure 4.2.1) of the $6 \text{ }\mu\text{m}$ mylar film were used to catch the detached particles. Immediately before the tests the set of such specimens was prepared, degreased by a spirit and dried out. Then the net mass m_l of each specimen was measured by the laboratory balance. The uncertainty of the measurements was less than 1%.

The surface of the conic model installed on a shaft of electric motor (Pos. 3, Figure 4.2.1) was also degreased, dried out and covered with the particles by the technique of the gravity deposition. During the covering the model was rotated very slowly by the motor in order to obtain the more uniform distribution of the particles along the surface. The duration of the deposition was (20...30) s. Immediately before the covering the powders were sieved with the help of the set of three sieves with the mesh size of 160, 400 and $700 \text{ }\mu\text{m}$ in order to exclude the large aggregates of the particles.

The removing of the particles from the model surface in every test was carried out with the help of the cardboard head (Pos. 6, Figure 4.2.1), which was brought into contact with the surface in the given cross-section, by the manual

rotating of the model. The removed particles were dumped onto the film specimen installed on a slab (Pos. 9). The width of the test cross-sections dx_L was approximately equalled to the width of the head which was 3 mm. The coordinate of the cross-section x_L counted from the model vertex with the help of the coordinate device (Pos. 7, 8).

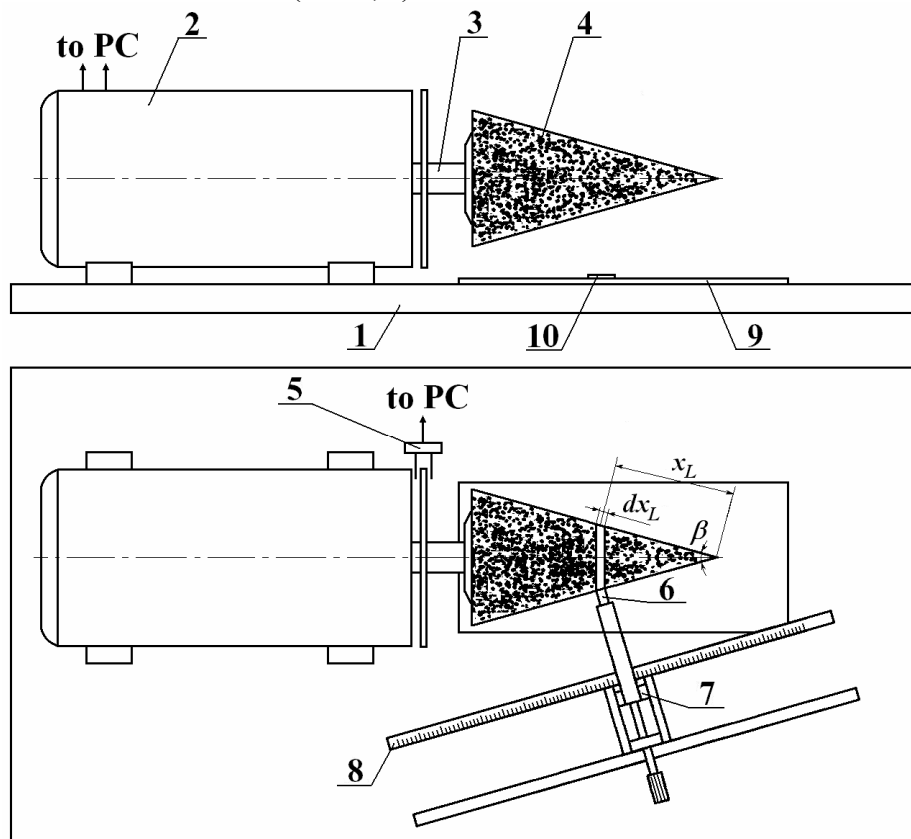


Figure 4.2.1 Test rig: 1 – fixed bed; 2 – DC electric motor; 3 – sleeve for installing of the model on the shaft of the electric motor; 4 – stainless steel hollow conic model; 5 – infrared transducer of the rotational speed of the model; 6 – special head for removing of dust from the model surface; 7, 8 – coordinate device; 9 – slab; 10 – film specimen for collecting of particles removed from the model surface

The first test was carried out without the rotation of the model. The particles were removed in the cross-sections $x_L = 0.01, 0.03$ and 0.09 m.

At the second test the rotational speed of the electric motor was increased gradually up to 14 rps. The rotational speed was varied with the help of the varistor and controlled by the infrared transducer (Pos. 5). The motor ran at this speed during (7...10) s. Then, the rotational speed was gradually decreased till zero, and the motor was switched off. The particles which remained at the

surface after the finishing of rotation were removed in the cross-sections $x_L=0.007, 0.027$ and 0.087 m.

At the third test the rotational speed was increased up to 28 rps, maintained at this value during (7...10) s and then gradually decreased till zero. The particles remained at the surface were removed in the cross-sections $x_L=0.013, 0.033$ and 0.093 m.

Then, the masses of all the film specimens covered with the particles were measured: m_{2i} for the test without rotation, m_{2j} for the test with the rotational speed of 14 rps, m_{2k} for the test with the rotational speed of 28 rps. After that the net masses of the particles were calculated for each specimen as follows:

$$m_{pi} = m_{2i} - m_{1i}, m_{pj} = m_{2j} - m_{1j}, m_{pk} = m_{2k} - m_{1k} \quad (4.2.1)$$

where m_{1i}, m_{1j}, m_{1k} are the net masses of the clean specimens. Indices i, j, k correspond to the tests without rotation of the model, with the rotational speed of 14 rps and 28 rps, respectively.

The net masses of the particles obtained for each test were related to the lateral surface of the model in the corresponding cross-sections:

$$m_{psi} = \frac{m_{pi}}{s_i}, m_{psj} = \frac{m_{pj}}{s_j}, m_{psk} = \frac{m_{pk}}{s_k} \quad (4.2.2)$$

where s is the lateral surface of the model in the given cross-section, $s = 2x_L \pi \sin(\beta/2) dx_L$.

The masses of the particles detached from the surface during the test were determined as follows:

$$M_{psj} = m_{psi} - m_{psj}, M_{psk} = m_{psi} - m_{psk} \quad (4.2.3)$$

It was assumed that in the neighbouring test cross-sections of the model (0.007, 0.01, 0.013 m; 0.027, 0.03, 0.033 m; 0.087, 0.09, 0.093 m) the initial, i.e. the taken place before the rotating, the distribution density m_{psi} of the particles along the surface was the same.

Then, in the considered cross-sections $x_L=0.01, 0.03$ and 0.09 m the particles adhesion number α was calculated for two values of the rotational speed as follows:

$$\alpha_j = \frac{M_{psj}}{m_{psi}}, \alpha_k = \frac{M_{psk}}{m_{psi}} \quad (4.2.4)$$

The given routine was carried out for the powders of $\delta_p=12, 23$ and $32 \mu\text{m}$.

The detaching centrifugal force was calculated for each value of δ_p for two values of the rotational speed, 14 and 28 rps, as follows:

$$F_{det} = 4\pi^2 n^2 R_i m_p \quad (4.2.5)$$

where n is the rotational speed of the model, R_i is the radius of the cross-sections of the model where the masses of the detached particles were measured,

$R_i = x_L \sin(\beta/2)$, m_p is the mass of a single particle, $m_p = (4/3)\pi(\delta_p/2)^3 \rho_p$. Here the particles were assumed to be spheric.

Thus, the expression of the detaching centrifugal force is as follows:

$$F_{det} = \frac{2}{3} \pi^3 x_L \sin(\beta/2) \rho_p \delta_p^3 n^2 \quad (4.2.6)$$

4.3. Results and Discussion.

The results of the experimental investigation concerning the adhesive behaviour of the particles and the surface were reported in Article IV.

The experimentally obtained dependencies $\alpha = f(\lg F_{det})$ were approximated by the linear law $\alpha = a + b \lg F_{det}$ (Figure 4.3.1), where a and b are the empirical coefficients derived from the approximating straight lines.

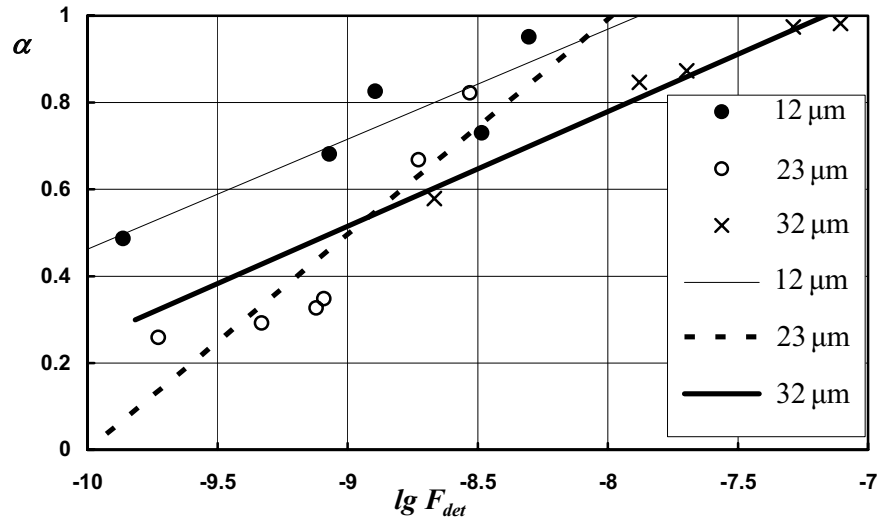


Figure 4.3.1 Distributions of the detaching centrifugal force for the different particles: the experimental data and the approximating trendlines

Thus, for the particle sizes $\delta_p = 12, 23$ and $32 \mu\text{m}$ the following empirical dependencies for the adhesion number from the detaching centrifugal force were obtained:

$$\begin{aligned} \delta_p = 12 \mu\text{m} & \quad \alpha = 2.99 + 0.25 \lg F_{det} \\ \delta_p = 23 \mu\text{m} & \quad \alpha = 4.96 + 0.50 \lg F_{det} \\ \delta_p = 32 \mu\text{m} & \quad \alpha = 2.89 + 0.26 \lg F_{det} \end{aligned} \quad (4.3.1)$$

The values of the coefficients a and b are presented in Table 4.3.1.

Table 4.3.1 Empirical coefficients a and b

Mean particle size $\delta_p, \mu\text{m}$	a	b
12	2.99	0.25
23	4.96	0.50
32	2.89	0.26

Some deviation of the experimental data from the linear law, which takes place at the low rotational speed (see Figure 4.3.1), can be explained by the combined effect of the aerodynamic drag force and the detaching centrifugal force. One can see from Eq. (4.2.6) that the centrifugal force is in proportion to n^2 . The expression for the aerodynamic drag force F_{ad} effected on a single particle upon the rotation of the model can be written according to Loicjanski (1987) as follows:

$$F_{ad} = C_x \rho S_p \frac{U_d^2}{2} \quad (4.3.2)$$

where C_x is the aerodynamic drag coefficient of a particle, S_p is the area of the midsection of a particle, U_d is the flow velocity near the centre of a particle. The flow velocity near the centre of a particle is substantially small, and the particle Reynolds number $Re_p \ll 1$, i.e. the Stokes streamlining takes place, and

according to Schlichting (1974) $C_x = \frac{24}{Re_p}$. Assuming the streamlining of the

rotating model to be laminar, U_d can be written according to Schlichting (1974) as follows:

$$U_d = U_0 \left(2 \frac{y}{\Delta_l} - \frac{y^2}{\Delta_l^2} \right) \quad (4.3.3)$$

where U_0 is the flow velocity at the outer boundary of the laminar boundary layer, Δ_l is the thickness of the boundary layer, y is the transverse coordinate of the boundary layer. The expression (4.3.3) is the approximation of Blasius' solution for the laminar boundary layer (Schlichting, 1974). The thickness of the laminar boundary layer, which is generated upon the rotation, is as follows:

$$\Delta_l = \sqrt{\frac{\nu}{\pi n}} \quad (4.3.4)$$

The flow velocity at the outer boundary of the laminar boundary layer is calculated as:

$$U_0 = 2\pi n x_L \sin\left(\frac{\beta}{2}\right) \quad (4.3.5)$$

Thus, the expression for the aerodynamic drag force F_{ad} can be written as follows:

$$F_{ad} = 6\sqrt{\frac{v}{\pi}} \rho \pi^3 \delta_p^2 x_L \sin\left(\frac{\beta}{2}\right) n^{\frac{3}{2}} \quad (4.3.6)$$

One can see from Eq. (4.3.6) that the drag force is in proportion to $n^{\frac{3}{2}}$. So, the rising of the rotational speed results in more stronger increase of the centrifugal force in compare with the drag force, and for the high rotational speed the detaching of the particles from the surface is stipulated only by the centrifugal force.

Basing on the expressions for the centrifugal and drag forces, Eqs. (4.2.6) and (4.3.6), respectively, where F_{ad} is in proportion to δ_p^2 and F_{det} is in proportion to δ_p^3 , one can expect that the increase of the particles size attenuates the influence of the drag force on the particles and simultaneously intensify the effect of the centrifugal force.

Figure 4.3.1 shows that the distributions of the adhesive force (in this case this is the detaching force) obtained for the 12, 23 and 32 μm electrocorundum particles obey the log-normal law that agree with the conclusions made by Zimon (1976), as well as the results obtained by Reeks & Hall (2001) who applied the similar measurement technique for the investigations of adhesion of the particles of the same sizes to the stainless steel surface.

The inclination of the approximating lines in Figure 4.3.1 determines the root-mean-square deviation of the distribution of the detaching force of the particles. The smaller inclination corresponds to the larger root-mean-square deviation. One can see from Figure 4.3.1 that this deviation is substantially smaller for 23 μm as compared with the 12 and 32 μm particles, for which it is approximately the same. The root-mean-square deviation characterizes the spread in values of the detaching force. This spread is considerably smaller for the 23 μm particles than for the 12 and 32 μm particles.

The total uncertainty of the given measurement technique is caused by the next factors: 1) uncertainty due to the aerodynamic drag force F_{ad} influenced on the particles while the rotating of model by means of the air friction of particles (it was less than 10%), 2) inaccuracy of measurements of the rotational speed of the model (it was less than 1%), 3) uncertainty due to different distances between the axis of revolution and the cross-section of thickness dx_L (it was less than 12%), 4) inaccuracy of weighing (it was less than 1%). So, according to Moffat (1988), the total uncertainty was within 15%.

Based on the results of the given experimental investigation one can draw the following conclusions:

- the log-normal distributions for the adhesion number from the detaching centrifugal force were obtained for various particle sizes;

- for the given measurement technique the detaching of the particles from the surface is stipulated by the combined effect of the aerodynamic drag force and the detaching centrifugal force at the low rotational speed;
- the increase of the rotational speed as well as the particles size results in the intensification of effect of the detaching centrifugal force;
- the obtained dependencies do not consider the environment parameters (humidity, temperature, chemistry), the surface electric charges of the particles, the material properties and shape of the particles as well as the material properties and roughness of the surface.

5. THE ESTIMATION TECHNIQUE FOR THE PARTICLES DEPOSITION AT THE FLAT PLATE.

5.1. Probabilistic Nature Of Particles Deposition.

According to Zimon (1976), when the single particles are brought into contact with a homogeneous surface, the occurred adhesive forces effected on each particle are the different. This difference appears when the detaching of the particles from a surface takes place and it is characterized by the curves of the dependence of the adhesion number α on the detaching force F_{det} (see Figure 1.2.2). The adhesion number $\alpha(F_{det})$ can be considered as the probability of the detaching of the particles due to the detaching force F_{det} , and α possesses the values in the range $(0 \dots 1)$. Changing from the ensemble of the identical particles to the ensemble of tests performed with one single particle, one can assign that $\alpha(F_A)$ is the probability of the adhesive forces, which values are less than F_A occurring at the contact of a particle and a surface.

Figure 5.1.1 shows the schematic of the forces that act on a spherical particle during the time of the contact with a vertical surface. Here F_{el} is the elastic force originated from the elastic collision, F_{fr} is the frictional force,

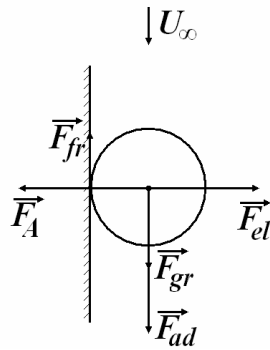


Figure 5.1.1 The forces acting on a particle during the contact

F_{ad} is the aerodynamic drag force, F_{gr} is gravity.

Gravity acting on the particles of the size smaller than $100 \mu\text{m}$ is negligible as compared with other forces. Therefore, the entrainment of the deposited particle by a surface is determined by the relation between the rest forces. Though the elastic and the aerodynamic drag forces are the deterministic, the entrainment of a particle is the stochastic process due to the probabilistic nature of the adhesive force. Assuming as a first approximation the adhesion of a particle and its available blowing-off from a surface by a flow to be the independent events, let us consider these two processes separately. Then, the probability of adhesion of a particle P_A is determined by the condition $F_A \geq F_{el}$, and since the probability of the rebound of a particle after the contact with a surface is $\alpha(F_{el})$ one can write:

$$P_A(F_{el}) = 1 - \alpha(F_{el}) \quad (5.1.1)$$

Now let us consider the blowing-off of a particle from a surface by the air flow, which is determined by the condition:

$$F_{ad} \geq F_{fr} \quad (5.1.2)$$

The expression for the frictional force acting during the time of the contact on condition that $P_A > 0$ (when $P_A < 0$ the blowing-off makes no sense) can be written as follows:

$$F_{fr} = \chi(F_A - F_{el}) \quad (5.1.3)$$

where χ is the dynamic friction coefficient. Generally, χ depends on the surface roughness and the collision angle. According to Matsumoto & Saito (1970), χ was chosen equalled 0.3 for the given quality of the surface treatment of the plate.

The blowing-off is determined by the correlation:

$$F_{ad} \geq \chi(F_A - F_{el}) \quad (5.1.4)$$

or

$$\left(\frac{F_{ad}}{\chi} + F_{el} \right) \geq F_A \quad (5.1.5)$$

In other words, when the condition (5.1.5) is complied, a particle is blown off from a surface, and the probability of this event P_{bl} is as follows:

$$P_{bl} = \alpha \left(\frac{F_{ad}}{\chi} + F_{el} \right) \quad (5.1.6)$$

5.2. Estimation of Deposition Intensity.

Assuming that the deposited particles do not change a surface in respect to both the hydrodynamics of a streamlining of a surface and interaction between a particle and a surface, one can consider the deposition of the particles as a process which does not depend on time. Then, the deposition is characterized by the intensity of the particle deposition I_d , $\text{kg/m}^2 \text{ s}$, which does not depend on time. This assumption is valid during the definite time interval for the dilute two-phase flows for the bodies having the low deposition intensity. For example, for the given experimental conditions $\rho_{s\infty} = 0.01 \text{ kg/m}^3$ and $U_\infty = 3 \text{ m/s}$ this assumption is valid during (2...3) hours depending on the particles size.

The intensity of the particle deposition taken place in the given cross-section of the streamlined surface is determined by the number of the particles N , which collide with a unit area per time unit, and the probability of the entrainment of these particles by the surface P_{en} :

$$I_d = N m_p P_{en} \quad (5.2.1)$$

and

$$N = (C_N V_s) \Big|_W \quad (5.2.2)$$

where C_N is the numerical concentration of the particles in the flow, V_s is the velocity of the particles normal to the surface, index “ W ” denotes the conditions occurred immediately close to the surface.

Hence,

$$I_d = (C_N V_s)_{|W} m_p P_{en} = (C V_s)_{|W} P_{en} \quad (5.2.3)$$

where C is the particle mass concentration.

Let us write the expression of the deposition intensity as follows:

$$I_d = I_A - I_{bl} \quad (5.2.4)$$

where I_A is the deposition intensity occurred under the absence of the blowing-off of the particles, I_{bl} is the intensity of the blowing-off of some portion of the deposited particles.

Then, one can write the expressions for I_A and I_{bl} as follows:

$$I_A = (C V_s)_{|W} P_A \quad (5.2.5)$$

$$I_{bl} = I_A P_{bl} \quad (5.2.6)$$

Then, Eq. (5.2.4) can be rewritten as follows:

$$I_d = I_A (1 - P_{bl}) = (C V_s)_{|W} P_A (1 - P_{bl}) \quad (5.2.7)$$

Thus, comparing Eqs. (5.2.3) and (5.2.7), one can write:

$$P_{en} = P_A (1 - P_{bl}) \quad (5.2.8)$$

where P_A and P_{bl} are calculated by Eqs. (5.1.1) and (5.1.6), respectively.

Taking into account that $\alpha(F_A) = a + blg F_A$ (see Chapter 1), one can obtain:

$$P_A = 1 - a - blg(F_{el}) \quad (5.2.9)$$

and

$$P_{bl} = a + blg\left(\frac{F_{bl}}{\chi} + F_{el}\right) \quad (5.2.10)$$

where the empirical coefficients a and b possess the values obtained in Chapter 4 (see Table 4.3.1).

The expression for the elastic force can be written as:

$$F_{el} = p_{max} S_z \quad (5.2.11)$$

where p_{max} is the maximum tension in the zone of contact of a particle and a surface, S_z is the area of the zone of contact. Assuming the surface to be perfectly solid and smooth, the maximum tension can be calculated according to Muller et al. (1986) as follows:

$$p_{max} = \frac{0.4}{3\pi\kappa} \left(\frac{5}{4} \pi \rho_p V_s^2 \kappa \right)^{\frac{1}{5}}, \left[\frac{\text{N}}{\text{m}^2} \right] \quad (5.2.12)$$

where $\kappa = \frac{1 - \mu_m^2}{E_m}$. The values of μ_m and E_m for the given flat plate are

presented in Chapter 4. The area of the contact zone in the given case is calculated as follows:

$$S_z = \pi l_{el} r_p \cdot 10^{-4}, [\text{m}^2] \quad (5.2.13)$$

where r_p is the radius of a particle, l_{el} is the approach of the centre of a spherical particle and the surface occurred for the elastic collision. Here the

particles are assumed to be spheric. According to Muller et al. (1986) the expression for l looks like:

$$l_{el} = r_p \left(\frac{5}{4} \pi \rho_p V_s^2 \kappa \right)^{\frac{2}{5}} \cdot 10^{-2}, [\text{m}] \quad (5.2.14)$$

Substituting the expressions for l_{el} , S_z and p_{max} into Eq. (5.2.11) one can obtain:

$$F_{el} = \frac{4}{3} \frac{r_p^2}{\kappa} \left(\frac{5}{4} \pi \rho_p V_s^2 \kappa \right)^{\frac{3}{5}} \cdot 10^{-5} = K_{el} r_p^2 V_s^{\frac{6}{5}} \cdot 10^{-5}, [\text{N}] \quad (5.2.15)$$

where $K_{el} = \frac{4}{3\kappa} \left(\frac{5}{4} \pi \rho_p \kappa \right)^{\frac{3}{5}}$ is the constant generally determined by the physical properties of materials of the surface and the particles. In the given specific case K_{el} is determined only by the properties of the particles. The surface is assumed to be perfectly solid that slightly understates the deposition intensity.

The aerodynamic drag force F_{ad} that causes the blowing-off of a particle from the surface is calculated according to Loicjanski (1987) as follows:

$$F_{ad} = C_x \rho S_p \frac{U_d^2}{2} \quad (5.2.16)$$

The flow velocity near the centre of a particle is substantially small, and the particle Reynolds number $Re_p \ll 1$, and according to Schlichting (1974) for the Stokes streamlining:

$$C_x = \frac{24}{Re_p} \quad (5.2.17)$$

Hence, the expression for the aerodynamic drag force can be rewritten as follows:

$$F_{ad} = 6\pi \nu \rho U_d r_p \quad (5.2.18)$$

The flow velocity near the centre of a particle U_d can be calculated according to Schlichting (1974) for the laminar boundary layer as follows:

$$U_d = U_\infty \left(2 \frac{y}{\Delta_{l_x}} - \frac{y^2}{\Delta_{l_x}^2} \right) \quad (5.2.18)$$

where y is the transverse coordinate of the boundary layer, Δ_{l_x} is the thickness of the laminar boundary layer calculated by Eq. (2.3.1).

Substituting the expressions for F_{el} and F_{ad} into Eqs. (5.2.9) and (5.2.10) one can obtain:

$$P_A = 1 - a - b \lg \left(K_{el} r_p^2 V_s^{\frac{6}{5}} \right) \quad (5.2.19)$$

$$P_{bl} = a + b \lg \left(\frac{6}{\chi} \pi \nu \rho U_d r_p + K_{el} r_p^2 V_s^{\frac{6}{5}} \right) \quad (5.2.20)$$

Then, after substituting the expressions for P_A and P_{bl} into Eq. (5.2.8) one can calculate the probability of entrainment of the particles by the surface P_{en} .

Finally, applying Eq. (5.2.3) one can obtain the intensity of the particles deposition in the given cross-section of the streamlined surface. The velocity of the particles normal to the surface V_{sw} and particle mass concentration C_w , occurred immediately close to the surface of the flat plate, were obtained from the calculations by the mathematical model of the two-phase laminar boundary layer, which was described in Chapter 3.

The above described method of the calculation was repeated for the considered particles sizes $\delta_p = 12, 23$ and $32 \mu\text{m}$ for the flow velocity 1.5 and 3 m/s.

The total uncertainty of the given technique was caused by the uncertainty of determination of coefficients a and b (see Chapter 4), which was less 15%.

5.3. Results And Discussion.

Figures 5.3.1 and 5.3.2 show the calculated distributions of the probability of entrainment P_{en} of the particles by the surface along the plate surface. Here the probability is presented versus the Reynolds number Re_x for the more convenience.

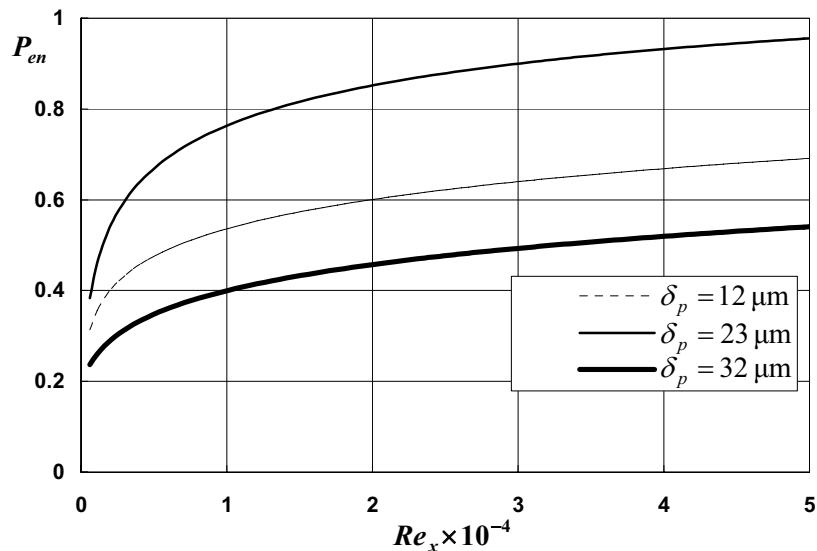


Figure 5.3.1 The entrainment probability of the particles for the flow velocity $U_\infty = 1.5 \text{ m/s}$

It is evident that the probability of entrainment by the plate surface is appreciably higher for the $23 \mu\text{m}$ particles as compared with other particles. This

can be explained by the fact that the probability of adhesion P_A of the 23 μm particles is much more than the probability of the blowing-off that arises from the predominance of the adhesive forces over the forces which determine the elastic rebound from the surface and the blowing-off.

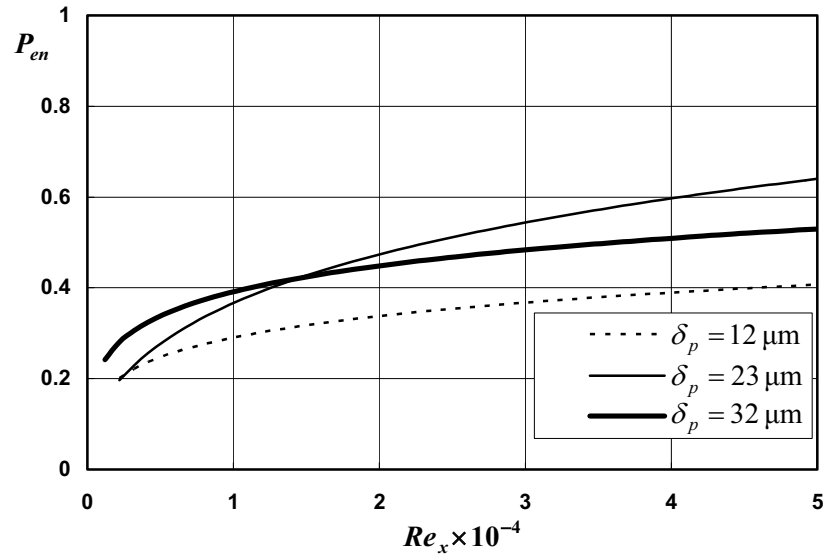


Figure 5.3.2 The entrainment probability of the particles for the flow velocity $U_\infty=3$ m/s

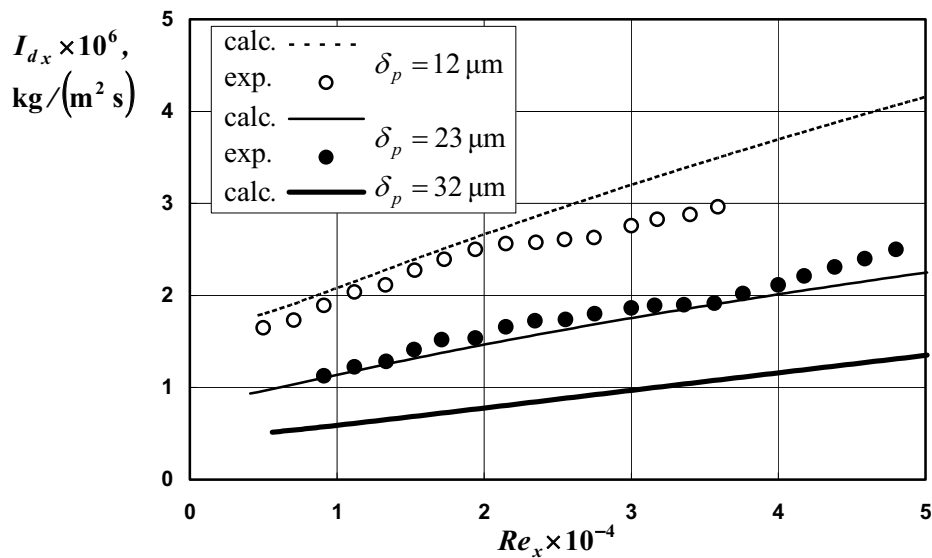


Figure 5.3.3 The comparison of the calculated and the experimental particles deposition for the flow velocity $U_\infty=1.5$ m/s

However, analysing the calculated distributions of the deposition intensity along the plate (see Figures 5.3.3 and 5.3.4) one can see that though the entrainment probability of the 23 μm particles is much more than for the 12 and

32 μm particles, the deposition intensity of the 12 μm particles is substantially larger, especially for the flow velocity 1.5 m/s. This arises from their appreciably higher concentration taken place immediately near the plate surface (see Figures 2.4.3 and 3.4.1).

Figures 5.3.3 and 5.3.4 demonstrate a satisfactory agreement between the experimental and calculated deposition intensity for the 12 and 23 μm particles.

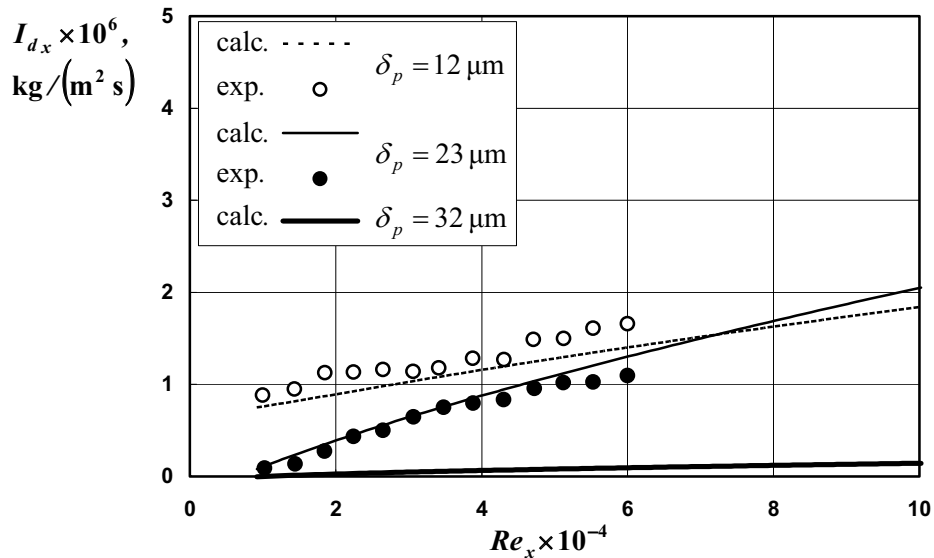


Figure 5.3.4 The comparison of the calculated and experimental particles deposition for the flow velocity $U_\infty = 3 \text{ m/s}$

Unfortunately, the obtained experimental data are not enough to derive the most reliable correlation for the prediction of the particles deposition for the wide range of the operating conditions. Therefore, there is some discrepancy between the distributions of the deposition obtained by the experiments and by the proposed calculation technique. This discrepancy can be attributed to the neglect of the microphysics of adhesion, e.g. the influence of the electric charges of the particles and surface, as well as the ambient conditions (humidity, temperature, chemistry). These factors are planned to be taken into account for the further investigations of the particles deposition.

But, in whole, though the given technique does not claim to be the comprehensive one, it can be applied with confidence for the calculation of the amount of various fine solid particles deposited from the two-phase aerosol flows for the conditions of the laminar flow past different flat surfaces which operate in various industrial and natural applications.

CONCLUSIONS

The results of the experimental and theoretical investigations on the deposition of solid particles from the aerosol flow in the laminar flat-plate boundary layer are reported and summarized in the given thesis.

The next topics were under investigation:

- the behaviour of fine solid aerosol particles in the laminar flat-plate boundary layer and the influence of parameters of the isothermal aerosol flow on the particles deposition on the plate,
- the adhesive properties of the pair “particle-surface”,
- the elaboration of the estimation technique of the particles deposition at the flat surface based on the integrated approach for this phenomenon.

The experimental set-up included the disconnected vertical two-phase wind-channel was developed and built up for these investigations. This set-up enabled to measure the distributions of the particle mass concentration and velocity inside the laminar flat-plate boundary layer by the techniques of the laser diagnostics.

The mathematical model was elaborated for the adequate description of the behaviour of the aerosol particles in the laminar flat-plate boundary layer.

The test rig was designed for the ascertainment of the adhesive properties of particles and surface.

The estimation technique was elaborated for the calculation of the intensity of the particles deposition at the flat plate based on the simultaneous account of the hydrodynamics of the flow past and the adhesive properties of the pair “particle-surface” with the applying of the probabilistic approach for the particles deposition.

The obtained results allow to draw the following conclusions:

1. The elaborated estimation technique takes into account both the hydrodynamics of the flow past the flat plate by the aerosol flow and the adhesive properties of the particles and the plate surface.
2. The particles deposition depends substantially on the behaviour of the aerosol particles in the laminar flat-plate boundary layer occurred near the surface, namely it is conditioned by the value of maximum of the distribution of the particle mass concentration taken place inside the boundary layer, maximum’s disposition relative to the surface as well as the gradient of the particle mass concentration inside the boundary layer.
3. The adhesion, which is taken place after the contact between a particle and surface and considered as the stochastic phenomenon, substantially determines the deposition amount of the aerosol particles at the streamlined flat plate.

The given technique can be applied for the assessment of amount of solid deposits at various surfaces streamlined by the air-solid particles aerosol flows, namely, the acting faces of the constructional elements of the solid fuel power plants, the pneumo-conveying devices as well as various gas-purifying equipment.

REFERENCES

1. Adhiwidjaja, I., Matsusaka, S., Tanaka, H., Masuda, H., 2000, Simultaneous phenomenon of particle deposition and reentrainment: Effects of surface roughness on deposition layer of striped pattern. *Aerosol Science and Technology*, Vol. 33, pp. 323-333.
2. Anderson, D. A., Tannehill, J. C., Pletcher, R. H., 1990, Computational fluid mechanics and heat transfer, Vols. 1 and 2, Mir, Moscow, (in Russian).
3. Asmolov, E. S., 1992, Particulate movement in the laminar boundary layer on a flat plate. *Proc. Acad. Sci. USSR Mekhanika Zhidkosti i Gaza*, Vol. 1, pp. 66-73, (in Russian).
4. Babukha, G. L., Shraiber, A. A., 1972, Interaction of particles of polydisperse material in two-phase flows. *Naukova Dumka*, Kiev, p. 175, (in Russian).
5. Botto, L., Lakehal, D., Narayanan, C., Soldati, A., 2003, Mechanisms of particle deposition in a fully developed turbulent open channel flow. *Phys. Fluids*, Vol. 15(3), pp. 763-775.
6. Bowling, R. A., 1986, A theoretical review of particle adhesion. *In: Mittal, K. L. (Ed.), Particles on Surfaces 1: Detection, Adhesion and Removal. Proc. Symposium Held in Conjunction with 17th Annual Meeting of the Fine Particles Society*, San Francisco, CA. Plenum Press, New York, pp. 129-142.
7. Braaten, D. A., Paw, U. K. T., Shaw, R. H., 1990, Particle resuspension in a turbulent boundary layer-observed and modeled. *J. Aerosol Sci.*, Vol. 21(5), pp. 613-628.
8. Braaten, D. A., Shaw, R. H., Paw, U. K. T., 1993, Boundary-layer flow structures associated with particle reentrainment. *Boundary-Layer Meteorol.* Vol. 65, pp. 255-272.
9. Brooke, J. W., Kontomaris, K., Hanratty, T. J., McLaughlin, J. B., 1992, Turbulent deposition and trapping of aerosols at a wall. *Phys. Fluids A* 4, pp. 825-834.
10. Chapman, S., Cowling, T. G., 1990, Mathematical theory of non-uniform gases: An account of the kinetic theory of viscosity, thermal conduction and diffusion in gases. Cambridge University Press, Cambridge, p. 423.
11. Cheng, W., Brach, R. M., Dunn, P. F., 2002, Surface roughness effects on microparticle adhesion. *J. Adhesion*, Vol. 78, pp. 929-965.
12. Cleaver, J. W., Yates, B., 1973, Mechanism of detachment of colloid particles from a flat substrate in turbulent flow. *J. Colloid Interface Sci.*, Vol. 44(3), pp. 464-474.
13. Cleaver, J. W., Yates, B., 1975, A sublayer model for deposition of the particles from turbulent flow. *Chem. Engng. Sci.*, Vol. 30, pp. 983-992.
14. Cleaver, J. W., Yates, B., 1976, The effect of re-entrainment on particle deposition. *Chem. Engng. Sci.*, Vol. 31, pp. 147-151.
15. Corn, M., 1961, The adhesion of solid particles to solid surfaces. *J. Air Pollut. Control Assoc.*, Vol. 11, pp. 566-575.

16. Crowe, C. T., Troutt, T. R., Chung, J. N., 1996, Numerical models for two-phase turbulent flows. *Ann. Rev. Fluid Mech.*, Vol. 28, pp. 11-43.
17. Cunningham, E., 1910, On the velocity of steady fall of spherical particles through fluid medium. *Proc. R. Soc. Lond.*, Vol. A83, pp. 357-365.
18. Davies, C. N., 1966, Deposition from moving aerosols. In: Davies, C. N. (Ed.), *Aerosol Science*, Academic Press, pp. 393-446.
19. Davis, R. H., Acrivos, A., 1985, Sedimentation of noncolloidal particles at low Reynolds numbers. *Ann. Rev. Fluid Mech.*, Vol. 17, pp. 91-118.
20. Fairchild, C. I., Tillery, M. I., 1982, Wind tunnel measurements of the resuspension of ideal particles. *Atmospheric Environment*, Vol. 16(2), pp. 229-238.
21. Fan, F.-G., Ahmadi, G., A model for turbulent deposition of particles in vertical ducts with smooth and rough surfaces. *J. Aerosol Sci.*, Vol. 24(1), pp. 45-64.
22. Fichman, M., Gutfinger, C., Pnueli, D., 1988, A model for turbulent deposition of aerosols. *J. Aerosol Sci.*, Vol. 19(1), pp. 123-136.
23. Friedlander, S. K., Johnstone, H. F., 1957, Deposition of suspended particles from turbulent gas streams. *Ind. Engng Chem.*, Vol. 49, pp. 1151-1156.
24. Frishman, F., Hussainov, M., Kartushinsky, A., Mulgi, A., 1997, Numerical simulation of a two-phase turbulent pipe-jet flow loaded with polydispersed solid admixture. *Int. J. Multiphase Flow*, Vol. 23(4), pp. 765-796.
25. Fuchs, N. A., 1955, The mechanics of aerosols. Acad. of Sci. of USSR Publishing House, 352 p., (in Russian).
26. Fuchs, N. A., 1989, The mechanics of aerosols. Dover Publ., New York, p. 375.
27. Hinze, J. O., 1975, Turbulence. McGraw-Hill, New York, p. 790.
28. Ibrahim, A. H., Dunn, P. F., Brach, R. M., 2003, Microparticle detachment from surfaces exposed to turbulent air flow: controlled experiments and modelling. *J. Aerosol Sci.*, Vol. 34(6), pp. 765-782.
29. Ingham, D. B., Yan, B., 1994, Re-entrainment of particles on the outer of a cylindrical blunt sampler. *J. Aerosol Sci.*, Vol. 25(2), pp. 327-340.
30. Johansen, S. T., 1991, The deposition of particles on vertical walls. *Int. J. Multiphase Flow*, Vol. 17(3), pp. 355-376.
31. Kline, S. J., Reynolds, W. C., Schraub, F. A., Runstadler, P. W., 1967, The structure of turbulent boundary layers. *J. Fluid Mech.*, Vol. 30, pp. 741-773.
32. Kottler, W., Krupp, H., Rabenhorst, H., 1968, Adhesion of electrically charged particles. *Z. Angew. Phys.* Vol. 24, pp. 219-223.
33. Kousaka, Y., Okuyama, K., Endo, Y., 1980, Re-entrainment of small aggregate particles from a plane surface by air stream. *Chem. Engng. Japan*, Vol. 13, pp. 143-147.
34. Kravtsov, M. V., 1968, Drag to the free steady motion of sphere in viscous medium. *J. Engng. Phys.*, Vol. 15(3), pp. 464-470, (in Russian).
35. Krupp, H., 1967, Particle adhesion theory and experiment. *Adv. Colloid Interface Sci.*, Vol. (1), pp. 111-239.

36. Lazaridis, M., Drossinos, Y., Georgopoulos, G., 1998, Turbulent resuspension of small nondeformable particles. *J. Colloid Interface Sci.*, Vol. 204(1), pp. 24-32.
37. Liu, B. Y. H., Agarwal, J. K., 1974, Experimental observation of aerosol deposition in turbulent flow. *J. Aerosol Sci.*, Vol. 5(2), pp. 145-148.
38. Loicjanski, L. G., 1987, Fluid and gas mechanics, Nauka, Moscow, p.840, (in Russian).
39. Löffler, F., 1977, Collection of particles in fibre filters. *In: Proceeding of 4th International Clean Air Congress.*, pp. 800-804.
40. Löffler, F., Muhr, W., 1972, Die Abscheidung von Feststoffteilchen und Tropfen an Kreiszyllindern infolge von Trägheitskräften. *Chem. Ing. Tech.*, Vol. (8), pp. 510-514.
41. Marchioli, C., Soldati, A., 2002, Mechanisms for particle transfer and segregation in a turbulent boundary layer. *J. Fluid Mech.*, Vol. 468, pp. 283-315.
42. Marchioli, C., Giusti, A., Salvetti, M. V., Soldati, A., 2003, Direct numerical simulation of particle wall transfer and deposition in upward turbulent pipe flow. *Int. J. Multiphase Flow*, Vol. 29(6), pp. 1017-1038.
43. Marcus, R. D., Leung, L. S., Klinzing, G. E., Rizk, F., 1997, Pneumatic conveying of solids. Chapman and Hall, New York, p 624.
44. Masironi, L. A., Fish, B. R., 1964, Direct observation of particle reentrainment from surfaces. *In: Fish, B. R. (Ed.), Surface contamination*, Tennessee, Pergamon Press, pp. 55-59.
45. Matsumoto, S., Saito, S. J., 1970, Monte Carlo simulation of horizontal pneumatic conveying based on the rough wall model. *Chem. Engng. Japan*, Vol. 3, pp. 223-230.
46. Matsusaka, S., Theerachaisupakij, W., Yoshida, H., Masuda, H., 2001, Deposition layers formed by a turbulent aerosol flow of micron and sub-micron particles. *Powder Technology*, Vol. 118, pp. 130-135.
47. McLaughlin, J. B., 1989, Aerosol particle deposition in numerically simulated turbulent channel flow. *Phys. Fluids A* 1, pp. 1211-1224.
48. Moffat, R. J., 1988, Describing the uncertainties in experimental results. *Exp. Thermal Fluid Sci.*, Vol. 1, pp. 3-17.
49. Muller, V. M., Mihovitch, N. S., Toporov, J. P., 1986, Contact electricity generating by the collisions of particles with rigid surface. *Colloid J.*, V. 48(4), pp. 728-740.
50. Niedra, J. M., Penny, G. W., 1965, Orientation and adhesion of particles. *IEEE Trans. Ind. Electron. Control Instrum*, IECI-12, pp. 46-50.
51. Nigmatulin, R. I., 1978, Fundamentals of mechanics of heterogeneous media. Nauka, Moscow, p. 336, (in Russian).
52. Osipsov, A. N., 1980, Structure of a laminar disperse-mixture boundary layer on a flat plate. *Proc. Acad. Sci. USSR Mekhanika Zhidkosti i Gaza*, Vol. 4, pp. 48-54, (in Russian).

53. Osipov, A. N., 1985, The boundary layer on the blunt body in the dust free stream. *Proc. Acad. Sci. USSR Mekhanika Zhidkosti i Gaza*, Vol. 5, pp. 99-107, (in Russian).
54. Osipov, A. N., Shapiro, E. G., 1988, The influence of fine solid admixture on a structure of the boundary layer for hypersonic streamlining of the blunt body. *Proc. Acad. Sci. USSR Mekhanika Zhidkosti i Gaza*, Vol. 5, pp. 55-62, (in Russian).
55. Ounis, H., Ahmadi, G., McLaughlin, J. B., 1991, Dispersion and deposition of Brownian particles from point sources in a simulated turbulent channel flow. *J. Colloid Interface Sci.*, Vol. 147(1), pp. 233-250.
56. Papavergos, P. G., Hedley, A. B., 1984, Particle deposition behavior from turbulent flows. *Chem. Engng. Res. Des.*, 1984, Vol. 62, pp. 275-295.
57. Pedinotti, S., Mariotti, G., Banerjee, S., 1992, Direct numerical simulation of particle behavior in the wall region of turbulent flows in horizontal channels. *Int. J. Multiphase Flow*, Vol. 18(6), pp. 927-941.
58. Penny, G. W., Klingler, E. H., 1962, Constant potential and the adhesion of dust. *IEEE Trans. Commun. Electron*, Vol. 81, pp. 200-205.
59. Phares, D. J., Smedley, G. T., Flagan, R. C., 2000, Effect of particle size and material properties on aerodynamic resuspension from surfaces. *J. Aerosol Sci.*, Vol. 31(11), pp. 1335-1353.
60. Ranade, M. B., 1987, Adhesion and removal of fine particles on surfaces. *Aerosol Science and Technology*, Vol. 7, pp. 161-176.
61. Rashidi, M., Hetsroni, G., Banerjee, S., 1990, Particle-turbulence interaction in a boundary layer. *Int. J. Multiphase Flow*, Vol. 16(6), pp. 935-949.
62. Reeks, M. W., Hall, D., 2001, Kinetic models for particle resuspension in turbulent flows: theory and measurement. *J. Aerosol Sci.*, Vol. 32(1), pp. 1-31.
63. Richardson, J. F., McLeman, M., 1960, Pneumatic conveying. *Trans. Inst. Chem. Engrs.*, Vol. 38, pp. 257-266.
64. Roache, P. J., 1980, Computational Fluid dynamics. Mir, Moscow, p. 616, (in Russian).
65. Robinson, S. K., 1991, Coherent motions in the turbulent boundary layer. *Ann. Rev. Fluid Mech.*, Vol. 23, pp. 601-639.
66. Rumpf, H., 1970, Zur Theorie der Zugfestigkeit von Agglomeraten bei Kraftübertragung an Kontaktpunkten. *Chemie Ingenieur Technik*, Vol. 42, pp. 538-540.
67. Saffman, P. G., 1965, The lift on a small sphere in a slow shear flow. *J. Fluid Mech.*, Vol. 22, pp. 385-400.
68. Schlichting, G., 1974, Theory of boundary layer. Nauka, Moscow, p. 712, (in Russian).
69. Shams, M., Ahmadi, G., Rahimzadeh, H., 2000, A sublayer model for deposition of nano- and micro-particles in turbulent flows. *Chem. Engng. Sci.*, Vol. 55, pp. 6097-6107.

70. Shraiber, A. A., Miliytin, V. N., Yatsenko, V. P., 1980, Hydromechanics of two-component flows with solid polydisperse substance. Naukova Dumka, Kiev, p. 249, (in Russian).
71. Smedley, G. T., Phares, D. J., Flagan, R. C., 1999, Entrainment of fine particles from surfaces by gas jets impinging at normal incidence. *Experiments in Fluids*, Vol. 26, pp. 324-334.
72. Soltani, M., 1993, Mechanisms of particle removal due to turbulent flow or substrate acceleration. M.Sc. Thesis, Clarkson University.
73. Soltani, M., Ahmadi, G., 1994, On particle adhesion and removal mechanisms in turbulent flows. *J. Adhesion Sci. Technol.* Vol. 8, pp. 763-785.
74. Soltani, M., Ahmadi, G., 1995, Direct numerical simulation of particle entrainment in turbulent channel flow. *Phys. Fluids*, Vol. 7(3), pp. 647-657.
75. Soo, S. L., 1971, Fluid dynamics of multiphase systems. Blaisdell, Waltham, pp. 524.
76. Spokoinij, F. E., Gorbis, Z. R., 1981, The features of sedimentation of finely divided particles from refrigerated gas flow onto the cross-streamlined heat-exchange surfaces. *Teplofizika Visokich Temperatur*, Vol. 19, pp. 182-199, (in Russian).
77. Squires, K. D., Eaton, J.K., 1991a, Measurements of particle dispersion obtained from direct numerical simulations of isotropic turbulence. *J. Fluid Mech.*, Vol. 226, pp. 1-35.
78. Squires, K. D., Eaton, J.K., 1991b, Preferential concentration of particles by turbulence. *Phys. Fluids A* 3, pp. 1169-1178.
79. Stokes, G. G., 1851, On the effect of internal friction of fluids on the motion of a pendulum. *Transactions of the Cambridge Philosophical Society*, Vol. 9, pp. 8-16.
80. Stulov, V. P., 1979, About the equations of the laminar boundary layer in the two-phase medium. *Proc. Acad. Sci. USSR Mekhanika Zhidkosti i Gaza*, Vol. 1, pp. 51-60, (in Russian).
81. Taheri, M., Bragg, G. M., 1992, A study of particle resuspension in a turbulent flow using a Preston tube. *Aerosol Sci. Technol.*, Vol. 16, pp. 15-20.
82. Theerachaisupakij, W., Matsusaka, S., Akashi, Y., Masuda, H., 2003, Reentrainment of deposited particles by drag and aerosol collision. *J. Aerosol Sci.*, Vol. 34(3), pp. 261-274.
83. Tsirkunov, J. M., 1993, The simulation admixture motion in the tasks two-phase fluid dynamics. The effects of the boundary layer. *Modelirovanije v mehanike*, Vol. 2, pp. 151-193, (in Russian).
84. Vainstein, P., Ziskind, G., Fichman, M., Gutfinger, C., 1997, Kinetic model of particle resuspension by drag force. *Phys. Rev. Lett.*, Vol. 78, pp. 551-554.
85. Varaksin, A. Yu., 2003, Turbulent gas flows with solid particles. Nauka, Moscow, p. 192, (in Russian).

86. Wang, J., Levy, E. K., 2003, Particle motions and distributions in turbulent boundary layer of air-particle flow past a vertical flat plate. *Exp. Thermal Fluid Sci.*, Vol. 27, pp. 845-853.
87. Wen, H. Y., Kasper, G., 1989, On the kinetics of particle reentrainment from surfaces. *J. Aerosol Sci.*, Vol. 20(4), pp. 483-498.
88. Wood, N. B., 1981, A simple method for calculation of turbulent deposition to smooth and rough surfaces. *J. Aerosol Sci.*, 1981, Vol. 12(3), pp. 275-290.
89. Wu, Y., Cliff, I. D., Russell, A. G., 1992, Controlled wind tunnel experiments for particle bounce-off and resuspension. *Aerosol Science and Technology*, Vol. 17, pp. 245-262.
90. Young, J., Leeming, A., 1997, A theory of particle deposition in turbulent pipe flow. *J. Fluid Mech.*, Vol. 340, pp. 129-159.
91. Yung, B. P. K., Merry, H., Bott, T. R., 1989, The role of turbulent bursts in particle re-entrainment in aqueous systems. *Chem. Engng. Sci.*, Vol. 44, pp. 873-882.
92. Zaichik, L. I., Alipchenkov, V. M., 2001, A statistical model for transport and deposition of high-inertia colliding particles in turbulent flow. *Int. J. Heat Fluid Flow*, Vol. 22, pp. 365-371.
93. Zhang, H., Ahmadi, G., 2000, Aerosol particle transport and deposition in vertical and horizontal turbulent duct flows. *J. Fluid Mech.*, Vol. 406, pp. 55-80.
94. Zhang, H., Ahmadi, G., Fan, F.-G., McLaughlin, J. B., 2001, Ellipsoidal particles transport and deposition in turbulent channel flows. *Int. J. Multiphase Flow*, Vol. 27(6), pp. 971-1009.
95. Zimon, A. D., 1976, Adhesion of dust and powders. Khimija, Moscow, p 432, (in Russian).
96. Ziskind, G., Fichman, M., Gutfinger, C., 1995, Resuspension of particulates from surfaces to turbulent flows – Review and analysis. *J. Aerosol Sci.*, Vol. 26(4), pp. 613-644.

ORIGINAL PUBLICATIONS

ARTICLE I

Hussainov, M., Kartushinsky, A., Mulgi, A., Shcheglov, I., Tisler, S., 1994, Properties of solid particle distribution in two-phase laminar boundary layers of various shapes and particle sedimentation. *Proc. Estonian Acad. Sci. Physics Mathematics*, Vol. 43(4), pp. 237-249.

PROPERTIES OF SOLID PARTICLE DISTRIBUTION IN TWO-PHASE LAMINAR BOUNDARY LAYERS OF VARIOUS SHAPES AND PARTICLE SEDIMENTATION

Medhat HUSSAINOV, Alexander KARTUSHINSKY, Anatoly MULGI,
Igor SHCHEGLOV, and Sergei TISLER

Eesti Teaduste Akadeemia Energeetika Instituut (Institute of Energy Research, Estonian Academy of Sciences), Paldiski mnt. 1, EE-0001, Tallinn, Eesti (Estonia)

Received June 22, 1994; revised July 7, 1994; accepted November 14, 1994

Abstract. The behaviour of solid particles in two-phase laminar boundary layer for various streamlining shapes (flat plate, curved surface and cone) was experimentally investigated. The velocity distributions of gas and particles as well as particle mass concentration were measured in the vicinity of surfaces. Particle sedimentation on surfaces was measured simultaneously. Parameters of the experiments were the following: free stream velocity – 1.5 and 3 m/s; particle size – 12, 23 and 32 μm ; particle mass concentration – 0.01 kg/m^3 .

Key words: dispersed phase, streamlining of various shapes, distributions of particle velocity and mass concentration, dust sedimentation on surfaces.

1. INTRODUCTION

A large number of technological and natural processes is bound with the motion of solid particles in gaseous flows, e.g., combustion of solid fuels, processes in scrubbers, pneumotransport, diffusion of solid suspension in the atmosphere. These processes are accompanied by the deposition of solid particles on the working surfaces of various devices.

The process of sedimentation on a body surface streamlined by two-phase flow, is substantially stipulated by the particle motion and their distribution near the wall. The object of our experimental investigation was to obtain data for building and improving a numerical model of particle sedimentation. This model may be applied for sedimentation prediction on real objects for the conditions differing from those in the laboratory.

2. AERODYNAMICAL BENCH

The experiments were carried out in a disconnected vertical two-phase wind-channel with an open working space (Fig.1).

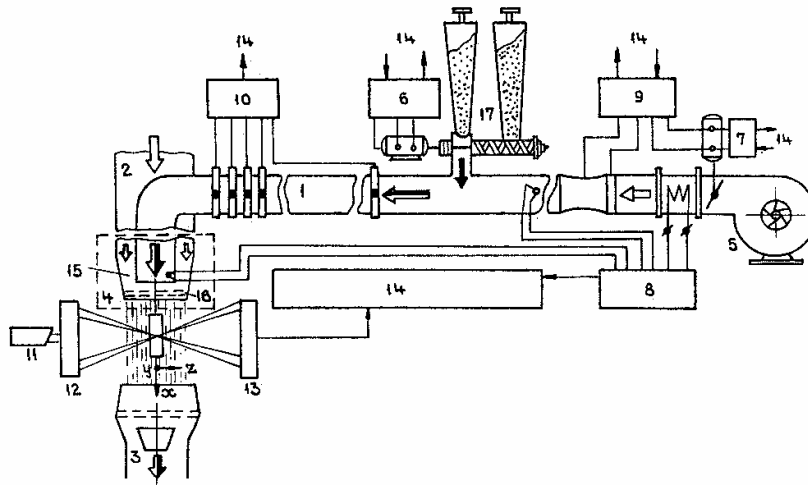


Fig. 1. Aerodynamical bench: 1 – main channel; 2 – channel of accompanying pure air flux; 3 – a dust suck-out channel; 4 – a device for the formation of the given flow field; 5 – blower; 6 – dispersed phase dosimeter; 7 – pure air dosimeter; 8 – thermocontroller; 9 – flowmeter; 10 – pressure converter; 11 – He-Ne laser; 12 – sending optics; 13 – receiving optics; 14 – registering, processing and controlling system; 15 – confuser; 16 – system of grates; 17 – particle screw feeder.

The aerodynamical bench consisted of the following parts: main channel (Pos. 1) for two-phase flow formation and transportation; a channel of accompanying pure air flux (Pos. 2); a device (Pos. 4) for the formation of a flow field with the given parameters in the working space of the wind-channel; a dust suck-out channel (Pos. 3). Besides, the aerodynamical bench contained various power (Pos. 5, 17), processing (Pos. 6, 7, 8), controlling (Pos. 9, 10) and measuring (Pos. 11, 12, 13, 14) equipment, which provided the formation and transport of two-phase flow with the given parameters.

The wind-channel started functioning by injecting solid suspension into the open working space with its following ejection through the diffuser. Two-phase flow was formed by the forming device (Pos. 4) consisting of a cylindrical tube with a diameter of 100 mm and a length of 3 m, which was installed along the axis of the forming device for the input of two-phase admixture. After the exit from the cylindrical tube and passing through the system of grates (Pos. 16), the formed two-phase suspension expanded and entered the open working space supported by the flux of pure air on either side. Three grates with the mesh sizes of 0.63, 0.315 and 0.315 mm and with the distance of 12 mm between them, are used for smoothing the parameters of the inflow, i.e., a uniform free stream was formed. Uniformity of the two-phase flow with the given parameters was obtained by varying pure air flow in one of the channels, two-phase flow in another and in the diffuser.

3. EXPERIMENTAL CONDITIONS

A flat plate, curved and conical surfaces were used as models for investigation (see Figs. 2, 3). The models had the following dimensions:

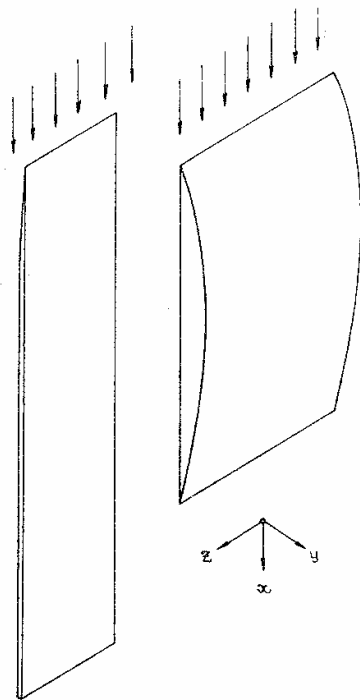
- stainless steel flat plate - length 500 mm, width 100 mm, thickness 2 mm;
- aluminium alloy model with a curved surface - length 320 mm, the curvature radius 300 mm, thickness in middle cross section 50 mm, width 170 mm;
- four aluminium alloy cones with the values of vertex angle of 30, 45, 60 and 90 degrees and with the base diameter of 100 mm.

The surface quality was characterized by the height of unevennesses of the surface profile in ten points, which equaled 6.3 mkm for all the models. This value corresponds to the N14 of surface quality according to the international classification.

Each model was installed vertically in the working space of the wind-channel with the help of a special holder. The design of the holders enabled to vary the value of the attack angle.

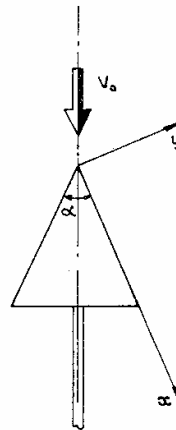
Electrocorundum powders with the density of 3950 kg/m^3 were used with the average particle sizes 12, 23 and 32 mkm. The deviation from the average size did not exceed 30%.

The main parameters of laboratory tests (flow velocity V_0 , particle size δ_p , particle mass concentration C_0) were stipulated by the steady



← Fig. 2. The flat plate and the curved surface.

Fig. 3. The cone model.



formation of a two-phase laminar boundary layer on streamlining models and by uniform inflow of the dispersed phase into the working space of the wind-channel. The values of flow velocity V_0 were 1.5 and 3 m/s. The value of particle mass concentration C_0 was 0.01 kg/m³ for the flat plate and curved surface streamlining and 0.0044 kg/m³ for the conical surface streamlining.

4. MEASURING OF VELOCITY AND PARTICLE MASS CONCENTRATION

The distributions of local averaged parameters (velocity and particle mass concentration) of two-phase flow in the vicinity of various shapes were measured with the help of an optic-electronic system which included a specially devised laser Doppler anemometer (LDA) and a laser concentration measurer (LCM) for determining relative particle concentration with the aid of methods described in [1].

The LDA consists of two channels (each channel for the concrete phase of dispersed flow), the sending sections of the LDA-channels are combined. One of the LDA beams is used in the optic scheme of the LCM. The peculiarity of the LDA is the operative changing of the direction of the sensitivity vector, i.e., the direction of a measured projection of the particle velocity vector. Furthermore, the changing of the direction of the sensitivity vector does not change effectiveness of laser beam splitting and it is not necessary to adjust the optical LDA scheme again.

The receiving section of the optic-electronic system consists of two LDA registration units for scattered radiation and the LCM registration units for scattered and attenuated radiation. Each of the LDA receiving units can pick the signals of particles of a certain size by means of changing the geometrical conditions for receiving, and by varying the sensitivity of the photoelectronic multiplier.

Signals of instantaneous particle velocities from the LDA photoreceivers enter the channels of carrier and dispersed phases of the processing system, which contain counters described by Pavlovski et al. [2]. These counters process the Doppler signals from the particles of corresponding phase of the dispersed flow.

With the help of special imitator the tuning of the measuring channel for the micron-size particles forming carrier-gas flow is realized in the direction of small receiving angles, where the diffraction component of scattered laser radiation is prevalent. Here, according to [3], the signals from fine particles are picked out distinctly independently of their physical nature. With that it satisfies the condition

$$m > m_p,$$

where $m = A \sim / A =$; m_p is the threshold value of the counter; $A \sim$ is the Doppler component of the signal; $A =$ is the constant component of the signal.

In this channel the selection of signals proceeding from the particles of dispersed phase is carried out both by amplitude when signals are neglected as signals of overloading [4], and by modulating the depth ($m < m_p$) automatically with the help of the counter.

The conditions for registering signals only from the dispersed phase particles are created in the measuring channel of the dispersed phase by varying the receiving geometry and by reducing photoreceiver sensitivity. For processing the signals, the Doppler component is picked out, and amplified to the level of

$$A_{\sim S} > U_p,$$

where $A_{\sim S}$ is the Doppler component of a signal from the dispersed phase particles; U_p is the working threshold of the counter and comes to the input of the counter.

The LCM receiving system for the direct attenuated beam is oriented to the probing beam, while the LCM registration system of scattered radiation in the measuring volume is oriented, under some small angle, to the probing beam. The system "lens-apertures" which forms the field of vision of the device in the channel of scattered light, permits to choose the measuring fields proceeding from the requirements of the experiment.

The optic-electronic system was installed on a special coordinate device controlled by PC, which permitted to scan the flow continuously or interruptedly in three directions.

Fig. 4 depicts the distribution of the particle mass concentration inside the two-phase boundary layer in the case of the streamlining of a flat plate installed at zero attack angle into the aerosol flow for the particle size of 32 mkmm and flow velocity of 1.5 m/s in various cross-sections downstream. Here and below the values of the velocity and particle mass concentration related to the ones in free stream are laid along the abscissa

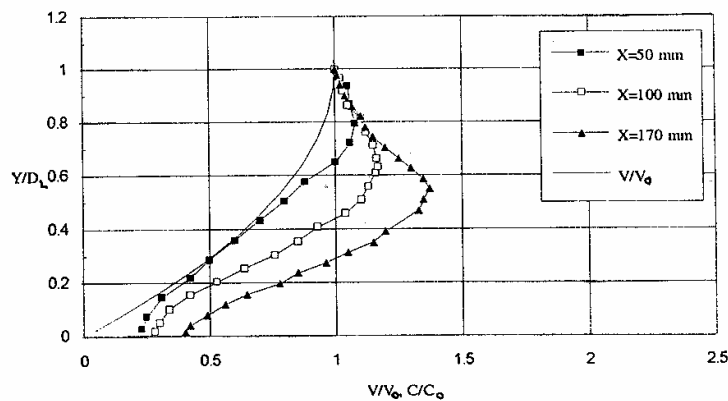


Fig. 4. Axial velocity of gas V/V_0 and concentration C/C_0 profiles on a flat plate. $\delta_p = 32$ mkmm, $V_0 = 1.5$ m/s.

axis ($V/V_0, C/C_0$); transversal coordinate of the boundary layer Y related to the theoretical thickness of laminar boundary layer D_L is laid along the ordinate axis. It is evident that the distribution of the particle mass concentration has its maximum within the two-phase boundary layer. The value of this maximum grows downstream while it immerses into the boundary layer.

Fig. 5 depicts the distribution of the particle mass concentration in the cross-section of 100 mm downstream for various values of the particle size and flow velocity of 1.5 m/s. The attack angle is zero. One can see that the value of the concentration maximum for fine particles is greater than that for rougher particles.

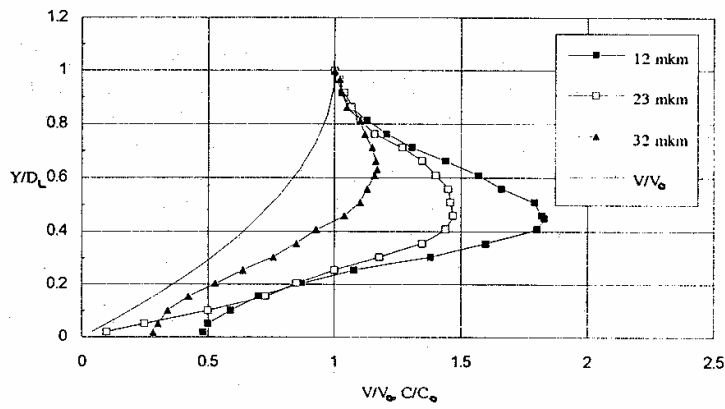


Fig. 5. Axial velocity of gas V/V_0 and concentration C/C_0 profiles on a flat plate. $V_0 = 1.5$ m/s, $X = 100$ mm.

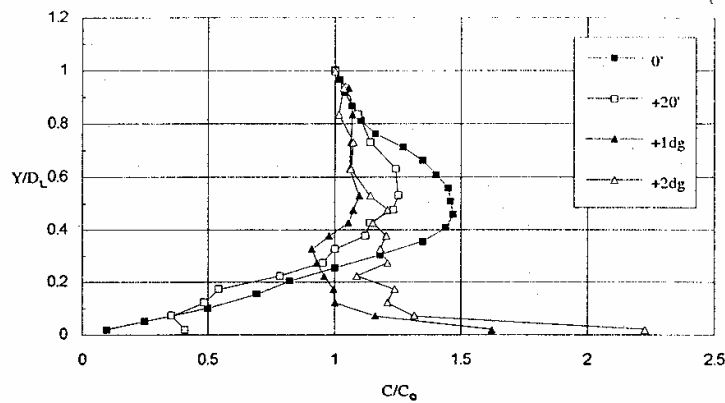


Fig. 6. Concentration C/C_0 profiles on a flat plate. $\delta_p = 23$ mkm, $V_0 = 1.5$ m/s, $X = 100$ mm.

The transformation of the concentration profile caused due to changing the attack angle is represented in Fig. 6 in the cross-section of 100 mm for the particle size of 23 mkm and flow velocity of 1.5 m/s. Substantial transformation takes place with changing the value of the attack angle from 0 to 1 degree. The subsequent increasing of the attack angle causes the concentration growth in the vicinity of a flat plate (Fig. 6).

The distributions of the particle mass concentration in various cross sections of the curved surface for the particle size of 23 mkm and flow velocity of 3 m/s is depicted in Fig. 7. The concentration profile is transformed along the surface. In upper cross sections the concentration maximum is located in the vicinity of the surface, but downstream it moves away from the surface and its value decreases (Fig. 7).

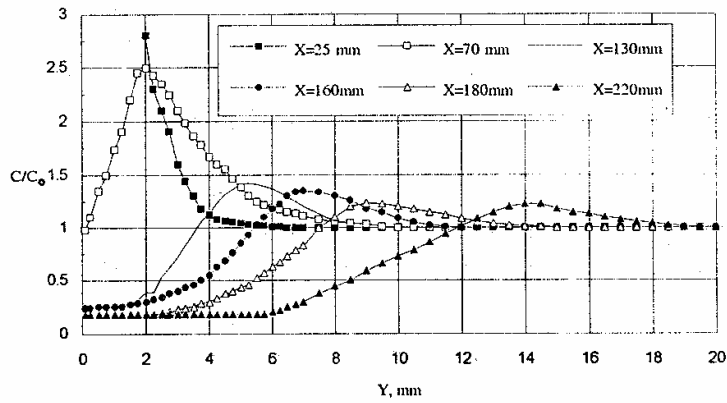


Fig. 7. Concentration C/C_0 profiles on the curved surface. $\delta_p = 23$ mkm, $V_0 = 3$ m/s.

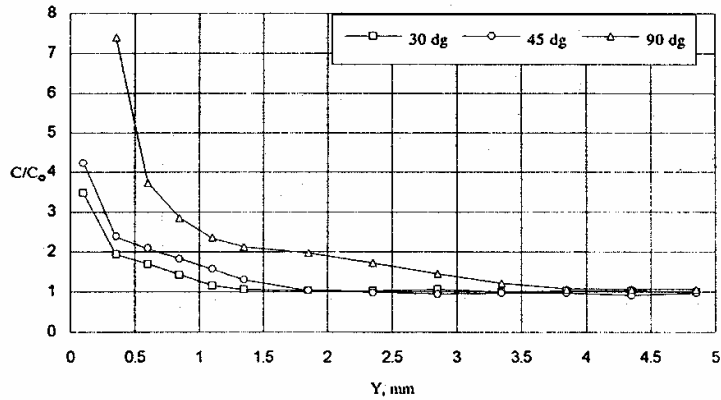


Fig. 8. Distribution of particle mass concentration C/C_0 near the wall for different vertex angles α of cone.

Fig. 8 represents the distributions of the particle mass concentration in the vicinity of conical surface for various values of the vertex angle, the particle size of 23 mkm and flow velocity of 1.5 m/s. Here concentration profiles have maxima near the conical surface. The increase of the value of the attack angle results in the growth of the concentration.

Figs. 9 and 10 show the distributions of tangential dV_t and normal dV_n velocity lag in the cross section of 50 mm for various values of the cone vertex angle. The velocity lag slightly depends on the attack angle outside the boundary layer. But inside it the increase of attack angle leads to a decrease in the tangential lag and the growth of the normal lag.

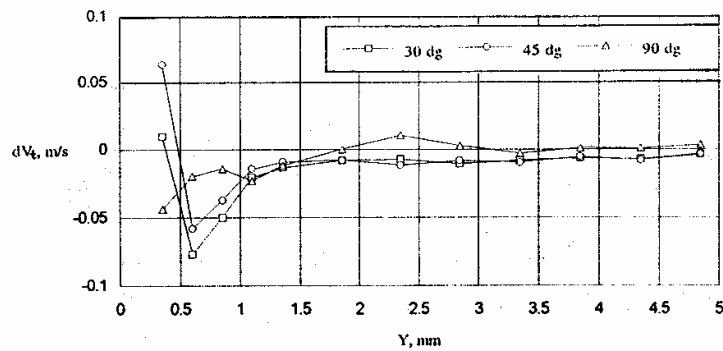


Fig. 9. The tangential velocity lag dV_t for different vertex angles α of cone.

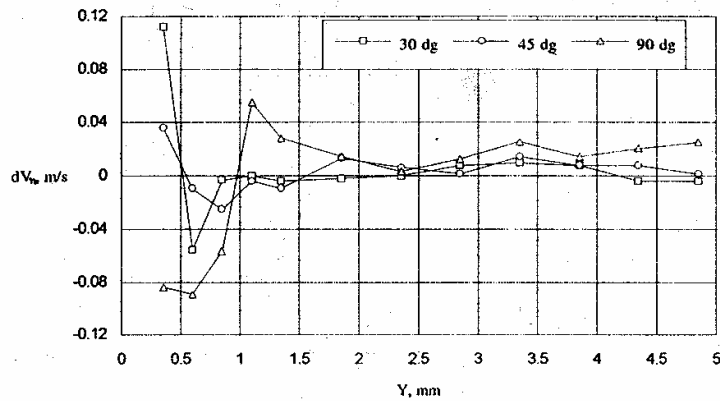


Fig. 10. The normal velocity lag dV_n for different vertex angles α of cone.

5. PARTICLE SEDIMENTATION MEASURING

The amount of sedimented particles and their distribution along the surfaces were measured by a special weighing method.

A special bench for removing dust from the surface of the flat-plate and curved surface is shown in Fig. 11. After blowing by two-phase flow during the given period of time t the model (Pos. 4) with sedimented dust on its surface was installed on the fixed plate (Pos. 3) by means of a holder (Pos. 2). The sedimented particles were removed from the surface with the help of a head (Pos. 1), which could move along a rod (Pos. 5). The removed dust fell down on the surface of the film specimen (Pos. 6), which was installed on the slab (Pos. 7). The mass of the specimen had been measured beforehand. The width of the head determined the width of the stripe on the model surface from which the particles were removed. The width of the head was 3 mm. Then the film specimen with dust on its surface was weighed. The difference of its masses with and without dust was mass M of the particles sedimented on the model surface in the given cross section during the given period of time t . The dimensionless intensity of particle sedimentation I was determined as

$$I = \frac{M}{V_0 C_0 S t},$$

where V_0 , C_0 , are the parameters of free stream; S – area of the stripe on the model surface from which dust was removed.

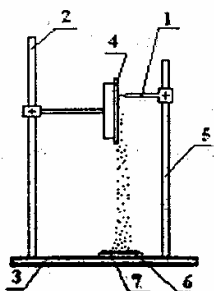


Fig. 11. Bench for dust removing from the flat plate and the curved surface.

Fig. 12 depicts a bench for dust removing from the cone surface. After blowing by two-phase flow, the model (Pos. 4) was installed on the shaft of an electric motor (Pos. 2) by means of a sleeve (Pos. 3). The model was rotated slowly by hand. A special head (Pos. 6), which was shifted by means of the coordinate device (Pos. 7, 8), removed sedimented particles from the model surface. The particles fell down on the surface of the film specimen (Pos. 10), which was installed on the slab (Pos. 9). The width of pure stripes on the model surface was determined by the width of the head and was equal to 3 mm. The subsequent determination of the

sedimentation intensity I was similar to that in the case of the flat-plate and curved surface.

Fig. 13 shows that the sedimentation intensity for a flat plate installed at zero attack angle grows downstream, but it reduces with the growth in flow velocity and particle size. Here and below I is dimensionless sedimentation intensity; Re_x is the Reynolds number along the surface. Particle sedimentation substantially depends on the value of the attack angle (Fig. 14). It grows with the increase of the angle.

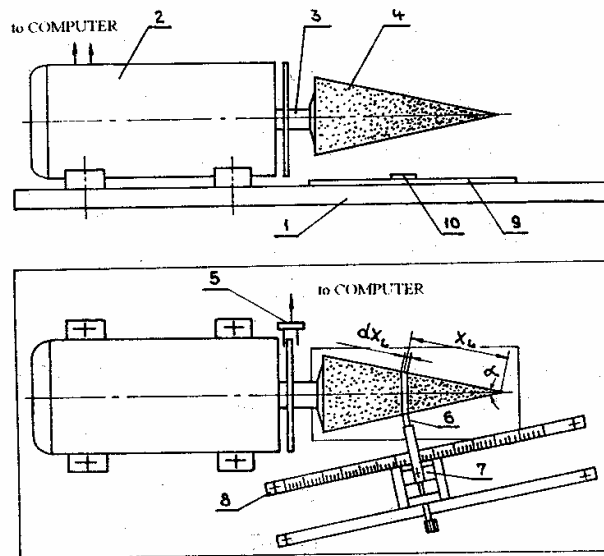


Fig. 12. Bench for dust removing from the cone surface.

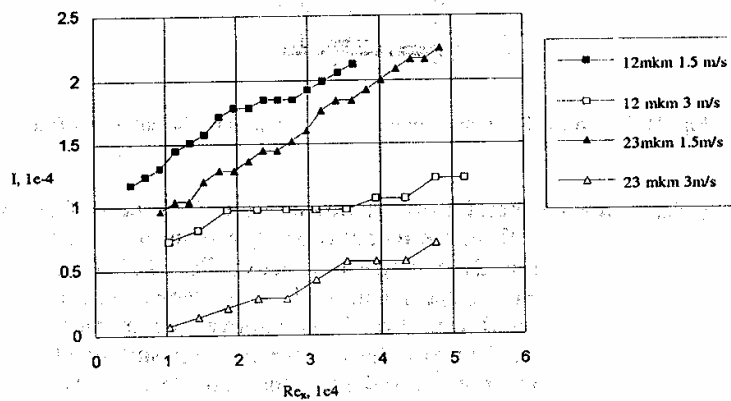


Fig. 13. Intensity of particle sedimentation I along the plate.

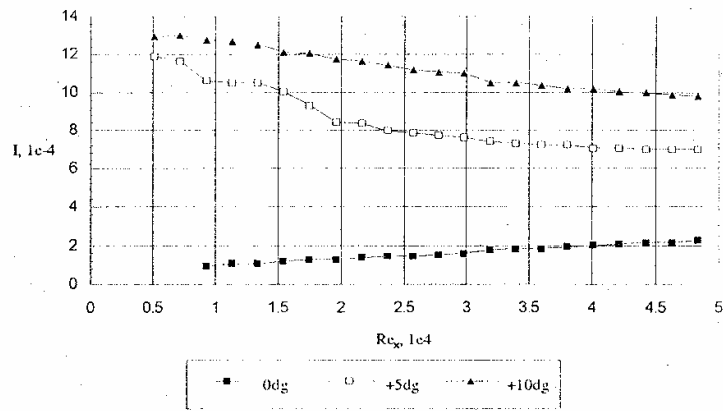


Fig. 14. Intensity of particle sedimentation I along the plate. $\delta_p = 23$ mkm, $V_0 = 1.5$ m/s.

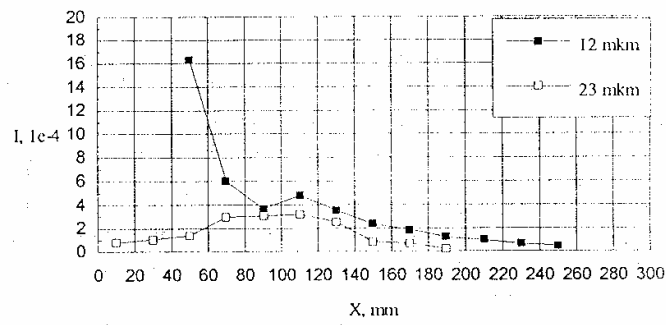


Fig. 15. Intensity of particle sedimentation I along the curved surface. $V_0 = 3$ m/s.

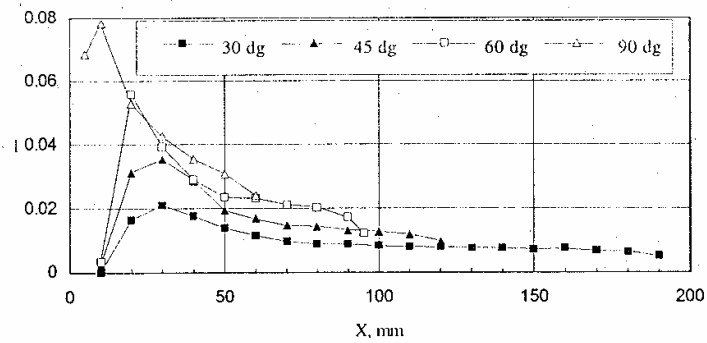


Fig. 16. Intensity of particle sedimentation I for different vertex angles α of cone.

Fig. 15 represents the dependence of particle sedimentation on their size in the case of curved surface streamlining.

The distributions of particle sedimentation with respect to the cone vertex angle are represented in Fig. 16. Intensity increases with the growth of the cone angle and the shift of its maximum towards the cone vertex (Fig. 16).

6. CONCLUSIONS

As our experimental investigations have shown, the sedimentation is very closely related to the particle motion near the wall. Thus, the mathematical prediction must consist of the criterial numbers that take into account particle motion and the dimensions of real objects and atmospheric conditions. To begin with the investigation, good approximation of numerical results and test data for laboratory conditions should be available. This data afford the sedimentation prediction under different conditions of further studies.

Summary

- the profile of the particle mass concentration has its maximum value inside the boundary layer. The maximum location and magnitude are defined by the following parameters: a) the coordinate X ; the maximum value of particle concentration increases and immerses downstream into the boundary layer; b) the particle size; the maximum value for fine particles is higher than that for rougher particles; c) the attack angle value; transformation from the concentration profile with its maximum inside the boundary layer to the maximum on the model surface results with the increase of the attack angle;
- particle sedimentation on a flat plate depends on flow velocity, also on particle size and the attack angle. The sedimentation is intensified with the reduction in flow velocity and particle size and with the growth of the attack angle;
- the particle concentration profile has its maximum in the vicinity of a curved surface; the maximum location and magnitude depends on the value of coordinate X discounted downstream from the model vertex. In the upper cross section the maximum is located near the surface and it shifts downstream from the surface with the decrease in its value;
- the particle sedimentation on the curved surface depends on the particle size, and for fine particles it is stronger than it is for rougher particles;
- in the vicinity of the cone surface the maximum of the particle mass concentration is located immediately on the surface;
- the distribution of the intensity of particle sedimentation on the cone surface has its maximum value in the vicinity of the vertex. The maximum value increases with the vertex angle.

REFERENCES

1. Злобин В.В., Розенштейн А. З. Ж. прикл. мех. и тех. физ., 1975, 1, 142–146.
2. Павловский Б. А., Заманский В. И., Семидетнов Н. В., Юрас С. Ф. Применение лазерных доплеровских анемометров в теплоэнергетике. ЛДНТП, Ленинград, 1989.
3. Картушинский А. И., Розенштейн А. З., Щеглов И. Н. Физические методы исследования прозрачных неоднородностей. МДНТП, Москва, 1987, 29–33.
4. Фришман Ф. А., Щеглов И. Н. В сб.: Лаатс М. К. (ред.) Турбулентные двухфазные течения и техника эксперимента. АН ЭстССР, Таллинн, 1985, 149–153.

TANKE LISANDI JAOTUS ERIKUJULISTE KEHADE LAMINAARSES PIIRIKIHIS JA KEHADE PINNAL

Medhat HUSSAINOV, Aleksander KARTUŠINSKI, Anatoli MULGI,
Igor ŠTŠEGLOV, Sergei TISLER

Ekspimentaalselt on uuritud erikujuliste kehade uhtmist kahefaasilise laminaarse voolusega. On määratud mõlema faasi kiirusjaotused ning osakeste kontsentratsioon piirikihis ja nende väljasadenemine kehade pinnal.

РАСПРЕДЕЛЕНИЕ ТВЕРДОЙ ПРИМЕСИ В ЛАМИНАРНОМ ПОГРАНИЧНОМ СЛОЕ НА ТЕЛАХ РАЗЛИЧНОЙ ФОРМЫ И ЕЕ ОСАЖДЕНИЕ НА ПОВЕРХНОСТИ

Медхат ХУСАИНОВ, Александр КАРТУШИНСКИЙ, Анатолий
МУЛЬГИ, Игорь ЩЕГЛОВ, Сергей ТИСЛЕР

Проведено экспериментальное исследование обтекания тел различной формы двухфазным ламинарным потоком. Измерены распределения скоростей фаз и концентрации частиц в пограничном слое, а также осаждение частиц на эти поверхности.

ARTICLE II

Hussainov, M., Kartushinsky, A., Mulgi, A., Rudi, Ü., Tisler, S., 1995, Experimental and theoretical study of the distribution of mass concentration of solid particles in the two-phase laminar boundary layer on a flat plate. *Int. J. Multiphase Flow*, Vol. 21(6), pp. 1141-1161.



EXPERIMENTAL AND THEORETICAL STUDY OF THE DISTRIBUTION OF MASS CONCENTRATION OF SOLID PARTICLES IN THE TWO-PHASE LAMINAR BOUNDARY LAYER ON A FLAT PLATE

M. HUSSAINOV, A. KARTUSHINSKY†, A. MULGI, Ü. RUDI and S. TISLER

Department of Aeromechanics, Institute of Energy Research, Estonian Academy of Sciences,
Paldiski Rd 1, EE0001 Tallinn, Estonia

(Received 25 January 1994; in revised form 26 April 1995)

Abstract—The essential non-uniform distribution of particle mass concentration, with vivid maximum value inside the two-phase laminar boundary layer developed in the flow past a flat plate, has been found by experimental investigation. The mathematical model based on the approximation of the dispersed phase within the viscous fluid, taking into consideration pseudoviscosity coefficients, has been elaborated for description of the motion and distribution of solid admixture. The dispersed phase is considered as a polydispersed phase, which consists of a finite number of particle fractions. The numerical results from the simplest version of the model are in good agreement with the experimental results, which indicates a principal possibility of applying the given mathematical model for flows of similar type.

Key Words: laminar boundary layer, self-similar co-ordinates, dispersed phase, particle mass concentration, interparticle collision, pseudoviscosity coefficients, particle fraction, particle angular momentum, restitution and friction coefficients

1. INTRODUCTION

A large number of manufacturing and natural processes are connected with the motion of particles in gas flows, e.g. combustion of solid fuels in thermal power stations, dust collection, pneumatic conveying and admixture diffusion in the atmosphere. The sedimentation of solid particles on streamlined surfaces can be included in these processes. The given investigation was carried out within the international project "Mars 94/96". The definition of the quantity of Martian dust sedimentation on the apparatus surfaces is of great importance in forecasting their security performance. One of the problems was to estimate the maximum possible value of particle sedimentation on the balloon surface. The sedimentation quantity was stipulated by particle motion near the streamlined surface. The laminar boundary layer was formed on the surface of the balloon while it was moving in the dusty Martian atmosphere. Thus, the object of the given investigation was to study the mechanism of particle motion and distribution inside the laminar boundary layer. Laminar flow past the unyawed flat plate by vertical two-phase flow for the Reynolds numbers 10^3 – 10^4 was considered. Knowing the distribution of particle mass concentration in such a two-phase laminar boundary layer, we can determine the sedimentation intensity of solid particles on the surface.

A suitable experimental rig has been built in our laboratory for investigating the motion of solid admixture in the vicinity of streamlining bodies. The measurements of relative particle mass concentration and velocities of both phases were carried out using laser diagnostics. Experimental investigations have essentially shown non-uniform distribution of particle mass concentration with the maximum value inside the boundary layer, which substantially differs from that obtained according to well-known theoretical conceptions (Soo 1971; Osyptsov 1981; Amsolov 1992). According to these conceptions, the maximum particle concentration is on the plate surface. The mathematical model, not considering the dispersed medium as an ideal gas, but as a Newtonian

†To whom all correspondence should be addressed.

viscous fluid and introducing pseudoviscosity coefficients, was elaborated for describing such a distribution of particle mass concentration. These pseudoviscosity coefficients are determined by the consideration of the interparticle collision mechanism and they characterize the diffusion of mass and the momentum of the dispersed phase. Since in manufacturing and in nature the composition of real powders are polydispersed and the particles have an irregular form, the assumption of monodispersity of the dispersed phase cannot adequately describe the motion of particles in various phenomena. Therefore, to describe the behaviour of the dispersed phase, it is necessary to take into account its real composition. The presented mathematical model considers the dispersed phase as polydispersed, consisting of a finite number of particle fractions with different sizes. Since the particles of different sizes have different velocities along their paths, the interparticle collisions are taken into account. Simulation of specific boundary conditions on the surface and in the outer part of the boundary layer is a peculiarity of the presented model. By applying such a method we can correctly describe the experimentally observed distribution of particle mass concentration near the surface.

2. EXPERIMENTAL STUDY

The experiments were carried out in a disconnected vertical two-phase wind-channel with an open working space (figure 1). The aerodynamical bench consisted of the following parts: a main channel for formation and transportation of two-phase flow; a channel of concurrent pure air flow; a device for formation of a flow field with the given parameters in the working space of the wind-channel; and a dust suck-out channel. Also, the aerodynamical bench included a blower, a particle screw feeder, an air flow governor, a thermocontroller, a particle screw feeder, a flowmeter, a pressure converter and optical registering, controlling and processing systems.

The wind-channel functioned by injecting a solid suspension into the open working space with given parameters and subsequent ejection through the diffuser. The two-phase flow was set up by forming a device consisting of a cylindrical tube with a diameter of 100 mm and length of 3 m. The tube was installed along the axis of the forming device. After exiting the cylindrical tube and passing

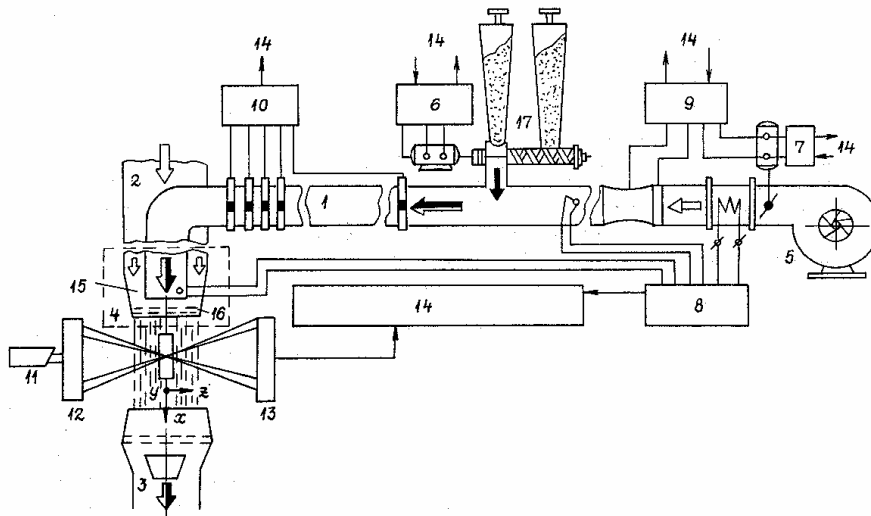


Figure 1. Aerodynamical bench: 1, main channel; 2, channel of concurrent pure air flux; 3, a dust suck-out channel; 4, a device for formation of the given flow field; 5, blower; 6, particle screw feeder; 7, air flow governor; 8, thermocontroller; 9, flowmeter; 10, pressure converter; 11 He-Ne laser; 12, transmitting optics; 13, receiving optics; 14, registering, processing and controlling system; 15, confuser; 16, system of grates; 17, particle screw feeder.

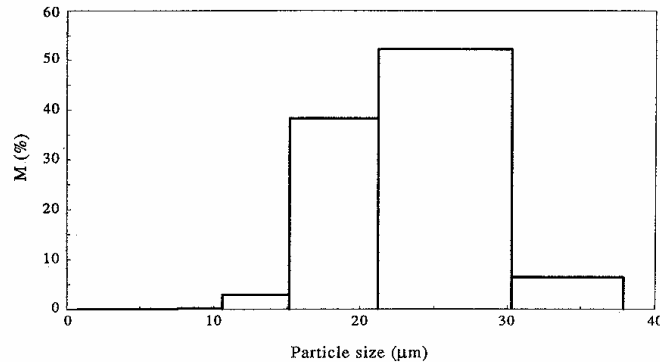


Figure 2. The particle mass distribution for the average particle diameter $\delta = 23 \mu\text{m}$.

through the system of grates, the formed two-phase suspension expanded and entered the open working space supported by the concurrent flow of pure air on either side. Three grates, with mesh sizes of 0.63, 0.315 and 0.15 mm at an interval of 12 mm, were used for smoothing the parameters of inflow. The uniformity of the two-phase flow with the given parameters was obtained by varying the pure air flow in one of the channels, the two-phase flow in another and also in the dust suck-out channel.

The distributions of the local averaged parameters (velocity and particle mass concentration) of the two-phase flow in the vicinity of a flat plate were measured with the help of a forward-scatter laser Doppler anemometer (LDA) and laser concentration measurer (LCM) (He-Ne laser, sending and receiving optics in figure 1). The optical parts of the LDA and LCM have been installed on a special coordinate device controlled by a PC. This allowed scanning of the flow continuously or discretely in any given direction with an accuracy of 0.1 mm. The optical system included a 50 mW helium-neon laser. The LDA receiving optics contained two channels: one has been tuned for registering signals from small flow tracers and the second for measuring the dispersed phase. Each channel consisted of receiving optics, fiber cable, a photomultiplier (PM) and a special counter processor. Tuning of the channels was based on the amplitude discrimination of the Doppler signals. The channel of the dispersed phase has been tuned for registering signals only from the particles of this phase by selecting the geometry of reception and sensitivity of the PM. The measurements of particle mass concentrations were based on measuring the light intensity of the beam scattered at some angle and an attenuated direct beam in the optical heterogeneous medium.

Manufactured abrasive electrocorundum powders (Al_2O_3 ; $\rho_p = 3950 \text{ kg/m}^3$), while average particle sizes of 12, 23 and $32 \mu\text{m}$, were used in the experiments. A large number of natural and manufactured dispersed abrasive materials have a granulous form and a high polydispersity, i.e. they contain particles with different sizes. Since the physical properties of the dispersed systems depend significantly on the fractional composition of the powders, it is necessary to know the particle size distributions and thus analysis of the polydispersity of the applied powders was made beforehand. The results of this analysis for the standard powder M28, as an example, are presented in figure 2 (here the mass content M of the given fraction is laid out along the ordinate and the lower and upper limits are given on the abscissa). A stainless steel flat plate was used as a model for investigations. It has the following dimensions: length 500 mm, width 100 mm, thickness 2 mm. The leading edge of the plate is wedge-shaped with a single bevel of the rear surface of the plate.

The model was installed into the uniform, completely formed, vertical, two-phase flow with the settled parameters. The distributions of gas velocity U_∞ and relative mass particle concentration α/α_∞ in the working space of the wind-channel are presented in figure 3 where $\alpha_\infty = \rho_{s00}/\rho$ and ρ, ρ_∞ are densities of the gas and dispersed phase in the stream flow, respectively. The diameter of the uniform flow in the working space was 150–180 mm depending on the stream velocity. The main parameters of the experiments ($U_\infty, \delta, \rho_\infty$) were stipulated by the steady formation of the two-phase

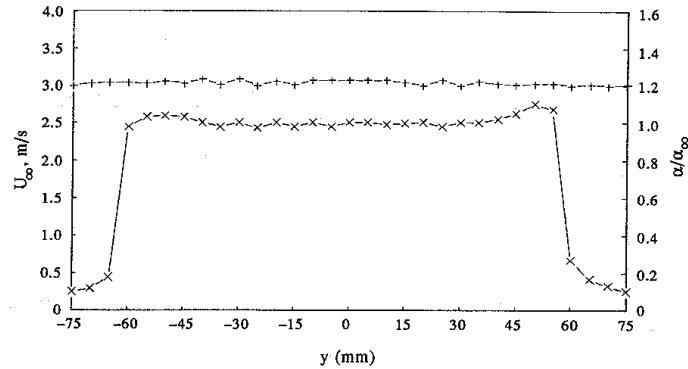


Figure 3. Profiles of the axial velocity component (---+) and particle mass concentration (---x---) in the working space of the wind-channel.

laminar boundary layer on a plate and by uniform feeding of the dispersed phase into the working space of the wind-channel. The values of stream velocity were 1.5 and 3 m/s. The Reynolds number Re_x in the investigated cross-sections of the plate did not exceed 4×10^4 . The concentration of solid admixture was due to the absence of feedback of the solid phase to the carrier flow ($\rho_s \ll 1$) and equalled $\rho_{s\infty} = 0.01 \text{ kg/m}^3$.

The main error in the measurements of particle mass concentration in the boundary layer is stipulated by time instability and by the non-uniformity of the particle concentration over the cross-section of the stream flow. The non-uniformity of the particle mass concentration for various particle sizes is almost the same and does not exceed 5%. The time instability of the concentration is caused by functioning of the particle screw feeder and by particle sedimentation on the walls of the main channel of transportation of the two-phase flow and on the surfaces of the forming device. This instability became apparent only for $12 \mu\text{m}$ particles due to their high adhesiveness. The concentration profiles have been obtained by averaging data from more than 10 measuring series for every cross-section of the plate. Experimental uncertainties for particle mass concentration were as follows: for $12 \mu\text{m}$ particles $< 15\%$; for 23 and $32 \mu\text{m}$ particles $< 10\%$.

Profiles of the relative particle mass concentration in the two-phase laminar boundary layer on a flat plate in the cross-sections $X = 50, 100$ and 170 mm are presented in figures 4 and 5. The experiments show that the given non-uniform concentration profiles have already been formed at

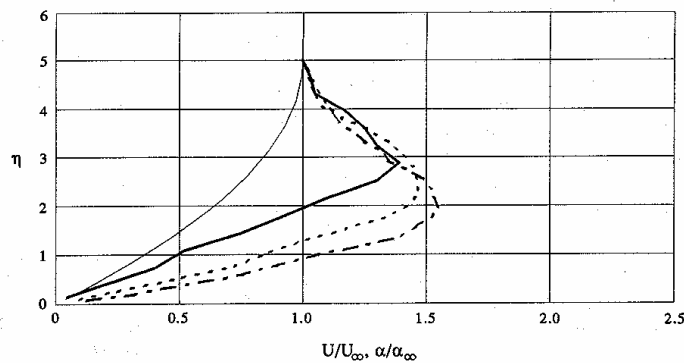


Figure 4. Experimental profiles of the axial velocity component of gas (—, U/U_∞) and particle mass concentration α/α_∞ for the free stream velocity $U_\infty = 1.5 \text{ m/s}$ and $\delta = 23 \mu\text{m}$: —, $X = 50 \text{ mm}$; ----, $X = 100 \text{ mm}$; -·-·-, $X = 170 \text{ mm}$.

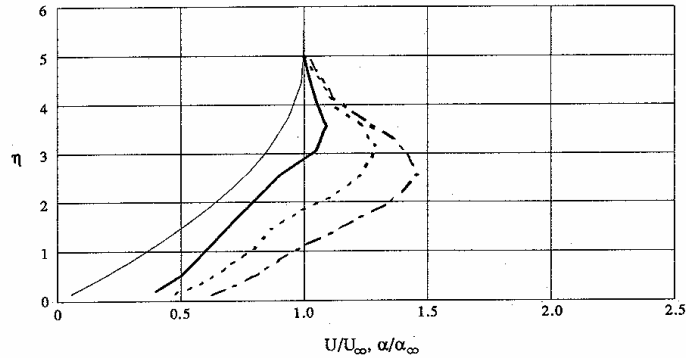


Figure 5. Experimental profiles of the axial velocity component of gas (—, U/U_∞) and particle mass concentration α/α_∞ for the free stream velocity $U_\infty = 3$ m/s and $\delta = 23$ μm : —, $X = 50$ mm; ----, $X = 100$ mm; - · - · -, $X = 170$ mm.

the leading edge of a flat plate (at a distance of 10 mm from the leading edge) and remained almost the same downstream. As follows from these charts, the distribution of particle mass concentration reaches a maximum for both free stream velocities (1.5 and 3 m/s). The value of concentration maximum increases along the plate from the leading edge and holds downstream while its self-similar coordinate decreases. Figures 6 and 7 show the influence of particle size on the distribution of particle mass concentration. The distribution of particle mass concentration has a maximum for all the investigated particle sizes (12, 23 and 32 μm).

3. THEORETICAL MODEL

3.1. General remarks

The solid particle-laden laminar boundary layer, developed when flowing past an unyawed flat plate, is considered within the Eulerian approach where the dispersed phase is modelled as a continuous medium. The dispersed phase is described within mutually-penetrating continua by Nigmatulin's theory (1978), since the interparticle distance e is much smaller than the characteristic flow scale, which here is the thickness of the boundary layer Δ . This also emanates from the

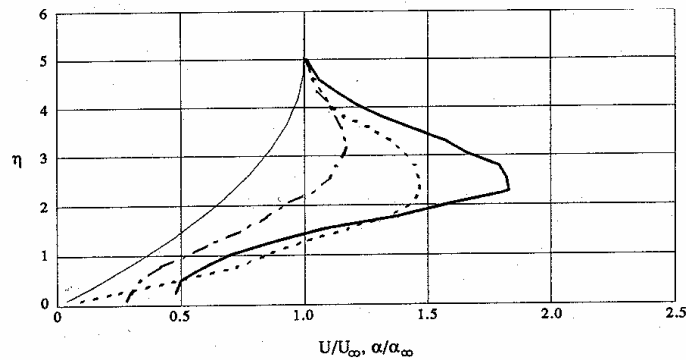


Figure 6. Experimental profiles of the axial velocity component of gas (—, U/U_∞) and particle mass concentration α/α_∞ for the free stream velocity $U_\infty = 1.5$ m/s and cross-section $X = 100$ mm: —, $\delta = 12$ μm ; ----, $\delta = 23$ μm ; - · - · -, $\delta = 32$ μm

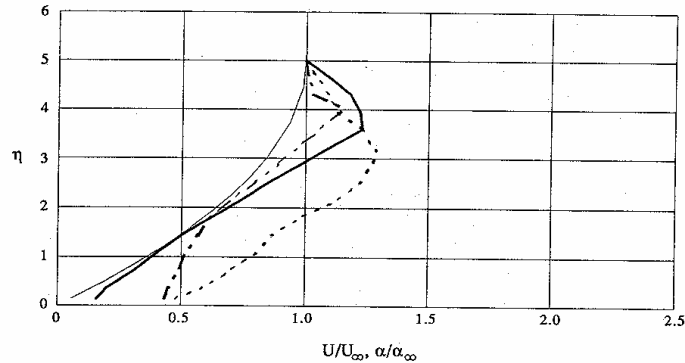


Figure 7. Experimental profiles of the axial velocity component of gas (—, U/U_∞) and particle mass concentration α/α_∞ for the free stream velocity $U_\infty = 3$ m/s and cross-section $X = 100$ mm: —, $\delta = 12$ μm ; ----, $\delta = 23$ μm ; - · - · -, $\delta = 32$ μm .

necessity of theory validation. As our calculations show, e.g. for 10 μm particles with a particle mass concentration $\alpha_\infty = 0.01$, the ratio l/Δ is an order of $(l/\Delta) \approx O(10^{-1})$.

Unlike the approach of an ideal gas for description of the dispersed phase in a two-phase laminar boundary layer (Soo 1971; Osypstov 1980; Asmolov 1992), the transport equations of particle mass, linear and angular momenta of the dispersed phase are written using the approximation of the Newtonian viscous fluid for that phase. Soo (1971), Osypstov (1980) and Asmolov (1992) calculated the two-phase laminar boundary layer on a flat plate with monodispersed particles and, also, Asmolov (1992) took into account the influence of the Saffman force on the motion and distribution of the dispersed phase. Therefore they considered only the convective transfer of the dispersed phase in the boundary layer. We account for, in addition to the convective transfer and particle–gas and particle–wall interactions, the diffusion transfer of the particles, which is described by considering the interparticle collision mechanism. As a result of such a theoretical description, the pseudoviscosity coefficients of the dispersed phase $v_s^1, v_s^2, v_s^3 D_s$ are brought into consideration. Interparticle collision results from velocity differences of single particles in the real two-phase flows. The differences in particle velocities in turn have been stipulated by the polydispersity of the real solid admixture content. As experimental data show, the content of the electrocorundum powder is non-uniform and the particles themselves have an irregular form. The particle mass distribution against the particle size is shown in figure 2 for the electrocorundum powder with a mean particle size $\delta = 23$ μm . The root-mean-square deviation of particle sizes is up to 30%.

For the mathematical description of the solid admixture the real continuous particle size distribution is modelled by the finite number of particle fractions of discrete size. Each fraction is characterized by its own properties, such as particle size, concentration and velocity. This allows the collision process between particles having different velocities to be taken into consideration. We can write the transport equations and set the boundary conditions for each particle fraction. The correlations between the different particle fractions are calculated by introducing the pseudoviscosity coefficients derived from the collision mechanism.

We restrict our consideration by the description of two-dimensional motion of a two-phase flow in the laminar boundary layer. The composition of the polydispersed admixture is modelled by three fractions of particles: the fraction which contained the particles with the largest percent by mass (the so-called ‘‘main fraction’’ and denoted by index 2) and two additional particle fractions with smaller percents by mass. One of these additional fractions (index 1) consists of particles of a smaller size than the size of the particles from the main fraction. The other additional fraction (index 3) includes particles of a larger size in comparison with the particles from the main fraction. The dispersed phase is considered in the model as a polydispersed phase and is characterized by the following quantities: the particle sizes of the fractions $\delta_1 < \delta_2 < \delta_3$; velocity projections

$u_{s1}, v_{s1}, u_{s2}, v_{s2}, u_{s3}, v_{s3}$ in the streamwise and transversal directions, respectively; angular particle velocities $\omega_{s1}, \omega_{s2}, \omega_{s3}$ and particle mass concentration of the fractions $\alpha_1, \alpha_2, \alpha_3$.

The impact of the carrier fluid on the motion of the dispersed phase in the laminar boundary layer is realized via the drag force and two lift forces—those of Magnus & Saffman. The particles obtain their rotation by interaction with the surface of a plate. In addition to the transport equation of particle mass and the linear momentum of the dispersed phase, the transport equation of the angular momentum of particles is considered in the presented model. This equation is derived from the formula which describes the damping of the angular velocity of a single particle in the viscous medium (Rubinow & Keller 1965). By applying the spatial averaging method (Nigmatulin 1978) to this equation and to the equations of the translational motion of a single particle, we obtain the equations for describing the dispersed phase as a continuum. There is a prerequisite for the action of the Saffman force in the laminar boundary layer, since the parameter $u/\sqrt{\nu(\partial u/\partial y)}$ (Saffman 1961) is of a unit value unlike in the turbulent boundary layer, where it is much higher than a unit. Here u is the streamwise velocity component of gas and ν is the laminar viscosity of gas. The gravity force is neglected due to the insignificance of the particle settling velocity relative to the particle velocity originating from the drag force. Other force factors (the Basset force, the force of added masses) have also been neglected, since the ratio of particle material density to the gas density is very high.

3.2. The equations and boundary conditions

Let us consider the two-dimensional motion of both phases in the laminar boundary layer. The equations of the two-phase laminar boundary layer in the Cartesian coordinate system are:

$$\frac{\partial \rho u}{\partial x} + \frac{\partial \rho v}{\partial y} = 0, \quad [1]$$

$$\rho u \frac{\partial u}{\partial x} + \rho v \frac{\partial u}{\partial y} = \frac{\partial \tau}{\partial y}, \quad [2]$$

$$\frac{\partial(\rho_s u_s)}{\partial x} + \frac{\partial(\rho_s v_s)}{\partial y} = \frac{\partial}{\partial y} \left(D_s \frac{\partial \rho_s}{\partial y} \right), \quad [3]$$

$$\rho_s u_s \frac{\partial u_s}{\partial x} + \rho_s v_s \frac{\partial u_s}{\partial y} = \frac{\partial \tau_s}{\partial y} + \frac{\rho_s}{\rho_p} \left[\frac{18 C'_D v (u - u_s)}{\delta^2} + \frac{3}{4} (v - v_s) \left(\omega_s - \frac{\partial u}{2 \partial y} \right) \right], \quad [4]$$

$$\rho_s u_s \frac{\partial v_s}{\partial x} + \rho_s v_s \frac{\partial v_s}{\partial y} = \frac{\partial p_s}{\partial y} + \frac{\rho_s}{\rho_p} \left[\frac{18 C'_D v (v - v_s)}{\delta^2} + \frac{3}{4} (u - u_s) \left(\omega_s - \frac{\partial u}{2 \partial y} \right) + \frac{6 \cdot K_s \sqrt{\nu}}{\pi \delta} (u - u_s) \sqrt{\frac{\partial u}{\partial y}} \right], \quad [5]$$

$$\rho_s u_s \frac{\partial \omega_s}{\partial x} + \rho_s v_s \frac{\partial \omega_s}{\partial y} = - \frac{\partial \rho_s \langle \omega_s v_{sd} \rangle}{\partial y} - \frac{60 \rho_s v}{\rho_p \delta^2} \left(\omega_s - \frac{\partial u}{2 \partial y} \right), \quad [6]$$

where v is the transversal gas velocity component and v_{sd} is the particle diffusion velocity and ρ and ρ_p are the gas and particle material densities, respectively. The drag coefficient C'_D for different Reynolds numbers of a particle $Re_p = \delta \sqrt{(u - u_s)^2 + (v - v_s)^2} / \nu$ is determined according to Kravtsov (1968) by the formula

$$C'_D = \frac{24}{Re_p} = 1 + 0.275 \sqrt{Re_p} + 0.0138 Re_p. \quad [7]$$

The density of the dispersed phase ρ_s is related to the density of incompressible gas ρ by $\rho_s = \alpha \rho$, which is valid if the volumetric concentration of particles is very low, i.e. $\beta \ll 1$. τ, τ_s are the shear stresses of the gas and dispersed phases, respectively, and p_s is the normal stress for the dispersed phase. $K_s = 1.61$ is the numerical constant (Shraiber *et al.* 1980).

We suggest that the behaviour of the dispersed phase obeys the approximation of the Newtonian fluid. Therefore, analogously to the gaseous carrier fluid the stress tensor components of the dispersed phase are correlated with the rate of strain via the introduced pseudoviscosity coefficients,

which can be written in the simplest form using the approximation of laminar boundary layer (Schlichting 1974):

$$\tau = \rho\nu \frac{\partial u}{\partial y}, \quad [8]$$

$$\tau_s = \rho_s \nu_s^1 \frac{\partial u_s}{\partial y}, \quad [9]$$

$$p_s = 2\rho_s \nu_s^2 \frac{\partial v_s}{\partial y}. \quad [10]$$

We consider that the cross-product term $\langle \omega_s v_{sd} \rangle$ in [6], describing the transport of particle rotation, can be analogously obtained by using the approach of the mixing-length theory according to Tennekes & Lumley (1972). Introducing the pseudoviscosity coefficients ν_s^3 , we can write:

$$\rho_s \langle \omega_s v_{sd} \rangle = -\rho_s \nu_s^3 \frac{\partial \omega_s}{\partial y}, \quad [11]$$

where $\langle \dots \rangle$ and further means an ensemble average. We also assume that the diffusive flow rate of particle mass is determined via the gradient of the concentration and pseudoviscosity coefficients analogously to the procedure for the molecular diffusion of gases.

The pseudoviscosity coefficients for the particle mass transport equation, for the momentum balance in streamwise and transversal directions and for the angular momentum balance of the dispersed phase are $D_s, \nu_s^1, \nu_s^2, \nu_s^3$, respectively. These coefficients describe the transfer of mass, momentum and angular momentum of the dispersed phase by the diffusion process (originating from the interparticle collisions). This transfer is considered in addition to convectational transfer and the interphase momentum exchange, which is caused by various forces (the viscous drag force, the Saffman and Magnus lift forces). The pseudoviscosity coefficients are varied both over the width and length of the boundary layer. As the calculations show, the values of these coefficients at the leading edge of the plate, where the distribution of velocity of the dispersed phase changes from uniform in the free stream flow to typical in the boundary layer, are comparable with the value of coefficient of laminar viscosity of the carrier fluid.

These transport equations are the continuity equation [1] and the momentum balance of gas [2], the transport equation of particle mass [3], the momentum balance of dispersed phase in streamwise and transversal directions [4] and [5], respectively and the transport equation of angular momentum [6] of the dispersed phase. The equations are obtained by applying Nigmatulin's theory of mutually-penetrating continua. On the right-hand side of the equations of the momentum balance of the dispersed phase in the streamwise [4] and transversal directions [5], the drag force and Magnus and Saffman lift forces are taken into account. We write transport equations for each particle fraction denoted by the index "i". The pseudoviscosity coefficients ν_{si}^j, D_{si} for each particle fraction can be determined by knowing the velocity and mass concentration fields of interacting fractions, i.e. $u_{si}, v_{si}, \omega_{si}, \alpha_i$. We consider one-way coupling because of the small particle mass loading (0.01 kg dust/kg air).

For transformation of the equations to the new coordinate system with the self-similar variables $x = x, \eta = y\sqrt{U/\nu x}$, i.e. using transformation as in the work by Anderson *et al.* (1990), let us write [1]–[6] with [8]–[11] in the following form:

$$x \frac{\partial \bar{U}}{\partial x} - \frac{\eta}{2} \frac{\partial \bar{U}}{\partial \eta} + \frac{\partial \bar{V}}{\partial \eta} = 0, \quad [12]$$

$$x \bar{U} \frac{\partial \bar{U}}{\partial x} + \left[\bar{V} - \frac{\eta \bar{U}}{2} \right] \frac{\partial \bar{U}}{\partial \eta} = \frac{\partial^2 \bar{U}}{\partial \eta^2}, \quad [13]$$

$$\sqrt{x} \frac{\partial}{\partial x} [\sqrt{x} \bar{\alpha}_i \bar{U}_{si}] + \frac{\partial}{\partial \eta} \left[\bar{\alpha}_i \left(\bar{V}_{si} - \frac{\eta \bar{U}_{si}}{2} \right) \right] = \frac{\partial}{\partial \eta} \left[\frac{D_{si}}{\nu} \frac{\partial \bar{\alpha}_i}{\partial \eta} \right], \quad [14]$$

$$x\bar{U}_{si} \frac{\partial \bar{U}_{si}}{\partial x} + \left[\bar{V}_{si} - \frac{\eta \bar{U}_{si}}{2} \right] \frac{\partial \bar{U}_{si}}{\partial \eta} = \frac{\partial}{\partial \eta} \left[\frac{v_{si}^1 \partial \bar{U}_{si}}{v} \right] + \frac{\rho}{\rho_p} \frac{x}{\delta_i} \left[\frac{18C'_{Di}(\bar{U} - \bar{U}_{si})}{\text{Re}_{pi}} + \frac{3(\bar{V} - \bar{V}_{si})}{4\sqrt{\text{Re}_x}} \left(\bar{\omega}_{si} - \frac{\text{Re}_{pi}}{4\sqrt{\text{Re}_x}} \frac{\partial \bar{U}}{\partial \eta} \right) \right], \quad [15]$$

$$x\bar{U}_{si} \frac{\partial \bar{V}_{si}}{\partial x} + \left[\bar{V}_{si} - \frac{\eta \bar{U}_{si}}{2} \right] \frac{\partial \bar{V}_{si}}{\partial \eta} = \frac{\partial}{\partial \eta} \left[\frac{2v_{si}^2 \partial \bar{V}_{si}}{v} \right] + \frac{\rho}{\rho_p} \frac{x}{\delta_i} \left[\frac{18C'_{Di}(\bar{V} - \bar{V}_{si})}{\text{Re}_{pi}} + \frac{3}{2} \sqrt{\text{Re}_x} (\bar{U} - \bar{U}_{si}) \left(\bar{\omega}_{si} - \frac{\text{Re}_{pi}}{4\sqrt{\text{Re}_x}} \right) + \frac{6 \cdot K_s (\bar{U} - \bar{U}_{si})}{\pi} \frac{\sqrt{\partial \bar{U}}}{4\sqrt{\text{Re}_x}} \right] + \frac{\bar{U}_{si} \bar{V}_{si}}{2}, \quad [16]$$

$$x\bar{U}_{si} \frac{\partial \bar{\omega}_{si}}{\partial x} + \left[\bar{V}_{si} - \frac{\eta \bar{U}_{si}}{2} \right] \frac{\partial \bar{\omega}_{si}}{\partial \eta} = \frac{\partial}{\partial \eta} \left[\frac{v_{si}^3 \partial \bar{\omega}_{si}}{v} \right] - \frac{60\rho}{\rho_p \text{Re}_{pi}} \frac{x}{\delta_i} \left[\bar{\omega}_{si} - \frac{\text{Re}_{pi}}{4\sqrt{\text{Re}_x}} \frac{\partial \bar{U}}{\partial \eta} \right], \quad [17]$$

where $\bar{U} = u/U_\infty$, $\bar{U}_{si} = u_{si}/U_\infty$, $\bar{V} = v\sqrt{x/vU_\infty}$, $\bar{V}_{si} = v_{si}\sqrt{x/vU_\infty}$, $\bar{\omega}_{si} = \omega_{si}\delta_i/2U_\infty$, $\bar{\alpha}_i = \alpha_i/\alpha_\infty$ are non-dimensional stretched variables, the local Reynolds number $\text{Re}_x = U_\infty x/v$, the Reynolds number of particles for different fraction $\text{Re}_{pi} = U_\infty \delta_i \sqrt{(\bar{U} - \bar{U}_{si})^2 + (\bar{V} - \bar{V}_{si})^2}/v$ and U_∞ , α_∞ are the velocity and particle mass concentration of free stream, respectively.

One can see that the equations of the two-phase laminar boundary layer include non-self-similar terms, which depend on the axial (streamwise) coordinate "x". They characterize the influence of the force factors in the equations of momentum balance and angular momentum balance of the dispersed phase. One can also see that, as far as the axial coordinate extends, the ratio δ_i/x decreases resulting in the reduction of the influence of force terms. The first terms on the right-hand side of the equations of particle mass transfer [14], momentum transfer in axial [15] and transversal directions [16] and angular momentum transfer [17] describe the diffusion of mass, momentum and angular momentum of different fractions and are determined via the introduced pseudoviscosity coefficients of the dispersed phase $v_{si}^1, v_{si}^2, v_{si}^3, D_s$. The terms in square brackets on the right-hand side of the equations of momentum balance, [15] and [16], characterize the impact of the drag force and the Magnus and Saffman lift forces, respectively. The fourth term takes into account the influence of the Saffman force and the last term on the right-hand side of [16] is a sequence of the transform of equations into a new self-similar coordinate system. The second term on the right-hand side of the equation of angular momentum balance of the dispersed phase [17] reflects decaying of the rotation of solid particles in the viscous medium.

3.3. The initial and boundary conditions

Since one-way coupling is considered in the given model and, hence, the non-self-similar terms (the force factors) on the right-hand side of [12] and [13] are absent, we have self-similar velocity distribution of gas in the new coordinates x, η . This solution results from the joint decision of [12] and [13] for $x = 0$. The initial fields of axial velocity components of the solid phase of different fractions and particle mass concentrations are set as uniform distributions in the cross-section of the boundary layer:

$$\bar{U}_{si} = 1, \quad [18]$$

$$\bar{\alpha}_1 = \bar{\alpha}_3 = 0.2, \quad \bar{\alpha}_2 = 0.6, \quad [19]$$

where $\bar{\alpha}_2$ is the initial value of relative particle mass concentration for the main particle fraction, $\bar{\alpha}_1$ and $\bar{\alpha}_3$ are the initial values of relative particle mass concentration for other particle fractions.

The distribution of transversal velocity components of the dispersed phase at $x = 0$ is set as:

$$\bar{V}_{si} = 0. \quad [20]$$

The initial fields of angular velocity of different particle fractions are set uniform in the cross-section of the boundary layer and their values are obtained using the formula from Babukha & Shraiber (1972):

$$\bar{\omega}_{si} = (1 - k_i) \bar{U}_{si}. \quad [21]$$

Thus, the solid particles entering the boundary layer collide with the plate surface and obtain rotation due to the roughness of the plate surface. The rotation of particles depends also on the friction coefficient k_i (in calculations $k_i = 0.75$), which can be varied, in general, according to Babukha & Shraiber (1972) in the range $-1 \leq k_i \leq 1$.

We set the boundary conditions for the equations of the gaseous phase as sticking and impenetrability conditions at the surface:

$$\bar{U}|_w = 0, \quad [22]$$

$$\bar{V}|_w = 0. \quad [23]$$

At the outer part of the boundary layer we set the axial velocity component of gas equal to the velocity in free stream and the gradient of the transversal velocity equal to zero:

$$\bar{U}|_\infty = 1, \quad [24]$$

$$\left. \frac{\partial \bar{V}}{\partial \eta} \right|_\infty = 0. \quad [25]$$

The boundary conditions for the equations of the dispersed phase, i.e. for the equations of the streamwise particle velocity component and the particle angular velocity, are set assuming the relative particle velocity along the surface as in the theory of rarefied gases (Chapman & Cowling 1960). The given expressions include the recovery coefficients of linear and angular momenta of particles at the interaction with the surface:

$$\bar{U}_{si}|_w = \gamma_u \left. \frac{\partial \bar{U}_{si}}{\partial \eta} \right|_w, \quad [26]$$

$$\bar{\omega}_{si}|_w = \gamma_\omega \left. \frac{\partial \bar{\omega}_{si}}{\partial \eta} \right|_w, \quad [27]$$

where the recovery coefficients γ_u, γ_ω , according to Chapman & Cowling (1960), are determined as:

$$\gamma_u = \frac{(1 - f_u)}{f_u} l, \quad [28a]$$

$$\gamma_\omega = \frac{(2 - f_\omega)}{f_\omega} l. \quad [28b]$$

The formulae for f_u and f_ω are obtained using the results of Babukha & Shraiber (1972). Then one can write:

$$f_u = \frac{(5 + 2k_i)}{7}, \quad [29a]$$

$$f_\omega = \frac{(2 + 5k_i)}{7}. \quad [29b]$$

The friction coefficient k_i introduced by Babukha & Shraiber (1972) neglects the relative velocity of particles along the surface and thus differs from those introduced by Matsumoto & Saito (1970), who considered two types of particle-wall interaction—with and without relative velocity along the surface.

For the transversal velocity component of the dispersed phase the impenetrability conditions at the surface for each particle fraction are set as:

$$\bar{V}_{si}|_w = 0. \quad [30]$$

To explain the boundary conditions for particle mass concentration at the surface we consider the balance of mass flow rates near the surface in the volume element with thickness Δ_i and length

Δ_2 along the plate surface. For a given volume element the difference between the input and output mass flow rates in the axial direction is not equal to zero due to the sliding friction of particles against the plate surface. The total mass flow rate in the axial direction can be balanced by the convective and diffusion particle transfers in the transversal direction. But, as the convective transfer in the transversal direction is negligible due to the insignificance of the transversal particle velocity component near the surface, we only take into account the diffusion transfer. Thus, we may write the boundary condition for the particle mass concentration as follows:

$$\left. \frac{D_{st}}{v} \frac{\partial \bar{\alpha}_i}{\partial \eta} \right|_w = \bar{\alpha}_i f(x). \quad [31]$$

The expression for function $f(x)$ in the new coordinates is written as follows:

$$f(x) = C_1 \cdot x \left(\sqrt{1 + \frac{\Delta_2}{x} \bar{U}'_{st}} - \bar{U}_{st} \right). \quad [32]$$

During the interaction of a particle with the surface it loses velocity. This velocity loss is determined as $\bar{U}'_{st} = \bar{U}_{st}[(5 + 2k_t)/7]$ according to Babukha & Shraiber (1972). We calculate the velocity loss on the length Δ_2 . The coefficient C_1 in [32] equals a ratio of Δ_1 and Δ_2 . We assume in the calculations that $\Delta_1 = \Delta\eta$ and $\Delta_2 = \Delta x$, where $\Delta\eta$ and Δx are the calculation steps in the transversal and streamwise directions, respectively. So we may write that $C_1 = \Delta\eta/\Delta x$.

In the outer part of the boundary layer the streamwise velocity component of the particles and particle mass concentration of different fractions are set equal to those in the free stream

$$\bar{U}_{st}|_{\infty} = 1, \quad [33]$$

$$(\bar{\alpha}_1 = \bar{\alpha}_3)|_{\infty} = 0.2, \quad \bar{\alpha}_2|_{\infty} = 0.6. \quad [34]$$

The gradient type of boundary conditions are set similar to those of the gaseous phase for the transversal velocity component and particle angular velocity in the outer part of the layer. But, unlike gas, we equal the velocity gradient to the constant, which in turn may be determined as a streamline inclination in the outer part of the layer towards the particle velocity direction of the free stream. Thus, we suggest the existence of some definite particle flow rate coming from the free stream into the boundary layer. This constant does not depend on particle size. The boundary conditions for both the transversal and angular particle velocities in that case can be written:

$$\left. \frac{\partial \bar{V}_{st}}{\partial \eta} \right|_{\infty} = \left. \frac{\partial \bar{\omega}_{st}}{\partial \eta} \right|_{\infty} = -C_2. \quad [35]$$

The constant C_2 is computed from good agreement with the experimental data and according to our investigations $C_2 = 0.1$ for all experiments.

Equations [12]–[17], with [18]–[21] and boundary conditions [22]–[27], [30], [31], [33]–[35], are numerically calculated by the tridiagonal algorithm using the six-point formula for the numerical scheme. Linearization of a non-linear terms on the left-hand side of the transport equation is carried out by Newton's method (Anderson *et al.* 1990) and for the approximation of the derivatives in the transversal direction the upwind differences were used (Roache 1980).

3.4. Pseudoviscosity coefficients

For the definition of the pseudoviscosity coefficients D_{st} , v_{st}^i let us start by considering binary particle collision with using the formulae from Chapman & Cowling (1960). Let the principle diameter be δ_1, δ_2 , particle masses m_1, m_2 , their inertia moments I_1, I_2 and the linear velocity V_1, V_2 and angular velocities ω_1, ω_2 , respectively. Then, according to Chapman & Cowling (1960), taking into account the restitution coefficient k'_n for the normal velocity component and the friction coefficient k'_t for the tangential velocity component of colliding particles introduced by Babukha & Shraiber (1972), the velocity differences after and before collision can be calculated:

$$V'_1 - V_1 = \gamma_{21} \left\{ (1 - k'_n) [\mathbf{e} \cdot (V_2 - V_1)] \mathbf{e} + \frac{(1 - k'_t) \zeta}{(1 + \zeta)} \left[\mathbf{e} \times (V_2 - V_1) - \frac{(\delta_1 \omega_1 + \delta_2 \omega_2)}{2} \right] \times \mathbf{e} \right\}, \quad [36]$$

$$V'_2 - V_2 = \gamma_{12} \left\{ (1 - k'_n) [\mathbf{e} \cdot (V_2 - V_1)] \mathbf{e} + \frac{(1 - k'_t) \zeta}{(1 + \zeta)} \left[\mathbf{e} \times (V_2 - V_1) - \frac{(\delta_1 \omega_1 + \delta_2 \omega_2)}{2} \right] \times \mathbf{e} \right\}, \quad [37]$$

$$\omega'_1 - \omega_1 = \frac{\gamma_{21}(k'_1 - 1)}{(1 + \zeta)} \left\{ \frac{2}{\delta_1} \mathbf{e} \times (V_2 - V_1) + \omega_1 + \frac{\delta_2}{\delta_1} \omega_2 - \left(\mathbf{e} \cdot \omega_1 + \frac{\delta_2}{\delta_1} \mathbf{e} \cdot \omega_2 \right) \mathbf{e} \right\}, \quad [38]$$

$$\omega'_2 - \omega_2 = \frac{\gamma_{12}(k'_1 - 1)}{(1 + \zeta)} \left\{ \frac{2}{\delta_2} \mathbf{e} \times (V_2 - V_1) + \omega_2 + \frac{\delta_1}{\delta_2} \omega_1 - \left(\mathbf{e} \cdot \omega_2 + \frac{\delta_1}{\delta_2} \mathbf{e} \cdot \omega_1 \right) \mathbf{e} \right\}, \quad [39]$$

where the unit vector direction \mathbf{e} is determined by the angle θ and the distance χ between the colliding particles at the moment of their collision, for the fixed angle φ according to figure 8. The linear velocities of both particles after collision are V'_1, V'_2 and the angular velocities of the particles after collision are ω'_1, ω'_2 . The relative particle mass for the first and second particles are calculated as $\psi_{12} = (m_1/m_1 + m_2)$ and $\psi_{21} = (m_2/m_1 + m_2)$, respectively. The coefficient ζ is determined as $\zeta = 4I/(m\delta^2)$ and for the spherical particles $\zeta = 0.4$.

These velocity differences can be considered as the particle velocity fluctuations. Let us write them in the coordinate system related to the first particle. For this reason let us direct the axis 0ξ along the particle velocity vector \mathbf{V}_1 , and axis 0η normal to it in the plane of linear velocity vectors $\mathbf{V}_1, \mathbf{V}_2$ and the axis $0z$ normal to the plane $\xi 0\eta$, i.e. along the particle angular velocity vector (figures 8 and 9). The expressions for the velocity differences in the new coordinate system for the first and the second particles are defined by [A1]–[A6] in appendix A. By rewriting the obtained expressions within the Cartesian coordinate system, which is related to the plate, one can obtain [A7]–[A10] for the velocity differences, as presented in appendix A.

In order to determine the stress tensor components, we multiply the different fluctuating velocities of the particles [A3], [A6]–[A10], as presented in appendix A, and average the product over the two angles θ, φ and the parameter χ . Let us consider the following combinations:

$$\begin{aligned} &\langle (u'_{12} - u_1)(v'_{12} - v_1) \rangle, \quad \langle (u'_{12} - u_1)^2 \rangle, \quad \langle (v'_{12} - v_1)^2 \rangle, \quad \langle (\omega'_{12} - \omega_1)(v'_{12} - v_1) \rangle, \\ &\langle (u'_{21} - u_2)(v'_{21} - v_2) \rangle, \quad \langle (u'_{12} - u_1)^2 \rangle, \quad \langle (v'_{12} - v_1)^2 \rangle, \quad \langle (\omega'_{12} - \omega_1)(v'_{12} - v_1) \rangle. \end{aligned}$$

For example, in one particular case the averaging procedure is as follows:

$$\langle (u'_{12} - u_2)(v'_{12} - v_1) \rangle = \frac{1}{2\pi} \frac{1}{\varphi_{21}} \frac{\int_0^{2\pi} d\theta \int_0^1 \chi d\chi \int_0^{\varphi_{21}} (u'_{12} - u_1)(v'_{12} - v_2) d\varphi}{\int_0^1 \chi d\chi}, \quad [40]$$

which is the same for other combinations.

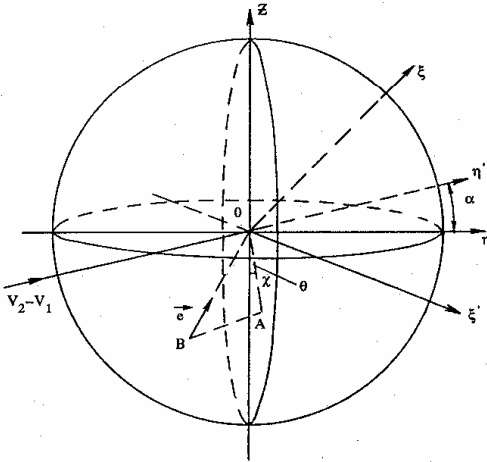


Figure 8. Schematic diagram of particle collision in space.

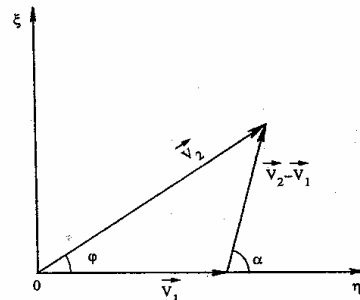


Figure 9. Schematic diagram of particle collision in plane.

The angle θ changes in the range $0 \leq \theta \leq 2\pi$ and the parameter χ , written in polar coordinates, is varied as $0 \leq \chi \leq 1$. The range of variation for the angle φ is determined from the correlation of transversal and streamwise velocity components of different particle fractions:

$$\operatorname{tg} \varphi_{21} = \operatorname{tg}(\gamma_2 - \gamma_1) = \frac{v_2 u_1 - v_1 u_2}{u_1 u_2 + v_1 v_2}. \quad [41]$$

For the turbulent motion Babukha & Shraiber (1972) have assumed that this angle changes within $0 \leq \varphi \leq 2\pi$, which results from the suggestion that the particles approach each other with equiprobability from all directions. This approximation fails for the laminar ordered flow. Thus, we suggest that in this case the particles collide only from the windward side of their surface. The application of the averaging method to all the above written correlations gives the stress tensor components of the dispersed phase. To obtain the sought pseudoviscosity coefficients, we multiply the stress tensor components by the interparticle collision time, thus we determine this stress tensor over the volume element. The time period between collisions of two particles Δt is determined via the probability of collision as presented by Sommerfeld & Zivkovic (1992). Considering the probability of collision, which obeys a binomial distribution and which can be converted into a Poisson distribution, the authors estimate this time for the simplest case—for at least one collision. In this particular case, they assume the probability of collision is less than 0.02, when the interparticle collision time Δt is small (in their cases of mass loading 0.1–3 kg dust/kg air). Hence, by knowing this probability of collision the authors determine the interparticle collision time. For determining the probability of collision of particles Trushin & Lipatov (1963) considered the case of the ordered oncoming motion of suspended particles. The found probability is proportional to the square of the collision cross-section of colliding particles, with the diameters δ_1 and δ_2 . Using the expression for the probability in the simplest case for at least one collision

$$P = \frac{\pi(\delta_1 + \delta_2)^2}{4l^2}, \quad [42]$$

we can estimate the order of magnitude of the probability of collision. Since the average distance between the particles is an order of $l \approx (20-30)\delta$ for considered mass loading, then in our case the probability is less than 0.01. As we can see, this value is compared with that obtained by Sommerfeld & Zivkovic (1992). The obtained expression for the probability of collision is used for determining the interparticle collision time and, thus, the pseudoviscosity coefficients.

Let us define the expression for the pseudoviscosity coefficients. For this we consider the collision of a single particle of the first particle fraction (index 1) with a number of particles from the second particle fraction (index 2), and so the probability of collision can be written in this particular case according to [42] as:

$$P = \frac{\pi(\delta_1 + \delta_2)^2}{4l_2^2}, \quad [43]$$

where the interparticle distance l_2 is taken for the second particle fraction and is calculated as $l_2 = \delta_2 \sqrt[3]{(\rho_p / \rho \alpha_2)}$. Then the interparticle collision time can be calculated according to Marble (1964) as follows:

$$\Delta t = \frac{4P}{\pi(\delta_1 + \delta_2)^2 n_2 |V_1 - V_2|}. \quad [44]$$

n_2 is the numerical concentration of particles of the second fraction. Taking into account the above, one can obtain the pseudoviscosity coefficients, for example, for the first fraction of particles, as follows:

$$v_{s1}^1 = \langle (u'_{12} - u_1)(v'_{12} - v_1) \rangle \Delta t = \frac{\sqrt[3]{\rho_p} \delta_2 \varphi_{21} \langle (u'_{12} - u_1)(v'_{12} - v_1) \rangle}{\sqrt{\rho \alpha_2} (V_1 + V_2) E^{21}}, \quad [45]$$

$$v_{s1}^2 = \langle (v'_{12} - v_1)^2 \rangle \Delta t = \frac{\sqrt[3]{\rho_p} \delta_2 \varphi_{21} \langle (v'_{12} - v_1)^2 \rangle}{\sqrt{\rho \alpha_2} (V_1 + V_2) E^{21}}, \quad [46]$$

$$v_{s1}^3 = \langle (\omega'_{12} - \omega_1)(v'_{12} - v_1) \rangle \Delta t = \frac{\sqrt[3]{\rho_p} \delta_2 \varphi_{21} \langle (\omega'_{12} - \omega_1)(v'_{12} - v_1) \rangle}{\sqrt{\rho \alpha_2} (V_1 + V_2) E^{21}}, \quad [47]$$

$$D_{si} = [\langle (u'_{i2} - u_i) \rangle + \langle (v'_{i2} - v_i)^2 \rangle] \Delta t = \sqrt[3]{\frac{\rho_p}{\rho \alpha_2}} \frac{\delta_2 \varphi_{2i} [\langle (u'_{i2} - u_i)^2 \rangle + \langle (v'_{i2} - v_i)^2 \rangle]}{(V_1 + V_2) E^{2i}}, \quad [48]$$

where $E^{2i} = \int_0^{\varphi_i} \sqrt{1 - k_{i2}^2 \cos^2 0.5\varphi} d\varphi$ is the incomplete elliptic integral of the second type calculated by Byrd & Friedman (1971) with the parameter $k_{i2}^2 = 4V_i V_2 / (V_2 + V_2)^2$. The upper index in the expressions of pseudoviscosity coefficients points out the corresponding transport equation where it is used. For example, index "1" refers to the equation of momentum balance of the dispersed phase in the streamwise direction, index "2" to the equation of momentum balance in the transversal direction and index "3" to the equation of angular momentum balance. The lower index in the expressions denotes the specific particle fraction. Analogously we can obtain the expressions for the second particle fraction. As mentioned above, we consider that the polydispersed phase consists of three particle fractions and thus, for these fractions the pseudoviscosity coefficients can be written as follows:

$$v_{si}^1 = \sqrt[3]{\frac{\rho_p}{\rho}} \frac{\cos 2\gamma_i}{2} \sum_{j=1, j \neq i}^3 \frac{\delta_j (V_i + V_j)}{\sqrt[3]{\alpha_j}} \{A_{ij} [\operatorname{sgn}(i-j) O_i^j - O_i^j \operatorname{tg} 2\gamma_i] - \operatorname{sgn}(i-j) C_{ij} [P_i^j - P_i^j \operatorname{tg} 2\gamma_i] - D_{ij} \operatorname{sgn}(i-j) [Q_i^j - \operatorname{sgn}(i-j) (Q_i^j - \varphi_{ij}) \operatorname{tg} 2\gamma_i]\}, \quad [49]$$

$$v_{si}^2 = \sqrt[3]{\frac{\rho_p}{\rho}} \sum_{j=1, j \neq i}^3 \frac{\delta_j (V_i + V_j)}{2\sqrt[3]{\alpha_j}} \left\{ \frac{B_{ij} H_{ij}}{3} + \cos 2\gamma_i [A_{ij} (O_i^j + \operatorname{sgn}(i-j) O_i^j \operatorname{tg} 2\gamma_i) - \operatorname{sgn}(i-j) \times C_{ij} (P_i^j + P_i^j \operatorname{tg} 2\gamma_i)] + D_{ij} \left[\frac{\varphi_{ij}}{E_{ij}^2} (3 + \cos 2\gamma_i) - \cos 2\gamma_i (Q_i^j + \operatorname{sgn}(i-j) Q_i^j \operatorname{tg} 2\gamma_i) \right] \right\}, \quad [50]$$

$$v_{si}^3 = \sqrt[3]{\frac{\rho_p}{\rho}} \frac{\cos \gamma_i}{6} \sum_{j=1, j \neq i}^3 \frac{\delta_j (V_i + V_j)}{\sqrt[3]{\alpha_j}} \{F_{ij} \operatorname{sgn}(i-j) [R_i^j - R_i^j \operatorname{tg} \gamma_i] + G_{ij} [S_i^j \operatorname{tg} \gamma_i + \operatorname{sgn}(i-j) S_i^j] - 16 \operatorname{sgn}(i-j) D_{ij} [T_i^j + \operatorname{sgn}(i-j) T_i^j \operatorname{tg} \gamma_i]\}, \quad [51]$$

$$D_{si} = \sqrt[3]{\frac{\rho_p}{\rho}} \frac{1}{3} \sum_{j=1, j \neq i}^3 \frac{\delta_j (V_i + V_j)}{\sqrt[3]{\alpha_j}} \left[B_{ij} H_{ij} + \frac{9D_{ij} \varphi_{ij}}{E_{ij}^2} \right], \quad [52]$$

where the coefficients are determined as

$$a_{ij} = (1 - k_n') \psi_{ij}, \quad b_{ij} = \frac{(1 - k_n') \zeta \psi_{ij}}{(1 + \zeta)}, \quad \psi_{ij} = \frac{m_i}{(m_i + m_j)},$$

the angle γ_i is determined via the correlation as $\operatorname{tg} \gamma_i = (v_{si}/u_{si})$, the angle φ_{ij} is determined via the correlation as

$$\varphi_{ij} = \left| \frac{v_{si}}{u_{si}} - \frac{v_{sj}}{u_{sj}} \right|,$$

the functions are determined as

$$A_{ij} = \left(\frac{a_{ij} + b_{ij}}{2} \right)^2, \quad B_{ij} = A_{ij} + a_{ij}^2 + b_{ij}^2, \quad C_{ij} = \frac{2}{15} (2a_{ij} + 3b_{ij}) b_{ij} \left(\frac{\delta_i \omega_i + \delta_j \omega_j}{V_i + V_j} \right),$$

$$D_{ij} = \frac{b_{ij}^2}{16} \left(\frac{\delta_i \omega_i + \delta_j \omega_j}{V_i + V_j} \right)^2, \quad F_{ij} = (a_{ij} - b_{ij}) b_{ij}, \quad G_{ij} = \frac{5}{16} (5a_{ij} + 7b_{ij}) b_{ij} \left(\frac{\delta_i \omega_i + \delta_j \omega_j}{V_i + V_j} \right)$$

and the total velocity is $V_i = \sqrt{u_{si}^2 + v_{si}^2}$ and $V_j = \sqrt{u_{sj}^2 + v_{sj}^2}$, $i = 1, 3$. The formulae for incomplete elliptic integrals of the first and second type K^i , E^i are presented in appendix B. The function H^i , O_i^j , O_i^j , P_i^j , P_i^j , Q_i^j , Q_i^j , R_i^j , R_i^j , S_i^j , S_i^j , T_i^j , T_i^j are the functions of the total velocity V_i and V_j , and the angle φ_{ij} . All of these are defined by [B1]–[B13] in appendix B.

Expansion of the expressions in terms of the Taylor series for small angles $\varphi_{ij} \ll 1$ gives the following pseudoviscosity coefficients, which are in the self-similar coordinates (in the non-dimensional form):

$$\frac{v_{si}^1}{v} = \sqrt[3]{\frac{\rho_p}{\rho}} \frac{\cos 2\bar{\gamma}_i}{2} \sum_{j=1, j \neq i}^3 \frac{\text{Re} p_j(\bar{V}_i + \bar{V}_j)}{\sqrt[3]{\bar{\alpha}_j}} \left[-\frac{\bar{A}_{ij}}{\bar{E}_{ij}} (\bar{H}_{ij} - \bar{L}_{ij}) - \text{sgn}(i-j) \bar{C}_{ij} [\bar{N}_{ij} + \bar{O}_{ij} \text{tg } 2\bar{\gamma}_i] - \frac{\bar{D}_{ij}}{\bar{E}_{ij}} \text{sgn}(i-j) [\bar{P}_{ij} - \text{sgn}(i-j) (\bar{Q}_{ij} - \text{tg } 2\bar{\gamma}_i)] \right]. \quad [53]$$

$$\frac{v_{si}^2}{v} = \sqrt[3]{\frac{\rho_p}{\rho}} \frac{1}{2} \sum_{j=1, j \neq i}^3 \frac{\text{Re} p_j(\bar{V}_i + \bar{V}_j)}{\sqrt[3]{\bar{\alpha}_j}} \left\{ \frac{\bar{B}_{ij}}{3} - \frac{\bar{A}_{ij} \cos 2\bar{\gamma}_i}{\bar{E}_{ij}} (1 - \bar{k}_{ij}^2 + \bar{H}_{ij} \bar{M}_{ij}) - \text{sgn}(i-j) \bar{C}_{ij} \cos 2\bar{\gamma}_i (\bar{O}_{ij} - \bar{N}_{ij} \text{tg } 2\bar{\gamma}_i) + \frac{\bar{D}_{ij}}{\bar{E}_{ij}} [3 + \cos 2\bar{\gamma}_i (1 - \bar{Q}_{ij} - \text{sgn}(i-j)) \bar{P}_{ij} \text{tg } 2\bar{\gamma}_i] \right\}, \quad [54]$$

$$\frac{v_{si}^3}{v} = \sqrt[3]{\frac{\rho_p}{\rho}} \frac{\cos \bar{\gamma}_i}{6} \sum_{j=1, j \neq i}^3 \frac{\text{Re} p_j(\bar{V}_i + \bar{V}_j)}{\sqrt[3]{\bar{\alpha}_j}} [-\bar{F}_{ij} \bar{R}_{ij} + \bar{G}_{ij} \bar{S}_{ij} - 16 \bar{D}_{ij} \bar{T}_{ij} \text{sgn}(i-j)]. \quad [55]$$

$$\frac{D_{si}}{v} = \sqrt[3]{\frac{\rho_p}{\rho}} \frac{1}{3} \sum_{j=1, j \neq i}^3 \frac{\text{Re} p_j(\bar{V}_i + \bar{V}_j)}{\sqrt[3]{\bar{\alpha}_j}} \left[\bar{E}_{ij} \bar{E}_{ij} + \frac{9 \bar{D}_{ij}}{\bar{E}_{ij}} \right], \quad [56]$$

where the coefficients a_{ij} , b_{ij} , ψ_{ij} are the same.

The coefficients A_{ij} , B_{ij} , F_{ij} and the functions \bar{C}_{ij} , \bar{D}_{ij} , \bar{G}_{ij} depend on the angle $\bar{\gamma}_i$, which varies according to the correlation $\text{tg } \bar{\gamma}_i = \bar{V}_{si} / \bar{U}_{si}$, and the angle $\bar{\varphi}_{ij}$, which varies according to the correlation

$$\bar{\varphi}_{ij} = \left| \frac{\bar{V}_{si}}{\bar{U}_{si}} - \frac{\bar{V}_{sj}}{\bar{U}_{sj}} \right|.$$

The functions are:

$$\bar{C}_{ij} = \frac{4(2a_{ij} + 3b_{ij})b_{ij}(\bar{\omega}_i + \bar{\omega}_j)}{15(\bar{V}_i + \bar{V}_j)}, \quad \bar{D}_{ij} = b_{ij}^2 \left(\frac{\bar{\omega}_i + \bar{\omega}_j}{\bar{V}_i + \bar{V}_j} \right)^2, \quad \bar{G}_{ij} = \frac{5}{8}(5a_{ij} + 7b_{ij})b_{ij} \left(\frac{\bar{\omega}_i + \bar{\omega}_j}{\bar{V}_i + \bar{V}_j} \right)$$

and the total velocity is $\bar{V}_i = \sqrt{\bar{U}_{si}^2 + \bar{V}_{si}^2}$ and $\bar{V}_j = \sqrt{\bar{U}_{sj}^2 + \bar{V}_{sj}^2}$. The functions \bar{E}_{ij} , \bar{H}_{ij} , \bar{L}_{ij} , \bar{M}_{ij} , \bar{N}_{ij} , \bar{O}_{ij} , \bar{P}_{ij} , \bar{Q}_{ij} , \bar{R}_{ij} , \bar{S}_{ij} , \bar{T}_{ij} , are the functions of the total velocity \bar{V}_i and \bar{V}_j and angle $\bar{\varphi}_{ij}$, which are defined by [C1]–[C12] in appendix C. These coefficients and functions are obtained using the transformations of the self-similar coordinate system.

As one can see, the obtained pseudoviscosity coefficients are conditioned by the flow (linear and angular velocity components of colliding particles and their mass concentration), and relaxation (the particle sizes, ratio of particle material density and the density of the carrier fluid) and also the collision parameters (restitution coefficient of the normal velocity component and friction coefficient of the tangential velocity component of colliding particles). One can see that the pseudoviscosity coefficients generally consist of three terms which describe three correlations: the correlations of linear–linear, linear–angular and angular–angular particle velocities. By means of this the peculiarities of the motion of particles in two-phase boundary layers are described. As the calculations show, the values of the pseudoviscosity coefficients vary due to the value of the pseudoviscosity coefficient of dispersed phase, which is a factor of 10^3 – 10^4 greater than that obtained according to the formula of Einstein $v_s = 2.5\beta v$ (Soo 1971) for a small volumetric concentration of particles ($\beta \ll 1$), for the values close to the coefficient of laminar viscosity v of the carrier flow. While using the Einstein formula for calculating the pseudoviscosity coefficients, the numerical distribution of particle mass concentration will slightly differ from those obtained by Soo (1971), Osypstov (1980) and Asmolov (1992). This contradicts our experimental concentration profiles. While using the given interparticle collision model, the influence of the diffusion processes and hence the pseudoviscosity coefficients on the mass and momentum transfer intensifies. This provides a satisfactory agreement with the experimental data.

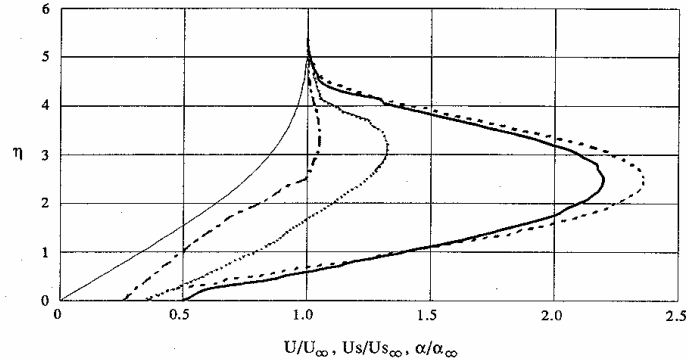


Figure 10. Numerical profiles of the axial velocity component of gas and solid phases (—, $U/U_\infty, U_s/U_{s_\infty}, X = 100 \text{ mm}, \delta = 12 \mu\text{m}$) and particle mass concentration α/α_∞ : - - -, $X = 100 \text{ mm}, \delta = 12 \mu\text{m}$; ····, $X = 100 \text{ mm}, \delta = 23 \mu\text{m}$; - · - ·, $X = 100 \text{ mm}, \delta = 32 \mu\text{m}$. The stream flow velocity $U_\infty = 1.5 \text{ m/s}$.

4. RESULTS AND DISCUSSION

Figures 10 and 11 represent the numerical distributions of the streamwise velocity components of the gaseous and the dispersed phases and relative particle mass concentration expressed in self-similar coordinates for the cross-sections of 100 and 170 mm. Comparison of our experimental and theoretical results with calculations of other models (Soo 1971; Osyptsov 1980; Asmolov 1992) is presented in figure 12.

As one can see from figures 10 and 11, the numerical distribution of relative particle mass concentration in the laminar boundary layer is substantially non-uniform. The concentration grows monotonously from the outer part of the boundary layer, reaches its maximum at some distance from the surface and decreases towards the wall up to 20% of its value in the free stream. The growth of particle mass concentration in the outer part of the boundary layer can be explained by the penetration of inertia particles inside the boundary layer where the particles slow down. The following reduction of mass concentration towards the surface can probably be explained by the diffusion mechanism imposed by the interparticle collision and by their collisions with the surface. The prevalence of diffusion transfer over the convective transfer near the surface is connected, first,

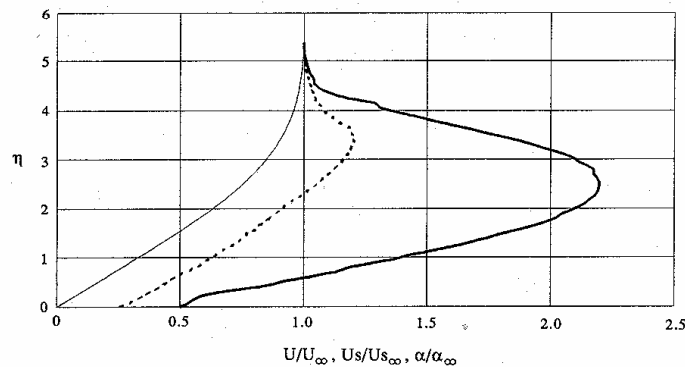


Figure 11. Numerical profiles of the axial velocity component of gas and solid phases (—, $U/U_\infty, U_s/U_{s_\infty}, U_\infty = 1.5 \text{ m/s}$) and particle mass concentration α/α_∞ for $\delta = 12 \mu\text{m}$ in cross-section $X = 100 \text{ mm}$ for various stream flow velocities: —, $U_\infty = 1.5 \text{ m/s}$; - - -, $U_\infty = 3 \text{ m/s}$.

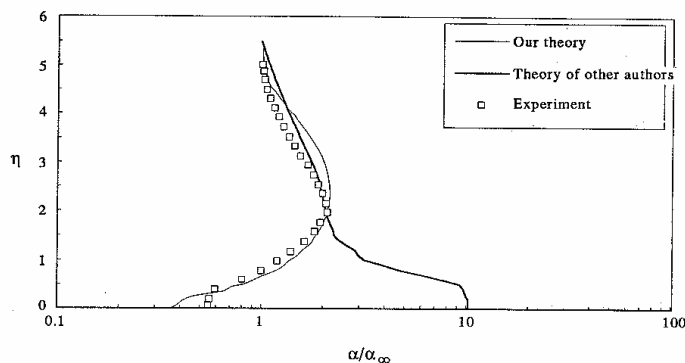


Figure 12. Comparison of experimental and numerical profiles of particle mass concentration with different models. The stream flow velocity $U_\infty = 1.5$ m/s and particle average diameter $\delta = 12 \mu\text{m}$ in cross-section $X = 170$ mm.

with the decrease of convective transfer near the surface, and second, with the intensification of the diffusion processes. This intensification emanates from the increase of particle velocity disturbance originated both from their interaction with the surface and from the different influence of the drag force and two lift forces, those of Magnus and Saffman, imposed on the particles of different sizes.

According to the numerical investigations, the distribution of particle mass concentration has its maximum value for fine particles (figure 10, $\delta = 12 \mu\text{m}$). The maximum mass concentration decreases with the growth of particle size and the profile becomes less non-uniform (figure 10, $\delta = 23$ and $32 \mu\text{m}$). It also follows from this figure that the concentration maximum shifts towards the outer part of the boundary layer for large particles. The influence of increasing free stream velocity on the concentration distribution is analogous to the influence of the growth of particle size, as is shown in figure 11. The same tendencies of modification of the distribution of particle mass concentration have been observed in the experiments.

The existing modes of two-phase laminar boundary layer on a flat plate (Soo 1971; Osypov 1980; Asmolov 1992), based on the description of the dispersed phase within the ideal gas conception, cannot provide the experimentally observed distributions of relative particle mass concentration (figure 12) since the mass transfer from the diffusion is not taken into account within those models. The authors calculated the two-phase laminar boundary layer with the monodispersed particles. Thus they excluded the interparticle collision mechanism from the consideration and, therefore, the diffusion transfer.

Presenting the dispersed phase within the concept of Newtonian fluid, by introducing the pseudoviscosity coefficients and specifying the boundary conditions for the dispersed phase, one can obtain the distributions of particle mass concentration by numerical calculations, which agree with our experimental data. The given model also describes the tendency of variation of the particle mass concentration with the parameters of free stream. Thus, the pseudodiffusion coefficient [56] increases with the growth of particle size or free stream velocity which leads to more uniform distribution of particle mass concentration.

Some discrepancy in the experimental and numerical results is due to the approximate description of the composition of the polydispersed admixture and the boundary conditions on the surface, specifically, when the impenetrability condition on the surface is set in the form [30] (the particle collision with the surface is implied to be elastic).

Thus, the model shows the principle possibility for applying the pseudoviscosity approach for the description of the motion and distribution of solid admixture in two-phase laminar boundary layer developed on the flow past the unyawed flat plate.

5. CONCLUSIONS

The distributions of solid admixture in the particle-laden laminar boundary layer on a flat plate for the Reynolds numbers of flow past $Re_x \approx 10^4$ have been experimentally obtained. The profiles of particle mass concentration essentially and systematically differ from those obtained by up-to-date theoretical models. The presented mathematical model based on the approximation of the dispersed phase within the Newtonian viscous fluid, taking into consideration the introduced pseudoviscosity coefficients, was elaborated for describing the experimental results. The dispersed phase is considered as polydispersed with finite number of particle fractions that permit determination of the pseudoviscosity coefficients by the interparticle collision mechanism. The given model and specific boundary conditions, with the assumption of particle mass flux input into the boundary layer from undisturbed free stream flow and the diffusion of particles from the surface inside the boundary layer due to the collisions with the surface allow us to correctly describe the experimental data. The discrepancy between theoretical and experimental results probably comes from using both the simplest version of the model, where the dispersed phase is restricted because only three fractions of particles and the boundary conditions are set for the elastic collisions of particles with the surface.

Acknowledgements—The theoretical part of this work was supported by a Grant of the International Science Foundation No. LG 6000. The authors are grateful to Mrs H. Käbi for correcting the English.

REFERENCES

- Anderson, D. A., Tannehill, J. C. & Pletcher, R. H. 1990 *Computational Fluid Mechanics and Heat Transfer*, Vols 1 & 2. Mir, Moscow (in Russian).
- Asmolov, E. S. 1992 Particulate movement in the laminar boundary layer on a flat plate. *Izv. Akad. Nauk SSSR Mekh. Zhidk. Gasa* **1**, 66–73 (in Russian).
- Babukha, G. L. & Shraiber, A. A. 1972 *Interaction of Particles of Polydispersive Material in Two phase Flows*. Naukova Dumka, Kiev (in Russian).
- Byrd, P. F. & Friedman, M. D. 1971 *Handbook of Elliptic Integrals for Engineers and Scientists*. Springer, New York.
- Chapman, S. & Cowling, T. G. 1960 *The Mathematical Theory of Non-uniform Gases*. Inostrannaja Literatura, Moscow (in Russian).
- Kravtsov, M. V. 1968 Drag to the free steady motion of sphere in viscous medium. *J. Engng Phys.* **XV**, 464–470 (in Russian).
- Marble, F. E. 1964 Mechanism of particle collision in the one-dimensional dynamics of gas–particle mixtures. *Phys. Fluids* **7**, 1270–1282.
- Nigmatulin, R. I. 1978 *Fundamentals of Mechanics of Heterogeneous Media*. Nauka, Moscow (in Russian).
- Osyptsov, A. N. 1980 Structure of a laminar disperse-mixture boundary layer on a flat plate. *Izv. Akad. Nauk SSSR Mekh. Zhidk. Gasa* **4**, 48–54 (in Russian).
- Roache, P. J. 1980 *Computational Fluid Dynamics*. Mir, Moscow (in Russian).
- Rubinow, S. I. & Keller, J. B. 1961 The transverse force on a spinning sphere moving in a viscous fluid. *J. Fluid Mech.* **11**, 447–459.
- Saffman, P. G. 1965 The lift on a small sphere in a shear flow. *J. Fluid Mech.* **22**, 385–400.
- Schlichting, G. 1974 *Theory of Boundary Layer*. Nauka, Moscow (in Russian).
- Shraiber, A. A., Milyutin, V. N. & Yatsenko, V. P. 1980 *Hydromechanics of Two-component Flows with Solid Polydispersive Substance*. Naukova Dumka, Kiev (in Russian).
- Soo, S. L. 1971 *Fluid Dynamics of Multiphase Systems*. Mir, Moscow (in Russian).
- Tennekes, H. & Lumley, J. L. 1972 *A First Course in Turbulence*. MIT Press, Cambridge, MA.
- Trushin, G. I. & Lipatov, N. N. 1963 The probability of collision of the suspended particles in their oriented motion. *Izv. Vizshich Uchebnich Zavedeniy. Pischevaya Technol.* **5**, 110–114 (in Russian).

APPENDIX A

The expressions of the velocity differences for the first particle:

$$V'_{12\xi} - V_{1\xi} = a_{12}\sqrt{1-\chi^2}[\sqrt{1-\chi^2}(V_2 \cos \varphi - V_1) - \chi V_2 \sin \varphi \sin \theta] \\ + b_{12}\chi[\chi(V_2 \cos \varphi - V_1) + \sqrt{1-\chi^2}V_2 \sin \varphi \sin \theta] - c_{12}[\sqrt{1-\chi^2} \sin \alpha + \chi \cos \alpha \sin \theta]. \quad [\text{A1}]$$

$$V'_{12\eta} - V_{1\eta} = a_{12}\sqrt{1-\chi^2}[\sqrt{1-\chi^2}V_2 \sin \varphi + \chi \sin \theta (V_2 \cos \varphi - V_1)] \\ + b_{12}\chi[\chi V_2 \sin \varphi - \sqrt{1-\chi^2}(V_2 \cos \varphi - V_1) \sin \theta] + c_{12}[\sqrt{1-\chi^2} \cos \alpha - \chi \sin \alpha \sin \theta], \quad [\text{A2}]$$

$$\omega'_{12} - \omega_1 = -\frac{b_{12}}{\zeta} \left[\left(\omega_1 + \frac{\delta_1}{\delta_2} \omega_2 \right) (1 - \chi^2 \cos^2 \theta) - \frac{2}{\delta_1} \chi \sin \theta \sqrt{V_1^2 + V_2^2 - 2V_1 V_2 \cos \varphi} \right] \quad [\text{A3}]$$

and for the second particle:

$$V'_{21\xi} - V_{2\xi} = a_{21}\sqrt{1-\chi^2}[\sqrt{1-\chi^2}(V_1 \cos \varphi - V_2) - \chi V_1 \sin \varphi \sin \theta] \\ + b_{21}\chi[\chi(V_1 \cos \varphi - V_2) - \sqrt{1-\chi^2}V_1 \sin \varphi \sin \theta] + c_{21}[\sqrt{1-\chi^2} \sin \alpha + \chi \cos \alpha \sin \theta] \quad [\text{A4}]$$

$$V'_{21\eta} - V_{2\eta} = a_{21}\sqrt{1-\chi^2}[\sqrt{1-\chi^2}V_1 \sin \varphi - \chi \sin \theta (V_1 \cos \varphi - V_2)] \\ + b_{21}\chi[\chi V_1 \sin \varphi + \sqrt{1-\chi^2}(V_1 \cos \varphi - V_2) \sin \theta] + c_{21}[\sqrt{1-\chi^2} \cos \beta - \chi \sin \beta \sin \theta], \quad [\text{A5}]$$

$$\omega'_{21} - \omega_2 = -\frac{b_{21}}{\zeta} \left[\left(\omega_2 + \frac{\delta_1}{\delta_2} \omega_1 \right) (1 - \chi^2 \cos^2 \theta) - \frac{2}{\delta_2} \chi \sin \theta \sqrt{V_1^2 + V_2^2 - 2V_1 V_2 \cos \varphi} \right] \quad [\text{A6}]$$

which differ from [A1]–[A3] by the coefficients a_{ij} , b_{ij} before the square brackets and transposition of the velocities V_1 , V_2 .

Here the variables are:

$$\cos \alpha = \frac{(V_2 \cos \varphi - V_1)}{\sqrt{V_1^2 + V_2^2 - 2V_1 V_2 \cos \varphi}}, \quad \sin \alpha = \frac{V_2 \sin \varphi}{\sqrt{V_1^2 + V_2^2 - 2V_1 V_2 \cos \varphi}}, \\ \cos \beta = \frac{-(V_1 \cos \varphi - V_2)}{\sqrt{V_1^2 + V_2^2 - 2V_1 V_2 \cos \varphi}}, \quad \sin \beta = \frac{V_1 \sin \varphi}{\sqrt{V_1^2 + V_2^2 - 2V_1 V_2 \cos \varphi}}$$

and coefficients are:

$$a_{12} = (1 - k'_n)\psi_{21}, \quad b_{12} = \frac{(1 - k'_r)\zeta\psi_{21}}{(1 + \zeta)}, \quad c_{12} = \frac{(\delta_1\omega_1 + \delta_2\omega_2)b_{12}}{2}, \\ a_{21} = (1 - k'_n)\psi_{12}, \quad b_{21} = \frac{(1 - k'_r)\zeta\psi_{12}}{(1 + \zeta)}, \quad c_{21} = \frac{(\delta_1\omega_1 + \delta_2\omega_2)b_{21}}{2}.$$

$$u'_{12} - u_1 = a_{12}\sqrt{1-\chi^2}[\sqrt{1-\chi^2}(V_2 \cos(\varphi + \gamma_1) - V_1 \cos \gamma_1) - \chi \sin \theta (V_2 \sin(\varphi + \gamma_1) - V_1 \sin \gamma_1)] \\ + b_{12}\chi[\chi(V_2 \cos(\varphi + \gamma_1) - V_1 \cos \gamma_1) + \sqrt{1-\chi^2} \sin \theta (V_2 \sin(\varphi + \gamma_1) - V_1 \sin \gamma_1)] \\ - c_{12} \left[\frac{\sqrt{1-\chi^2}(V_2 \sin(\varphi + \gamma_1) - V_1 \sin \gamma_1)}{\sqrt{V_1^2 + V_2^2 - 2V_1 V_2 \cos \varphi}} + \frac{\chi \sin \theta (V_2 \cos(\varphi + \gamma_1) - V_1 \cos \gamma_1)}{\sqrt{V_1^2 + V_2^2 - 2V_1 V_2 \cos \varphi}} \right], \quad [\text{A7}]$$

$$v'_{12} - v_1 = a_{12}\sqrt{1-\chi^2}[\sqrt{1-\chi^2}(V_2 \sin(\varphi + \gamma_1) - V_1 \sin \gamma_1) + \chi \sin \theta (V_2 \cos(\varphi + \gamma_1) \\ - V_1 \cos \gamma_1)] + b_{12}\chi[\chi(V_2 \sin(\varphi + \gamma_1) - V_1 \sin \gamma_1) + \sqrt{1-\chi^2} \sin \theta (V_2 \cos \\ \times (\varphi + \gamma_1) - V_1 \cos \gamma_1)] + c_{12} \left[\frac{\sqrt{1-\chi^2}(V_2 \cos(\varphi + \gamma_1) - V_1 \cos \gamma_1)}{\sqrt{V_1^2 + V_2^2 - 2V_1 V_2 \cos \varphi}} \right. \\ \left. - \frac{\chi \sin \theta (V_2 \sin(\varphi + \gamma_1) - V_1 \sin \gamma_1)}{\sqrt{V_1^2 + V_2^2 - 2V_1 V_2 \cos \varphi}} \right], \quad [\text{A8}]$$

$$\begin{aligned}
u'_{21} - u_2 &= a_{21}\sqrt{1-\chi^2}[\sqrt{1-\chi^2}(V_1 \cos(\varphi + \gamma_2) - V_2 \cos \gamma_2) + \chi \sin \theta(V_1 \sin(\varphi + \gamma_2) - V_2 \sin_2 \gamma_2)] \\
&\quad + b_{21}\chi[\chi(V_1 \cos(\varphi + \gamma_2) - V_2 \cos \gamma_2) - \sqrt{1-\chi^2} \sin \theta(V_1 \sin(\varphi + \gamma_2) - V_2 \sin \gamma_2)] \\
&\quad + c_{21}\left[\frac{\sqrt{1-\chi^2}(V_1 \sin(\varphi + \gamma_2) - V_2 \sin \gamma_2)}{\sqrt{V_1^2 + V_2^2 - 2V_1 V_2 \cos \varphi}} - \frac{\chi \sin \theta(V_1 \cos(\varphi + \gamma_2) - V_2 \cos \gamma_2)}{\sqrt{V_1^2 + V_2^2 - 2V_1 V_2 \cos \varphi}}\right], \quad [\text{A9}] \\
v'_{21} - v_2 &= a_{21}\sqrt{1-\chi^2}[\sqrt{1-\chi^2}(V_1 \sin(\varphi + \gamma_2) - V_2 \sin \gamma_2) - \chi \sin \theta(V_1 \cos(\varphi + \gamma_2) - V_2 \cos \gamma_2)] \\
&\quad + b_{21}\chi[\chi(V_1 \sin(\varphi + \gamma_2) - V_2 \sin \gamma_2) + \sqrt{1-\chi^2} \sin \theta(V_1 \cos(\varphi + \gamma_2) - V_2 \cos \gamma_2)] \\
&\quad - c_{21}\left[\frac{\sqrt{1-\chi^2}(V_1 \cos(\varphi + \gamma_2) - V_2 \cos \gamma_2)}{\sqrt{V_1^2 + V_2^2 - 2V_1 V_2 \cos \varphi}}\right. \\
&\quad \left. + \frac{\chi \sin \theta(V_1 \sin(\varphi + \gamma_2) - V_2 \sin \gamma_2)}{\sqrt{V_1^2 + V_2^2 - 2V_1 V_2 \cos \varphi}}\right], \quad [\text{A10}]
\end{aligned}$$

where the angles γ_1, γ_2 are determined from the following relations: $u_1 = V_1 \cos \gamma_1, v_1 = V_1 \sin \gamma_1$ and $u_2 = V_2 \cos \gamma_2, v_2 = V_2 \sin \gamma_2$. Formulae for the particle angular velocity fluctuations are the same as [A3] and [A6], since all transformations have occurred in the plane $\xi_0 \eta$.

APPENDIX B

Some expressions used in section 3.4 are listed in this appendix:

$$H^{\theta} = \left[1 - \frac{k_{\theta}^2}{2} \left(\frac{\sin \varphi_{\theta}}{\varphi_{\theta}}\right)\right] \frac{\varphi_{\theta}}{E^{\theta}}, \quad [\text{B1}]$$

$$O_{ij}^{\theta} = \frac{k_{\theta}^2 \sin^2 0.5\varphi_{\theta}}{E^{\theta}} \left(1 - \frac{V_j}{V_i} \cos^2 0.5\varphi_{\theta}\right) \quad [\text{B2}]$$

$$O_{ij}^{\theta} = \frac{k_{\theta}^2}{4E^{\theta}} \left[\sin \varphi_{\theta} \left(1 - \frac{V_j}{V_i} \cos \varphi_{\theta}\right) - \varphi_{\theta} \frac{V_i}{V_j} \left(1 - \frac{V_j \sin \varphi_{\theta}}{V_i \varphi_{\theta}}\right)\right], \quad [\text{B3}]$$

$$P_{ij}^{\theta} = 1 - \frac{2}{3} \frac{V_j (2 - k_{\theta}^2)}{V_i k_{\theta}^2} + \frac{4}{3} \frac{V_j (1 - k_{\theta}^2) K^{\theta}}{V_i k_{\theta}^2 E^{\theta}} - \frac{2}{3} \frac{V_j \Delta^{\theta} \sin \varphi_{\theta}}{V_i E^{\theta}}, \quad [\text{B4}]$$

$$\begin{aligned}
P_{ij}^{\theta} &= \frac{4V_j(1-k_{\theta}^2)}{E^{\theta} V_i k_{\theta}^2} \left[1 - \left(\frac{1-k_{\theta}^2 \cos^2 0.5\varphi_{\theta}}{1-k_{\theta}^2}\right)^{0.5}\right] \left\{ \text{sgn}(V_i - V_j) - \text{sgn}(i-j) \frac{\sqrt{1-k_{\theta}^2}}{3} \right. \\
&\quad \left. \times \left[1 + \left(\frac{1-k_{\theta}^2 \cos^2 0.5\varphi_{\theta}}{1-k_{\theta}^2}\right)^{0.5} + \frac{1-k_{\theta}^2 \cos^2 0.5\varphi_{\theta}}{1-k_{\theta}^2}\right] \right\}, \quad [\text{B5}]
\end{aligned}$$

$$Q_{ij}^{\theta} = \frac{2V_j}{E^{\theta} V_i} \left[\sin^2 0.5\varphi_{\theta} - \text{sgn}(i-j) \text{sgn}(V_i - V_j) \frac{\sqrt{1-k_{\theta}^2}}{k_{\theta}^2} \ln \left(\frac{1-k_{\theta}^2 \cos^2 0.5\varphi_{\theta}}{1-k_{\theta}^2}\right)\right], \quad [\text{B6}]$$

$$Q_{ij}^{\theta} = \frac{V_j \varphi_{\theta}}{V_i E^{\theta}} \left[\frac{2(1-k_{\theta}^2)}{k_{\theta}^2} + 1 + \frac{\sin \varphi_{\theta}}{\varphi_{\theta}} - \frac{4\sqrt{1-k_{\theta}^2}}{k_{\theta}^2 \varphi_{\theta}} \arctg \left(\frac{\text{tg } 0.5\varphi_{\theta}}{\sqrt{1-k_{\theta}^2}}\right)\right], \quad [\text{B7}]$$

$$R_{ij}^{\theta} = k_{\theta} \sqrt{\frac{V_i}{V_j}} \left[1 + \left(\frac{2-k_{\theta}^2}{3k_{\theta}^2} - \frac{2(1-k_{\theta}^2) k^{\theta}}{3k_{\theta}^2 E^{\theta}} - \frac{2\Delta^{\theta} \sin \varphi_{\theta}}{3E^{\theta}}\right) \frac{V_i}{V_j}\right], \quad [\text{B8}]$$

$$\begin{aligned}
R_{ij}^{\theta} &= \frac{4}{3} \sqrt{\frac{V_j(1-k_{\theta}^2)^{1.5}}{V_i k_{\theta} E^{\theta}}} \left[1 - \left(\frac{1-k_{\theta}^2 \cos^2 0.5\varphi_{\theta}}{1-k_{\theta}^2}\right)^{0.5}\right] \left[1 + \left(\frac{1-k_{\theta}^2 \cos^2 0.5\varphi_{\theta}}{1-k_{\theta}^2}\right)^{0.5} \right. \\
&\quad \left. + \frac{1-k_{\theta}^2 \cos^2 0.5\varphi_{\theta}}{1-k_{\theta}^2}\right], \quad [\text{B9}]
\end{aligned}$$

$$S^{ij} = \frac{\varphi_{ij} k_{ij}}{E^{ij}} \sqrt{\frac{V_i}{V_j}} \left(1 - \frac{V_j \sin \varphi_{ij}}{V_i} \right), \quad [\text{B10}]$$

$$S^{ij} = \frac{2k_{ij} \sin^2 0.5\varphi_{ij}}{E^{ij}} \sqrt{\frac{V_j}{V_i}}, \quad [\text{B11}]$$

$$T^{ij} = \frac{2}{k_{ij}} \sqrt{\frac{V_j}{V_i}} \left[1 - \operatorname{sgn}(i-j) \operatorname{sgn}(V_i - V_j) \sqrt{1 - k_{ij}^2} \frac{K^{ij}}{E^{ij}} \right], \quad [\text{B12}]$$

$$T^{ij} = \frac{4}{k_{ij}} \sqrt{\frac{V_j}{V_i}} \frac{\sqrt{1 - k_{ij}^2}}{E^{ij}} \left[1 - \left(\frac{1 - k_{ij}^2 \cos^2 0.5\varphi_{ij}}{1 - j_{ij}^2} \right)^{0.5} \right], \quad [\text{B13}]$$

where the parameter

$$k_{ij}^2 = \frac{4V_i V_j}{(V_i + V_j)^2}$$

and the variable $\Delta^{ij} = \sqrt{1 - k_{ij}^2 \cos^2 0.5\varphi_{ij}}$ are calculated. The values of

$$K^{ij} = \int_0^{\varphi_{ij}} \frac{d\varphi}{\sqrt{1 - k_{ij}^2 \cos^2 0.5\varphi}} \quad \text{and} \quad E^{ij} = \int_0^{\varphi_{ij}} \sqrt{1 - k_{ij}^2 \cos^2 0.5\varphi} d\varphi$$

are the incomplete elliptic integrals of the first and second type, respectively.

APPENDIX C

Some expressions used in section 3.4 are listed in this appendix:

$$\bar{k}_{ij} = \frac{4V_i V_j}{(V_i + V_j)^2}, \quad [\text{C1}]$$

$$\bar{E}_{ij} = \sqrt{1 - \bar{k}_{ij}^2 + \frac{\bar{k}_{ij}^2 \bar{\varphi}_{ij}^2}{4}}, \quad [\text{C2}]$$

$$\bar{H}_{ij} = \bar{\varphi}_{ij} \bar{k}_{ij} \sqrt{\frac{V_j}{V_i}} \left[\sqrt{1 - \bar{k}_{ij}^2} \operatorname{sgn}(V_i - V_j) - \operatorname{sgn}(i-j) \bar{k}_{ij} \sqrt{\frac{V_j \bar{\varphi}_{ij}^2}{V_i}} \right], \quad [\text{C3}]$$

$$\bar{L}_{ij} = (1 - \bar{k}_{ij}^2) \operatorname{tg} 2\bar{\gamma}_i, \quad [\text{C4}]$$

$$\bar{M}_{ij} = \operatorname{tg} 2\bar{\gamma}_i - \operatorname{sgn}(i-j) \frac{\bar{\varphi}_{ij}}{2}, \quad [\text{C5}]$$

$$\bar{N}_{ij} = 1 - \frac{V_j \bar{k}_{ij}^2 \bar{\varphi}_{ij}^2}{3V_i E_{ij}^2}, \quad [\text{C6}]$$

$$\bar{O}_{ij} = \frac{\bar{\varphi}_{ij} V_j}{E_{ij}^2 V_i} \left[\sqrt{1 - \bar{k}_{ij}^2} \operatorname{sgn}(V_i - V_j) - \frac{\operatorname{sgn}(i-j)}{3} (1 - \bar{k}_{ij}^2 + \bar{E}_{ij} \sqrt{1 - \bar{k}_{ij}^2 + \bar{E}_{ij}^2}) \right], \quad [\text{C7}]$$

$$\bar{P}_{ij} = \frac{\bar{\varphi}_{ij} V_j}{V_i} \left[1 - \frac{\sqrt{1 - \bar{k}_{ij}^2}}{\bar{E}_{ij}} \operatorname{sgn}(i-j) \operatorname{sgn}(V_i - V_j) \right], \quad [\text{C8}]$$

$$\bar{Q}_{ij} = \frac{V_i \bar{\varphi}_{ij}^2}{2V_i E_{ij}^2}, \quad [\text{C9}]$$

$$\bar{R}_{ij} = 2\sqrt{1 - \bar{k}_{ij}^2} \operatorname{sgn}(V_i - V_j) - \operatorname{sgn}(i-j) \frac{\bar{k}_{ij}^2 \bar{\varphi}_{ij}^2}{6E_{ij}^2} \sqrt{\frac{V_j}{V_i}} + \frac{\operatorname{tg} \gamma_i \bar{k}_{ij} \bar{\varphi}_{ij}}{3} \sqrt{\frac{V_j}{V_i}} (1 - \bar{k}_{ij}^2 + \sqrt{1 - \bar{k}_{ij}^2} \bar{E}_{ij} + \bar{E}_{ij}^2), \quad [\text{C10}]$$

$$\bar{S}_{ij} = -\frac{\operatorname{sgn}(i-j)}{\bar{E}_{ij}} \left(2 \operatorname{sgn}(V_i - V_j) \sqrt{1 - \bar{k}_{ij}^2} \operatorname{tg} \bar{\gamma}_i - \sqrt{\frac{V_j}{V_i}} \bar{k}_{ij} \bar{\varphi}_{ij} \right), \quad [\text{C11}]$$

$$\bar{T}_{ij} = \frac{2V_j}{V_i \bar{k}_{ij}^2} \left[1 - \frac{\operatorname{sgn}(i-j) \operatorname{sgn}(V_i - V_j) \sqrt{1 - \bar{k}_{ij}^2 + \bar{\varphi}_{ij} \bar{k}_{ij}^2}}{\bar{E}_{ij}^2} \right], \quad [\text{C12}]$$

ARTICLE III

Hussainov, M., Kartushinsky, A., Shcheglov, I., Tisler, S., 1998, Some results of investigation of solid particles distribution in the vicinity of various shapes in two-phase flow and sedimentation on their surfaces. *Proc. of 27th Israel Conference on Mechanical Engineering*, Haifa, Israel, 19-20 May, pp. 356-358.

SOME RESULTS OF INVESTIGATION OF SOLID PARTICLES DISTRIBUTION IN THE VICINITY OF VARIOUS SHAPES IN TWO-PHASE FLOW AND SEDIMENTATION ON THEIR SURFACES

M. Hussainov, A. Kartushinsky*, I. Shcheglov and S. Tisler
Estonian Energy Research Institute, Paldiski road.1, EE0001 Tallinn, Estonia

*Conference Lecturer

ABSTRACT

The behaviour of solid particles in a two-phase laminar boundary layer for various streamlining shapes (flat plate, curved surface and cone) was experimentally investigated. The velocity of gas and the particle mass concentration were measured in vicinity of these surfaces while the intensity of the particle sedimentation was measured on the surfaces for various flow conditions (for the different stream velocities and particle sizes, for the different attack angles of a streamlining plate as well as different vertex angles of a cone).

INTRODUCTION

A large number of technological, and natural processes is bound with the motion of solid particles in gaseous flows, e.g., combustion of solid fuels, processes in scrubbers, pneumotransport, diffusion of solid suspension in the atmosphere. These processes are accompanied by the deposition of solid particles on the working surfaces of various devices.

The process of sedimentation on a body surface streamlined by a two-phase flow, is substantially stipulated by the particle motion and their distribution near the wall. The object of our experimental investigation was to obtain the data for building and improving the numerical models of the particle sedimentation, which can be applied for sedimentation prediction on the real objects.

EXPERIMENTAL CONDITIONS

The experiments were carried out using the facility for formation of vertical two-phase flow (Hussainov et al. [1]). A flat plate, curved and conical surfaces were used as models for investigation (see Figs. 1, 2). The models had the following dimensions:

- stainless steel flat plate: length 500 mm, width 100 mm, thickness 2 mm;
- aluminium alloy model with a curved surface: length 320 mm, width 170 mm, the curvature radius 300 mm, thickness in middle cross section 50 mm;
- four aluminium alloy cones with the values of the vertex angle α of 30°, 45°, 60° and 90° and with the base diameter of 100 mm.

The surface quality was characterised by the roughness height of the surface profile, which was about 6 μm for all models.

Each model was installed vertically in the working space of the wind channel with the help of a special holder. The design of the holders enabled to vary the value of attack angle.

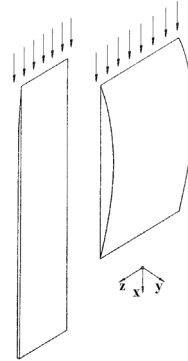


Fig.1. The flat plate and the curved surface.

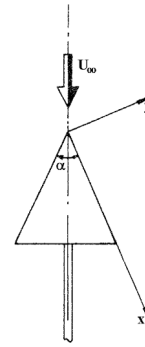


Fig.2. The cone model.

Electrocorundum powders (Al_2O_3) with the density of 3950 kg/m^3 and the average particle sizes 12, 23 and 32 μm were used for experiments.

The main parameters of laboratory tests (flow velocity U_∞ , particle size δ , particle mass concentration α_∞) were stipulated by the steady formation of a two-phase laminar boundary layer on the streamlining models and by uniform inflow of the dispersed phase in the working space of a wind-channel. The values of the stream flow velocity U_∞ were 1.5 and 3 m/s, the particle mass concentration in a free stream α_∞ was 0.01 kg dust/kg air for the streamlining of a flat plate and curved surface and 0.0044 kg dust/kg air for the streamlining of a conical surface.

MEASURING OF THE VELOCITY AND PARTICLE MASS CONCENTRATION

Distributions of the local averaged parameters (velocity of gas and particle mass concentration) in a two-phase flow in vicinity of the various shapes were measured with the help of the optic-electronic system which included the laser Doppler anemometer (LDA) and the laser concentration measurer (LCM) for determining the relative particle concentration by the methods described in [2].

The LDA consisted of the two channels (each channel for the concrete phase of the dispersed flow), the sending sections of the LDA-channels were combined. One of the LDA beams was used in the optic scheme of the LCM. The receiving section of the optic-electronic system consisted of the two LDA registration units for the scattered

attenuated radiation. Each of the LDA receiving units could pick up signals from the particles of a certain size. Signals of the instantaneous particle velocities from the LDA photoreceivers entered the channels of the carrier and dispersed phases of the processing system, which contained counters described by Pavlovski et al. [3]. These counters processed the Doppler signals from the particles of the dispersed flow.

As showed our experimental investigations, distribution of the particle mass concentration has the maximum located inside the boundary layer. The value of this maximum grows downstream while it immerses into the boundary layer.

The transformation of the concentration profile due to changing the attack angle is presented in Fig. 3 in the cross-section of 100 mm for the particle size $\delta = 23 \mu\text{m}$ and stream flow velocity $U_\infty = 1.5 \text{ m/s}$. Here and below the values of the particle mass concentration are related to the same in free stream (α/α_∞), the transversal coordinate of the boundary layer Y is related to the thickness of the laminar boundary layer D_L . The substantial transformation in the distribution of the particle mass concentration takes place while changing the value of the attack angle from 0° to 1° . The subsequent increasing of the attack angle results in growth of concentration in the vicinity of a flat plate (Fig. 3).

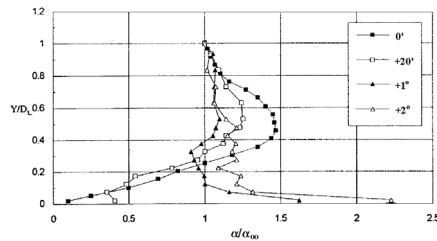


Fig.3. Concentration profiles on a flat plate.

Distributions of the particle mass concentration in various cross-sections of the curved surface for the particle size $23 \mu\text{m}$ and the stream flow velocity 3 m/s are shown in Fig. 4. The concentration profile is transformed, the concentration maximum, observed in vicinity of the surface upstream, moves away from the surface and decreases downstream (Fig. 4).

Fig. 5 represents the distributions of the particle mass concentration in vicinity of the conical surface for various values of the vertex angle, for $23 \mu\text{m}$ particles and for the stream flow velocity 1.5 m/s . Here the concentration profiles have the maximum values near the conical surface. The increase of the attack angle results in the growth of the concentration.

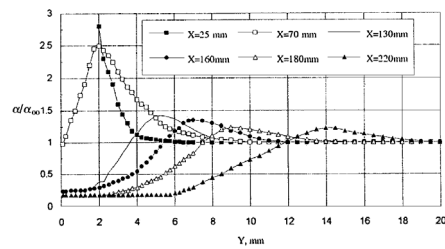


Fig.4. Concentration profiles on the curved surface.

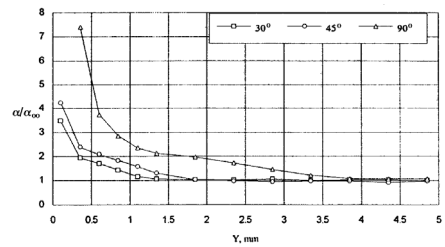


Fig.5. Concentration profiles near the cone surface for different vertex angles.

MEASURING OF THE PARTICLE SEDIMENTATION

The amount of the sedimented particles and their distribution along the surfaces were measured by a special weighing method. A special bench for removing the dust from the surface of flat plate and curved surface is shown in Fig. 6. After blowing by the two-phase flow during the given period of time T the model (Pos. 4) with sedimented dust on its surface was installed on the fixed plate (Pos. 3) by means of a holder (Pos. 2). The sedimented particles were removed from the surface with the help of a head (Pos. 1), which could move

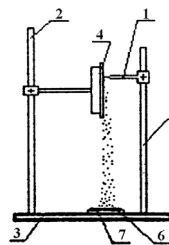


Fig.6. Bench for dust removing.

along a rod (Pos. 5). The removed dust fell down on the surface of the film specimen (Pos. 6), which was installed on the slab (Pos. 7). The mass of the specimen had been measured beforehand. The width of the head was determined by the width of the stripe on the model surface from which the particles were removed. The width of the head was 3 mm . Then the film specimen with the dust on its surface was weighed. The difference of the masses with and without dust was the mass M of the particles sedimented on the model surface in the given cross-section during the

given period of time T. The dimensionless intensity of the particle sedimentation I was determined as follows:

$$I = \frac{M}{U_{\infty} \rho \alpha_{\infty} S T}, \quad (1)$$

where U_{∞} , α_{∞} are the parameters of a free stream; ρ is the density of gas; S is the area of the stripe on the model surface from which the dust was removed.

Fig. 7 shows that the sedimentation intensity for a flat plate installed at zero attack angle grows downstream, but it reduces with the growth of the stream flow velocity and the particle size. Here and below I is the dimensionless sedimentation intensity; Re_x is the Reynolds number along the surface. The particle sedimentation substantially depends on the value of attack angle (Fig. 8). It grows with the increase of the angle.

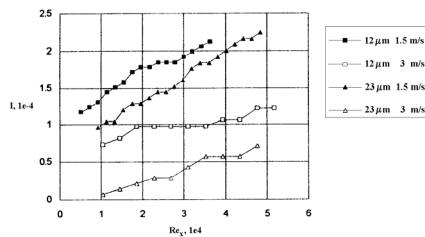


Fig.7. Intensity of particle sedimentation along the plate.

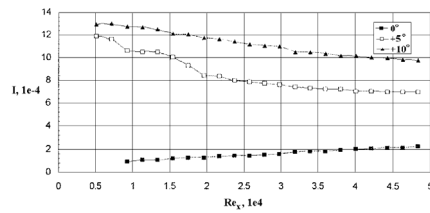


Fig.8. Intensity of particle sedimentation along the plate for various attack angles; $\delta = 23 \mu m$, $U_{\infty} = 1.5 m/s$.

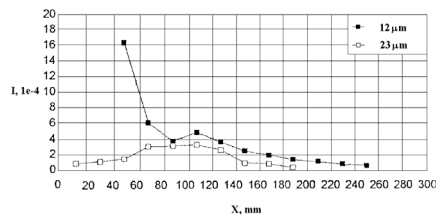


Fig.9. Intensity of particle sedimentation along the curved surface; $U_{\infty} = 3 m/s$.

Fig. 9 represents the distribution of the particle sedimentation intensity along the curved surface for the particles of two sizes.

The distributions of the particle sedimentation with respect to the cone vertex angle are represented in Fig. 10. The intensity increases with the growth of the cone angle and the maximum shifts towards the cone vertex (Fig. 10).

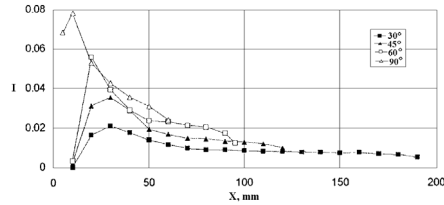


Fig.10. Intensity of particle sedimentation for different vertex angles of cone.

CONCLUSIONS

Our experimental investigations have revealed the following tendencies in the particle behaviour near the surfaces of various shapes and the particle sedimentation on their surfaces:

1. The profile of the particle mass concentration has its maximum value inside the boundary layer for all the shapes.
2. The maximum location and its magnitude are defined by the stream flow velocity, the particle size and the attack angle. The maximum increases and immerses into the boundary layer downstream with decreasing of the stream flow velocity and the particle size. The concentration maximum shifts towards the surface with increasing of the attack angle.
3. The particle sedimentation on a flat plate intensifies with the reduction in the stream flow velocity and the particle size and with the growth of the attack angle. The intensity of the particle sedimentation on the curved surface becomes stronger for the smaller particles, while for the cone surface it increases with the vertex angle.

The given experimental investigations were fulfilled within the international project "Mars 94/96" in the frame of the co-operation between the Russian and French Space Agencies.

REFERENCES

- [1] M. Hussainov, A. Kartushinsky, A. Mulgi, Ü. Rudi and S. Tisler, *Int. J. Multiphase Flow* **21**, 1141 (1995).
- [2] V. Zlobin and A. Rosenstein, (in Russian), *J. Appl. Mech. and Tech. Phys.* **1**, 142 (1975).
- [3] B. Pavlovsky, V. Zamansky, N. Semidetrov and S. Juras, in *Applying of Laser Doppler Anemometers for Heat Power Engineering* (in Russian, Leningrad), (1989).

ARTICLE IV

Hussainov, M., Kartushinsky, A., Tisler, S., 2002, Experimental study of adhesive behaviour of pair “solid particle-streamlined surface”. *Proc. of 10th Workshop on Two-Phase Flow Predictions*, Merseburg, Germany, April 9-12, pp. 401-405.

EXPERIMENTAL STUDY OF ADHESIVE BEHAVIOUR OF PAIR “SOLID PARTICLE–STREAMLINED SURFACE”

M. Hussainov, A. Kartushinsky, S. Tisler
Laboratory of Energy Processes Diagnostics,
Estonian Energy Research Institute
Paldiski Rd. 1, 10137, Tallinn, Estonia
Phone: (372) 6621822, Fax: (372) 6613655
e-mail: aeromeh@online.ee

Introduction

A large number of technological and natural processes is bound with the motion of solid particles in gaseous flows, e.g., combustion of solid fuels, processes in scrubbers, pneumotransport, diffusion of solid suspension in the atmosphere etc. These processes are accompanied by the deposition of solid particles on the working surfaces of various devices that often results in deterioration of their performance. The amount of deposited particles in many respects depends on the adhesive properties of particles and a surface. The object of the given investigation was to obtain data for analysing the physical nature of sticking of particles deposited from the flow to the surface and their holding on the surface.

Experimental conditions

The electrocorundum powders (the physical density $\rho_p=3950 \text{ kg/m}^3$, Young's modulus of elasticity $E_p=7 \cdot 10^{11} \text{ N/m}^2$, Poisson's ratio $\eta_p=0.3$) with the particle average sizes $\delta_p=12, 23$ and $32 \text{ }\mu\text{m}$ were used in the experiments. The surface of the aluminium alloy conic model with the vertex angle $\beta=60^\circ$ and the base diameter of 100 mm was used as the surface for particles' deposition. The surface material had the next properties: the physical density $\rho_s=2790 \text{ kg/m}^3$, Young's modulus of elasticity $E_s=6.6 \cdot 10^{10} \text{ N/m}^2$, Poisson's ratio $\eta_s=0.3$. The surface quality was characterised by the roughness height of the surface profile, which was about $6 \text{ }\mu\text{m}$.

Measurement technique

The experiments were carried out at the special test rig (Fig. 1) designed for the investigations of the adhesive properties of particles and a surface.

During the tests the dependence of the particles adhesion number α from the detaching force F_d was determined by the centrifugal technique consisted in the separating of particles from the rotating surface initially covered by the particles.

The square $20 \times 20 \text{ mm}$ specimens (10, Fig. 1) of the polyethylene terephthalate film of $6 \text{ }\mu\text{m}$ thickness were used to catch the removed particles. Immediately before the tests the set of such specimens was prepared, degreased by technical alcohol and dried. Then the net mass m_1 of each specimen was measured by the weigher with the accuracy of 0.05 mg .

The surface of the conic model installed on a shaft of electric motor was also degreased, dried and covered with the particles by the technique of the gravity deposition. During the covering the model was rotated very slowly by the motor in order to obtain more uniform distribution of the particles along the surface. The duration of deposition was $20 \dots 30$ seconds. Immediately before the covering the powders were bolted with the help of the set of three sieves with the mesh size of 160, 400 and $700 \text{ }\mu\text{m}$ in order to exclude the large aggregates of particles.

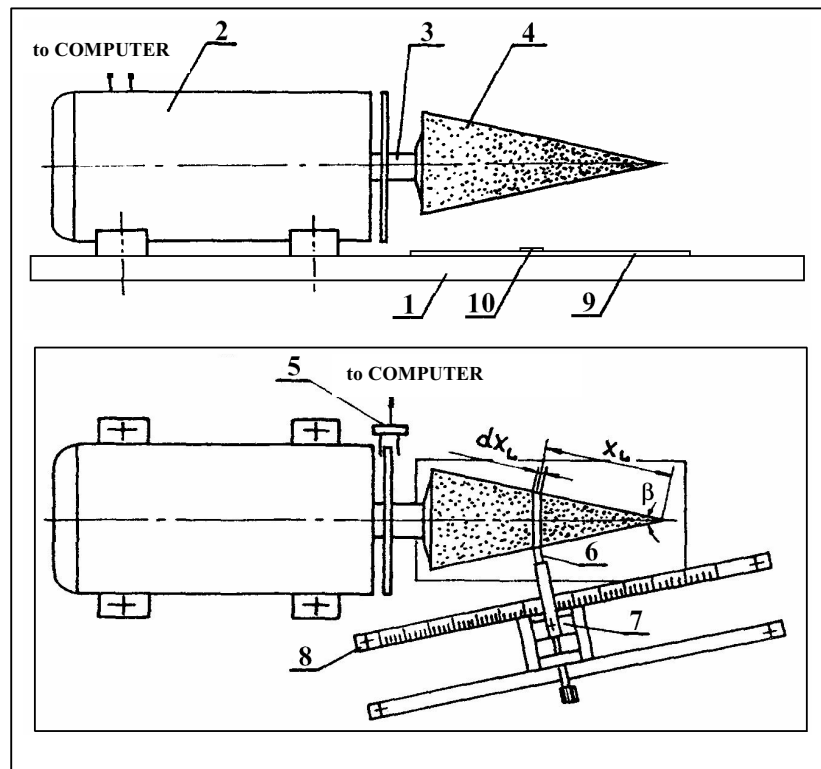


Fig. 1. The test rig: 1 – the fixed bed; 2 – the DC electric motor; 3 – the sleeve for installing of the model on the shaft of the electric motor; 4 – the aluminium alloy conic model; 5 – infrared transducer of the rotational speed of the model; 6 – the special head for removing of dust from the model's surface; 7, 8 – the coordinate device; 9 – a slab; 10 – the film specimen for collecting of particles removed from the model surface.

The removing of particles from the model surface in every test was carried out with the help of the head (6, Fig. 1) which was brought into contact with the surface in the given cross-section, by the manual rotating of the model. The removed particles were dumped onto the film specimen installed on a slab (9, Fig. 1). The width of the test cross-sections dx_L was approximately equalled to the width of the head which was 3 mm. The coordinate of the cross-section X_L was counted from the model vertex with the help of the coordinate device (7, 8, Fig. 1).

The first test was carried out without rotation of the model. The particles were removed in the cross-sections $X_L=10, 30$ and 90 mm.

At the second test the rotational speed of the electric motor was increased fluently up to 14 rps. The rotational speed was varied with the help of the varistor and controlled by the infrared transducer (5, Fig. 1). The motor ran at this speed during 7...10 seconds. Then the speed was fluently decreased till zero and the motor was switched off. The particles which remained at the surface after finishing of rotation were removed in the cross-sections $X_L=7, 27$ and 87 mm.

At the third test the rotational speed was increased up to 28 rps, maintained at this speed during 7...10 seconds and then fluently decreased till zero. The particles remained at the surface was removed in the cross-sections $X_L=13, 33$ and 93 mm.

Then, the masses of all the film specimens covered with the particles were measured: m_{2i} for the test without rotation, m_{2j} for the test with the rotational speed of 14 rps, m_{2k} for the test with the rotational speed of 28 rps. After that the net masses of particles from each specimen were calculated as: $m_{pi}=m_{2i}-m_{1i}$; $m_{pj}=m_{2j}-m_{1j}$; $m_{pk}=m_{2k}-m_{1k}$. Here m_{1i} , m_{1j} , m_{1k} are the net masses of the clean specimens. Indices i, j, k corresponds to the tests without rotation of the model, with the rotational speed of 14 rps and 28 rps, respectively.

The net masses of particles for each test was related to the lateral surface of the model in the corresponding cross-sections:

$$m_{psi} = \frac{m_{pi}}{S_i}, \quad m_{psj} = \frac{m_{pj}}{S_j}, \quad m_{psk} = \frac{m_{pk}}{S_k}, \quad (1)$$

where $S = 2X_L \pi \sin(\beta/2) dX_L$ is the lateral surface of the model in the given cross-section.

The masses of the particles detached from the surface during the test were determined as follows:

$$M_{psj} = m_{psi} - m_{psj}, \quad M_{psk} = m_{psi} - m_{psk}. \quad (2)$$

It was assumed that in the neighbouring test cross-sections of the model (7, 10, 13 mm; 27, 30, 33 mm; 87, 90, 93 mm) the initial, i.e. before the rotating, distribution density m_{psi} of particles along the surface was the same.

Then in the considered cross-sections $X_L=10, 30$ and 90 mm the particles adhesion numbers α for two values of the rotational speed were calculated as follows:

$$\alpha_j = \frac{M_{psj}}{m_{psi}}, \quad \alpha_k = \frac{M_{psk}}{m_{psi}}. \quad (3)$$

The given routine was carried out for the powders with the particle average sizes $\delta_p=12, 23$ and 32 μm .

The detaching centrifugal force was calculated for each particle average size δ_p for two values of the rotational speed (14 and 28 rps) as follows:

$$F_d = 4\pi^2 n^2 R_i m_p, \quad (4)$$

where n is the rotational speed of the model, R_i is the radius of the cross-sections of the model where the masses of the detached particles were measured, $R_i = X_L \sin(\beta/2)$, m_p is the mass of a single particle, $m_p = (4/3)\pi(\delta_p/2)^3 \rho_p$. Here the spheric shape of particles was assumed.

Results and discussion

Experimentally obtained dependencies $\alpha=f(\lg F_d)$ were approximated by the linear law $\alpha=a+b \cdot \lg F_d$ (s. Fig. 2), where a and b are the empirical coefficients derived from the approximating straight lines. Thus, for the particle sizes $\delta_p=12, 23$ and 32 μm the following empirical dependencies for the adhesion number from the detaching centrifugal force were obtained:

$$\begin{aligned} \delta_p=12 \mu\text{m} & \quad \alpha = 3.08 + 0.26 \lg F_d, \\ \delta_p=23 \mu\text{m} & \quad \alpha = 5.02 + 0.50 \lg F_d, \\ \delta_p=32 \mu\text{m} & \quad \alpha = 2.92 + 0.26 \lg F_d. \end{aligned}$$

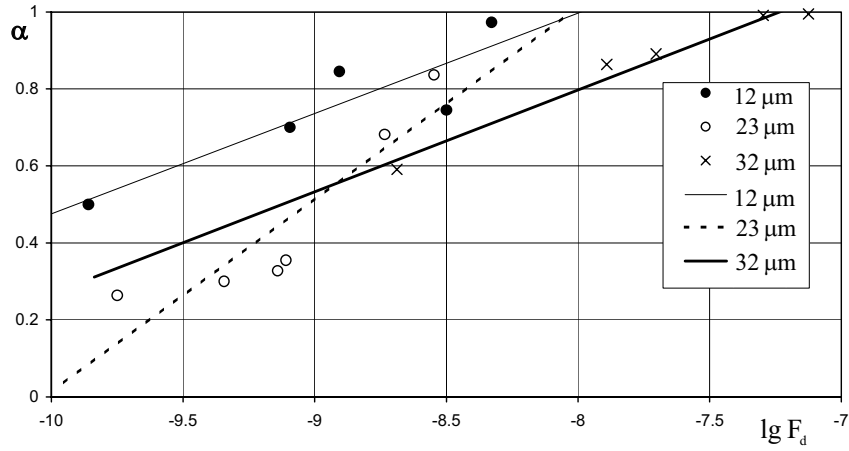


Fig. 2. Distributions of the detaching centrifugal force for various particles.

Some deviation of the experimental data from the linear law, which takes place at low rotational speed, can be explained by the combined effect of the aerodynamic drag force and detaching centrifugal force. One can see from expression (4) that centrifugal force is in proportion to $(n)^2$. The expression for the drag force F_{ad} acted on particle upon rotation of the model can be written according to Loicjanski (1987) as follows:

$$F_{ad} = C_x \rho S \frac{v_d^2}{2}, \quad (5)$$

where C_x is the aerodynamic drag coefficient, ρ is the air density, S is the area of the midsection of particle, v_d is the flow velocity near the centre of particle. Assuming the streamlining of the rotating model to be laminar, v_d can be written according to Schlichting (1974) as:

$$v_d = v_0 \left(2 \frac{y}{\delta_{bl}} - \frac{y^2}{\delta_{bl}^2} \right), \quad (6)$$

where v_0 is the flow velocity at the outer boundary of the laminar boundary layer, δ_{bl} is the thickness of the boundary layer, y is the transverse coordinate of the boundary layer. For the rotating model $\delta_{bl} = \sqrt{\nu / \pi n}$, where ν is the kinematic viscosity of air, and $v_0 = 2\pi n X_L \sin(\beta/2)$.

Thus, the expression for the drag force F_{ad} can be written as follows:

$$F_{ad} = 6 \sqrt{\frac{\nu}{\pi}} \rho \pi^3 \delta_p^2 X_L \sin(\beta/2) n^{3/2}, \quad (7)$$

i.e., the drag force is in proportion to $(n)^{3/2}$. So, the rising of the rotational speed results in more stronger increase of the centrifugal force in compare with the drag force, and for high rotational speed the detaching of particles from the surface is stipulated only by the centrifugal force.

Basing on the expressions for the centrifugal and drag forces, where $F_{ad} \sim (\delta_p)^2$ and $F_d \sim (\delta_p)^3$, respectively, one can expect that the increase of the particles size attenuates the influence of the drag force on the particles and simultaneously intensify the effect of the centrifugal force.

Conclusions

1. The empirical normal-logarithmic dependencies for the adhesion number from the detaching centrifugal force were obtained for various particle sizes. These dependencies are the initial for the calculation of the adhesive interaction of particles and the surface.

2. The detaching of particles from the surface is stipulated by the combined effect of aerodynamic drag force and detaching centrifugal force at low rotational speed.

3. The increase of the rotational speed as well as the particles size results in the intensify of effect of the centrifugal force.

The obtained dependencies do not consider the environment parameters (humidity, temperature, chemistry), the surface electric charges of particles, the material properties and shape of the particles as well as the material properties and roughness of the rotating surface.

The given test series can be taken as the preliminary step which allows to check the measurement technique and estimate all limitations of the given method.

References

1. Loicjanski, L.G., 1987: Fluid and Gas Mechanics; Moscow, Science, 840 (in Russian).
2. Schlichting, G., 1974: Theory of Boundary Layer; Nauka, Moscow, 712 (in Russian).

ARTICLE V

Hussainov, M., Kartushinsky, A., Rudi, U., Shcheglov, I., Tisler, S., 2004, An experimental investigation of effect of the velocity slip on modification of the grid-generated turbulence in a gas-solid particles flow. In: Proceedings of 3rd International Symposium in Two-Phase Flow Modelling and Experimentation, Pisa, Italy, September 22-25, CD-ROM, as04.

AN EXPERIMENTAL INVESTIGATION OF EFFECT OF THE VELOCITY SLIP ON MODIFICATION OF THE GRID-GENERATED TURBULENCE IN A GAS- SOLID PARTICLES FLOW

Medhat Hussainov, Alexander Kartushinsky, Ülo Rudi, Igor Shecheglov, Sergei Tisler

Laboratory of Multiphase Media Physics, Faculty of Science, Tallinn University of Technology,
Akadeemia tee 23A, 12618 Tallinn, Estonia
e-mail: aeromeh@online.ee

ABSTRACT

The experimental data on an initial period of decay of the grid-generated turbulence in a gas-solid particles downward flow for the flow mass loading ratio 0.14 kg dust/kg air are presented. The distributions of the averaged and fluctuating velocities of gas and particles were obtained by the laser Doppler Anemometer (LDA). The turbulence decay curves along the flow axis were built for grids of three types with the Reynolds number $Re_M = 3040, 6333$ and 10133 , respectively, for the flow mean velocity 9.5 m/s. The velocity slip was varied in the range 0–5 m/s. Investigations showed that the influence of 700 μm glass beads on turbulence was different depending on a type of a grid. The particles enhanced turbulence in case of small grids ($Re_M = 3040$ and 6333) on the contrary to the large grid ($Re_M = 10133$), where the particles attenuated turbulence. It was obtained that the increasing of the velocity slip between gas and particles resulted in an increase of the rate of the turbulence generation. The character of the turbulence modification changed from an attenuation for a small velocity slip to the turbulence enhancement for a large velocity slip. Analysis of the experimental data allowed to propose the parameter Re_p/Re_L as the criterion for an assessment of a character as well as the degree of influence of particles on the grid-generated turbulence.

Keywords: Grid-generated turbulence; Modification of turbulence; Velocity slip

INTRODUCTION

Two-phase turbulent flows research has application to a vast number of natural and technological processes. A typical listing of the general technological areas dealt with such flows includes fluidized bed reactors, particle generation and reaction processes, solids transport, separation processes etc. To predict the behaviour of the two-phase system it is necessary to have an insight into the interaction process between particles and fluid, which is the key problem in multiphase flows. The grid-generated two-phase flow, being the simplest case of the turbulent flow, is under consideration in this paper.

The effect of solid particles on turbulence is a prime issue of numerous experimental researches. In [1, 2] all available data were summarized and the generalizing dependencies were obtained. However, there is a lack of investigations concerning the grid-generated turbulence in two-phase flows, although it seems to be the most relevant subject of inquiry with respect to the effect of particles on turbulence. Firstly, it is well studied theoretically and experimentally for a single-phase flow, secondly, there are no complicative factors of analysis, like a non-uniformity of the flow fields or the walls, and, thirdly, it is easy to vary the turbulence conditions only by changing the grid parameters etc. However, the experimental investigations of the grid-generated turbulence in case of gas-solid particles flow are complicated in the first place by large transverse dimension of a flow that conditions the high mass flow of particles even for the moderate mass loading ratio and rises the difficulties in optical probing, as

well the problems concerning the entering of particles into the flow. The only studies devoted to the grid-generated turbulence in two-phase flows were presented in works [3–5]. For example, authors of [3] observed both attenuation and enhancement of turbulence while studying the effect of a gas bubbles on the turbulence intensity behind a grid in liquid. The authors of [4] investigated a short section of the initial period of the turbulence decay ($15 < X/M < 33$) in a water flow loaded by 655 μm plastic or glass particles. They found that the light plastic particles resulted in a growth of the turbulent energy, whereas heavy glass particles decreased it. It is essential to note that the experimental results of effect of particles on turbulence of a liquid flow are hardly comparable with the similar ones obtained for an air flow, since the same values of the mass loading of flow by the same particles can be obtained for the volume concentration of particles in water of 3 orders of magnitude higher than in air. Unfortunately, the similar studies in case of a gas-solid particles flows were not carried out. Thereupon, it can be mentioned the investigations [5], where the effect of solid 120 and 480 μm particles on attenuation of the grid-generated turbulence in a downward air flow was studied. It was found that 120 μm particles with $Re_p \approx 13$ decreased turbulence, whereas 480 μm particles with $Re_p \approx 170$ showed the enhancement effect. Unfortunately, these experiments were conducted only for one type of a grid.

EXPERIMENTAL CONDITIONS

The given experiments were carried out in a vertical two-phase open-loop wind-channel with a closed test section [6]. The difference from the previous investigations concerned the way particles were accelerated and entered into the flow. The present work used the gravity acceleration device. Three types of mono-plane grids with square meshes were used in the experiments. The mesh size M was 4.8, 10 and 16 mm; solidity for the first two grids was 0.49 and for the third one it was equal 0.36. The grid Reynolds number Re_M for the given mean flow velocity 9.5 m/s was 3040, 6333 and 10133, respectively. Glass beads ($\rho_p = 2500 \text{ kg/m}^3$) with an average diameter of 700 μm were used as the dispersed phase.

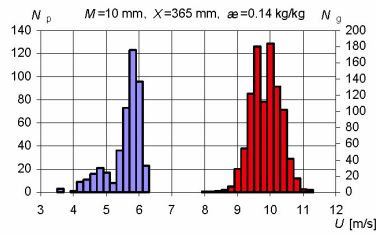


Fig. 1a. The velocity distributions of particles (left) and gas (right) for a large velocity slip.

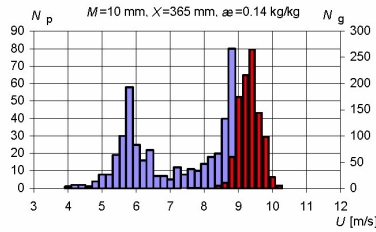


Fig. 1b. The velocity distributions of particles (left) and gas (right) for a small velocity slip.

The present work dealt with the investigation of influence of the velocity slip for the loading ratio $\alpha=0.14 \text{ kg dust/kg air}$. The velocity slip was controlled by varying of the initial velocity of the dispersed phase at the fixed gas velocity. As the accelerated particles were entered the flow before the grid, they were separated into two velocity groups behind the grid (s. Fig. 1a): the particles that passed the grid without collisions with the grid rods and the particles collided with a grid. In both histograms of the particles velocity the particles, having the smaller velocity, were the particles that collided with a grid. When the particles had the larger velocity before

a grid (s. Fig. 1b), the particles, that collided with a grid, rebound upward from a grid and entered the measurement volume, preliminary passing the longer distance and having the larger velocity. Therefore, the group of particles in Fig. 1b, collided with a grid, had the larger velocity as compared to ones shown in Fig. 1a.

The decreasing of the velocity slip, i.e. the increasing of the particles velocity before the grid, resulted in a growth of difference between the average velocities of the particles groups (roughly 0.8 m/s in Fig. 1a versus 3 m/s in Fig. 1b) and in enlargement of share of particles that collided with a grid (s. Fig. 1b). The observed separation of particles by their velocity allows to clarify the experimental data obtained for the grids $M=4.8$ and 10 mm, that showed a lack of the turbulence attenuation for a small velocity slip.

RESULTS

Fig. 2 shows the decay curves behind various grids in a single- and two-phase flow for the loading ratio $\alpha=0.14 \text{ kg dust/kg air}$. The velocity slip was in the range 3.5–4.5 m/s depending on the grid mesh size.

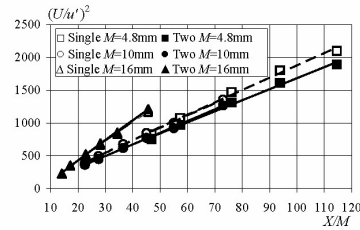


Fig. 2. The turbulence attenuation behind various grids.

Table 1. The constants for the decay curves

Grid (M , mm)	C	A
4.8 (unladen)	18.832	0.414
4.8 (laden)	16.839	-0.0004
10 (unladen)	18.985	1.469
10 (laden)	17.811	2.217
16 (unladen)	29.280	5.629
16 (laden)	30.590	6.043

As follows from Fig. 2, the pronounced turbulence enhancement by particles is observed for the grids with $M=4.8$ and 10 mm, while for $M=16$ mm attenuation takes place. The decay curves for the cross-sections up to $X=730$ mm are approximated by the linear law:

$$\frac{U^2}{u_{rms}^2} = C \cdot \left(\frac{X}{M} - A \right), \quad (1)$$

where the coefficients C and A possess the values according to Table 1.

Figs. 3, 4 and 5 present the dependencies of the degree of influence of particles on turbulence, so-called Effect, on the Reynolds numbers Re_p and Re_L as well as their ratio Re_p/Re_L .

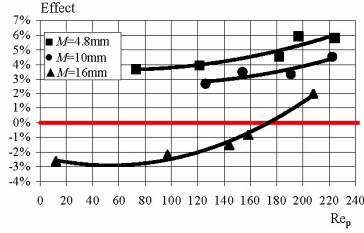


Fig. 3. The degree of influence of particles vs Re_p in the cross-section $X=365$ mm.

Effect is determined according to [1]:

$$\text{Effect} = \frac{(\sigma_{TP} - \sigma_F)}{\sigma_F} \times 100, \quad (2)$$

where σ is calculated from Eq. (1), $\sigma = u'_{rms}/U$.

The character and the degree of influence of particles on turbulence according to [2] depend on Re_p , which is determined by the velocity difference of gas and particles $(U-U_p)$ (s. Fig. 3). Fig. 3 shows that in case of $M=16$ mm the turbulence attenuation takes place up to the critical value of $Re_p = Re'_p \approx 175$, whereas turbulence is enhanced for $Re_p > Re'_p$. The curves $\text{Effect}(Re_p)$ in case of $M=4.8$ and 10 mm do not cross the zero line. This is connected with the separation of particles into two velocity groups (s. Fig. 1b), which affect the flow turbulence in different ways. The group of particles, having $Re_p > 200$, enhances turbulence owing to the vortex break-down, and the group of particles, having $Re_p < 50$, attenuates turbulence. The net effect of particles is the increasing of turbulence by 3–4%. At the same time, the particle Reynolds number calculated by the average velocity slip of all particles can be smaller than 100, and, if taking into account that $\delta_p/L_E < 0.064$, the turbulence attenuation should be observed and the curves for $M=4.8$ and 10 mm (s. Fig. 3) should cross the zero line.

Re_p reflects the influence of the averaged velocities of gas and particles on turbulence and does not consider the turbulence conditions of the initial single-phase flow. Therefore, it is necessary to appoint the parameter, which could characterize turbulence of the initial single-phase flow. The turbulent Reynolds number Re_L corresponded to the

turbulence length-scale L_E can be chosen as the given parameter.

Let us clarify in what way the conditions of turbulence of the initial single-phase flow, which is characterized by Re_L , affects on the particles effect on turbulence of the two-phase flow. It is evident that in the flow strength the share of energy, supplemented by particles owing to the eddies break-down for $Re_p = \text{const}$, decreases with a growth of the turbulent energy of the initial single-phase flow. At the same time, the particles effect for $\delta_p = \text{const}$ moves towards the turbulence attenuation with a growth of the eddy size L_E of the initial single-phase flow. This implies that the particles effect is in inverse proportion to Re_L , that was verified by the experimental data (s. Fig. 4), where the dependencies of the degree of influence of particles on turbulence from Re_L are shown for various, almost permanent values of Re_p .

Based on all aforesaid, it seems to be logical to integrate both criteria, Re_p and Re_L , into the single encompassing criterion Re_p/Re_L . The given approach is the improvement of Crowe's approach [1], since the ratio $Re_p/Re_L = (\delta_p/L_E) \cdot (U-U_s)/u'$ considers in addition the velocity characteristics of gas and particles. Thus, this criterion enables to consider the all-inclusive influence of parameters of the dispersed phase and the initial single-phase flow on turbulence of the carrier phase of the two-phase flow. On basis of the processing of the experimental data obtained at the fixed flow mass loading for various grids, various velocity slip, in various cross-sections of the flow, it can draw the dependence of the degree of influence of particles on turbulence Effect from ratio Re_p/Re_L (s. Fig. 5). It is very difficult to obtain the condition $Re_p = \text{const}$ in experiments, since the velocity slip depends on both the grid type and the streamwise location. Therefore, the curves in Fig. 4 were drawn for the narrow range of Re_p . The ratio Re_p/Re_L was calculated in every gage point for every grid type and the velocity slip in order to draw the curve in Fig. 5. As Fig. 5 shows, all experimental data are fitted by the curve, which has the point of transition from the turbulence attenuation to its enhancement at $Re_p/Re_L \approx 0.4$.

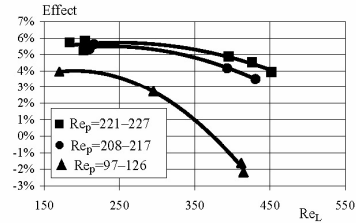


Fig. 4. The degree of influence of particles vs the turbulent Reynolds number Re_L .

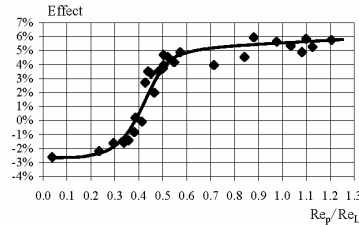


Fig. 5. The degree of influence of particles vs Re_p / Re_L .

CONCLUSION

There were performed the experimental investigations of effect of the velocity slip on the grid-generated turbulence in a gas-solid particles flow. The velocity slip was achieved by the preliminary acceleration of particles before their entering the flow, when the parameters of the gas and dispersed phases were invariable.

The obtained results allow to draw the following conclusions:

- the influence of 700 μm glass beads on turbulence, depending on the parameters of turbulence of the initial single-phase flow, appears as both enhancement and attenuation of the turbulent energy of the gas flow;
- the velocity slip determines the character of the particles effect on turbulence for the grid $M=16$ mm for the given experimental conditions. The turbulence attenuation is observed for a small velocity slip, whereas enhancement takes place for the velocity slip larger 3.5 m/s;
- the ratio Re_p / Re_L is proposed as the criterion

for considering the all-inclusive influence of parameters of the dispersed phase and the initial single-phase flow on turbulence of the carrier phase of the two-phase flow;

- $Re_p / Re_L \approx 0.4$ is the limit value for the given experimental conditions, which defines the character of influence of particles on turbulence. At $Re_p / Re_L < 0.4$ the turbulent energy is attenuated and at $Re_p / Re_L > 0.4$ it is enhanced.

NOMENCLATURE

A	see Eq. (1) and Tab. 1, [dimensionless]
C	see Eq. (1) and Tab. 1, [dimensionless]
Effect	see Eq. (2); measure of degree of influence on turbulence, [%]
L_E	Euler's turbulence length-scale, [m]
M	the grid mesh size, [m]
N	number of records of velocity, [1/s]
Re_L	the Reynolds number of turbulence; $Re_L = u' L_E / \nu$, [dimensionless]
Re_M	the Reynolds number of the grid mesh; $Re_M = UM / \nu$, [dimensionless]
Re_p	the particle Reynolds number, $Re_p = (U - U_p) \delta_p / \nu$, [dimensionless]

Re'_p	the critical value of Re_p , [dimensionless]
U	the mean gas flow velocity, [m/s]
U_p	velocity of a single particle, [m/s]
U_s	velocity of the dispersed phase, [m/s]
u'	fluctuating velocity of gas, [m/s]
u'_{rms}	root mean square value of the gas velocity, [m/s]
X	the streamwise coordinate counted down the stream behind the grid, [m]

Greek symbols

δ_p	the average particle diameter, [m]
α	the mass loading ratio of flow, [kg dust/kg air]
ν	kinematic viscosity of the gas flow, [m^2/s]
ρ_p	physical density of the particles material, [kg/m^3]
σ	the turbulent intensity of the flow, [dimensionless]

Subscripts

F	single-phase flow
L	the turbulence length-scale
M	grid
TP	two-phase flow
g	gas
rms	root mean square
p	particle
s	dispersed phase

REFERENCES

1. R.A. Gore, C.T. Crowe, Effect of Particle Size on Modulating Turbulent Intensity, Brief communication, *Int. J. Multiphase Flow*, vol. 15, 2, pp. 279-285, 1989.
2. G. Hetsroni, Particles-Turbulence Interaction, *Int. J. Multiphase Flow*, vol. 15, 5, pp. 735-746, 1989.
3. M. Lance, J. Bataille, Turbulence in the Liquid Phase of a Uniform Bubbly Air-Water Flow, *J. Fluid Mech.*, vol. 222, pp. 95-118, 1991.
4. S. Schreck, S.J. Kleis, Modification of Grid-Generated Turbulence by Solid Particles, *J. Fluid Mech.*, vol. 249, pp. 665-688, 1993.
5. Z. Stojanovic, M. Chrighi, A. Sadiki, A. Dreizler, S. Geiß, J. Janicka, Experimental Investigation and Modeling of Turbulence Modification in a Dilute Two-Phase Turbulent Flow, *Proc. The 10th Workshop on Two-Phase Flows Predictions*, 2002.
6. M. Hussainov, A. Kartushinsky, Ü. Rudi, I. Shcheglov, G. Kohnen, M. Sommerfeld, Experimental Results of Turbulence Modulation by Rough Solid Particles in a Grid-Generated Flow, *Proc. Estonian Acad. Sci. Engineering*, vol. 6, 3, pp. 217-229, 2000.

ARTICLE VI

Kartushinsky, A., Mulgi, A., Tisler, S., Michaelides, E. E., 2005, An experimental study of the effect of particles on the shear stress in particulate turbulent pipe flow. Proc. Estonian Acad. Sci. Engineering, Vol. 11(2), pp. 161-168.

An experimental study of the effect of particles on the shear stress in particulate turbulent pipe flow

Alexander Kartushinsky^a, Anatoly Mulgi^a, Sergei Tisler^a and Efstathios E.
Michaelides^b

^a Laboratory of Multiphase Media Physics, Tallinn University of Technology, Akadeemia tee 23A,
12618 Tallinn, Estonia; aeromeh@online.ee

^b School of Engineering, Tulane University, New Orleans, LA 70118, USA;
emichael@mailhost.tcs.tulane.edu

Received 27 November 2003, in revised form 30 March 2004

Abstract. Experimental data on the shear stress, exerted by a flowing mixture of solid particles in air, are presented. The data were obtained in a facility with a steel or vinyl test section. The Reynolds numbers were close to 10^5 , thus the flow was turbulent. Several types of particles with different material properties were used. Low as well as intermediate-to-high values of the loading ratio were investigated. It was found that the reduction of the data with respect to the Gastershtadt coefficient K highlights certain trends of the flow and makes it possible to derive some general conclusions on the behaviour of the mixture.

Key words: gas–solid pipe flow, turbulence, loading ratio, shear stress, Gastershtadt coefficient.

1. INTRODUCTION

Pressure loss (pressure change) in gas–solid pipelines has been a subject of several investigations [1–5]. Several sets of experimental data have been published and relationships for the pressure drop have been formulated, which exhibit various degrees of accuracy in predicting data, different from the ones derived in [6]. Most of these relationships are for low to intermediate values of the loading ratio and utilize few types and sizes of particles.

The authors of [3], considering turbulent gas–solid flow in a horizontal pipe, revealed a dependence of the pressure drop for particle transport on the ratio of the densities of the solid and fluid phases of the flow. They explained this ratio as representing the mean velocity slip between the fluid and the solid material. The

authors of [4] investigated a vertical upward gas–solid two-phase flow. They showed experimentally that the frictional pressure drop is an important component of the total pressure gradient in the riser of the vertical pneumatic conveying system and that at low gas velocities negative frictional pressure gradients occur.

Today a reliable metering of the flow rate of solids is of great importance for effective operation and control of gas–solid transport systems in industry. The authors of [5] experimentally examined the principle of measuring the pressure loss, experienced by a gas–solid flow in a straight section of piping in order to obtain the flow rates for a wide range of powders and granular materials. The results of [7] verified the possibility of widespread industrial application of the pressure drop metering devices.

The purpose of this study is to determine experimentally the effect of the solids loading on the total shear stress and the pressure drop, under steady-state turbulent flow conditions, utilizing several types of particles. The Reynolds number Re varied from 2×10^4 to 3×10^5 , the pipeline inner diameter was in the range of 16–66 mm and the pipeline materials were stainless steel and vinyl. Experiments were conducted with the mass loading ratio m in the low range ($0 < m < 15$) as well as in the intermediate-to-high range ($0 < m < 15$).

2. EXPERIMENTAL FACILITY

The experiments were carried out in a horizontal two-phase system, a schematic diagram of which is shown in Fig. 1. The power to run the system was supplied by a blower of 3.2 kW. The maximum mass flow rate of air was 0.2 kg/s. An automatic control system determined the air flow through the system and kept the flow constant during the experiments. The air flow rate was measured by a Venturi flowmeter with an uncertainty less than 10%. The thermal controller maintained the desired level of air temperature at the inlet, which was in the range of 20–40°C.

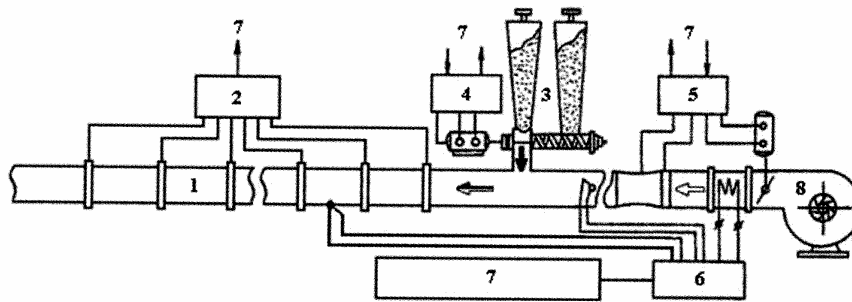


Fig. 1. Experimental set-up: 1 – test section; 2 – pressure converter; 3 – particle screw feeder; 4 – control unit of the particle screw feeder; 5 – flowmeter; 6 – thermocontroller; 7 – registering, processing and controlling system; 8 – blower.

Particles were introduced into the flow stream by a screw feeder, which was supplied with its own control unit. The test section was 4 m long and was made of stainless steel or vinyl. The test section itself consisted of 16 smaller pipe sections that were joined by flanges. A straight pipe section of 3 m before the test section assured uniform acceleration of the particles before they reached the test section. A series of sixteen pressure transducers recorded the pressure along the test section. At the end of the test section, a cyclone separator (not shown in Fig. 1) was used to separate the particles from air. The experimental facility was equipped with an automatic data acquisition system, which also helped to control the experiments and to keep the flow parameters at a steady-state level.

The pressure sampling was carried out along the whole length of the pipe test section at every 0.25 m (a total of sixteen transducers were used). Uncertainty of the pressure measurements was caused mainly by the procedural and instrumental errors. In order to reduce the overall uncertainty, the data array contained 50 000 measurements at each gage point for every experimental condition. Such data array allowed to obtain the overall uncertainty not exceeding 12%.

The powders of electrocorundum (Al_2O_3), silicon carbide (SiC) and bronze particles were used as the dispersed phase. Their material density ρ_s was 3970, 3200 and 8900 kg/m^3 , respectively. The size of the particles δ varied in the range of 15–200 μm , which is the range of small but non-cohesive particles. The weight-average size of the particles was in the range of 16–88 μm . The particles were obtained from industrially used samples and were highly polydispersed. Thus in the case of electrocorundum with nominal sizes 16 and 32 μm , an analysis of the actual sizes of the particles used revealed histograms, shown in Fig. 2. The standard deviation of these distributions was approximately 30%.

The velocity slip for the given flow conditions varied in the range of 0–25% of the mean flow velocity depending on the particle size [8]. The transport velocity of the carrier fluid for the given range of the Reynolds number 2×10^4 – 3×10^5 was sufficient to keep the particles away from the bottom wall, thus excluding the precipitation process. Besides, the observed distribution of the particle mass concentration at the pipe exit is axisymmetric for these regimes [8].

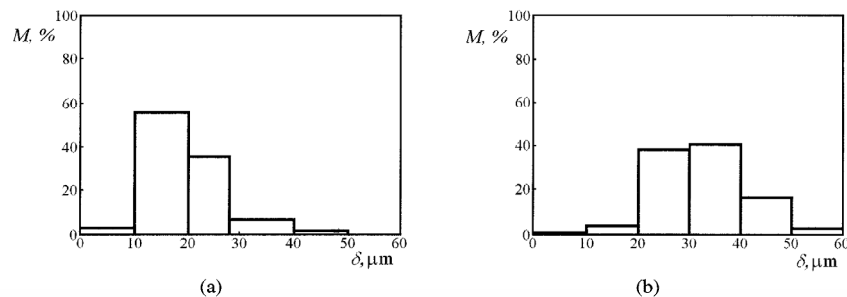


Fig. 2. The weight-average size distributions of electrocorundum particles of nominal sizes: (a) $\delta = 16 \mu\text{m}$; (b) $\delta = 32 \mu\text{m}$; M – the weight fraction.

3. EXPERIMENTAL RESULTS

From the measurements of the pressure gradient, one may easily obtain the shear stress and, hence, the friction coefficient of the two-phase mixture. From theoretical considerations on the behaviour of solid particles carried by a fluid in a pipe, one concludes that the best way to express the total shear stress τ_m is as the sum of the shear stress, induced by the flow of air alone, and the shear stress due to the presence of the particles [9-11]. Thus we used the following equation for modelling our data:

$$\tau_m = \tau + \Delta\tau_s, \quad (1)$$

where τ is the shear stress for $m=0$ and $\Delta\tau_s$ is the part of the shear stress due to the addition of the solid particles. In the case of dilute flows, where particle-to-particle interactions are not important, the excess shear due to the presence of particles is mainly due to two causes: a) the interaction of particles with the wall, and b) the interaction of particles with the fluid. Hence, the excess shear stress may be expressed in terms of two separate quantities: $\Delta\tau_s = \Delta\tau_1 + \Delta\tau_2$. The last two terms are related to the particle-wall interactions ($\Delta\tau_1$) and to the gas-particle interactions ($\Delta\tau_2$). The component $\Delta\tau_1$ is a result of several complex forces, such as the Coulomb friction and particle-wall impacts. The part due to the gas-particle interactions ($\Delta\tau_2$) also has a complex origin and includes the effects of the local modification of the gas velocity field, caused by the presence of particles, velocity slip between particles as well as by the gas and turbulence modulation by the particles [6,12-14].

Given the complex nature of $\Delta\tau_1$ and $\Delta\tau_2$, we did not model separately these two components of the excess shear stress $\Delta\tau_s$. Thus, for the reduction of the experimental data, we assumed that $\Delta\tau_s$ is proportional to the loading ratio m :

$$\Delta\tau_s = Km\tau, \quad (2)$$

where K is the proportionality constant, which is sometimes referred to as the Gastershtadt coefficient [15]. Now Eq. (1) can be written as

$$\tau_m = \tau(1 + Km). \quad (3)$$

In [9], K was given by the following expression:

$$K = \frac{2m \sqrt{Dg}}{c_f u} \frac{1-\xi}{1+\xi}, \quad (4)$$

where D is the pipe diameter, c_f is the friction coefficient at $m=0$, ξ is the bouncing coefficient of the particles with the wall, u is the fluid velocity and g is the gravitational acceleration.

Equation (2) implies that the contribution of particles to the shear stress is proportional to the fluid stress τ and to the mass loading ratio m of the particles.

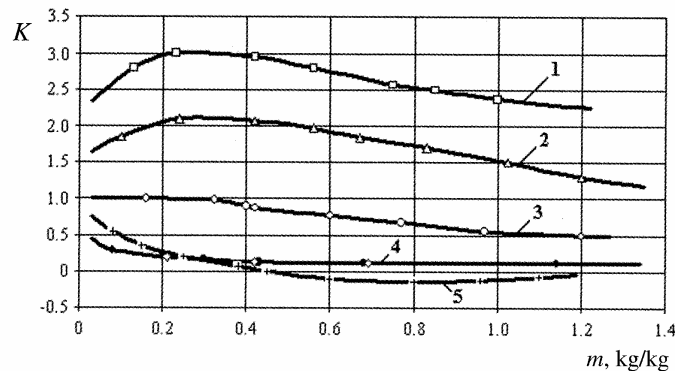


Fig. 3. The coefficient K vs the particle mass loading and the particle size for the stainless steel pipe by $Re = 6.2 \times 10^4$, $D = 32.7$ mm: 1 – Al_2O_3 , $\delta = 88$ μm ; 2 – Al_2O_3 , $\delta = 70$ μm ; 3 – SiC, $\delta = 55$ μm ; 4 – Al_2O_3 (\bullet), $\delta = 32$ μm , SiC (\diamond), $\delta = 32$ μm ; 5 – Al_2O_3 , $\delta = 16$ μm .

Figure 3 shows the dependence of the coefficient K on the mass loading for very dilute flows, where m is less than 1.5. It is evident that in this case K depends on the mass loading as well as on the size of the particles. Smaller particles tend to have lower values of K , and the smallest ones even exhibit negative values; this implies that the total shear stress is reduced. We believe that this is due to the turbulence modulation in the gaseous phase, which is usually experienced in the fine particle range [13,14]. In terms of the two components of the excess shear stress $\Delta\tau$ we have a significant reduction of $\Delta\tau_2$, which counteracts any increase of the component $\Delta\tau_1$. This reduction is expected to persist only at small values of the loading ratio ($m < 3$) even with fine particles. Figure 3 shows that in the case of the particles with $\delta = 55$ μm , K would become positive at values of the loading ratio higher than 1.2. This means that the gains of any turbulence reduction would not be sufficient to counteract the shear stress increase due to the other causes, such as particle–wall collisions, acceleration of particles and simple Coulomb friction due to particles.

It is also evident in Fig. 3 that the curves, corresponding to the larger particles (for which turbulence reduction is not expected), reach a maximum value and then level off. This is a manifestation of the fact that the marginal cost (in terms of the pressure drop) associated with the transport of solids is reduced with an increase of the solids loading.

At low values of the loading ratio, the coefficient K apparently varies with the loading ratio and may reach a maximum or a minimum value as Fig. 3 indicates. However, at high values of the loading ratio, we expect that equilibrium will be reached between the overall gas–particle–walls interactions and that K will approach a constant value. A series of experiments we performed with bronze particles at high values of m shows that K is almost constant over a very large range of loading ratios and gas Reynolds numbers. In this series of experiments we

used three sizes of bronze particles (35, 45 and 67 μm) and two types of pipes made of stainless steel and vinyl. The results of these experiments are shown in Fig. 4 as the ratio τ_m/τ vs the mass loading. Despite some deviations from the norm, the data show a markedly linear trend, which implies that K is almost constant over a long range of the loading ratio m .

The function $K(m)$ was calculated from Fig. 4 and Eq. (3). The actual results for K are shown in Fig. 5, where it is observed that K is almost constant (equal

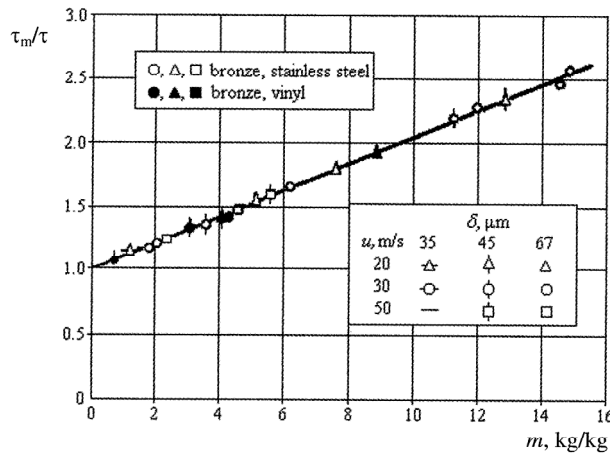


Fig. 4. The shear stress ratio vs mass loading for bronze particles.

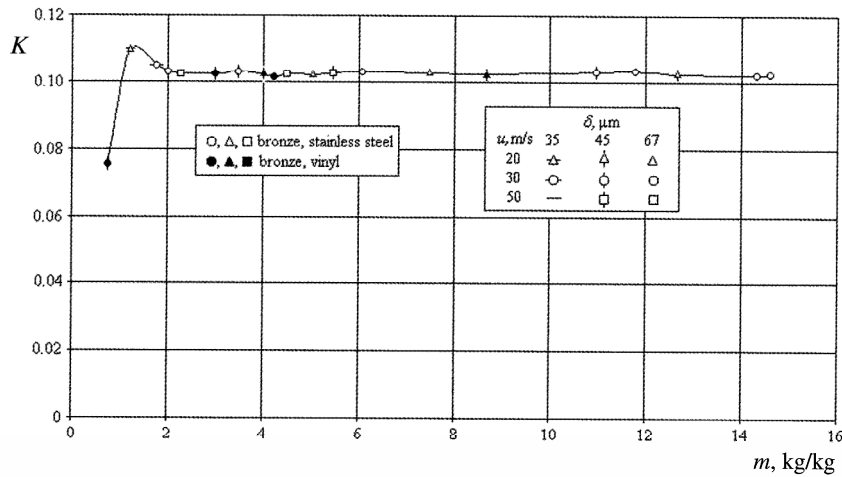


Fig. 5. The Gastershtadt coefficient vs the loading ratio for bronze particles.

to 0.102) in the range of $2 < m < 15$, which covers the low and intermediate loadings. The uncertainty of data for K and τ_m/τ , presented in Figs. 3 to 5, is caused by the uncertainty of the pressure measurement and does not exceed 12%. It must be pointed out that in the dense range of solids transport ($m > 20$) it is expected that the value of K will change, because different effects govern the flow and transport of solids.

4. CONCLUSIONS

Experiments, performed in an automated horizontal facility, show that the total shear stress is a sum of the stress at zero loading and of an excess stress, due to the presence of the particles. The excess shear stress of a gas–solids mixture is a linear function of the mass loading for a wide range of loadings. The constant of proportionality depends on the type of solids conveyed. At very low loadings, this constant K is a function of the loading. The experimental data indicate that K reaches maximum (for large particles, which contribute to the turbulence increase) or minimum (for small particles, where turbulence modulation may be expected) value and then levels off to a constant value. The value of K reaches a constant value at intermediate values of the loading ratio.

REFERENCES

1. Hetsroni, G. *Handbook of Multiphase Systems*. McGraw-Hill, New York, 1982.
2. Peters, L. K. and Klinzing, G. E. Friction in turbulent flow of solids–gas systems. *Can. J. Chem. Eng.*, 1972, **50**, 441–444.
3. Molerus, O. and Heucke, U. Pneumatic transport of coarse grained particles in horizontal pipes. *Powder Technol.*, 1999, **102**, 135–150.
4. Rautiainen, A., Stewart, G., Poikolainen, V. and Sarkomaa, P. An experimental study of vertical pneumatic conveying. *Powder Technol.*, 1999, **104**, 139–150.
5. Venkatasubramanian, S., Klinzing, G. E. and Ence, B. Flow rate measurements of a fibrous material using a pressure drop technique. *Flow Meas. Instrum.*, 2000, **11**, 177–183.
6. Hoyt, J. W. The effect of additives on fluid friction. *J. Basic Eng.*, 1972, **94**, 1–32.
7. Lee, H. J. and Lee, S. Y. Pressure drop correlations for two-phase flow within horizontal rectangular channels with small heights. *Int. J. Multiphase Flow*, 2001, **27**, 783–796.
8. Hussainov, M., Kartushinsky, A., Mulgi, A. and Rudi, Ü. Gas–solid flow with the slip velocity of particles in a horizontal channel. *J. Aerosol Sci.*, 1996, **27**, 41–59.
9. Michaelides, E. E. and Roy, I. Evaluation of several correlations used for the prediction of pressure drop in particulate flows. *Int. J. Multiphase Flow*, 1987, **13**, 433–442.
10. Babukha, G. L. and Shraiber, A. A. *Interaction of the Particles of Polydispersed Material in Two-Phase Flows*. Naukova Dumka, Kiev, 1972 (in Russian).
11. McCarthy, H. E. and Olson, I. H. Turbulent flow of gas–solids suspensions. *Ind. Eng. Chem. Fund.*, 1968, **7**, 471–483.
12. Barenblatt, G. I., Bulina, I. G. Kalashnikov, V. N. and Kalinichenko, N. M. Of the structure of low mass loading polymer solution with effect of turbulence reduction. *Prikladnaya Mekhanika i Tekhnicheskaya Fizika*, 1966, **6**, 106–110 (in Russian).
13. Gore, R. A. and Crowe, C. T. Effect of particle size in modulating turbulent intensity. *Int. J. Multiphase Flow*, 1989, **15**, 279–285.

14. Yuan, Z. and Michaelides, E. E. Turbulence modulation in particulate flows – a theoretical approach. *Int. J. Multiphase Flow*, 1992, **18**, 279–285.
15. Gorbis, Z. R. *Heat Exchange and Hydromechanics of Dispersed Through Flows*. Energiya, Moscow, 1970 (in Russian).

**Osakeste mõju nihkepingele tahkete osakestega õhu
turbulentsel voolamisel kanalis.
Eksperimentaalne uurimus**

Alexander Kartušinski, Anatoli Mulgi, Sergei Tisler
ja Efstathios E. Michaelides

On kirjeldatud horisontaalse, turbulentsel, tahkete osakestega koormatud õhu toruvooluse eksperimentaalset uurimist ja esitatud erinevate osakeste põhjustatud nihkepingete mõõtmise tulemusi. Voolusi uuriti nii osakeste madalate, keskmiste kui ka suurte masskontsentratsioonide korral. Leiti, et osakestest põhjustatud nihkepinge suurenemine on lineaarses sõltuvuses osakeste masskontsentratsioonist selle laiades piirides. Võrdelisuse teguri Gastershtadi koefitsiendi väärtus sõltub oluliselt osakeste tüübist.

ARTICLE VII

Hussainov, M., Kartushinsky, A., Rudi, U., Shcheglov, I., Tisler, S., 2005, Experimental study of the effect of velocity slip and mass loading on the modification of grid-generated turbulence in gas-solid particles flows. Proc. Estonian Acad. Sci. Engineering, Vol. 11(2), pp. 169-180.

Experimental study of the effect of velocity slip and mass loading on the modification of grid-generated turbulence in gas–solid particles flows

Medhat Hussainov, Alexander Kartushinsky, Ylo Rudi, Igor Shcheglov
and Sergei Tisler

Laboratory of Multiphase Media Physics, Tallinn University of Technology, Akadeemia tee 23A,
12618 Tallinn, Estonia; aeromeh@online.ee

Received 4 May 2004

Abstract. Experimental data on the effects of the velocity slip and mass loading on a grid-generated turbulence in gas–solid particles flow are presented. Glass beads (700 μm) were used as the dispersed phase. Velocities of both phases were measured with a Laser Doppler Anemometer. Turbulence decay curves, obtained for different grids, show that particles enhance turbulence for small grids and attenuate it for the large ones. Turbulence enhancement and attenuation are intensified with the increase of the flow mass loading. The particles effect on turbulence changes from turbulence attenuation for a small velocity slip to its enhancement for a large velocity slip. A criterion for the evaluation of turbulence modification in gas–solid particles flow is proposed.

Key words: gas–solid particles flow, grid-generated turbulence, turbulence modification, mass loading ratio, velocity slip.

1. INTRODUCTION

The effect of solid particles on turbulence has been a prime issue of many experimental studies during last decades. New results about the dependence of turbulence on both the ratio between the particle size and the Euler turbulence length-scale δ/L_E and the particle Reynolds number Re_p were obtained in [1,2]. Later on, the dependence of the attenuation of the turbulent energy on the particle mass loading was established in [3]. The data were classified into two groups: the first group consisted of light particles with low Stokes numbers St_E , based on the Euler turbulence time scale T_E with a weak dependence of the turbulence

attenuation on the mass loading; the second one consisted of heavy particles with more sharp dependence of the turbulence attenuation on the mass loading. However, the influence of particles on turbulence, depending on the Stokes number, is still an open issue. For instances, the authors of [4] found that the turbulence attenuation for a given mass loading depends weakly on the Stokes number; on the contrary, the authors of [3] found a considerable increase of the turbulence attenuation with the increase of St_E . Therefore experiments with various Reynolds and Stokes numbers of the particles would clarify the effect of particles on turbulence.

The grid-generated turbulence is an appropriate subject to study the effect of particles on the turbulence modification since, first, it is well studied theoretically and experimentally for the single-phase flow and, secondly, there are no complicating factors for analysis such as non-uniformity of the flow fields or the influence of the confining surfaces. Besides, it is easy to vary the Stokes number by changing only the grid parameters. However, experimental investigation of the grid-generated turbulence in gas–solid particles flows is complicated, first of all due to large transverse dimension of the flow that results in high mass flow of particles and also because of the difficulties in optical probing. Problems concerning entering of particles into the flow make the task even more complicated. Because of that, there is a lack of experimental studies concerning the grid-generated turbulence in two-phase flows. The papers [5–7] are among the few papers devoted the given problem. For example, while studying the effect of the air bubbles on the turbulence intensity behind a grid, the authors of [5] observed both attenuation and enhancement of the turbulence for a wide range of the energy spectrum of the liquid phase. The grid-generated turbulence in a water flow, loaded by 655 μm plastic or glass particles, was investigated in [6]. Here the mean flow velocity was 1 m/s and the Reynolds number Re_M , calculated for the grid mesh size M , was 15 600. A short section of the initial period of the turbulence decay for $15 < X/M < 33$, was studied (X is the streamwise coordinate counted down the stream behind the grid). It was found that the light plastic particles caused an increase of the longitudinal component of the turbulent energy, but heavy glass particles decreased the transversal component of the latter. It should be noted that experimental results on the effect of particles on turbulence in the water flow are hardly comparable with similar ones obtained for the air flow, because in case of the water flow the same values of the mass loading of the flow by the same particles can be obtained for the volume concentration of particles of 3 orders of magnitude higher than in air. As numerous investigations have shown, the character and the amount of change of the turbulence by particles in many respects depend on both the volume concentration and the mass loading. Unfortunately, no much attention has been paid to similar studies in gas–solid particles flows until now. As an exception, paper [7] can be mentioned, where the effect of 120 and 480 μm glass beads on the decay of the grid-generated turbulence in the downward air flow was studied. It was found that 120 μm particles with $Re_p \approx 13$ decreased turbulence, whereas

480 μm particles with $Re_p \approx 170$ increased it. However, these experiments were conducted for only one type of the grid. Thus the parameters of the initial turbulence were not varied and it was not possible to reveal their influence on the turbulence modification in the case of the two-phase flow.

Thus experimental investigations of the effect of parameters of the initial turbulence as well as of the velocity slip and flow mass loading on the turbulence of the gas phase of flow are needed. This study tries to fill partly this gap.

2. EXPERIMENTAL CONDITIONS

The experiments were carried out in a vertical two-phase open-loop wind channel with a closed test section described in detail in [8]. The instantaneous velocities of the tracer particles and particles of the dispersed phase were measured with a Laser Doppler Anemometer (LDA) [9]. Glass beads of the density $\rho_p = 2500 \text{ kg/m}^3$ with a diameter of $\delta = 700 \mu\text{m}$ were used as the dispersed phase. A gravity acceleration device was used. This device allowed to obtain the required velocity slip for high values of the mass loading ratio of the flow. Three different grids were used (Table 1, where d is the diameter of the grid rods and S is the solidity of the grid).

The grid Reynolds number Re_M , which is calculated as

$$Re_M = \frac{uM}{\nu} \quad (1)$$

for the given mean gas flow velocity $u = 9.5 \text{ m/s}$ was 3040, 6333 and 10 133, respectively. Here ν is the kinematic viscosity of gas.

The investigation of the influence of the velocity slip on turbulence was carried out for the positive velocity slip, i.e. when particles lagged the gas. The velocity slip was set only by the preliminary acceleration of particles before their entering into the flow, without changing the parameters of the particles or of the initial single-phase flow.

The influence of the flow mass loading α on turbulence was explored for the range of α from 0 to 1 (kg dust)/(kg air). The mass flow of the dispersed phase was measured by the isokinetic sampling technique [10] and on-line monitored by the Laser Concentration Measurer [11].

Table 1. Parameters of the grids

$M, \text{ mm}$	M/d	S
4.8	2.53	0.487
10	2.50	0.490
16	4.00	0.360

3. RESULTS

Figure 1 shows decay curves of the turbulence u^2/u_{rms}^2 (u'_{rms} is the root mean square value of the gas fluctuation velocity) behind different grids in the single- and two-phase flow for the mass loading of 0.14 (kg dust)/(kg air). The velocity slip $u_r = u - u_s$ was about 4 m/s (u_s is the mean particles velocity). As follows from Fig. 2, the pronounced turbulence enhancement by particles is observed for the grids $M = 4.8$ and 10 mm, while for the grid $M = 16$ mm the turbulence attenuation takes place. The character of the turbulence attenuation

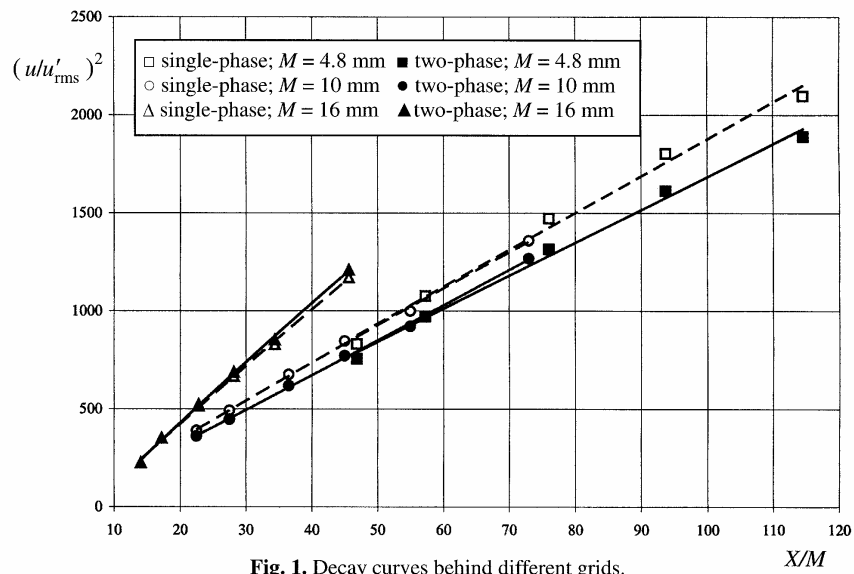


Fig. 1. Decay curves behind different grids.

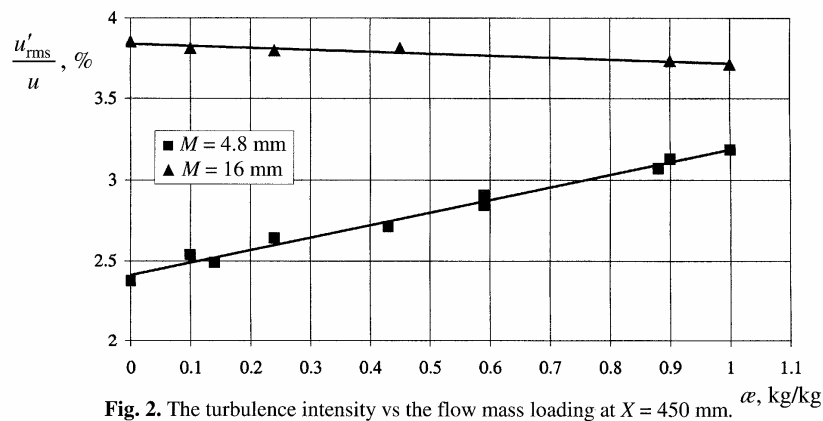


Fig. 2. The turbulence intensity vs the flow mass loading at $X = 450$ mm.

Table 2. Constants of the decay curves of different grids

M , mm	C	A
4.8; single-phase flow	20.09	2.62
4.8; two-phase flow	17.59	-0.01
10; single-phase flow	18.80	0.91
10; two-phase flow	18.0	3.15
16; single-phase flow	29.28	5.63
16; two-phase flow	30.57	6.04

behind the grids agrees with the well-known behaviour of the decay curves in grid-generated turbulent flows described in [12]:

$$\frac{u^2}{u_{\text{rms}}^2} = C \left(\frac{X}{M} - A \right), \quad (2)$$

where C and A are coefficients according to Table 2.

Experimental results (Fig. 2) show that increase in the mass loading of the flow results in the intensification of the additional turbulence generation for the grid $M = 4.8$ mm and in the attenuation of the turbulence for the grid $M = 16$ mm. As it can be seen from Fig. 2, the turbulence intensity depends linearly on the mass loading at least up to 1 (kg dust)/(kg air).

Most interesting are the results concerning the turbulence modification by particles with various velocity slip (Fig. 3). The influence of the velocity slip on turbulence is distinctly apparent in case of the grid $M = 16$ mm. The turbulence attenuation is observed for this grid for small velocity slip, while for large slip (larger than 3.5 m/s) the character of the particles effect changes to the opposite, i.e. the turbulence enhancement takes place. Thus for the given experimental conditions for $M = 16$ mm, the velocity slip determines the character of the particles effect. The turbulence enhancement by particles with larger values of the velocity slip was observed also for the grids $M = 4.8$ and 10 mm.

The turbulence structure of a single-phase flow behind the grid is determined by such flow parameters as the mean flow velocity u , the grid mesh size M and the ratio M/d [12]. The character of the particles effect on turbulence of the gas phase in the two-phase flow depends both on the turbulence parameters of the initial single-phase and the parameters of the dispersed phase, such as diameter δ , the material density ρ_p , the flow mass loading α , the particle Reynolds number Re_p and the Stokes number St_E . In order to analyse the experimental results, the experimental parameters of the single- and two-phase flows at the location $X/M = 50$ along the flow axis are presented in Table 3. In Table 3 the following notations are used:

$$\text{the Euler integral turbulence time scale } T_E = \frac{L_E}{u}, \quad (3)$$

$$\text{the Kolmogorov turbulence time scale } t_K = \left(\frac{v^3}{\varepsilon} \right)^{1/4}, \quad (4)$$

η_K is the Kolmogorov turbulence length scale, k is the turbulence kinetic energy and ε is the dissipation rate of the turbulence kinetic energy.

Table 4 shows the parameters of the dispersed phase. The change of the turbulence intensity by the particles Ch is calculated according to [1]:

$$Ch = \frac{(\sigma_{TP} - \sigma_F)}{\sigma_F} \times 100, \quad (5)$$

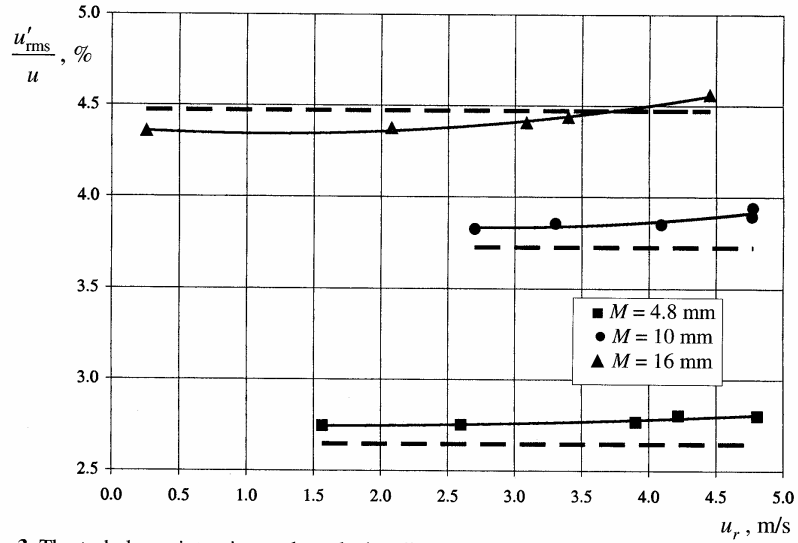


Fig. 3. The turbulence intensity vs the velocity slip at the location $X = 365$ mm. Heavy dash lines denote the turbulence intensity for different grids in the single-phase flow.

Table 3. Experimental parameters of the single- and two-phase (bold) flows at the location $X/M = 50$

Parameter	M , mm		
	4.8	10	16
T_E , s	2.51×10^{-2} 2.53×10^{-2}	5.11×10^{-2} 5.03×10^{-2}	7.47×10^{-2} 7.40×10^{-2}
t_K , s	1.61×10^{-3} 1.54×10^{-3}	2.28×10^{-3} 2.18×10^{-3}	3.28×10^{-3} 3.32×10^{-3}
η_K , m	1.55×10^{-4} 1.52×10^{-4}	1.85×10^{-4} 1.81×10^{-4}	2.22×10^{-4} 2.23×10^{-4}
L_E , m	9.54×10^{-3} 1.01×10^{-2}	1.96×10^{-2} 2.01×10^{-2}	2.41×10^{-2} 2.35×10^{-2}
k , m^2/s^2	1.45×10^{-1} 1.61×10^{-1}	1.47×10^{-1} 1.59×10^{-1}	1.04×10^{-1} 1.01×10^{-1}
ε , m^2/s^3	5.786 6.364	2.876 3.162	1.394 1.360

where σ_{TP} and σ_F are the turbulence intensities of the two-phase and single-phase flow, respectively; σ is calculated from Eq. (2) as follows:

$$\sigma = \frac{u'_{rms}}{u}. \quad (6)$$

The volume concentration of the dispersed phase is calculated as

$$\beta = \frac{\rho \alpha u}{\rho_p u_s}, \quad (7)$$

where ρ is the material density of gas.

Re_p is the particle Reynolds number:

$$Re_p = \frac{u_t \delta}{\nu}, \quad (8)$$

τ_p is the particle response time and St_K is the Stokes number based on the Kolmogorov turbulence time scale t_K . The ratio of the interparticle distance λ and the particle diameter δ is determined according to [13] as

$$\frac{\lambda}{\delta} = \left(\frac{\pi}{6\beta} \right)^{1/3} - 1. \quad (9)$$

As it can be seen from Table 4, the diameter of the particles used in experiments is substantially smaller than the energy-containing eddies ($\delta/L_E < 0.08$). Therefore, according to [1], only the turbulence attenuation should take place. However, the experimental data do show both turbulence attenuation and enhancement. At the same time, the increasing of the turbulence attenuation for $M = 16$ mm or reducing of the turbulence enhancement for $M = 4.8$ and 10 mm

Table 4. The parameters of the dispersed phase

Parameter	M , mm		
	4.8	10	16
Ch , %	5.31	4.05	-1.70
α , kg/kg	1.4×10^{-1}	1.4×10^{-1}	1.4×10^{-1}
β	1.35×10^{-4}	1.19×10^{-4}	1.15×10^{-4}
u_t , m/s	4.4	3.7	3.5
Re_p	2.0533×10^2	1.7267×10^2	1.6333×10^2
τ_p , s	3.76	3.76	3.76
St_K	2.45×10^3	1.73×10	1.13×10^3
St_E	1.49×10^2	7.48×10^1	5.08×10^1
λ/δ	1.472×10^1	1.541×10^1	1.559×10^1
δ/η_K	4.50	3.78	3.16
δ/L_E	7.34×10^{-2}	3.57×10^{-2}	2.90×10^{-2}

that were observed in experiments, are in agreement with the general concept of the turbulence attenuation by the particles with decreasing ratio of δ/L_E .

Let us analyse the experimental results using the diagram presented in Fig. 4 [14], which exhibits the domains of the particles effect on the turbulence modification depending on the interparticle distance, related to λ/δ as well as to the Stokes numbers St_E and St_K . The shaded area in the given diagram corresponds to the given experimental flow conditions and shows the turbulence enhancement by particles that should occur.

Another criterion of the particles effect on turbulence, suggested in [15], is the particle Reynolds number Re_p , which determines the velocity slip. Figure 5 shows the dependence of the turbulence on Re_p . This plot also demonstrates that the turbulence attenuation takes place up to $Re_p \approx 175$, and turbulence is enhanced for $Re_p > 175$.

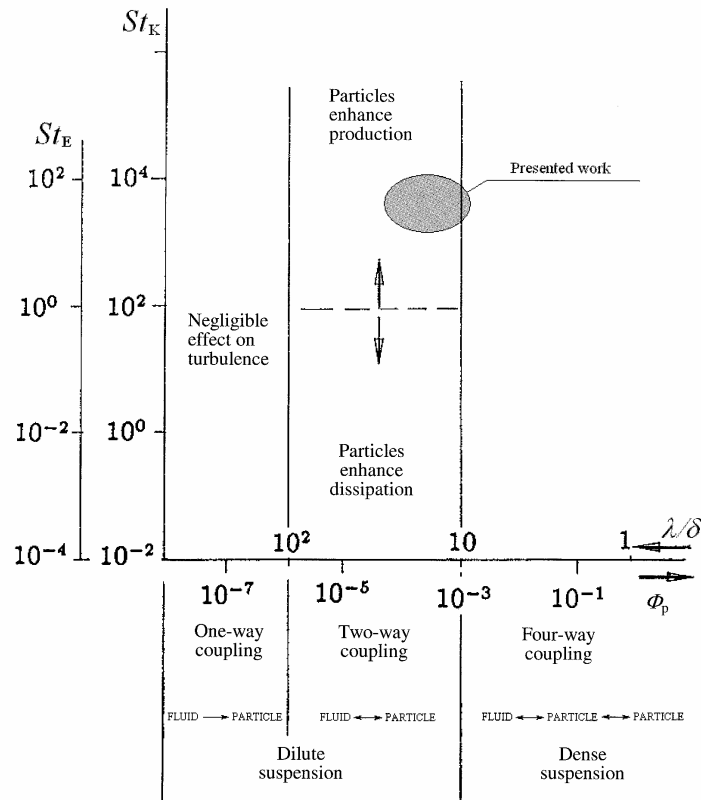


Fig. 4. The map of the flow regimes in particle-laden flows [14]; ϕ_p is the volume fraction of particles: $\phi_p = NV_p/V$ (N is the number of particles, V_p is volume of a particle and V is the volume occupied by particles and fluid).

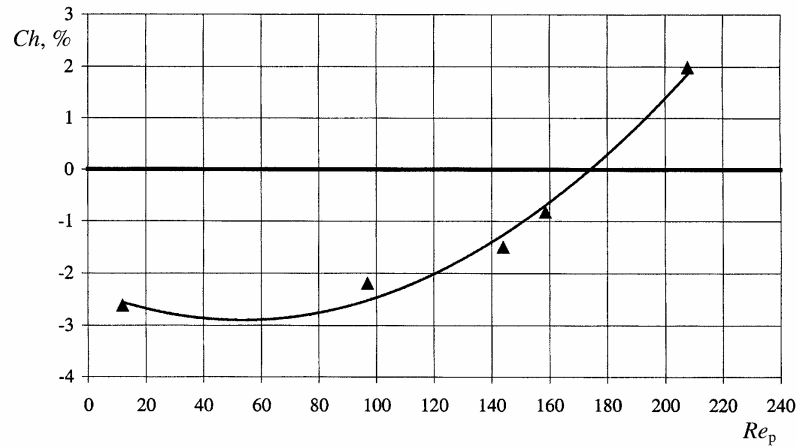


Fig. 5. The change of the turbulence intensity by particles vs Re_p for the grid $M = 16$ mm at the location $X = 365$ mm.

The criterion Re_p reflects the influence of the averaged velocities of the gas and particles and does not consider the turbulence parameters of the initial single-phase flow. Therefore, it is necessary to choose a criterion that would consider turbulence of the initial single-phase flow. The turbulence Reynolds number Re_L , determined by the Euler turbulence length-scale L_E and the fluctuating velocity of gas u'_{rms} as

$$Re_L = \frac{u'_{rms} L_E}{\nu}, \quad (10)$$

can be accepted as such a criterion.

Let us clarify in what way the conditions of turbulence of the initial single-phase flow, which is characterized by Re_L , affect the particles influence on turbulence in the two-phase flow. It is evident that the portion of energy, supplemented by particles owing to the shedding of vortices, decreases with the increase of the turbulent energy of the initial single-phase flow. At the same time, according to [1], the particles effect moves towards the turbulence attenuation with the growth of the eddy size L_E of the initial single-phase flow. This implies that the particles effect Ch is in inverse proportion to Re_L that was verified by experimental data (Fig. 6).

It seems logical to unify both criteria, Re_p and Re_L , into a single generalizing criterion Re_p/Re_L . This approach is a development of the Crowe's criterion [1], since the ratio $Re_p/Re_L = (\delta/L_E) \cdot (|u - u_s|/u'_{rms})$ considers the velocity characteristics of gas and particles in addition to Crowe's parameter δ/L_E . Thus the introduced criterion enables one to consider the combined influence of the parameters of the dispersed phase and of the initial single-phase flow on the turbulence of the carrier phase of the two-phase flow. Based on the

processing of the experimental data, obtained with the fixed mass loading for different grids at various velocity slips in different cross-sections of the flow, the dependence of the change of the turbulence intensity on the ratio Re_p/Re_L is obtained (Fig. 7). As Fig. 7 shows, all experimental data are fitted by the curve, which shows the point of transition from the turbulence attenuation to its enhancement at $Re_p/Re_L \approx 0.4$. Based on linear dependence of the change of the turbulence intensity by particles on the mass loading, stretch or shrink of this curve in vertical direction, depending on the flow mass loading, can be expected.

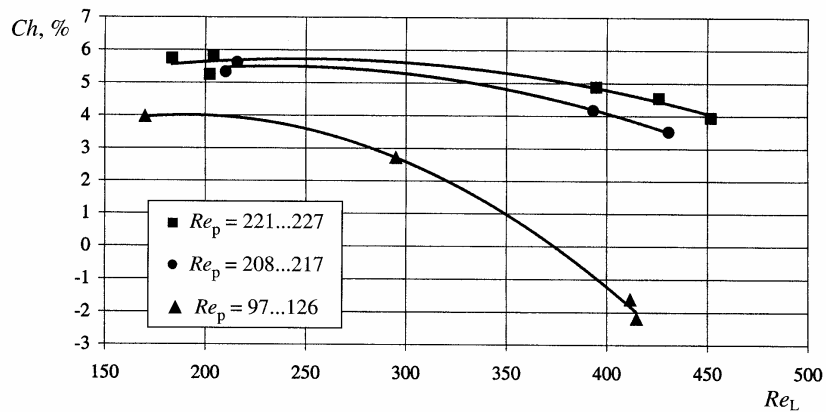


Fig. 6. The change of the turbulence intensity by particles vs Re_L for different values of Re_p .

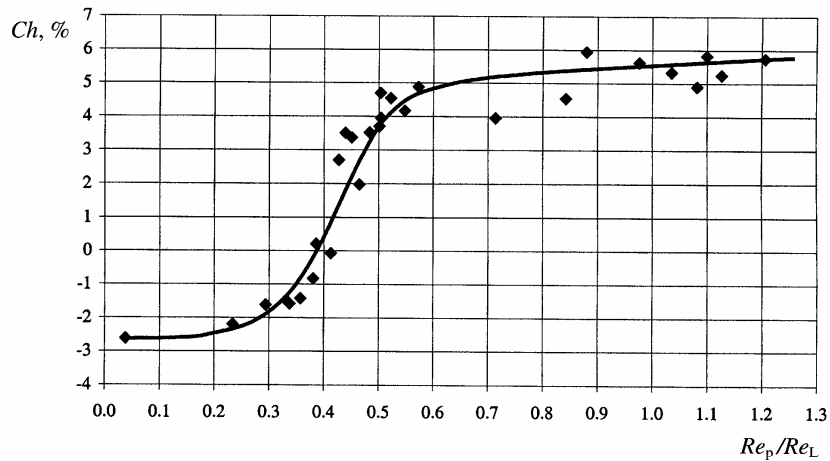


Fig. 7. The change of the turbulence intensity by particles vs Re_p/Re_L for the flow mass loading $\alpha = 0.14$ (kg dust)/(kg air).

4. CONCLUSIONS

Experimental investigations of the effect of the velocity slip and of the mass loading on the grid-generated turbulence in a gas–solid particles flow have been carried out. The velocity slip was achieved by preliminary acceleration of particles before their entering the flow, when the parameters of the gas and dispersed phases were invariable. The obtained results allow to draw the following conclusions:

- the 700 μm glass beads may attenuate or enhance the turbulence, depending on the parameters of turbulence of the initial single-phase flow;
- the velocity slip determines the particles effect on turbulence for the grid $M = 16$ mm for the given experimental conditions; the turbulence attenuation is observed for small velocity slips, whereas enhancement takes place for the velocity slips larger than 3.5 m/s;
- the ratio Re_p/Re_L is proposed as the criterion for considering the combined influence of the parameters of the dispersed phase and the initial single-phase flow on the turbulence of the carrier phase of the two-phase flow;
- $Re_p/Re_L \approx 0.4$ is the critical value for the given experimental conditions that determines the influence of particles on turbulence; at $Re_p/Re_L < 0.4$ the turbulent energy is attenuated and at $Re_p/Re_L > 0.4$ it is enhanced;
- the particles effect on turbulence depends linearly on the mass loading up to the loading of 1 (kg dust)/(kg air).

REFERENCES

1. Gore, R. A. and Crowe, C. T. Effect of particle size on modulating turbulent intensity. *Int. J. Multiphase Flow*, 1989, **15**, 279–285.
2. Hetsroni, G. Particles-turbulence interaction. *Int. J. Multiphase Flow*, 1989, **15**, 735–746.
3. Kulick, J. D., Fessler, J. R. and Eaton, J. K. *On the Interaction between Particles and Turbulence in a Fully-developed Channel Flow in Air*. Thermosciences Division, Department of Mech. Eng., Stanford University, Rep. No. MD-66, Stanford, California, 1993.
4. Squires, K. D. and Eaton, J. K. Particle response and turbulence modification in isotropic turbulence. *Phys. Fluids A*, 1990, **2**, 1191–1203.
5. Lance, M. and Bataille, J. Turbulence in the liquid phase of a uniform bubbly air-water flow. *J. Fluid Mech.*, 1991, **222**, 95–118.
6. Schreck, S. and Kleis, S. J. Modification of grid-generated turbulence by solid particles. *J. Fluid Mech.*, 1993, **249**, 665–688.
7. Stojanovic, Z., Chrigui, M., Sadiki, A., Dreizler, A., Geiß, S. and Janicka, J. Experimental investigation and modeling of turbulence modification in a dilute two-phase turbulent flow. In *Proc. 10th Workshop on Two-Phase Flows Predictions*. Merseburg, 2002, 52–60.
8. Hussainov, M., Kartushinsky, A., Rudi, Ü., Shcheglov, I., Kohnen, G. and Sommerfeld, M. Experimental results of turbulence modulation by rough solid particles in a grid-generated flow. *Proc. Estonian Acad. Sci. Eng.*, 2000, **6**, 217–229.
9. Hussainov, M., Kartushinsky, A., Rudi, Ü., Shcheglov, I., Kohnen, G. and Sommerfeld, M. Experimental investigation of turbulence modulation by solid particles in a grid-generated vertical flow. *Int. J. Heat Fluid Flow*, 2000, **21**, 365–373.
10. Laats, M. K. and Frishman, F. A. Assumptions used for the calculation of the two-phase turbulent jet. *Izv. Akad. Nauk SSSR, Mekh. Zhidk. Gaza*, 1970, No. 2, 186–191 (in Russian).

11. Hussainov, M., Kartushinsky, A., Mulgi, A., Shcheglov, I. and Tisler, S. Properties of solid particle distribution in two-phase laminar boundary layers of various shapes and particle sedimentation. *Proc. Estonian Acad. Sci. Phys. Math.*, 1994, **43**, 237–249.
12. Hinze, J. O. *Turbulence*. McGraw-Hill, New York, 1975.
13. Kenning, V. M. and Crowe, C. T. On the effect of particles on carrier phase turbulence in gas-particle flows. *Int. J. Multiphase Flow*, 1997, **23**, 403–408.
14. Elghobashi, S. Particle-laden turbulent flows: direct simulation and closure models. Spec. No. "Computational Fluid Dynamics for the Petrochemical Process Industry" (Oliemans, R. V. A., ed.). *Appl. Sci. Res.*, 1991, **48**, 301–314.
15. Hetsroni, G. Particles-turbulence interaction. *Int. J. Multiphase Flow*, 1989, **15**, 735–746.

Tahkefaasi kiirusliku nihke ja masskoormatuse mõju hindamine võreturbulentsi modifitseerumisele dispersses vooluses

Medhat Hussainov, Alexander Kartušinski, Ülo Rudi, Igor Štšeglov
ja Sergei Tisler

Eksperimentide läbiviimisel kasutati dispersse faasi moodustamiseks sfäärilisi klaasosakesi suurusega 700 µm, gaasi ja tahkete osakeste kiirusi mõõdeti laser-dopplermeetodiga. Turbulentsi sumbumiskõverad fikseeriti ruudukujuliste aken-dega võre taga, kusjuures võreakna suurused olid 4,8, 10,0 ja 16,0 mm. Nagu katsed näitasid, sumbus turbulents väikeste (4,8 ja 10,0 mm) võreakende puhul aeglasemalt kui samade parameetritega gaasivooluse puhul. See tõendab turbu-lentsi täiendavat genereerimist tahkete osakeste poolt. Samas põhjustasid osake-sed turbulentsi sumbumist suure (16,0 mm) võreakna puhul. Dispersse vooluse masskoormatuse suurendamisel võimendus osakeste mõju vooluse võreturbulent-sile mõlemal juhul. Faasidevahelise kiirusliku nihke mõju uurimisel dispersse vooluse turbulentsile nihkekiiruste vahemikus 0–5 m/s täheldati nii dispersse vooluse turbulentsi sumbumist kui ka genereerumist. Eksperimentaalsete and-mete baasil määrati kriteeriaalne parameeter, mis võimaldab arvestada dispersse faasi ja ühefaasilise lähtevooluse parameetrite mõju dispersse vooluse turbulent-sile.

CURRICULUM VITAE

Name Sergei
Surname Tisler
Date and place of birth 29.06.1967, Estonia
Family status Married
Contact Kellamäe 3-50, 74113 Maardu, Estonia,
 Telephone: +372 6001037;
 E-mail: sergei.tisler@ttu.ee

Workplace Tallinn University of Technology,
 Faculty of Science,
 Laboratory of Multiphase Media Physics,
 Akadeemia tee 23a, 12618 Tallinn

Appointment Researcher

Education:

<i>Educational institution</i>	<i>Year of graduation</i>	<i>Education</i>
26 th secondary school, Tallinn	1984	Secondary-level Educations
Leningrad Mechanical Institute (now Baltic State Technical University)	1990	Engineer in engines of the flying vehicles
Tallinn Technical University, Faculty of Mechanical Engineering	1999	M.Sc. (Eng)

Work experience:

2004 - present time	Tallinn University of Technology, Faculty of Science	researcher
2002 - 2003	Tallinn University of Technology, Estonian Energy Research Institute	researcher
1999 - 2002	Estonian Energy Research Institute	researcher
1996 - 1998	Estonian Energy Research Institute	extraordinary researcher
1990 - 1995	Energy Research Institute	junior researcher

Scientific degree Master of Science in Engineering
Certificate of education Tallinn Technical University, 1999
Scientific work Development of Theory of the Dispersed Gas-Solid Particles Flows

ELULOOKIRJELDUS (CV)

Eesnimi Sergei
Perekonnanimi Tisler
Sünniaeg ja-koht 29.06.1967, Eesti
Perekonnaseis Abielus
Kontaktandmed Kellamäe 3-50, 74113, Maardu, Eesti,
Telefon: +372 6001037,
E-mail: sergei.tisler@eri.ee
Töökoht TTÜ, Matemaatika-Loodusteaduskond,
Mitmefaasiliste keskkondade füüsika
teaduslaboratoorium,
Akadeemia tee 23A, 12618 Tallinn
Ametikoht Teadur

Hariduskäik

<i>Õppeasutus</i>	<i>Lõpetamise aeg</i>	<i>Haridus</i>
26. keskkool, Tallinn	1984	keskharidus
Leningradi Mehaanika Instituut	1990	insener-mehaanik, eriala: lennuaparaatide mootorid
Tallinna Tehnikaülikool, mehaanikateaduskond	1999	tehnikateaduste magister

Teenistuskäik

<i>Töötamise aeg</i>	<i>Organisatsiooni nimetus</i>	<i>Ametikoht</i>
2004- käesoleva ajani	Tallinna Tehnikaülikool, matemaatika-loodusteaduskond	teadur
2002 - 2003	Tallinna Tehnikaülikool, Eesti Energeetika Instituut	teadur
1999 - 2002	Eesti Energeetika Instituut	teadur
1996 - 1998	Eesti Energeetika Instituut	erakorraline teadur
1990 - 1995	Energeetika Instituut	nooremteadur

Teaduskraad Tehnikateaduste magister
Teaduskraadi välja andnud asutus, aasta Tallinna Tehnikaülikool, 15.12.1999
Teadustöö põhisuunad Disperssete (gaas-tahked osakesed)
vooluste teooria arendamine

LIST OF THE MOST IMPORTANT PUBLICATIONS

1. Hussainov, M., Kartushinsky, A., Mulgi, A., Shcheglov, I., Tisler, S., 1994, Properties of solid particle distribution in two-phase laminar boundary layers of various shapes and particle sedimentation. *Proc. Estonian Acad. Sci. Physics Mathematics*, Vol. 43(4), pp. 237-249.
2. Hussainov, M., Kartushinsky, A., Mulgi, A., Rudi, Ü., Tisler, S., 1995, Experimental and theoretical study of the distribution of mass concentration of solid particles in the two-phase laminar boundary layer on a flat plate. *Int. J. Multiphase Flow*, Vol. 21(6), pp. 1141-1161.
3. Hussainov, M., Kartushinsky, A., Mulgi, A., Shcheglov, I., Tisler, S., 1995, Experimental study of two-phase flow past various bodies and deposition of solid particles on the Surfaces. In: *Proceedings of 2nd Baltic Heat Transfer Conference*, Riga, Latvia, 21-23 August, 1995, Advances in Engineering Heat Transfer, (Eds.) B. Sunden, E. Blums, A. Zukauskas, Computational Mechanics Publ., Southhampton, Boston, 1995, pp. 267-276.
4. Hussainov, M., Kartushinsky, A., Shcheglov, I., Tisler, S., 1998, Some results of investigation of solid particles distribution in the vicinity of various shapes in two-phase flow and sedimentation on their surfaces. In: *Proceedings of 27th Israel Conference on Mechanical Engineering*, Haifa, Israel, 19-20 May, (Ed.) Ben-Haim, Ya., Technion - Israel Institute of Technology, Haifa, Israel, pp. 356-358.
5. Kartushinsky, A., Hussainov, M., Shcheglov, I., Tisler, S., Graham, D. I., 2001, Modulation of grid turbulence by small particles. In: *Proceedings of 4th International Conference on Multiphase flow*, New Orleans LA, USA, May 27 to June 1, CD-ROM, icmf472.
6. Hussainov, M., Kartushinsky, A., Tisler, S., 2002, Experimental study of adhesive behaviour of pair “solid particle-streamlined surface”. In: *Proceedings of 10th Workshop on Two-Phase Flow Predictions*, Merseburg, Germany, April 9-12, (Ed.) Sommerfeld, M., Martin-Luther-Universität, Halle, Germany, pp. 401-405.
7. Hussainov, M., Kartushinsky, A., Rudi, U., Shcheglov, I., Tisler, S., 2004, An experimental investigation of effect of the velocity slip on modification of the grid-generated turbulence in a gas-solid particles flow. In: *Proceedings of 3rd International Symposium in Two-Phase Flow Modelling and Experimentation*, Pisa, Italy, September 22-25, CD-ROM, as04.
8. Kartushinsky, A., Mulgi, A., Tisler, S., Michaelides, E. E., 2005, An experimental study of the effect of particles on the shear stress in particulate turbulent pipe flow. *Proc. Estonian Acad. Sci. Engineering*, Vol. 11(2), pp. 161-168.
9. Hussainov, M., Kartushinsky, A., Rudi, U., Shcheglov, I., Tisler, S., 2005, Experimental study of the effect of velocity slip and mass loading on the modification of grid-generated turbulence in gas-solid particles flows. *Proc. Estonian Acad. Sci. Engineering*, Vol. 11(2), pp. 169-180.

DISSERTATIONS DEFENDED AT
TALLINN UNIVERSITY OF TECHNOLOGY ON
MECHANICAL AND INSTRUMENTAL ENGINEERING

1. **Jakob Kübarsepp**. Steel-bonded hardmetals. 1992.
2. **Jakob Kõo**. Determination of residual stresses in coatings & coated parts.
3. **Mart Tamre**. Tribocharacteristics of journal bearings unlocated axis. 1995.
4. **Paul Kallas**. Abrasive erosion of powder materials. 1996.
5. **Jüri Pirso**. Titanium and chromium carbide based cermets. 1996.
6. **Heinrich Reshetnyak**. Hard metals serviceability in sheet metal forming operations. 1996.
7. **Arvi Kruusing**. Magnetic microdevices and their fabrication methods. 1997.
8. **Roberto Carmona Davila**. Some contributions to the quality control in motor car industry. 1999
9. **Harri Annuka**. Characterization and application of TiC-based iron alloys bonded cermets. 1999.
10. **Irina Hussainova**. Investigation of particle-wall collision and erosion prediction. 1999.
11. **Edi Kulderknup**. Reliability and uncertainty of quality measurement. 2000.
12. **Vitali Podgurski**. Laser ablation and thermal evaporation of thin films and structures. 2001.
13. **Igor Penkov**. Strength investigation of threaded joints under static and dynamic loading. 2001.
14. **Martin Eerme**. Structural modelling of engineering products and realisation of computer-based environment for product development. 2001.
15. **Toivo Tähemaa**. Assurance of synergy and competitive dependability at non-safety-critical mechatronics systems design. 2002.
16. **Jüri Resev**. Virtual differential as torque distribution control unit in automotive propulsion systems. 2002.
17. **Toomas Pihl**. Powder coatings for abrasive wear. 2002.
18. **Sergei Letunovitš**. Tribology of fine-grained cermets. 2003.
19. **Tatyana Karaulova**. Development of the modelling tool for the analysis of the production process and its entities for the SME. 2004.

20. **Grigori Nekrassov.** Development of an intelligent integrated environment for computer. 2004.
21. **Sergei Zimakov.** Novel wear resistant WC-based thermal sprayed coatings. 2004.
22. **Irina Preis.** Fatigue performance and mechanical reliability of cemented carbides. 2004.
23. **Medhat Hussainov.** Effect of solid particles on turbulence of gas in two-phase flows. 2005.
24. **Frid Kaljas.** Synergy-based approach to design of the interdisciplinary systems. 2005.
25. **Dmitri Neshumayev.** Experimental and numerical investigation of combined heat transfer enhancement technique in gas-heated channels. 2005.
26. **Renno Veinthal.** Characterization and modelling of erosion wear of powder composite materials and coatings. 2005.